universität
wien

DISSERTATION

**Cellular accumulation and DNA interaction studies
of antitumor metal complexes**

DI (FH) Caroline Bartel

angestrebter akademischer Grad
Doktor der Naturwissenschaften (Dr.rer.nat.)

Vienna, September 2011

Für meine Eltern

Acknowledgements

I am grateful that Prof. DDr. Bernhard Keppler gave me the opportunity to realize my PhD thesis in his prosperous working group and for the financial support.

I want to thank Dr. Michael Jakupec for his supervision, his motivation during the last years and his scientific suggestions and ideas.

Special thanks go to Dr. Anna Bytzek for her friendship and her scientific collegiality.

I want to thank my colleagues from the cell biology laboratory, DI (FH) Robert Trondl, BSc Simone Göschl, Michaela Hejl, MSc. Anton Legin, MSc Maria Novak, DDr. Mojtaba Valiahdi, DI (FH) Gerhard Mühlgassner, and BSc. Mahsa Razavi for the inspiring and friendly working atmosphere.

I´m also grateful for the support of my colleagues in the analytical and synthetic laboratory, Dr. Alexander Egger, PD Dr. Christian Hartinger, Mag. Yulia Scaffidi-Domianello, Mag. Gerlinde Grabmann and Prof. Dr. Markus Galanski, and I want to thank the rest of the working group for scientific discussions and good collaborations.

I also want to give thanks to Prof. Dr. Walter Berger and Dr. Petra Heffeter from the Institute of Cancer Research, Medical University Vienna, for their scientific support.

Many thanks go to Mag. Elfriede Limberger for helping with all administrative issues.

Last but not least I want to express my deepest gratitude to my parents Silvia and Günter, my boyfriend Arman, my sisters Cordula and Carina and my grannies Grete and Käthe who supported me during my studies, always encouraged me and never got tired of listening to my problems.

Abstract

The limitations of clinically used platinum-based anticancer drugs in a variety of solid tumors, severe side effects and the problem of acquired and intrinsic resistance necessitate the development of anticancer therapeutics with a different mode of action.

Hence, within this PhD thesis the ruthenium-based investigational anticancer drug KP1019 which showed promising results in a phase I clinical trial was investigated with regard to its mode of action. Based on the 'activation by reduction' hypothesis, the influence of the intracellular antioxidant ascorbic acid (vitamin C) was studied. Ascorbic acid enhanced the activity of KP1019 which was shown by higher cytotoxicity in the human colon carcinoma cell line SW480, human cervical carcinoma KB-3-1 cells, and the multidrug-resistant subline KBC-1. Moreover it was demonstrated by means of EMSA that ascorbic acid enhanced interaction of KP1019 with the model biomolecule plasmid DNA. To explain increased activity, cellular accumulation was investigated and ruthenium contents were measured by ICP-MS. Those studies revealed that ascorbic acid did not alter the intracellular ruthenium concentration compared to KP1019-only treated cells. During incubation with KP1019 intracellular reactive oxygen species (ROS) are produced. To elucidate whether generation of ROS is influenced by ascorbic acid and therefore may contribute to the enhanced cytotoxic potential of KP1019, ROS were analyzed by the DCFA-DH assay and subsequent FACS measurements. It was evinced that KP1019-induced ROS were reduced by ascorbic acid in a dose-dependent manner and thus can be excluded as a reason for increased activity of KP1019. Based on the obtained results, it is assumed that the direct interaction of KP1019 and ascorbic acid, resulting in reduction of the ruthenium center, is responsible for the enhanced reactivity.

A further scope was investigation of non-classical platinum drugs with regard to their biological behavior. Therefore three pairs of *cis-* and *trans*-configured 2-propanone oxime platinum(II) complexes and one pair of 3-pentanone oxime platinum(II) complexes, which displayed higher cytotoxicity for the *trans*-configured complexes than their *cis*-configured counterparts and proved more cytotoxic than cisplatin in the inherently cisplatin resistant cell line SW480, were selected. To explain the higher activity, cellular accumulation was determined, revealing enhanced concentrations in cells treated with the four *trans*-platinum(II) complexes compared to the respective *cis*-complexes as well as cisplatin and transplatin. Based on the assumption that DNA is the critical cellular target as it is with cisplatin, binding to DNA was investigated by *in vitro* DNA metalation experiments and determined by ICP-MS measurement. Again, the *trans*-complexes showed stronger effects resulting in higher r_b values (platinum per phosphorus). Studies on the genotoxic potential of the *trans*-platinum(II) complexes as well as their ability to induce cross-links were conducted by means of the Comet Assay and showed a distinct impact on the DNA compared to cisplatin. Additional information about the type of DNA interaction were obtained by cell free experiments with plasmid DNA and the

nucleobase dGMP which, in accordance with the other experiments, also indicated differences compared to cisplatin. The variations in DNA interactions between the novel *trans*-platinum(II) complexes and cisplatin give reason to think of a different mode of action.

Concluding, the presented investigations of cellular accumulation and interaction with biomolecules of metal-based anticancer drugs contribute to the understanding of the mode of action of those complexes. The emphasis for further clinical development is on substances that act differently from currently used drugs because such complexes may overcome resistance phenomena or bear a lower risk of severe side effects.

Zusammenfassung

Die unzureichende Wirkung platin-basierter Krebstherapeutika in einer Vielzahl solider Tumore, die schweren Nebenwirkungen und das Problem von erworbener und intrinsischer Resistenz machen die Entwicklung von Arzneimitteln mit einem anderen Wirkmechanismus notwendig.

Ein Schwerpunkt dieser Arbeit war daher die Untersuchung der Wirkungsweise des Ruthenium-Komplexes KP1019, der bereits in einer klinischen Phase I – Studie erfolgversprechende Resultate erzielte. Basierend auf der Hypothese einer Aktivierung durch Reduktion wurde der Einfluss des intrazellulären Antioxidans Ascorbinsäure (Vitamin C) untersucht. Ascorbinsäure verstärkte die Aktivität von KP1019, was sich durch höhere Zytotoxizität in der humanen Darmkrebszelllinie SW480, den humanen Gebärmutterkarzinomzellen KB-3-1 und der mehrfach resistenten Subzelllinie KBC-1 gezeigt hat. Darüberhinaus konnte in weiteren Versuchen unter dem Einfluss von Ascorbinsäure eine verstärkte Reaktivität von KP1019 mit dem Modell-Biomolekül Plasmid-DNA mittels EMSA nachgewiesen werden. Um die erhöhte Aktivität erklären zu können, wurde zunächst die zelluläre Akkumulation untersucht und der Ruthenium-Gehalt der Zellen mittels ICP-MS bestimmt. Dabei zeigte sich, dass Ascorbinsäure die intrazelluläre Ruthenium-Konzentration im Vergleich zu Zellen, die nur mit KP1019 behandelt wurden, nicht veränderte. Bei der Inkubation mit KP1019 kommt es zur Bildung reaktiver Sauerstoffspezies (ROS), die bei der zytotoxischen Wirkung eine Rolle spielen. Die Frage, ob die ROS-Bildung durch Ascorbinsäure beeinflusst wird und damit zur Erklärung der erhöhten zytotoxischen Wirkung von KP1019 beitragen kann, wurde durch den DCFA-DH Assay mit anschließender FACS Messung untersucht. Es zeigte sich, dass der Gehalt an durch KP1019 gebildete ROS durch Ko-Inkubation mit Ascorbinsäure dosisabhängig abnimmt und somit als Ursache der verstärkten Aktivität von KP1019 ausgeschlossen werden kann. Basierend auf den Resultaten wird angenommen, dass eine direkte Wechselwirkung zwischen KP1019 und Ascorbinsäure und die daraus resultierende Reduktion des Ruthenium-Zentrums für die verstärkte Reaktivität verantwortlich ist.

Eine weitere Aufgabenstellung war die Untersuchung biologischer Effekte nicht-klassischer Platinverbindungen. Hierzu wurden drei Paare *cis*- und *trans*- konfigurierter Platin(II)-Acetonoxim-Komplexe und ein Paar Platin(II)-Pentanonoxim-Komplexe ausgewählt, bei denen die *trans*-Komplexe deutlich zytotoxischer als ihre *cis*-konfigurierten Analoga wirken und vor allem in der cisplatin-resistenten Zelllinie SW480 aktiver als Cisplatin sind. Um die stärkere Aktivität erklären zu können, wurde zunächst die zelluläre Akkumulation gemessen. Dabei konnte eine erhöhte zelluläre Anreicherung im Falle der vier *trans*-Platin(II)-Komplexe im Vergleich zu den entsprechenden *cis*-Komplexen sowie zu Cisplatin und Transplatin nachgewiesen werden. Aufgrund der Annahme dass DNA, wie bei Cisplatin, das zelluläre Target ist, wurde die Anbindung an die DNA in Zellen untersucht und mittels ICP-MS gemessen. Auch hier zeigten die *trans*-Komplexe stärkere Effekte, die

III

in höheren r_b-Werten (Platin pro Phosphor) resultierte. Untersuchungen des genotoxischen Potenzials der *trans*-Platin(II)-Komplexe und die Fähigkeit der Verbindungen, Quervernetzungen zu verursachen, wurden mit Hilfe des Comet Assays durchgeführt und zeigten eine von Cisplatin deutlich abweichende Wirkung auf die DNA. Zusätzliche Informationen über die Art der DNA-Wechselwirkung brachten zellfreie Experimente mit Plasmid-DNA und der Nukleobase GMP, die in Übereinstimmung mit den zuvor erwähnten Versuchen eindeutige Unterschiede zu Cisplatin belegen. Die Abweichungen der DNA-Wechselwirkung der neuen *trans*-Platin(II)-Komplexe und Cisplatin lassen auf andersartige Wirkmechanismen schließen.

Zusammenfassend ist zu erwähnen, dass die vorliegenden Studien der zellulären Akkumulation von metall-basierten Krebstherapeutika und deren Wechselwirkung mit Biomolekülen zum Verständnis des Wirkmechanismus beitragen. Der Fokus der klinischen Weiterentwicklung liegt auf Verbindungen, die anders wirken als derzeit verwendete Medikamente. Solche Wirkstoffe könnten es ermöglichen, Resistenz-Phänomene zu überwinden, oder ein geringeres Risiko ernster Nebenwirkungen aufweisen.

Table of Contents

Index of Figures

List of abbreviations

AP	apurinic/apyrimidinic
ATP	adenosine triphosphate
BER	base excision repair
CAM	cell adhesion molecule
CE	capillary electrophoresis
cddp	cisplatin, (*SP*-4-2)-diamminedichloridoplatinum
Cdk	cyclin dependent kinase
Cdk-I	cyclin dependent kinase inhibitor
cis-GG	cisplatin – Guanin –Guanin adduct
cis-AG	cisplatin – Adenine –Guanin adduct
cis-GxG	cisplatin – Guanin – any Nucleotide – Guanin adduct
DMT1	divalent metal transporter 1
DNA	desoxyribonucleic acid
EMSA	electrophoretic mobility shift assay
EGF-R	epidermal growth factor receptor
FGF	fibroblast growth factor
G0/1/2	gap phase 0/1/2
ICP-MS	inductively coupled plasma-mass spectrometry
KP1019	indazolium *trans*-[tetrachlorobis(1*H*-indazole)ruthenate(III)]
KP1339	sodium *trans*-[tetrachlorobis(1*H*-indazole)ruthenate(III)]
KP46	tris(8-quinolinolato)gallium(III)
MAPK	mitogen activated protein kinase
NAMI-A	imidazolium *trans*-[tetrachloro-*S*-dimethylsulfoxideimidazole-ruthenate(III)],
	new antitumor metastasis inhibitor – A
NER	nucleotide excision repair
^{1}H-NMR	proton nuclear magnetic resonance spectroscopy

PDGF   platelet derived growth factor

RNR   ribonucleotide reductase

ROS   reactive oxygen species

tddp   transplatin, (*SP*-4-1)-diamminedichloridoplatinum

Tf   transferrin

TfR   transferrin receptor

TGFα   tumor growth factor α

VEGF   vascular endothelial growth factor

1. Introduction

1.1. Cancer – definition and epidemiological background

Cancer is classified as a cohort of diseases that are characterized by uncontrolled cell growth, invasion and the thereof resulting destruction of surrounding tissue, and the capability to form metastasis at different sites of the body. Malignant tumors emerge from a single mutated cell (monoclonal growth) and can occur in every tissue of the body. Carcinomas arise of endothelial cells and are responsible for about 80% of malignant deaths in the European countries. Sarcomas are cancers of mesenchymal cell types including tumors of muscles and bones and account for about 1% of cancers. Tumors of the third group are caused by hematopoietic tissues and include lymphomas as well as leukemias. Tumors of the neuroectodermal tissue are termed glioma and blastoma. The last groups add up to nearly 20% of cancers [1, 2].

In Austria, as in most other Western world countries, cancer is the second most common cause of death after cardiovascular diseases and is responsible for 25% of deaths. Among the most common types of cancer are prostate cancer in men and breast cancer in women. In both genders, colon and lung cancer are the second and third most abundant types of cancer (Figure 1). Together, these three kinds of cancer are causing more than 50% of malignancy-related deaths [3]. Due to preventive checkups as well as progress in surgery and treatment, today some types of cancer have curing rates of 80%, e.g.; testicular cancer, while others such as pancreatic cancer still are fatal for over 80% of the patients.
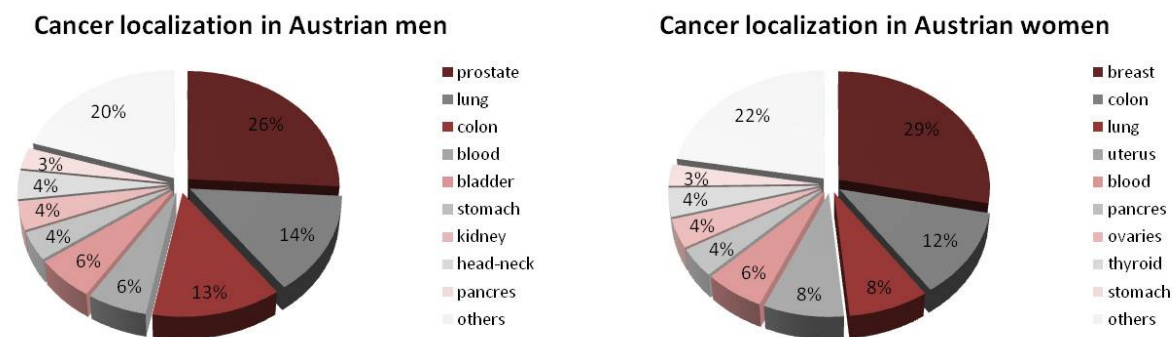

Figure 1. Cancer localization in Austrian men (left) and Austrian woman (right) [3]

1.2. Carcinogenesis

Cancer development is a multistage process. Within this process, which is called carcinogenesis, a normal cell is transformed into a tumor cell by various accumulated molecular mutations. The process is divided into three major phases: initiation, promotion and progression (Figure 2).
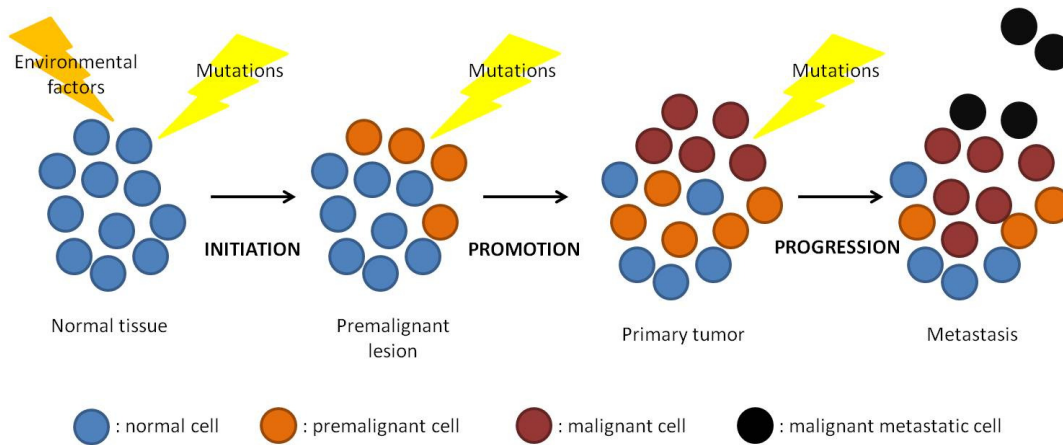
Figure 2. Carcinogenesis as a multistep process [4]

The initiation of tumorigenesis involves certain single mutations within a given cell. During cell cycle and cell division errors within the transcription of DNA occur frequently and various repair mechanisms are in place to deal with them (e.g. nucleotide excision repair, base excision repair, mismatch repair). One of the major important factors for the cell cycle is the p53 gene. This gene is a tumor suppressor gene that stops the cell cycle at the G1/S regulation check point as soon as a mismatch or another abnormality in the DNA occurs, thus giving the cellular repair machinery time to repair the DNA. If the damage is beyond repair, p53 initiates apoptosis. In some cases neither damage repair nor cell apoptosis are initiated, and the irreversibly altered DNA is given to the next generation of cells acting as a proto-oncogene, depending on the gene context of the mutation. Another possibility of initiation are mutations within tumor suppressor genes such as p53 itself, which inactivate the control and repair machinery of the cell [5].

A single mutation within a cell normally does not cause cancer, but in the course of several years various mutations can occur that promote tumor formation and initiate enhanced cell proliferation. The amplified proliferation leads to hyperplasia, an aggregate of cells that exceeds the normal cell number and can lead to enlarged organs. Due to mutations, the histological structure of those tissues differs from normal organs and is therefore called dysplasia. In any case the newly formed cell aggregates to malignant or benign tumors, with neoplasia being a preliminary stage to both [1, 2]. Mutations are promoted by various endogenous and exogenous factors such as nutrition, smoking, alcohol, inflammation, hormones, chemicals and UV exposure [6].

The promotion of tumorigenesis can last for several years or even decades and thus explains why most tumors occur in the second half of a human's lifespan. Within this stage, changes in life style can help to avoid further promotion of the tumor in many cases.

In the final step of the carcinogenic process the accumulated mutated cells are transformed into malignant cells. During progression, more mutations occur within the preneoplastic cell population and result in cancer. In this step malignant cells overcome tissue boundaries and are able to enter the blood stream. As a result, these cancer cells can enter other tissues and form tumors in distant locations of the body, i.e. metastasis [4].

1.3. Cancer cell characteristics

Even though cancer is basically an accumulation of DNA alterations and every cancer has its own unique genotype as well as phenotype, there are several characteristics that are found in most cancer cells [7]. Our understanding of these hallmarks is of great importance for drug development as they may inspire approaches for effective treatment strategies.

Proliferation of cancer cells is independent on growth signals. This autonomy can be achieved by three different mechanisms which can also accumulate within cancer cells. First, as opposed to normal cells which always depend on paracrine or endocrine growth signals, cancer cells have the ability to generate their own growth factors such as the platelet derived growth factor (PDGF) or the tumor growth factor α (TGFα) [8]. Furthermore, such cells have the possibility to over-express growth factor receptors in order to take full advantage of circulating growth factors. Frequently these receptors are tyrosine kinases, and they were shown to be over-expressed in a variety of human tumors, e.g. epidermal growth factor receptor (EGF-R/erbB) is over-expressed in stomach, brain and breast tumors [9]. The third and most sophisticated mechanism that can lead to growth signal independency involves alterations in the downstream pathways of growth signals. An important example is the Ras-Raf-MAPK cascade which is mutated in 25% of human tumors. In these cases the Ras proteins are able to give signals to cells even when their normal upstream regulators are no longer stimulated [10].

Besides the generation of growth signals cancer cells are also able to overcome antigrowth signals by disruption of two main mechanisms that prevent proliferation under normal conditions. Cancer cells can overcome the signals that force them to enter the G_0 phase in the cell cycle and become quiescent, and they are also able to evade differentiation [7, 11].

In order to keep a tissue healthy, the balance between cell proliferation and apoptosis is essential. Additionally to their independence of growth and anti-growth signals, cancer cells are also able to escape apoptosis. The major factor in this regard is the tumor suppressor gene p53 which is inactivated in over 50% of all cancers and leaves the DNA susceptible to unrepaired damage [12]. The apoptosis pathway is versatile and to date not fully understood. It is postulated that, besides changes in p53, mutations can arise in other tumor suppressor genes and oncogenes of all cancer cells enabling them to escape apoptosis [7].

While normal cells exhibit a limitation in cell division and enter senescence after a defined number of doublings, cancer cells acquire limitless replicative potential. The clue to being immortal is the preservation of telomeres, DNA sections at the end of chromosomes that protect genomic DNA. Telomeres normally are shortened with every cell cycle and indicate to enter senescence when a certain length is deceeded. Neoplastic cells are able to upregulate the telomere-maintaining enzyme telomerase and avoid entering senescence [7, 11].

Especially during tumor growth, cancer cells have a need for nutrients and oxygen which are delivered with the blood. After reaching a certain tumor size, this supply is insufficient and it becomes necessary for the tumor cells to trigger the formation of new blood vessels to the tumor. Vascular endothelial and fibroblast growth factors (VEGF, FGF) play an important role in neoangiogenesis and are over-expressed in many tumors [7, 11].

The last step in the transformation of a normal cell into a cancer cell is the ability to invade surrounding tissue and enter the blood and lymph stream to form metastases elsewhere in the body. Even though the mechanism of invasion and metastasis is still not completely elucidated, several proteins have been identified that play a crucial role. On the one hand proteins that mediate cell-cell interactions, such as cell-cell adhesion molecules (CAM), as well as proteins that trigger interactions of cells with the extracellular matrix, such as integrins, are of great importance. For example inhibition of the CAM E-cadherin was shown to promote invasion and metastasis while imposed expression led to inhibition of invasive activities [7, 13]. Furthermore the interaction with matrix degrading proteases plays a role in enabling cancer cells to spread out into surrounding tissue [7].

1.4.   The cell cycle – the role of oncogenes, tumor suppressor genes and repair mechanisms

1.4.1. The cell cycle

During the cell cycle one cell divides into two daughter cells sharing identical genomic material. The cell cycle is divided into 4 phases (Figure 3). In the first phase, i.e. the G1 phase, cells grow and the chromosomes are prepared for replication. During the next phase, the S phase, the genetic material is doubled, new DNA is synthesized and the centromers are duplicated. After this, the cell enters resting phase G2, in which preparations are made for cell division. The gaps between the synthesis of new DNA and the actual division into two daughter cells, G1 and G2, allow the cell also to double proteins and organelles. Additionally at the end of both phases checkpoints are installed to ensure proper replication of the cell in the following important phase. The final step of the cell cycle is the mitosis and the cytokinesis, namely the M phase. The mitosis is segmented in 4 periods: prophase, metaphase, anaphase, telophase during which the chromosomes condensate and, following the breakdown of the nuclear membrane, are aligned at the metaphase plate. Subsequently the sister chromatids are pulled towards the poles of the cell by the spindle apparatus and start to decondensate there. The cytosol divides, the nuclear membrane is rebuilt again and the two identical cells enter G1 phase [1, 14-16].
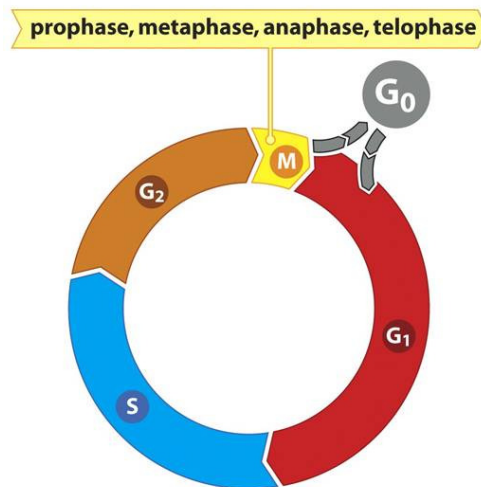
Figure 3. The cell cycle and the 4 phases of the mitosis [1]

Another phase which is associated with the cell cycle is the G0 phase. In this state, cells are quiescent which means that they do not prepare replication but are highly active in maintenance of the human body functions. The G0 phase is initiated by the lack of mitogenic factors (growth factors) or due to antimitogenic signals. Normally cells are able to leave G0 and re-enter the cell cycle. However, when cells differentiate this capability gets lost, and the cells are not able to replicate any more [1, 14-16].

1.4.2. *Regulation of the cell cycle checkpoints*

The components regulating the cell cycle are mainly cyclins, cyclin dependent kinases (Cdks) and Cdk inhibitors (Cdk-I).

Cdks are Ser/Thr specific protein kinases with an average size of 34-40 kDa. In order to become active, they must bind to the corresponding cyclin. The formation of such dimers is essential for the activity of Cdks and is regulated by phosphorylation. The crucial Cdks in cell cycle regulation are Cdk4, which is essential during the G1 phase, Cdk2 in the S phase, and Cdk1 in the mitotic phase.

Cyclins are a unit of the Cdk heterodimer and are important for activating Cdks and defining their substrate specificity. Their concentration varies periodically during the cell cycle and is strictly controlled by regulation of expression, degradation through the ubiquitin pathway as well as phosphorylation. Furthermore, the sub cellular distribution changes within the cell cycle from the nucleus to predominant localization in the plasma. In the cell cycle, cyclin D is essential in G1, cyclin E and A take control in the S phase and cyclin B regulates the mitotic events [15, 17].

Cdk-I can delay or stop the cell cycle whenever necessary. They are highly important for the passage from the G1 to the S phase and for enabling cells to enter as well as leave the G0 phase. Activated by antimitotic signals and DNA damage, Cdk-I themselves negatively regulate Cdks by binding to the Cdk/cyclin complex, distortion of its active side, prevention of substrate binding, fixation of inactive Cdk conformation, and competition with cyclins in the complexes [16, 18].

The cell cycle is equipped with various feedback mechanisms to avoid incomplete execution of the particular phases and uncontrolled cell proliferation as well as polyploid cells. Sensors detecting errors in the replication machinery stop the cell cycle, thus giving repair proteins time to fix the problem or induce apoptosis if the damage is beyond repair. To assure correct replication, each phase in the cell cycle harbors a checkpoint which must be passed before the cell can enter the next phase (Figure 4) [1, 19].

G1 includes the DNA damage checkpoint. Prior to a cell's transition into the S phase, it is checked whether the surrounding conditions are favorable for cell division: the cell has to be adequately large, the nutrient supply must be sufficient, and enough growth factors are required to stimulate the process. If all requirements are fulfilled, the start checkpoint is passed and the cell can enter the S phase and start the cell cycle. During the S phase the genomic material is checked and only in case of an unharmed genome the cell enters G2. At the G2/M checkpoint the completeness of DNA replication as well as the correct doubling in the S phase is assessed before the cell can proceed to the M phase and enter mitosis.

While the cell divides into two daughter cells in the M phase, it must be ensured that the chromosomes are correctly attached to the spindle and are aligned in a specific order on the metaphase plate. Only if this is the case, anaphase is induced and the cell can proceed with cytokinesis subsequent to the splitting of the chromosomes [15-17].
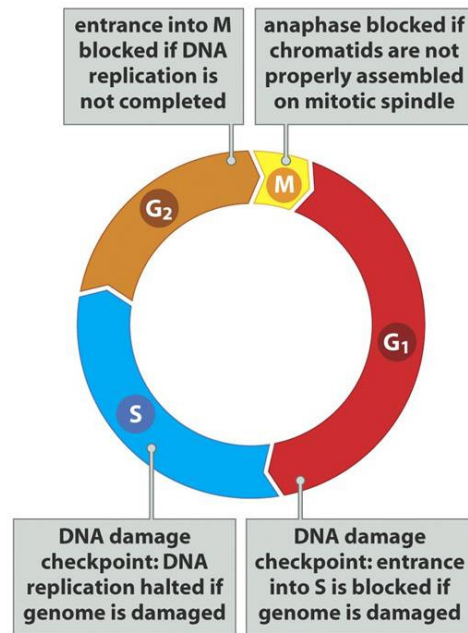
Figure 4. Checkpoints in the 4 phases of the cell cycle [1]

1.4.3. Oncogenes

Proto-oncogenes, acting as precursors of oncogenes, are parts of the DNA that encode growth factors and their receptors, *e.g.* tyrosine kinases, G-proteins such as the group of Ras proteins and nuclear transcription factors as well as genes that are involved in repair mechanisms and apoptosis inducing genes. They normally control and promote cell growth, proliferation and differentiation. Caused by environmental factors or viruses, mutations can occur within these sequences and turn proto-oncogenes into oncogenes, which promote tumor growth. The most important proto-oncogenes are the control genes of the cell cycle.

Changes in these sequences always lead to dysfunction of the normal cell division. While a single mutation even in a proto-oncogen is not sufficient to cause cancer, it triggers proliferation, thus producing many dividing cells which are susceptible to further mutations and therefore are at risk to become cancer cells. Some of the oncogenes are important prognostic factors concerning the aggressiveness in various cancers, *e.g.* n-myc in neuroblastoma and c-erbB-2 in ovarian and breast cancer [4, 14].

1.4.4. Tumor suppressor genes

Tumor suppressor genes are control points in the cell cycle and can lead to the differentiation of cells as well as apoptosis if lesions in the DNA occur that are not repaired. The balance between proliferation and apoptosis and also the elimination of incorrectly duplicated DNA is crucial for the maintenance of health, and therefore every malfunction increases the risk of cancer development.

One of the most important tumor suppressor genes is p53, which is also called the guardian of the genome. The p53 protein is a transcription factor, which is activated by kinase-dependent phosphorylation as a consequence of cellular stress and DNA damage. When activated, it blocks the cell cycle, thus giving the cellular repair machinery time to correct the DNA damage. If the damage is beyond repair, p53 induces apoptosis. As a response to cell growth and anti-growth signals, p53 can also provoke differentiation in cells and therefore limit the number of proliferating cells. p53 is mutated in over 50% of all cancers, emphasizing its outstanding role in cancer development and its importance as a target in anticancer therapy [20].

1.4.5. Cell repair mechanism

Various chemicals and other exogenous factors such as UV light and radiation trigger the occurrence of altered bases and even larger DNA lesions. Therefore defects in the DNA during the cell cycle arise often, but not every mistake leads to a mutated cell or enforces apoptosis. As soon as the cell cycle is paused by Cdk-I, the cell repair machinery has an opportunity to repair the defects, permitting the cell to continue the division.

1.4.5.1. Base excision repair (BER)

During the process of replication various defects can occur within the DNA strands such as methylation, deamination or oxidation of several bases. To remove these errors, a special group of enzymes, DNA glycosylases, are able to travel along the DNA and detect these damages by a base flipping mechanism. As soon as a disturbance is found, the enzyme removes the base, leaving the sugar in the backbone.

This gap is recognized by AP (apurinic/apyrimidinic) endonucleases which remove the sugar together with phosphodiesterases by cutting the phosphodiester backbone. The break in the DNA strand is filled in by DNA polymerases and DNA ligases closes the gap (Figure 5) [1, 16]
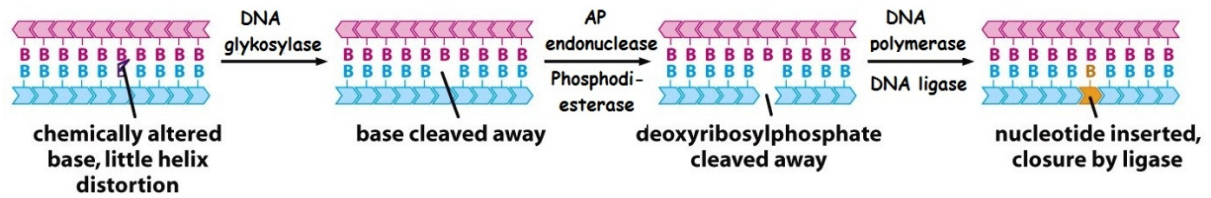
Figure 5. Base excision repair [1]

1.4.5.2. Nucleotide excision repair (NER)

If the structure of DNA is seriously changed, the NER is activated to remove the altered part of the DNA strand and replace it with functioning nucleotides. Such damages can be caused by covalent binding of the DNA with various substances, e.g. cisplatin and benzopyrene, but also by dimer formation as a reaction to UV light. After an enzyme complex detects a lesion in the DNA, excision nucleases and DNA helicases remove a considerable part of the DNA up- and downstream of the lesion. Subsequently the DNA polymerase together with the DNA ligase fills in and seals the gap. The enzymes of the NER are also used to repair strand breaks, which can be induced by various chemicals as well as ionizing radiation (Figure 6) [1, 14, 16, 21].
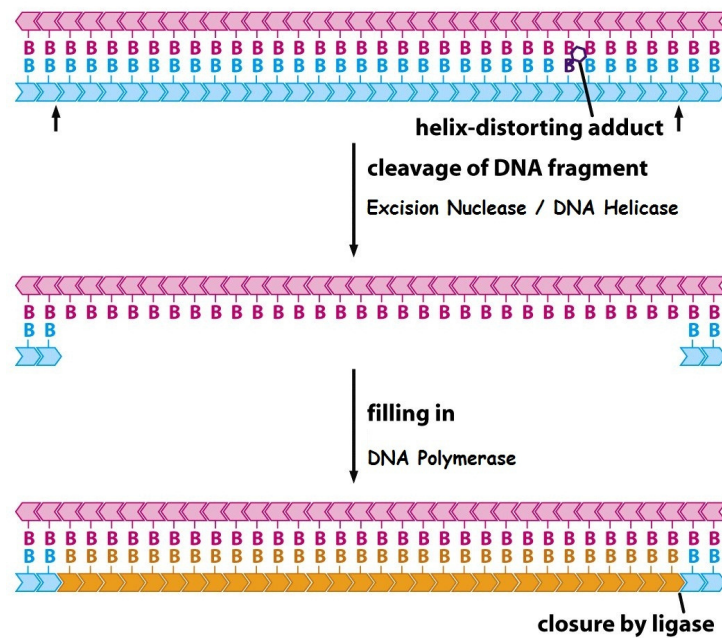
Figure 6. Nucleotide excision repair [1]

Even though a working repair system is beneficial for cell division, a problem arises in anticancer treatment. Various drugs, among them the prominent chemotherapeutic cisplatin, gain their antiproliferative property by formation of DNA adducts and resulting impairments in cell proliferation. The removal of such DNA lesions by the NER has been reported for cisplatin and is discussed as one of the mechanisms that lead to resistance during treatment [22, 23].

1.5. Anticancer therapy

The treatment of cancer is based on the three classical pillars surgery, radiation- and chemotherapy and also on newer approaches such as targeted therapy with antibodies as well as cryo- and fever-therapy. Even though surgery is the most promising treatment, it is limited to solid tumors that occur in accessible sites of the body and its use is especially restricted in case of metastases. Often surgery is followed by chemotherapy, which is then called adjuvant chemotherapy, to destroy malignant cells that may be left in the tissue and to avoid relapse and metastatic spread. Sometimes it is necessary to give antineoplastic drugs prior to surgery of the tumor, a treatment known as neo-adjuvant therapy, in order to reduce the size of the tumor to enable its removal. Therapy of inoperable tumors, either because of their localization or because of their systemic character such as leukemias, includes radiation- and chemotherapy.

Radiation therapy is the devastation of cancer cells by using ionizing radiation such as X-ray, neutron and proton beams and gamma rays [24]. The application can be made by the direction of a radiation beam to the tumor mass or by treatment with radionuclides such as ^{131}I for the treatment of thyroid diseases [25]. Radionuclides can be linked to transporters, *e.g.* antibodies, liposome emulsions and nanoparticles with tumor targeting ligands, to enable selective delivery to the cancer cells without causing damage of other organs [26].

Just as in the case of surgery, radiotherapy is often combined with chemotherapy to maximize therapy success based on interaction of radiation with the cell surface. This results in an increased permeability of cell membranes allowing enhanced uptake of chemotherapeutic drugs specifically into cancer cells. Furthermore, chemotherapeutics are used to reduce tumor mass and thereby allow subsequent treatment with radiation beams [27].

Chemotherapy is defined as the attack of pathogens and cancer cells with low molecular substances. Even though the term includes antibiotic and antimycotic therapy, it is often narrowed down to cytostatics. The roots of chemotherapy date back to World War I when lymphoid hypoplasia and myelosuppression were found in soldiers who got in touch with mustard gas (nitrogen mustard). After the discovery of the anticancer activity of nitrogen mustard, first clinical trials were conducted in 1942 showing the regression of non-Hodgkin lymphoma in a single patient.

This gave hope to the idea of cancer being treatable with chemicals [28, 29]. Over the years many different kinds of antineoplastic drugs that lead to a regression of various tumors when administered alone or, more often, in combination with other chemotherapeutics were introduced into the clinic. The first attempts to find new antitumor active substances took the form of big screenings of various natural and synthesized compounds by governmental programs. However, as molecular cancer biology was understood in greater detail, the search for new drugs started to focus on substances that specifically affect cancer cells and therefore cause fewer side effects.

The field of targeted therapy was established and specific proteins that were involved in cancer specific pathways were targeted, with one of the first examples being imatinib, a Bcr-Abl tyrosine kinase inhibitor which is used in the treatment of chronic myelocytic leukemia [30]. Even though today there is a broad range of chemotherapeutic drugs available, including alkylating agents (cyclophosphamide), antifolates (methotrexate), antimetabolites (5-fluorouracil), topoisomerase inhibitors (doxorubicin), antimitotic drugs (vinca alkaloids), monoclonal antibodies (cetuximab) and metal-based anticancer drugs (cisplatin), cisplatin and its two clinically used analogues carboplatin and oxaliplatin are used in >50% of chemotherapies alone or in combination with other drugs causing synergistic effects, *e.g.* bleomycin and vinblastin [31, 32].

1.6. Treatment strategies – exploiting the hallmarks of cancer cells

As mentioned above, cancer cells show a variety of special characteristics that distinguish them from normal cells. To avoid adverse effects during chemotherapy it would be beneficial to target such cancer cell specific hallmarks.

1.6.1. DNA interaction

Even though most of the drugs targeting DNA do not address certain sequences and therefore have a rather unspecific function, DNA is a suitable target as cancer cells proliferate at a very high rate. This makes their DNA more susceptible to damage and these cells more responsive than normal cells, keeping the risk of side effects acceptable. There are several ways of impairing DNA function, such as strand breaks and covalent binding. Bleomycin is an anticancer drug of the group of metal-binding glycopeptide antibiotics that breaks DNA strands by free radical-mediated cleavage of desoxyribose [33, 34]. A more common mechanism is the binding to DNA and the resulting disruption in the division process. Cisplatin, one of the clinically most frequently used antitumor drug, exerts its activity *via* this mechanism. It covalently binds to the N7 residue of the guanine bases and crosslinks

bases of the same or of the two different strands (Figure 7), causing bending of the DNA and local interruptions which impair replication processes [35].
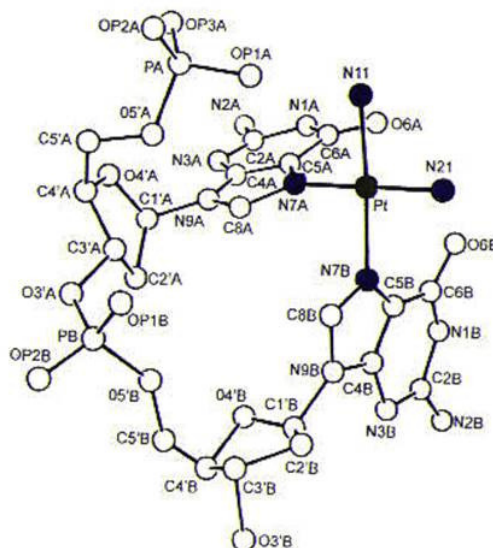
Figure 7. DNA binding of cisplatin [36]

Several drugs in clinical use and clinical trials are members of the group of nucleoside or nucleobase analogues. These substances are built-in into the newly synthesized DNA during replication but are unable to fulfill the function of nucleotides. Thus, these antimetabolites such as 5-fluorouracil, which is another frequently used chemotherapeutic, also cause lesions in the DNA which force the cell into apoptosis if not repaired in time [37]. Another mechanism to interact with DNA is the intercalation of planar structures between base pairs which also hinders replication and transcription and has been demonstrated for the anti-neoplastic drugs doxorubicin and mitomycin c [33].

1.6.2. *Transferrin mediated drug delivery*

Transferrin (Tf) is an iron transport protein in the human blood. It is a single chain, 80 kDa glycoprotein containing two iron binding sites that specifically bind Fe^{3+}. Diferric Tf, which is called holo-Tf, binds to the cell surface bound transferrin receptor (TfR) and the Tf/TfR complex is internalized to a clathrin-coated endosome. The clathrin coat gets lost during maturation of the endosome, and the pH becomes acidic by a proton pump based mechanism. The lower pH causes the release of iron which is transported into the plasma by divalent metal transporter (DMT1) and is there bound as Fe^{2+} to ferritin as storage iron or linked to heme, thus participating in oxygen transport.

The iron-free Tf/TfR complex is recycled on the cell surface and both proteins are re-used in the circulation (Figure 8) [38, 39].
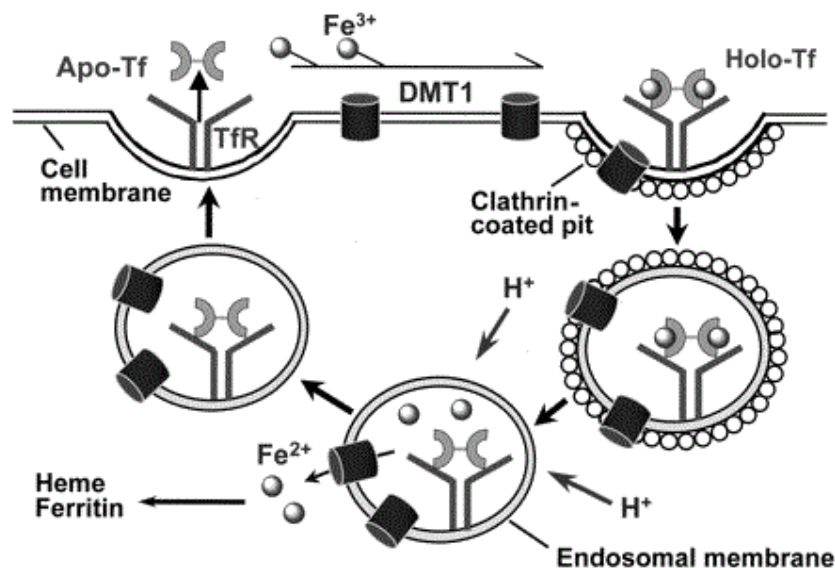
Figure 8. Iron uptake *via* the transferrin/transferrin receptor pathway [38]

Cancer cells have a high demand of iron, probably due to their enhanced proliferation and neoangiogenetic activities. This requirement is fulfilled by overexpression of TfR [40, 41]. Therefore the TfR is a plausible target in cancer cells while normal cells remain less affected. Additionally the transferrin saturation in the human blood is only about 30%, leaving a majority of the iron binding sites available for metal binding [39]. Because of the chemical similarities of iron to Ru^{3+} and Ga^{3+}, anticancer drugs based on these metals are supposed to be incorporated *via* this receptor-mediated pathway.

For the investigational anticancer drug indazolium *trans*-[tetrachlorobis(1*H*-indazole)ruthenate(III)], also known as KP1019, the protein binding has been shown and seems to be important for its mechanism of action [42]. Furthermore, it was demonstrated that titanium-based chemotherapeutics exploit the TfR system to reach cancer cells. Ti_2-Tf can block the TfR, thereby inhibiting iron supply of cancer cells whereas Ti^{4+} is transported into the cancer cells *via* TfR and exhibits its antitumor activity by DNA targeting [43]. Another utilization of the Tf/TfR system is to deliver drugs through the blood-brain barrier by receptor-mediated transcytosis of brain capillary endothelial cells [44].

1.6.3. Reactive oxygen species

Reactive oxygen species (ROS) are generated in every cell mainly by mitochondria during respiration (Figure 9) and contribute to important functions in cell signaling, metabolism, proliferation, differentiation and defense mechanisms. The most important ones of this species are the superoxide radical $O_2\bullet^-$, the hydroxyl radical $OH\bullet$ and hydrogen peroxide H_2O_2 [45]. ROS production is tightly controlled by regulation of the enzymes involved, the unstable nature of the species themselves and various antioxidative agents such as glutathione, ascorbate and thioredoxin reductase [45, 46]. The balance of oxidants and antioxidants is of great importance and imbalances lead to severe diseases such as Morbus Alzheimer, Morbus Parkinson and various types of cancer [47].

During the process of cancer development ROS are playing a crucial role. These species interact with biomolecules and as a result impair their functions. The interaction of ROS with DNA leads to different modifications in nucleobases such as formation of 8-hydoxyguanin and 5-hydoxyuracil. If these oxidized base lesions in the DNA are not repaired by NER or BER, the mutated cell proliferates and may eventually become malignant. In many tumors elevated levels of oxidative DNA lesions have been found, reinforcing the role of ROS [47]. Furthermore ROS can modify proteins, thereby affecting their function. The main target of ROS is the thiol group of cysteine. Oxidative reactions cause changes in the polypeptide conformation and cause formation of S-S disulfide bridges which alter the protein topology [46]. Such modifications can lead to constant activation of transcription factors and are jointly responsible for tumor progression [48].

Besides their role as cancer promoting agents, ROS may be utilized for chemotherapeutic strategies. Due to impairments in their redox homeostasis cancer cells may be selectively eliminated by targeting the redox system [49].

The ability of transition metals to participate in redox reactions plays a crucial role in ROS-dependent anticancer treatment. Interactions in the oxidation/reduction mechanisms were shown for a variety of metal-based antineoplastic compounds such as complexes with platinum, gold and arsenic [50]. Furthermore ROS are also generated by the ruthenium complex KP1019 and contribute to its cytotoxic activity [51].

The mode of action of this class of antitumor metal-based complexes is either based on direct enhancement of ROS levels or on inhibition of the antioxidant defense mechanisms in the cell, *e.g.* thioredoxin reductase. The elevated ROS levels induce protein oxidation, lipid peroxidation, DNA damage and mitochondrial membrane depolarization and as a consequence lead to apoptosis [45].
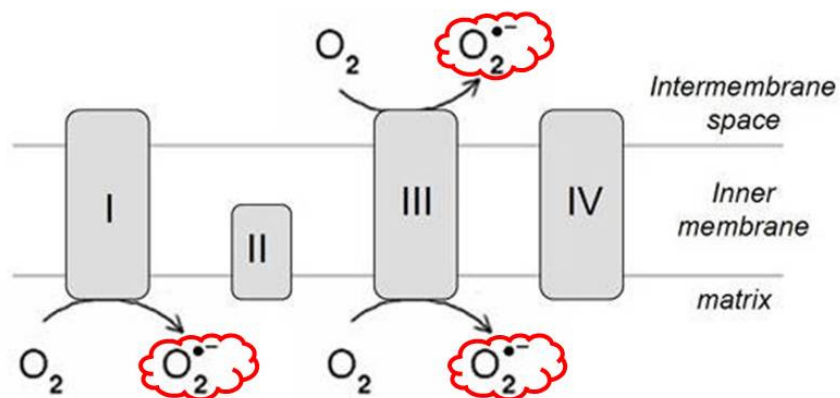
Figure 9. ROS production in the mitochondrial membrane as a consequence of the respiratory chain.

Complex I: NADH Dehydrogenase, Complex II: Succinate Dehydrogenase

Complex III: Cytochrome c Reductase, Complex IV: Cytochrome c Oxidase [52]

1.6.4. Mitochondria

Mitochondria are responsible for generating ATP, the energy unit in cells which is required for all cellular processes such as respiration, metabolism and biosynthesis. It was also found that mitochondria contribute to apoptosis which is not initiated by outer signals. The process is based on cytochrome c, a small protein between the outer and the inner membrane of the mitochondria exerting oxidative phosphorylation.

As a response to apoptotic signals and interaction with the proteins of the Bcl-2 family, the outer membrane becomes depolarized and cytochrome c is released into the cytosol where it triggers apoptosis [1].

The loss of function of the mitochondrial membrane and the associated liberation of soluble intermembrane proteins provokes bioenergetic imbalances, impairments in redox homeostasis as well as ion homeostasis and as a consequence initiates programmed cell death [53].

The ability to induce apoptosis by a caspase- and p53-independent way and the fact that during carcinogenesis several genes that contribute to mitochondrial functions such as Bcl-2 and Bax are altered constitute an interesting target in anticancer treatment. Various drugs that are able to disrupt the mitochondrial membrane potential and cause apoptosis, *e.g.* arsenite and lonidamine [53], are in clinical trials phase II and phase III. Moreover, the investigational anticancer complex KP1019 interacts with mitochondria, even though the relevance for cytotoxic activity has not yet been fully investigated [54].

1.6.5. *Ribonucleotide reductase inhibition*

Ribonucleotide reductase (RNR) is the enzyme converting ribonucleotide diphosphates to desoxyribonucleotide diphosphates which are required for DNA synthesis and DNA repair. Because RNR is the rate limiting factor in DNA synthesis this enzyme is essential in the cell cycle. Therefore it has been linked to cancer development and progression and represents an attractive target in anticancer therapy [55]. Various RNR inhibitors already showed activity in some tumors, *e.g.* non-small cell lung cancer, pancreatic cancer, bladder cancer and leukemias [56]. Currently one of the most promising RNR inhibitors is triapine (3-aminopyridine-2-carboxaldehyde thiosemicarbazone). It is an α-N-heterocyclic thiosemicarbazone and was already studied in a phase I and phase II clinical trial which showed promising results for the drug alone or in combination with other antineoplastic drugs [57, 58].

1.7. Metal complexes in cancer therapy

Metal based therapeutics have been used in a wide panel of diseases, such as lithium for the treatment of depression since 1952 and arsenic to treat syphilis since 1910, but it was not until 1969 that metal-based drugs were introduced to the field of antitumor therapy due to a serendipitous discovery of Barnett Rosenberg that showed cytostatic activity for platinum. Since then they have been well established and are part of at least 50% of chemotherapies nowadays.

1.7.1. *Platinum compounds*

After Barnett Rosenberg's discovery that *cis*-diamminedichloroplatinum(II) (cisplatin, cddp, Figure 10) exerts antiproliferative activity [59, 60] it was successfully introduced into the clinic in 1978 and achieved promising results in some cancers. While the cure rate for patients suffering from testicular cancer reached 80% [61] and other cancers such as ovarian malignancies, tumors of the head and neck as well as bladder, cervix and lung respond well to cisplatin treatment [62], a variety of cancers remained untreatable with this drug.

Besides the limited range of activity the occurrence of severe side effects such as nephrotoxocity, neurotoxicity, nausea, vomiting and ototoxicity [63] and the problem of resistance to the drug encouraged development of further platinum-based therapeutics. The goal was to find drugs with a similar effectiveness as that of cisplatin but with a higher tolerability, fewer side effects and the potential to overcome cisplatin resistance. In cisplatin-based cancer treatment two forms of resistance are possible: acquired resistance which develops in patients during chemotherapy and intrinsic resistance which leaves tumors in some patients totally unaffected by the drug right from the start.

Resistance is based on various mechanisms: decreased drug accumulation which can be caused by both, decreased influx and increased active efflux [64-66], increased cellular thiol levels leading to cytosolic inactivation of the drug mainly by binding to glutathione [66-69] and the removal of cytotoxic DNA lesions by repair machineries as well as alterations in the cisplatin-DNA adduct recognition by mismatch repair and HMG proteins [35, 62, 66, 70].

Out of many attempts for improved platinum anticancer drugs only two complexes succeeded for clinical application, namely *cis*-diammine(cyclobutane-1,1-dicarboxylato-O,O')platinum(II), also known as carboplatin, and (*trans*-L-diaminocyclohexane)oxalatoplatinum(II), commonly referred to as oxaliplatin (Figure 10). Whereas carboplatin is an improvement due to its lower cytotoxicity and the possibility to be administered in higher doses, it shows active potential only in the same panel of malignancies. Oxaliplatin exerts activity also in cisplatin-resistant tumors [71].
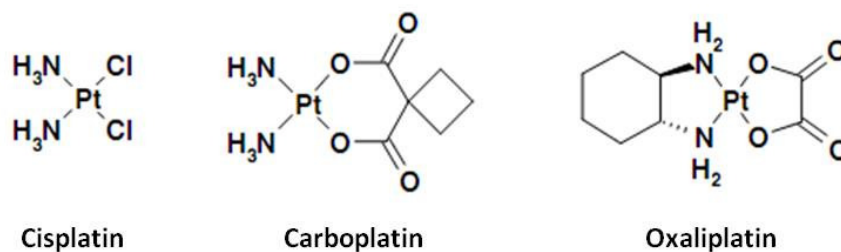
Figure 10. Chemical structures of the three platinum compounds that are used in the clinic worldwide

The main mode of action of the clinically used platinum compounds is interaction with DNA after formation of the active species by aquation and hydrolysis. These complexes are able to form DNA crosslinks causing distortion and structural damage of the DNA and thus inhibiting replication and transcription processes. The prevalent adducts induced by cisplatin are 1,2-intrastrand crosslinks, more precisely *cis*-GG adducts (47-50%) and *cis*-AG adducts (23-28%). Additionally 1,3 intrastrand crosslinks (*cis*-GXG) (8-10%) and monofunctional adducts (2-3%) are formed whereas interstrand crosslinks and intermolecular interactions such as DNA-protein crosslinks occur only rarely (Figure 11). Platinum binds to the N7 atom of purine bases in all cases of crosslinks [35, 72].

Adduct formation through carboplatin does not differ in the products but proceeds with slower kinetics [73], while oxaliplatin shows reduced adduct formation compared to cisplatin and adducts differ by the presence of the diaminocyclohexane ligand [74-76].
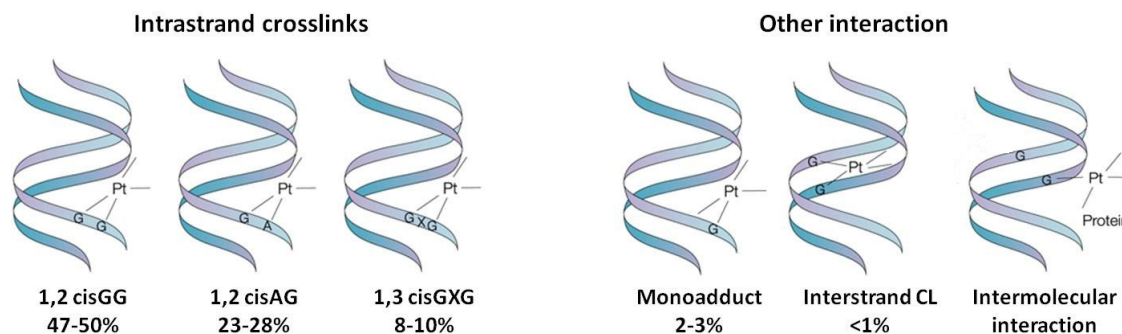
Figure 11. DNA adduct formation of cisplatin [77]

The success of the *cis*-configured isomers and the lack of activity of the transplatin and other *trans*-configured platinum complexes raised the idea of a structure-activity relationship that demanded *cis* configured, planar, uncharged complexes for antitumor potential [78, 79]. However, soon it turned out that these first rules have exceptions and more and more compounds clashing these assumptions were proven active. Besides polynuclear platinum compounds which can form different DNA adducts and therefore offer the possibility to overcome cisplatin resistance [80-82] and active platinum(IV) complexes that are suitable for oral administration and hence bear the hope to make chemotherapy more convenient for the patients [83-85], cytotoxic *trans*-platinum complexes became particularly interesting.

Different classes of *trans*-platinum complexes showed higher cytotoxicity than their *cis*-configured analogues and showed activity comparable to cisplatin. Among these are complexes with pyridine-like ligands [86-88], with iminoether ligands [89-92], with aliphatic amines [93, 94], with nonplanar heterocyclic ligands *e.g.* piperidin [95, 96], and acetoxime containing complexes [97, 98]. This class of non-classical platinum complexes is promising due to its different DNA binding behavior, varying protein interaction and enhanced accumulation in cells [79, 99, 100], and might be able to overcome the problem of cisplatin resistance because of a different mode of action.

1.7.2. Ruthenium compounds

The limitations of platinum-based anticancer therapy such as severe side effects and resistance soon led to investigations of antineoplastic drugs based on different metals. Besides gallium, titanium, rhodium and iron, ruthenium drew special attention. Because of the chemical similarities between ruthenium and iron, such as physiologically accessible redox potentials and the protein binding behavior it is hypothesized that the iron uptake mechanism *via* transferrin (Tf) and the transferrin receptor (TfR), which is overexpressed in most cancer cells, can be exploited for cancer cell specific delivery of the drug [42].

Out of many synthesized complexes only two entered clinical trials and proved successful in phase I, namely imidazolium *trans*-[tetrachloro-*S*-dimethylsulfoxideimidazole-ruthenate(III)] [39] [101], NAMI-A, and indazolium *trans*-[tetrachlorobis(1*H*-indazole)ruthenate(III)], also known as KP1019 (Figure 12).

NAMI-A   **KP1019**
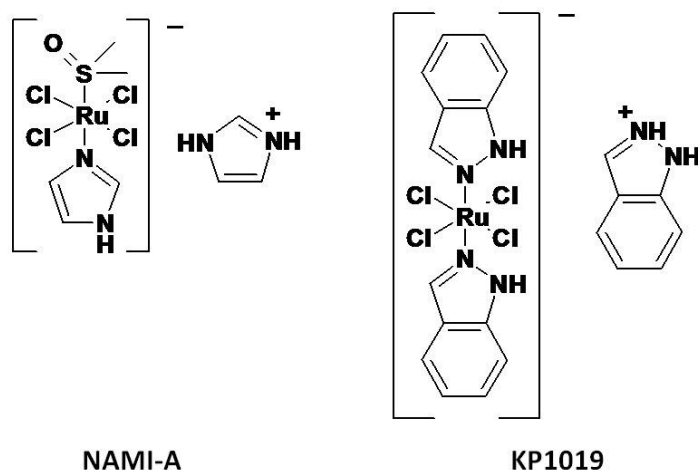
Figure 12. Chemical structures of the two ruthenium complexes in clinical trials

After showing high cytotoxicity in preclinical tests in colon carcinoma, KP1019 also revealed anticancer activity in a phase I clinical study and led to stable disease in some patients. It showed only mild toxicity which was not dose limiting and was well tolerated by the patients [102]. For further clinical development the sodium salt of KP1019, sodium *trans*-[tetrachlorobis(1*H*-indazole)ruthenate(III)], KP1339, was chosen due to its better solubility and has entered a phase I/IIa study in 2009 which is still in progress.

The mechanism of action of this drug so far is not completely clarified: following intravenous administration KP1019 undergoes hydrolysis and reacts with serum proteins such as Tf, which is believed to deliver the drug into the cell *via* the TfR. Once inside the cell the ruthenium(III) prodrug is reduced to the active Ru(II) species, and the acidic environment in solid tumors is supposed to favor this mechanism [103]. The active species then interact with biomolecules so far interaction with proteins and DNA have been demonstrated, but it is still uncertain whether there is a single critical target that is crucial for the cytotoxic effect [42, 104].

NAMI-A (new antitumor metastasis inhibitor – A) is the first of a series of ruthenium compounds synthesized for selective toxicity to tumor cells based on the activation by reduction hypothesis in hypoxic tumor environment. Unexpectedly it showed no activity in primary tumors and failed the NCI screening in a panel of 60 cancer cell lines but proved very effective against metastasis and therefore successfully finalized a phase I clinical trial [105].

The antimetastatic potential is based on the ability of NAMI-A to inhibit angiogenesis induced by the vascular endothelial growth factor and to reduce cell motility and invasiveness through integrin activation [101, 106].

Besides these two auspicious complexes another group of ruthenium compounds, namely Ru-arene complexes with a 1,3,5-triaza-7-phospha-adamantane (pta) ligand, called RAPTA complexes, were synthesized recently and similarly to NAMI-A inhibit metastasis while being only poorly active against primary tumors and non-toxic to healthy cells which makes them very interesting for further development [106].

1.7.3. *Other metal-based anti cancer compounds*

1.7.3.1. Gallium

Due to similarities of iron (Fe^{3+}) and gallium (Ga^{3+}) in size and charge, gallium is of great interest in drug development. Gallium is competing with iron for enzyme binding sites, *e.g.* ribonucleotide reductase is inactivated when gallium binds because of its lack of redox activity under physiological conditions [107]. Gallium nitrate has shown activity in malignant lymphomas and bladder cancer [108, 109], but as many other chemotherapeutics it has to be administered intravenously which is uncomfortable for the patients.
To improve their quality of life, orally applicable drugs were the goal of research. The complex tris(8-quinolinolato)gallium(III), known as KP46, meets this demand and entered clinical phase I trials in 2004 where it showed promising activity in renal cell cancer. *In vitro*, KP46 is especially active in melanoma cells [110].

1.7.3.2. Osmium

Several osmium(IV) complex salts and osmium(III) coordination compounds were shown to exert cytotoxic activity in cancer cells [111, 112]. Because of the similarities in oxidation states of osmium and ruthenium, a variety of osmium compounds were synthesized utilizing the same ligands as antiproliferative ruthenium complexes. Osmium NAMI-A analogues showed high cytotoxicity *in vitro* while not being hydrolyzed and staying stable in aqueous solution [113].

1.7.3.3. <u>Titanium</u>

After cisplatin, two titanium-based complexes entered clinical evaluation, namely budotitane ([*cis*-diethoxybis(1-phenylbutane-1,3-dionato)titanium(IV)]) and titanocene dichloride (dichloridobis(η^5-cyclopentadienyl)titanium). Even though their high activity against cisplatin-resistant tumors and their low toxicity were promising, they failed clinical evaluation due to formulation problems and insufficient response, respectively [114]. Out of the attempt to overcome these problems, titanocene Y (dichloridobis[(*p*-methoxybenzyl)cyclopentadienyl]titanium(IV)) was synthesized, showing high activity in renal cell, ovarian, non-small cell lung and colon cancer cells *in vitro* [115].

1.7.3.4. <u>Iron</u>

Several examples of iron compounds show promising antiproliferative potential. Among the first to exhibit antitumor activity were simple ferricenium salts [116, 117]. The most promising iron compounds are ferrocifens which are derivatives of tamoxifen, a selective estrogen receptor antagonist. Those substances are active against estrogen-dependent as well as estrogen-independent breast cancer cells [118]. The antiproliferative effect of the tamoxifen-like group is enhanced by the redox behavior of the ferrocene unit [119, 120]

2. Results

This PhD thesis can be divided in work with platinum- and ruthenium-based complexes and is based on the following publications and manuscripts.

Platinum:

Cellular accumulation and DNA interaction studies of active *trans*-platinum anticancer compounds

Bartel C., Bytzek A.K., Scaffidi-Domianello Y.Y., Grabmann G., Hartinger C.G., Jakupec M.A., Galanski M., Keppler B.K.

Journal of Biological Inorganic Chemistry, submitted September 14th 2011

A group of novel active *trans*-platinum oxime complexes was investigated with regard to their cellular accumulation and DNA interaction characteristics, and differences to the clinically used cisplatin and its inactive counterpart transplatin were shown.

I conducted accumulation experiments as well as DNA interaction studies both *in vitro* and in cell-free tests by means of the Comet Assay, analysis of DNA metalation and the electrophoretic mobility shift assay. Moreover I prepared the manuscript and wrote the discussion of the data.

Ruthenium:

Influence of ascorbic acid on the activity of the investigational anticancer drug KP1019

Bartel C., Egger A.E., Jakupec M.A., Heffeter P., Galanski M., Berger W., Keppler B.K.

Journal of Biological Inorganic Chemistry, **2011**, online first June 25th

Enhancement of cytotoxicity and DNA interactions of the investigational anticancer complex KP1019 by the reducing agent ascorbic acid were investigated with various cell biological methods and considerations about the mode of action of this drug were drawn.

I performed cytotoxicity tests, DNA interaction studies *in vitro* and in cell free experiments and the DCFH-DA assay. Beside the parts of the manuscript referred to the methods, I participated in writing of the introduction and the discussion of the publication.

Physicochemmical studies and anticancer potency of ruthenium(6η-p-cymene) complexes containing antibacterial quinolones

Kljun J., Kandioller W., Bytzek A.K., Bartel C., Jakupec M.A., Hartinger Ch.G., Keppler B.K., Iztok T.

Organometallics, **2011**, 30(9): 2506-2512

Ruthenium complexes of the antibacterial quinolones nalidixic acid and cinoxacin were synthesized to explore the anticancer potential of organometallic compounds with bioactive ligands. The complexes were characterized and their physicochemical properties were investigated. Moreover the cytotoxic potential was studied in various cancer cell lines.

I determined the *in vitro* anticancer activity of the synthesized complexes, finalized the data and contributed to the discussion and the preparation of the manuscript.

Intracellular protein binding patterns of the anticancer ruthenium drugs KP1019 and KP1339

Heffeter P., Boeck K., Atil B., Hoda M.A.R., Koerner W., Bartel C., Jungwirth U., Keppler B.K., Micksche M., Berger W

Journal of Biological Inorganic Chemistry, **2010**, 15, 737-748.

The intracellular uptake as well as protein binding patterns of KP1019 and its sodium salt 1339 which is currently in a clinical trial phase I/IIa study were investigated and compared to clinically used cisplatin. The distribution of ruthenium in the cytosolic and nucleic fraction was analyzed and the differences compared to cisplatin were pointed out.

I performed uptake experiments under a variety of experimental conditions and participated in the discussion and interpretation of the results.

Maltol-derived ruthenium-cymene complexes with tumor inhibiting properties: the impact of ligand-metal bond stability on anticancer activity *in vitro*

Kandioller W., Hartinger C.G., Nazarov A.A., Bartel C., Skocic M., Jakupec M.A., Arion V.B., Keppler B.K.

Chemistry – A European Journal, **2009**, 15, 12283-12291

Ruthenium cymene complexes with pyrone and thiopyrone ligands were synthesized and spectroscopically characterized. Furthermore, aquation studies were carried out and the cytotoxic activity was tested in different cancer cell lines.

My contribution to this paper was the performance of the cell biological assays to determine the cytotoxic potential of these complexes. Moreover, I assisted in writing of the manuscript and discussing the obtained data.

From pyrone to thiopyrone ligands-rendering maltol-derived ruthenium(II)-arene complexes that are anticancer active *in vitro*

Kandioller W., Hartinger C.G., Nazarov A.A., Kuznetsov M.L., John R.O., Bartel C., Jakupec M.A., Arion V.B., Keppler B.K.

Organometallics, **2009**, 28, 4249-4251.

Maltol-derived ruthenium(II)-arene complexes with thiopyrone ligands were synthesized to enhance the cytotoxic activity compared to the pyrone-bearing counterparts. The cytotoxic potential was evaluated in various cancer cell lines.

To contribute to this publication I conducted the cytotoxicity assays in various cancer cell lines and evaluated the results, additionally I took part in discussing the data and preparing the manuscript.

Synthesis, x-ray diffraction structure, spectroscopic properties and antiproliferative activity of a novel ruthenium complex with constitutional similarity to cisplatin

Grguric-Sipka S., Stepanenko I.N., Lazic J.M., Bartel C., Jakupec M.A., Arion V.B., Keppler B.K.

Dalton Transaction, **2009**, 17, 3334-3339.

Two novel ruthenium complexes with cymene ligands which are structurally similar to cisplatin were synthesized and characterized by x-ray crystallography and ^{1}H NMR spectroscopy. Furthermore the antiproliferative activity was tested in different cancer cell lines and a time dependence was investigated in the colon cancer cell line SW480.

I contributed to the paper by conduction of the cell biological experiments, discussion of the data and assistance to the manuscript.

2.1. Cellular accumulation and DNA interaction studies of active *trans*-platinum anticancer compounds

Bartel C.[a], Bytzek A.K.[a], Scaffidi-Domianello Y.Yu.[a], Grabmann G.[a], Hartinger C.G.[a,b], Jakupec M.A.[a,b], Galanski M.[a,b], Keppler B.K.[a,b]

[a] Institute of Inorganic Chemistry, University of Vienna, Waehringer Strasse 42, 1090 Vienna, Austria
[b] Research Platform ''Translational Cancer Therapy Research'', University of Vienna, Waehringer Strasse 42

Cellular accumulation and DNA interaction studies of active *trans*-platinum anticancer compounds

Caroline Bartel[a], Anna K. Bytzek[a], Yulia Yu. Scaffidi-Domianello[a], Gerlinde Grabmann[a], Michael A. Jakupec[a,b,✉], Christian G. Hartinger[a,b], Markus Galanski[a,b], Bernhard K. Keppler [a,b]

[a]Institute of Inorganic Chemistry, University of Vienna, Waehringer Str. 42, 1090 Vienna, Austria

[b]Research Platform "Translational Cancer Therapy Research", University of Vienna, Waehringer Str. 42, 1090 Vienna, Austria

✉ Corresponding Author: M.A. Jakupec, Fax: +43142779526, michael.jakupec@univie.ac.at

Abbreviations

AG   adenine-cisplatin-guanine DNA adduct

cddp   (*SP*-4-2)-diamminedichloridoplatinum(II), cisplatin

CZE   capillary zone electrophoresis

dGMP   deoxyguanosine monophosphate

D-PBS   Dulbecco's phosphate-buffered saline

EMSA   electrophoretic mobility shift assay

EtBr   ethidium bromide

FCS   fetal bovine serum

GG   guanine-cisplatin-guanine DNA adduct

ICP-MS   inductively coupled plasma mass spectrometry

MEM   Eagle's minimum essential medium

oc   open circular

sc   super-coiled

TBS   tris-buffered saline

tddp   (*SP*-4-1)-diamminedichloridoplatinum(II), transplatin

Abstract

40 years after the discovery of the anticancer effects of cisplatin, scientists are still pursuing the development of platinum complexes with improved properties regarding side effects and resistance, which are two main problems in cisplatin treatment. Among these compounds, *trans*-configured platinum complexes with oxime ligands emerged as a new class with distinct features to established anticancer agents, including different DNA binding behavior, increased cellular accumulation and different pattern of protein interaction. We report herein on the reactivity with biomolecules of three novel pairs of *cis*- and *trans*-configured 2-propanone oxime platinum(II) complexes and one pair of 3-pentanone oxime platinum(II) complexes. Cellular accumulation experiments and *in vitro* DNA platination studies were performed and platinum contents were determined with ICP-MS. The *trans*-configured complexes were accumulated in SW480 cells in up to 100 times higher amounts than cisplatin and up to 50 times higher amounts than their *cis*-configured counterparts; r_b values (platinum atoms per nucleotide) in cells treated with *trans*-complexes were more than 10-fold increased compared to cells treated with cisplatin. The interaction of the complexes with DNA was studied in cell-free experiments with plasmid DNA (pUC19), in capillary zone electrophoresis (CZE) with the DNA model dGMP as well as in *in vitro* experiments showing the degree of DNA damage in the Comet Assay. Whereas incubation with *cis*-compounds did not induce degradation of DNA, the *trans*-complexes led to pronounced strand cleavage.

Introduction

Cisplatin (cddp) was introduced into clinical development in the 1970s, after the discovery of its antiproliferative effects by Rosenberg in 1965 [1]. The success of cddp, especially against testicular cancer, led to the development of various analogous platinum complexes with the aim to obtain compounds which are more active in a broader spectrum of cancers and cause less adverse effects. However, only two complexes were successfully approved for clinical use, *viz.*, *cis*-diammine(cyclobutane-1,1-dicarboxylato-O,O')platinum(II) (carboplatin) and [(*1R,2R*)-diaminocyclohexane]oxalatoplatinum(II) (oxaliplatin), both *cis*-configured complexes that have been approved in 1989 and 2002, respectively [2, 3]. The anticancer inactivity of transplatin (tddp) and analogous *trans*-configured platinum complexes once led to the assumption that *cis*-configuration is a prerequisite for anticancer activity and several rules for structure-activity relationships were laid down (*e.g.* active complexes were supposed to require *cis*-configured leaving groups and to be neutral; the complexes should not be too labile to avoid toxicity but also not too inert to facilitate binding to DNA; complexes with fewer alkyl substituents in their amine groups are more active) [4, 5].

In recent years, more and more rule-breaking *trans*-platinum complexes with higher cytotoxicity than their *cis*-configured counterparts have been reported with anticancer activity similar to cddp. Anticancer *trans*-platinum(II) complexes are often composed of ligands of the following groups: pyridine-derived ligands, iminoethers, aliphatic amines and non-planar heterocyclic ligands. Beside those compounds, *trans*-platinum(IV) complexes with aliphatic amines as well as dinuclear platinum(II) and platinum(IV) species proved to be active and these and other *trans*-platinum complexes have been reviewed extensively [6-14]. Lately, another group of *trans*-

platinum compounds, namely acetoxime-containing complexes, was reported in which the *trans*-isomer showed higher antiproliferative activity than its *cis*-isomer [15] or led to apoptosis more extensively than its *cis*-configured counterpart [16].

Currently it is widely accepted that the main mode of action of cddp and other *cis*-configured platinum-based drugs is based on their interaction with DNA and the resulting inhibition of transcription. In case of cddp, the most common types of DNA adducts are 1,2-intrastrand crosslinks (GG and AG) that account for about 80% of the products, and approximately 10% 1,3-intrastrand crosslinks, whereas monofunctional binding occurs only in 2-3% of adducts. In contrast, the inactive *trans*-analogue tddp is not able to form 1,2-intrastrand crosslinks but tends to form 1,3-intrastrand as well as interstrand crosslinks [17]. In addition to the binding of cddp to DNA, the recognition of the adduct by high mobility group (HMG) proteins is of importance for the therapeutic success, preserving the DNA lesion from nucleotide excision repair. Deficiencies in this process lead to drug resistance [18]. In contrast to cddp, tddp-DNA conjugates are not recognized by those proteins making the adduct susceptible to repair. Hence, this mechanism together with the different DNA-binding behavior may contribute to the difference in the antitumor potential of those two complexes. Active *trans*-platinum complexes also show interaction with DNA, however the formed products vary depending on the ligand. For example, planar amine ligands favor interstrand crosslinks and also protein-associated strand breaks, iminoether complexes preferably form monofunctional adducts, whereas asymmetric aliphatic amine ligands enable the formation of interstrand crosslinks [13]. While protein-DNA adducts only play a minor role in the mechanism of action of classical platinum drugs, this kind of interaction seems to be more important for the activity of *trans*-platinum complexes, and activity

mimicking topoisomerase inhibitors has been demonstrated [8]. The cytotoxic activity of some *trans*-platinum complexes in cisplatin-resistant cell lines, their cellular accumulation characteristics and their different DNA-binding behavior give reason to think of a different mode of action [5, 13]. Furthermore, enhanced accumulation of some classes of *trans*-platinum species, *e.g.* complexes with iminoether ligands [13], give encouraging results with regard to their ability to accumulate inside the cell and induce less side effects.

Herein we report about the interactions of the *cis*- and *trans*-configured anticancer platinum(II) complexes $[PtX_2(R_2C=NOH)]$ (X = Cl, Br, I; R = Me, Et) (Figure 1) with DNA and DNA models [19]. Furthermore, the compounds were tested in a series of *in vitro* studies on their cellular accumulation and DNA strand cleaving ability, in order to obtain a more detailed picture of the differences between *cis*- and *trans*-complexes at the molecular level.

Materials and methodology

Compounds

Cddp [20], (*SP*-4-2)-[dichloridobis(acetone oxime)platinum(II)] (**1c**) and (*SP*-4-1)-[dichloridobis(acetone oxime) platinum(II)] (**1t**) [15], (*SP*-4-2)-bis(acetone oxime-κN)dibromidoplatinum(II) (**2c**), (*SP*-4-1)-bis(acetone oxime-κN)dibromidoplatinum(II) (**2t**), (*SP*-4-2)-bis(acetone oxime-κN)diiodidoplatinum(II) (**3c**), (*SP*-4-1)-bis(acetone oxime-κN)diiodidoplatinum(II) (**3t**), (*SP*-4-2)-dichloridobis(3-pentanone oxime-κN)platinum(II) (**4c**) and (*SP*-4-1)-dichloridobis(3-pentanone oxime-κN)platinum(II) (**4t**) [19] were synthesized according to literature procedures (for structures, see Figure 1). Tddp was purchased from Sigma Aldrich (Germany). The compounds were freshly dissolved for each experiment.
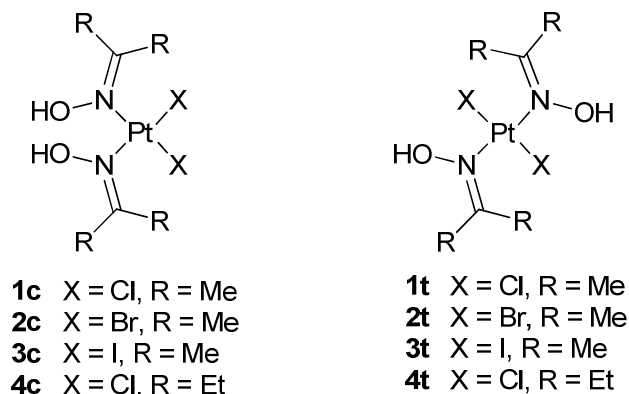
Figure 1. Structures of platinum(II) oxime complexes under investigation.

Cell lines and culture conditions

Human SW480 (colon carcinoma) cells were kindly provided by Dr. Brigitte Marian (Institute of Cancer Research, Department of Medicine I, Medical University of Vienna, Austria). Cells were grown in 75 cm² culture flasks as adherent monolayer cultures in complete culture medium, i.e. Eagle's minimum essential medium (MEM) supplemented with 10% heat-inactivated fetal bovine serum (FCS), 1 mM sodium pyruvate, 4 mM L-glutamine and 1% non-essential amino acids (from 100× stock). Cultures were maintained at 37 °C in a humidified atmosphere containing 5% CO_2. Cells were passaged twice weekly, and all experiments were carried out during the logarithmic growth phase. MEM, D-PBS, sodium pyruvate (100 mM), L-glutamine (200 mM), FCS, non-essential amino acids (100x) and trypsin were obtained from Sigma (Schnelldorf, Germany). 6-well plates, 90 mm culture dishes and 75 cm² culture flasks were purchased from Iwaki/Asahi Technoglass (Gyouda, Japan).

Cellular accumulation

Studies on cellular accumulation of the compounds were performed according to the method described previously [21]. Briefly, SW480 cells were seeded in 6-well plates in densities of 3×10^5 cells per well in aliquots of 2.5 mL complete culture medium (see cell culture conditions). Accumulation experiments and corresponding adsorption/desorption controls were located on the same plate. Plates were kept at 37 °C for 24 h prior to addition of the respective complex. Cells were incubated with compound concentrations of 10 µM and 50 µM, respectively, for 2 h at 37 °C. Afterwards, the medium was removed, cells were washed three times with D-PBS, lysed with 0.5 mL sub-boiled HNO_3 per well for 1 h at room temperature, and platinum (Pt) was quantified by ICP-MS in aliquots of 400 µL diluted to a total volume of 8 mL and internally standardized with 0.5 ppb indium (In). The adsorption/desorption blank was subtracted from the corresponding accumulation sample. Results are based on three independent experiments, each consisting of three replicates.

Metal concentrations were determined by an ICP-MS instrument (Agilent 7500ce, Waldbronn, Germany), equipped with a CETAC ASX-520 autosampler and a MicroMist nebulizer, at a sample uptake rate of approx. 0.25 mL/min. In and Pt standards were obtained from CPI International (Amsterdam, The Netherlands). Standards were prepared in matrices matching the sample matrix with regard to internal standard and concentration of the acid. Nitric acid (p.a.) was purchased from Fluka (Buchs, Switzerland) and further purified in a quartz sub-boiling point distillation unit. All samples and dilutions were prepared with Milli-Q water (18.2 MΩcm). Concentrations were determined by means of the isotopes [115]In and [195]Pt.

DNA platination

SW480 cells were seeded in 90 mm culture dishes and grown in a total volume of 10 mL complete culture medium (see cell culture conditions) at 37 °C. Complexes were dissolved in medium at a concentration of 10 µM. When cells were about 80% confluent the medium was sucked off and replaced by 10 mL of the compound solution (complex dissolved in complete culture medium). Cells were incubated for 24 hours at 37 °C. After exposure, medium was removed, cells were washed with Tris-buffered saline (TBS) and harvested by trypsinization. After centrifugation of the cell suspensions, pellets were resuspended in TBS, and the number of viable cells was determined after trypan blue staining of dead cells. 6 x 10^6 cells were transferred to a 15 mL tube and centrifuged for 2 min. Cells were washed three times by resuspending the pellets in 1 mL TBS and centrifugation at 900 g for 2 min in Eppendorf tubes. The supernatant was discarded, and the cell pellets were resuspended in 500 µL lysis buffer (10 mM Tris-HCl, 1 mM EDTA, 20 µg/mL RNase, 0.2 % Triton X-100, pH 7.4) and incubated for 30 min at 37 °C. The lysate was centrifuged at 10000 g for 8 min. The supernatant was transferred to fresh Eppendorf tubes, 350 µL isopropanol were added, the tubes were centrifuged at 10000 g for 30 min at 4 °C, pellets were washed with ethanol and finally centrifuged again. The pellets were dried in air and dissolved in 200 µL milli-Q water (18.2 MΩ cm) for at least 20 min at 65 °C in a gently shaking thermomixer. In order to minimize the impact of $^{15}N^{16}O$ interference with ^{31}P, aliquots (100 µL) of each DNA solution were analyzed in 2% (w/w) hydrochloric acid in a total volume of 5 mL. Beryllium (Be, 1 ppb) and In (0.5 ppb) were used as internal standards for phosphorus (P) and Pt, respectively, and concentrations were determined by means of the isotopes ^9Be, ^{31}P, ^{115}In and ^{195}Pt. All standards were obtained from CPI International

(Amsterdam, The Netherlands) and prepared in matrices matching the sample matrix with regard to internal standard and concentration of the acid. Hydrochloric acid (p.a.) was purchased from Fluka (Buchs, Switzerland) and was further purified in a quartz sub-boiling point distillation unit. Milli-Q water (18.2 MΩcm) was used for dilutions. As phosphate-containing reagents were strictly avoided, P was measured simultaneously with Pt by ICP-MS (see section cellular uptake) and taken for calculation of r_b values (number of Pt atoms per nucleotide). Results are based on three independent experiments, each consisting of three replicates.

Electrophoretic mobility shift assay

Plasmid pUC19 (2686 bp) was purchased from Bio-Rad Laboratories (Munich, Germany). For every time point of the kinetic studies, 1 µg plasmid DNA was incubated with the complexes in a total volume of 40 µL in 0.1-fold Tris-EDTA (TE) buffer at 37 °C. Incubation time varied from 15 min to 3 h. The concentration of the Pt complexes was 50 µM in all experiments. After incubation, 4 µL loading dye (6x loading dye, Fermentas, Germany) were added to 20 µL aliquot of the sample, and electrophoresis was performed for 90 min at 80 V in a 1% agarose gel (agarose from Sigma, Schnelldorf, Germany) using Tris-Borate-EDTA (TBE) buffer (5x TBE, Eppendorf, Hamburg, Germany). Gels were stained in 0.2 µg/mL ethidium bromide (EtBr) solution (Serva, Heidelberg, Germany), illuminated by UV light and photographed using the gel documentation system GelDoc-It (UVP, Upland, CA, USA).

Comet Assay

The alkaline single cell gel electrophoresis, also known as Comet Assay, was carried out according to a previously described method [22] with some modifications: briefly, SW480 cells were seeded in a density of 4 x 10^5 cells in a total volume of 2.5 mL complete medium (see cell culture conditions) in 6-well plates (CytoOne, Starlab, UK) and allowed to settle for 24 h. Cells were treated with 50 µM methyl methanesulfonate (MMS) as a positive control. Cddp was applied at concentrations between 10 µM and 500 µM, tddp at concentrations of 10 µM and 250 µM and the platinum(II) oxime complexes at 10 µM, all dissolved in medium without the use of additional solvents. Co-incubation of the respective compound (10 µM) and MMS (50 µM) was used to determine an impact of the complex on MMS-induced DNA damage, *e.g.* cross-linking activity. Incubation lasted for 2 h in all cases. Thereafter cells were harvested by trypsin, counted with trypan blue exclusion of dead cells, and 2 x 10^4 viable cells were aliquoted and centrifuged (3 min, 500 g). The cell pellet was suspended in low melting agarose (0.8%) and applied to frosted microscope slides pre-coated with a layer of normal melting agarose (0.5%). After addition of the cover slips, the slides were dried at 4 °C for 10 min. Subsequently the cover slips were removed and the slides were incubated in lysis buffer (89% lysis buffer stock solution: 2.5 mM sodium chloride, 100 mM EDTA, 10 mM Tris, 1% (w/v) N-laurylsarcosyl sodium salt; 1% Triton-X-100, 10% DMSO) for 1 h at 37 °C. After incubation the slides were placed in the electrophoresis chamber and DNA was allowed to unwind for 20 min in electrophoresis buffer (300 mM NaOH, 1 mM EDTA, pH 13.5). After electrophoresis (25 V, 300 mA, 20 min) slides were washed with 0.4 M Tris-HCl, pH 7.5 and each sample was stained with 40 µL ethidium bromide (20 µg/mL). Analysis was done under a fluorescence microscope (Olympus BX40, λ_{ex} ~

550 nm $\lambda_{em} \geq 590$ nm) by use of the Comet Assay IV system (Perceptive Instruments, Suffolk, GB). From each sample 100 individual cells were analyzed; cells were chosen randomly throughout the slide. Experiments were carried out independently at least 3 times. The results were evaluated with respect to the tail intensity (intensity of DNA fluorescence in the comet tail relative to the overall DNA fluorescence intensity in the cell).

dGMP binding studies

For the dGMP-binding experiments, a mixture containing 1 mM of the corresponding complex and disodium 2-deoxyguanosine 5'-monophosphate (dGMP) at a molar ratio of 1 : 2 in 20 mM phosphate buffer containing 4 mM NaCl (pH 7.4) was used. The capillary zone electrophoresis (CZE) experiments were carried out with a G7100A CE system (Agilent, Waldbronn, Germany) equipped with an on-column DAD. Detection was carried out by UV/vis at 200 nm. For all experiments capillaries of 48.5 cm total length (40 cm effective length; 50 μm id) were used (Polymicro Technologies, Phoenix, AZ, USA). Capillary and sample tray were thermostated at 37 °C. The sample injection was carried out by hydrodynamic injection at 50 mbar for 3 s, and the separation voltage was 20 kV. New capillaries were conditioned with 0.1 M HCl, water, 0.1 M NaOH and again with water (10 min each). As a daily routine, the capillary was flushed with 0.1 M NaOH, water, and the background electrolyte for 5 min each before the first run. Before each injection the capillary was purged with 0.1 M NaOH, water and the background electrolyte for 2 min each. Sodium hydroxide solution (0.1 M), hydrochloric acid, sodium dihydrogenphosphate and sodium chloride were obtained from Fluka (Buchs, Switzerland).

Disodium monohydrogenphosphate and disodium 2-deoxyguanosine 5'-monophosphate (dGMP) were purchased from Sigma-Aldrich (Vienna, Austria).

Results

Cellular accumulation

The cellular accumulation of the platinum(II) oxime complexes was compared to cddp and tddp in the inherently cisplatin-resistant cell line SW480 at concentrations of 10 µM and 50 µM. The measured Pt amounts per cell are listed in Table 1. The comparison of cellular accumulation of the *cis*-configured complexes and their *trans*-isomers is depicted in Figure S1 (supporting information).

Even though tddp is less cytotoxic than cddp (IC$_{50}$ values 19 µM *vs.* 3 µM in SW480 cells, respectively [19]) the accumulation inside the cell is slightly higher. The *cis*-complexes **1c**, **2c** and **4c** show cellular accumulation comparable to cddp and tddp, whereas the iodido complex **3c** shows enhanced uptake. The *trans*-configured complexes **1t**, **2t** and **4t** lead to considerably higher accumulation of the metal in the cells. In particular, the cellular amount in cells treated with those complexes is 15 to 50 times higher than if treated with the *cis*-counterparts. In contrast, the accumulation of Pt in cells treated with 50 µM of **3t** was only 4 times higher than in cells treated with 50 µM of its *cis*-analogue **3c** whereas 10 µM of **3t** also caused 20 times higher Pt accumulation than in cells treated with **3c**. Interestingly, incubation with the *cis*-complexes in the 5-fold concentration caused a 4- to 8-fold enhancement of the intracellular Pt amount

whereas the 5-fold increased concentration during incubation with the *trans*-complexes only doubled the intracellular Pt content.

Table 1. Cellular accumulation of cddp, tddp and the complexes under investigation. SW480 cells were incubated for 2 h at 37 °C with 10 µM and 50 µM of the complex. Cellular accumulation is indicated as mean fg/cell ± standard deviation.

	cis-configuration				*trans*- configuration		
compound	IC$_{50}$ [µM]	accumulation [fg/cell]		compound	IC$_{50}$ [µM]	accumulation [fg/cell]	
		10µM	50µM			10µM	50µM
cddp	3.3 ± 0.4	2.8 ± 0.3	12 ± 0.5	tddp	19 ± 3	15.2 ± 2.1	84 ± 6.6
1c	3.4 ± 0.3	3.7 ± 0.9	31 ± 1.6	1t	0.22 ± 0.05	577 ± 73	1278 ± 205.4
2c	45 ± 6	7.8 ± 0.7	39 ± 2.8	2t	2.5 ± 0.4	1051 ± 141	2184 ± 263.5
3c	1.8 ± 0.5	51 ± 11	402 ± 12.3	3t	2.8 ± 0.3	1027 ± 194	1845 ± 170.5
4c	15 ± 1	19.8 ± 4.4	72 ± 7.8	4t	1.9 ± 0.6	392 ± 69	1064 ± 105.6

DNA Platination

The platination of DNA in SW480 cells by the platinum(II) oxime complexes was compared to cddp and tddp. The measured Pt concentrations were referred to P concentrations, and r_b values [Pt/P] are listed in Table S1 (supporting information). The comparison of platination of DNA in

cells treated with the *cis*-configured complexes and their *trans*-configured isomers is depicted in Figure 2.

Complexes **1c**, **2c** and **4c** show platination levels in the range of cddp and tddp, whereas the iodido complex **3c**, in agreement to the enhanced cellular accumulation, shows a higher degree of platination. In sharp contrast, the *trans*-configured complexes **1t**, **2t** and **4t** lead to higher levels of platination in the cells with the amount of Pt bound to DNA being 10-fold elevated compared to their *cis*-counterparts. Again, the iodido complex **3t** deviates, showing only a doubling of the DNA-bound platinum compared to its *cis*-analogue **3c**.
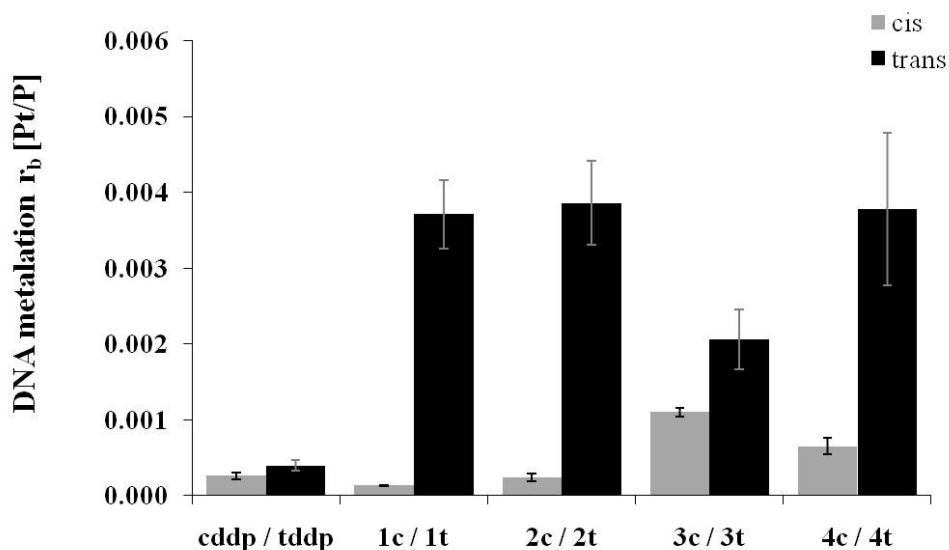

Figure 2. Comparison of intracellular DNA platination after treatment with cddp, tddp and the oxime complexes. SW480 cells were incubated for 24 h at 37 °C with 10 µM of the respective compound.

Electrophoretic mobility shift assay

The impact of the compounds on the secondary structure of DNA was investigated with pUC19 plasmid DNA. Platinum-based anticancer complexes interact with DNA by unwinding, cross-linking or bending DNA, depending on the compound. Therefore, analysis of the alterations on the secondary structure of circular plasmid DNA and the resulting changes in the migration pattern can provide information about the type of adduct formation. Unwinding of the DNA causes a retardation of the fast running band of the super-coiled form (sc) whereas condensation and cross-linking of DNA accelerates the migration of the open circular form (oc). The electrophoretic patterns of plasmid DNA incubated with 50 µM of cddp and the *trans*-configured platinum(II) complexes at various time intervals are shown in Figure 3.

Complexes **1t** and **4t** did not show any impact on the DNA mobility within this time period, whereas the non-chlorido complexes **2t** and **3t** showed retardation of the sc band indicting local unwinding of the plasmid DNA.
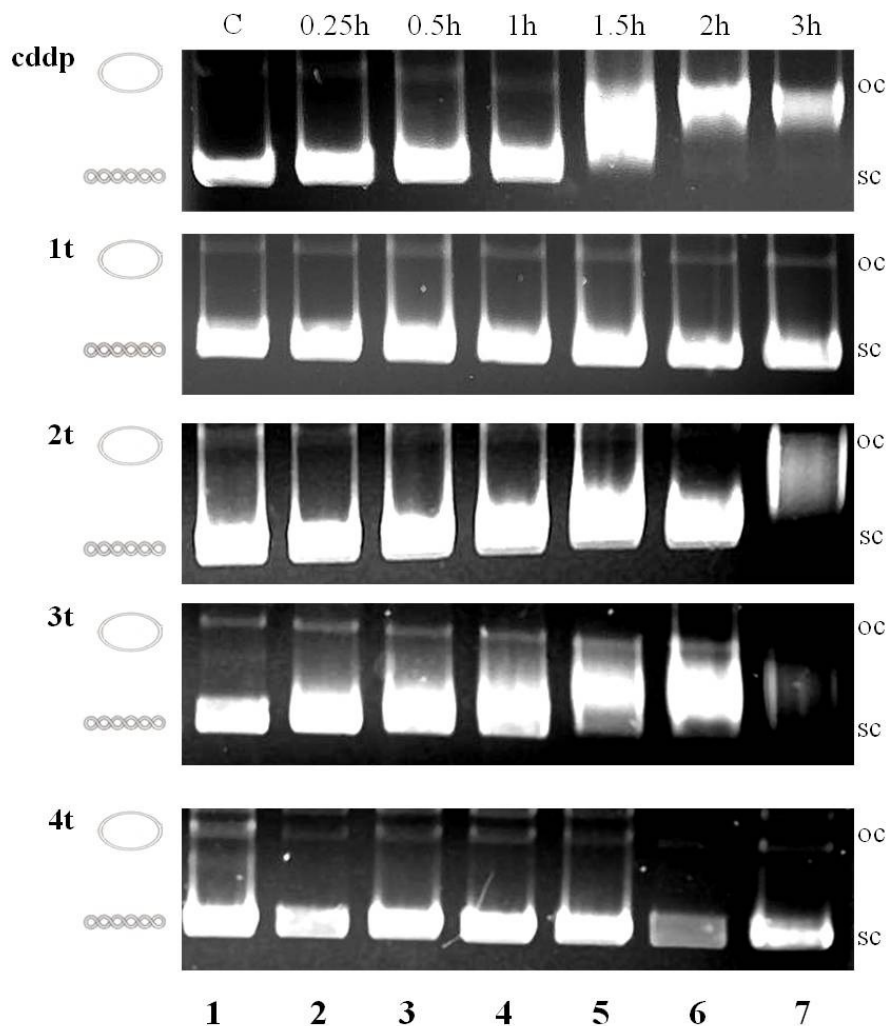
Figure 3. Interaction of cddp and the *trans*-platinum(II) oxime complexes with dsDNA of plasmid pUC19. 1 µg DNA was incubated with 50 µM of the compound for the indicated time period. Electrophoretic separation was performed in a 1% agarose gel, followed by EtBr staining. Lane C (1) indicates untreated control plasmid DNA.

Comet Assay

The potential to damage DNA and the ability to induce cross-links were investigated for the *cis*- and *trans*-configured platinum(II) complexes by means of the comet assay. Whereas strand

breaks directly cause comet formation in comparison to untreated cells, cross-links can be detected by co-incubation of the investigated compound with methyl methanesulfonate (MMS), a substance that is commonly known to induce DNA strand breaks by methylation of *N7-deoxyguanine*. Based on its capability of partially linking the DNA fragments produced by MMS, cddp shows an apparent dose-dependent reduction of MMS-caused DNA damage [23] (Figure S2, supporting information). Tddp also reduces MMS-induced DNA damage at a concentration of 250 µM but with lower extent than cddp (Figure 4).
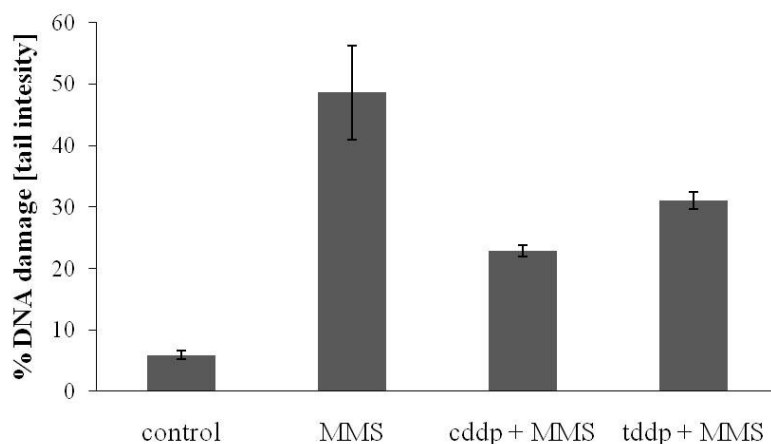
Figure 4. DNA damage of SW480 cells co-incubated with 250 µM cddp and tddp, respectively, and 50 µM MMS for 2 h at 37 °C, in the Comet Assay.

Because of the high cytotoxicity of the investigated *trans*-configured compounds at concentrations of 250 µM, which in the case of cddp and tddp obviously reduced MMS-induced damage without destruction of the cells, the oxime complexes were investigated in lower concentrations. Incubation of SW480 cells with 10 µM of the respective *trans*-complex caused DNA damage to an extent roughly comparable with MMS. Incubation with the *cis*-complexes

showed no influence on the cells in the case of **1c**, **2c** and **4c**. Only **3c** induced DNA damage comparable to MMS and the *trans*-complexes. Co-incubation with MMS led to excessive comet formation, which even made analysis difficult for the *trans*-complexes and **3c**, whereas incubation with **1c**, **2c** and **4c** together with MMS did not alter the comet pattern compared to MMS-only treated cells. Tail intensities are listed in Table 2 and exemplary images of comet formation are displayed in Figure 5.

Table 2. Tail intensities in SW480 cells treated with 10 µM of the respective complex for 2 h at 37 °C (left column) and with co-incubation of 10 µM of the complex and 50 µM MMS (right column).

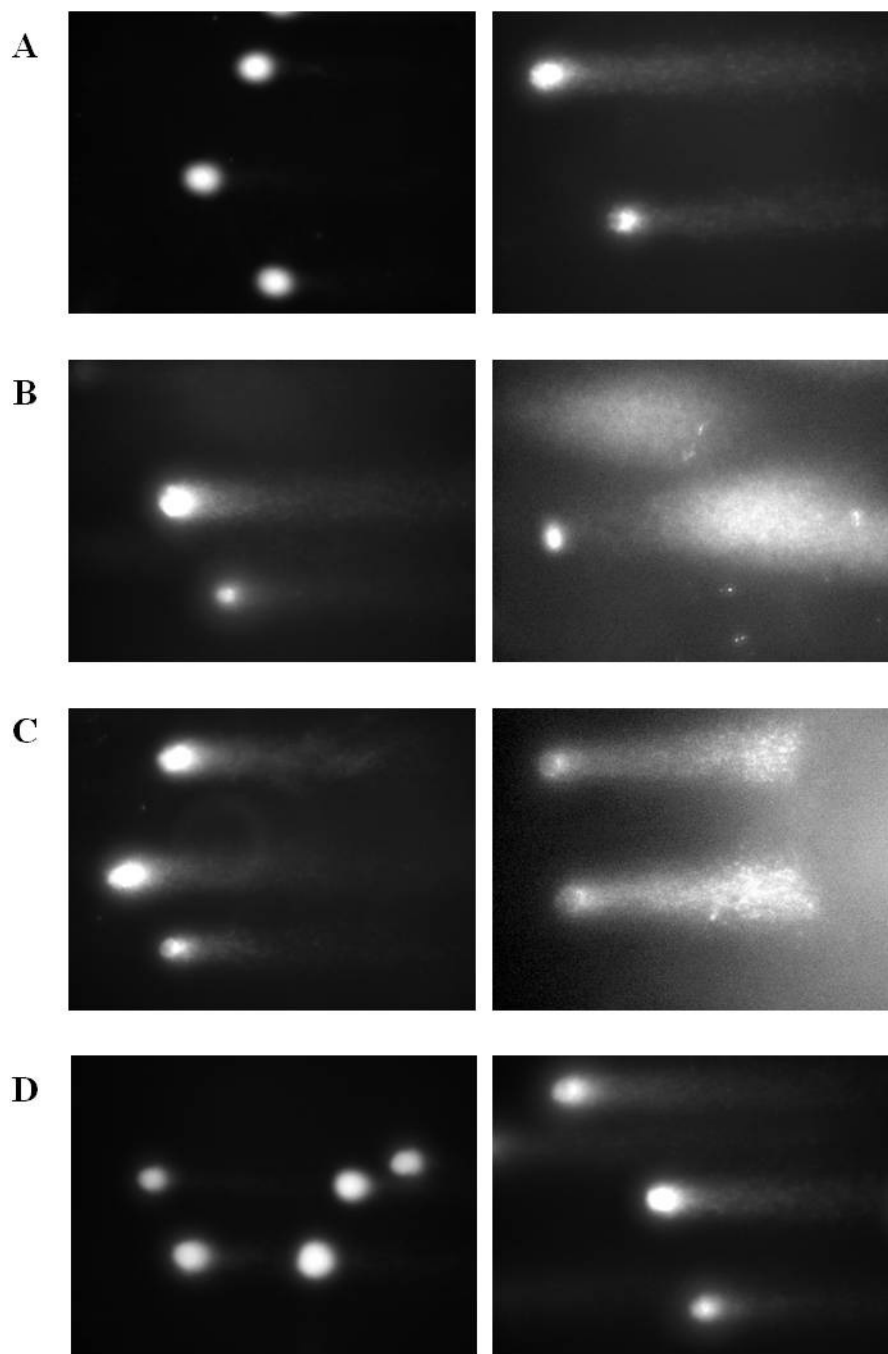| compound 10 µM	tail intensity [%]	compound 10 µM + MMS 50 µM	tail intensity [%]
control	7.3 ± 0.9	MMS	46.0 ± 6.3
1c	8.5 ± 0.3	1c	45.4 ± 2.0
1t	42.1 ± 3.8	1t	87.7 ± 1.3
2c	5.7 ± 0.9	2c	34.3 ± 2.6
2t	38.5 ± 5.5	2t	94.7 ± 1.9
3c	33.3 ± 5.4	3c	86.2 ± 5.1
3t	39.9 ± 4.0	3t	93.6 ± 1.4
4c	7.8 ± 0.9	4c	43.1 ± 1.7
4t	36.3 ± 0.6	4t	86.7 ± 1.5

Figure 5. Comet formation of SW480 cells after 2 h incubation at 37 °C with the respective

complex. The left column shows the compound-only treated cells (10 µM), right pictures depict

cells co-incubated with 10 µM of the complexes and 50 µM MMS. Control (A, left), MMS-only treated cells (A, right), **3t** (B), **3c** (C) and **4c** (D).

dGMP binding studies

The binding of novel anticancer drugs towards nucleotides serves as a model system to indicate the affinity of a compound to DNA. dGMP is of particular interest because the *N7* position has been identified as the primary binding site for cddp and is therefore considered as a possible target for other Pt drugs. The reactivity of the investigated compounds towards dGMP was studied by CZE. In order to simulate physiological conditions, the dGMP binding studies were performed in phosphate buffer containing 4 mM NaCl at pH 7.4. Under these conditions cddp and tddp are neutral, whereas the oxime-containing complexes are negatively charged [24, 25]. The results of the dGMP-binding experiments are summarized in Figure 6. Reactivity decreases in the following order: cddp > tddp > *trans*-configured oximes > *cis*-configured oximes. The comparison of the binding kinetics of cddp and tddp reveals that tddp reacts slightly faster than the *cis*-analog during the first hours of incubation. After approximately 4 h, rate of conversion for tddp decreases compared to cddp, indicating that the binding of a second dGMP to the *cis*-isomer is kinetically favored. Similar observations were already made by other groups [26] and were explained by the faster exchange of the second chlorido ligand in cddp with water because aquation is considered a prerequisite for adduct formation [27, 28]. In contrast, the *trans*-configured oxime complexes are more reactive than their *cis*-configured congeners over the whole incubation time and the amount of the dGMP adducts is higher.
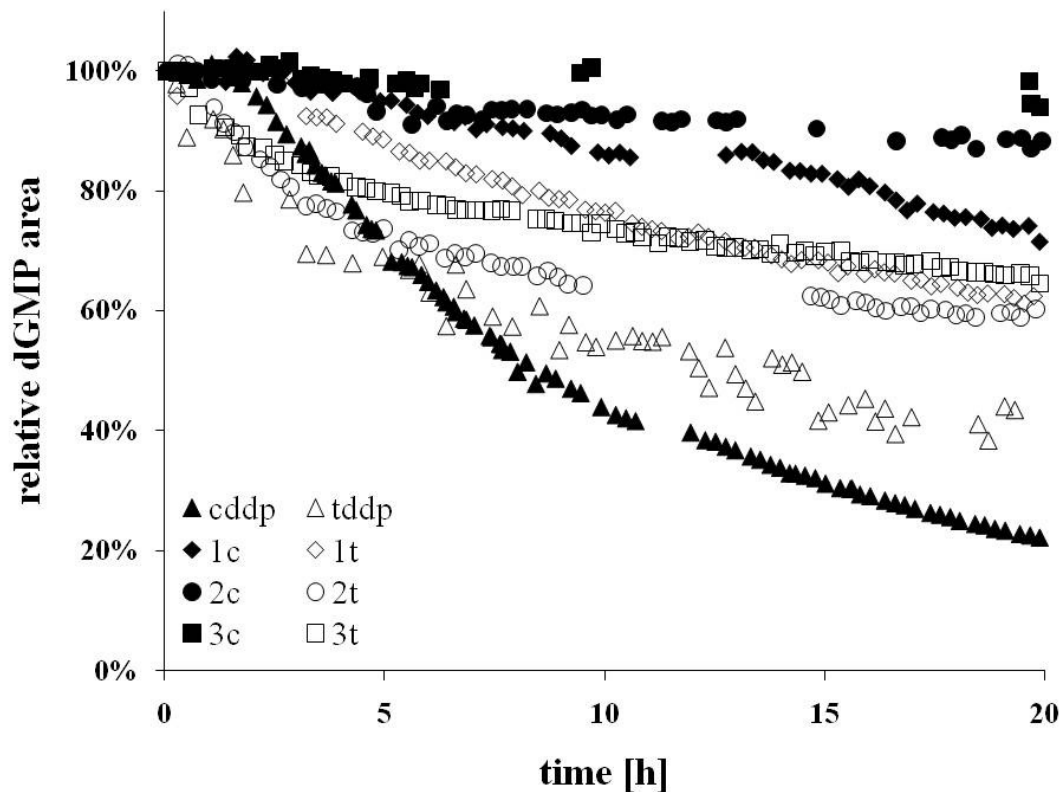
Figure 6. Time courses of the dGMP binding reaction of all studied substances

Discussion

The rule-breaking properties of *trans*-platinum(II) oxime complexes with higher cytotoxicity than the corresponding *cis*-congener and IC_{50} values lower than or comparable to that of cisplatin in the cisplatin-resistant cell line SW480 make them interesting candidates for further studies and in particular to elucidate their mode of action at the molecular level.

One major factor that contributes to the cytotoxicity of metal-based anticancer drugs is the accumulation in the cell. Incubation with two different doses of the *trans*-platinum complexes

1t–**4t** led to much higher accumulation of Pt in the cells in both cases, compared to cddp, tddp and their *cis*-configured counterparts. While the variation of the halogenido ligand did not result in significant differences in cytotoxicity and cellular accumulation of the *trans*-complexes, the *cis*-iodido complex **3c** showed outstandingly high accumulation among the *cis*-isomers. The IC_{50} values of the *trans*-complexes, which are in the same range as those of cisplatin, do not reflect the drastically enhanced cellular accumulation. In accordance with our findings, Halámiková *et al.* also reported strongly enhanced accumulation of a *trans*-platinum(II) amine complex in tumor cells, while the cytotoxicity was still comparable to that of cddp [29]. Furthermore, we found that a five-fold increase of the concentration of the *cis*-complexes led to a four- to eight-fold higher accumulation in cells, while the Pt content in cells treated with the *trans*-isomers only doubled under the same conditions. Those data suggest different uptake mechanisms for the *cis*- and *trans*-isomers.

DNA is considered the main intracellular target of platinum-based anticancer drugs and hence the DNA binding behavior of the oxime compounds was investigated. dGMP binding studies were conducted to analyze adduct formation with the nucleotide deoxyguanosine 5'-monophosphate, with its *N*7 atom being known as the preferred binding partner of cddp. The experiments revealed that the *trans*-complexes interact with GMP initially faster than their *cis*-configured counterparts. Furthermore, the *in vitro* platination of DNA in SW480 cells was studied. Corresponding to the higher accumulation in cells treated with the *trans*-configured complexes, elevated levels of Pt bound to DNA were detected in this *in vitro* setup. DNA platination was up to 15-fold enhanced for the *trans*-complexes compared to cddp and 6–10 times higher than for their *cis*-configured congeners. An exception was **3t**, which led to r_b values

only twice as high as its *cis*-analogue **3c**. While the other *cis*-compounds caused r_b values in the same range as cddp and tddp, DNA binding of **3c** was increased being in line with its enhanced cytotoxicity in SW480 cells and its higher cellular accumulation. According to our findings that the enhanced *in vitro* binding to DNA does not correspond with the cytotoxic activity, Khazanov *et al.* reported that *trans*-platinum(II) piperidine derivates penetrate cells more effectively and bind to DNA to a higher extent than cddp and tddp whereas the complexes show lower cytotoxicity than cddp [30]. Therefore it must be considered that high accumulation and strong affinity to DNA alone are not decisive for cytotoxic potency but that the form of DNA interaction is of great importance. In order to elucidate the nature of DNA interaction single cell electrophoresis assays were conducted (Comet Assay). The ability of cddp to cross-link MMS-damaged DNA has been demonstrated by Pfuhler and Wolf [23] and was confirmed under the applied conditions. In addition, the cross-linking capacity of MMS-induced DNA fragments by tddp was demonstrated which was less pronounced than for cddp. This observation might be explained by different kinds of DNA adducts formed for *cis*- and *trans*-isomers of platinum(II) complexes [17]. These results are consistent with earlier reports of Heringova *et al*. [31] who investigated the cross-linking potential of these drugs on H_2O_2-induced DNA fragments. An apparent reduction of MMS-induced damage by about 50% was achieved by incubation with cddp at a concentration of 250 µM and was therefore chosen as the initial test concentration. While treatment of SW480 cells for 2 h with this high dose of cddp did not affect their microscopic appearance, exposure to the same concentrations of the *trans*-complexes **1t**–**4t** for 2 h drastically reduced their viability. As a consequence the test concentration was reduced for further experiments. Cddp did not cause comet formation even when added at very high

concentrations (500 µM) and treatment with the *cis*-oxime complexes yielded basically the same electrophoretic pattern at the concentration applied (10 µM), with the exception of **3c**. Unlike the other *cis*-complexes, **3c** induced DNA damage comparable to MMS and co-incubation with MMS led to destruction of DNA, with >85% of the DNA found in the comet. The four *trans*-complexes **1t–4t** also caused DNA damage at the applied concentration (10 µM) to an extent comparable to MMS and together with MMS more than 85% of fluorescence intensity was found in the comet, indicating interaction with DNA that leads to strand breaks under alkaline conditions.

The outstanding results of the *cis*-configured iodido complex in all experiments may derive from the different reactions caused by the halogenido ligand. It has been demonstrated by Messori *et al.* [32] that a *cis*-configured iodido platinum(II) complex with isopropylamine ligands showed higher cytotoxic activity in a panel of cancer cell lines than cddp and reacts in a different way with biomolecules, which was suggested to arise from the loss of the amine ligand instead of the iodido moiety. Preliminary hydrolysis experiments reveal differences between the iodido oxime complex and the other *cis*-configured compounds (data not shown) but the reason is not fully understood and requires further studies. While some *trans*-platinum complexes such as *trans*-platinum(II) amine quinolines are able to form intrastrand cross-links, which are the crucial DNA adduct caused by cddp, other groups of compounds such as *trans*-platinum(II) iminoether complexes, which are closely related to the investigated compounds, only show a reduced ability to form DNA intrastrand cross-links. Therefore other kinds of DNA interaction are suggested to contribute to the cytotoxicity of those complexes, and monoadducts are the most likely candidates [33]. It was previously reported that various cytotoxic *trans*-platinum compounds

form monofunctional adducts that are able to bend DNA [34, 35], which can be shown by local untwisting of the sc plasmid DNA. Complexes **2t** and **3t** showed such retardation of the sc band within 3 h incubation, whereas the two chlorido compounds failed to show such a pattern within this time frame. Zorbas-Seifried *et al.* demonstrated reaction of **1t** with pTZ18u DNA within 7 h incubation and assumed monofunctional adducts as a reason [15]. Such monofunctional adducts have been detected for the closely related *trans*-platinum(II) iminoether complexes, and it was shown that those adducts are kinetically stable and are able to inhibit DNA and RNA synthesis [36]. There is further evidence that monofunctional adducts distort DNA and are able to reduce the thermal stability by local unwinding and may therefore also affect the replication and transcription processes [37].

A possible explanation for the observation that enhanced cellular accumulation and higher binding to DNA of the *trans*-platinum(II) oxime complexes do not result in drastically increased cytotoxicity may be involvement of repair mechanisms. While cddp-DNA adducts are recognized by HMG proteins and are thereby shielded against nucleotide excision repair (NER) [38], monofunctional adducts are less likely to be protected. Monofunctional DNA adducts of *e.g.* [PtCl(NH$_3$)$_3$]Cl are not recognized by HMG proteins and are therefore susceptible to repair [37].

Concluding remarks

We investigated four pairs of *cis*-and *trans*-configured platinum(II) oxime complexes with regard to their DNA interaction and compared them to cddp and tddp. We found significant differences in all experiments conducted that suggest a differing mode of action. The most likely

explanation for the influence of the configuration of the complexes is the formation of platinum-DNA monoadducts in case of the *trans*-complexes that contribute to the cytotoxic effect. However, further experiments are required to verify this hypothesis, as are in order to explain non-conventional behavior of the *cis*-iodido platinum(II) acetoxime complex compared to its chlorido and bromido analogues. These observations render the class of complexes with their different behavior compared to cddp interesting candidates for further studies, in order to reveal the chemical basis for the properties observed.

Acknowledgements

References

1.   Rosenberg B, Vancamp L, Krigas T (1965) Nature 205:698-699
2.   Jakupec MA, Galanski M, Keppler BK (2003) Rev Physiol, Biochem. Pharmacol. 146:1-53
3.   Galanski M, Jakupec MA, Keppler BK (2005) Met Compd Cancer Chemother:155-185
4.   Cleare MJ, Hoeschele JD (1973) Plat Met Rev 17:2-13
5.   Hambley TW (1997) Coord Chem Rev 166:181-223
6.   Arandjelovic S, Tesic Z, Radulovic S (2005) Med Chem Rev--Online 2:415-422
7.   Coluccia M, Natile G (2007) Anti-Cancer Agents in Medicinal Chemistry 7:111-123
8.   Farrell N (1996) Metal Ions in Biol Syst 32:603-639
9.   Guo J-x, Sun S-x, Wang H-c (2002) Wuji Huaxue Xuebao 18:125-129

10. Kalinowska-Lis U, Ochocki J, Matlawska-Wasowska K (2008) Coord Chem Rev 252:1328-1345

11. Natile G, Coluccia M (2004) Metal Ions in Biol Syst 42:209-250

12. Natile G, Coluccia M (2001) Coord Chem Rev 216-217:383-410

13. Perez JM, Fuertes MA, Alonso C, Navarro-Ranninger C (2000) Crit Rev Onc Hematol 35:109-120

14. Radulovic S, Tesic Z, Manic S (2002) Curr Med Chem 9:1611-1618

15. Zorbas-Seifried S, Jakupec MA, Kukushkin NV, Groessl M, Hartinger CG, Semenova O, Zorbas H, Kukushkin VY, Keppler BK (2007) Mol Pharmacol 71:357-365

16. Quiroga AG, Cubo L, de Blas E, Aller P, Navarro-Ranninger C (2007) J Inorg Biochem 101:104-110

17. Jamieson ER, Lippard SJ (1999) Chem Rev (Washington, D. C.) 99:2467-2498

18. Heffeter P, Jungwirth U, Jakupec M, Hartinger C, Galanski M, Elbling L, Micksche M, Keppler B, Berger W (2008) Drug Resist Update 11:1-16

19. Scaffidi-Domianello YY, Meelich K, Jakupec MA, Arion VB, Kukushkin VY, Galanski M, Keppler BK (2010) Inorg Chem (Washington, DC, United States) 49:5669-5678

20. Dkhara SC (1970) Indian J Chem 8:193-194

21. Egger AE, Rappel C, Jakupec MA, Hartinger CG, Heffeter P, Keppler BK (2009) J Anal Atom Spectrom 24:51-61

22. Singh NP, McCoy MT, Tice RR, Schneider EL (1988) Exp Cell Res 175:184-191

23. Pfuhler S, Wolf HU (1996) Environ Mol Mutagen 27:196-201

24. Kukushkin VY, Tudela D, Pombeiro AJL (1996) Coord Chem Rev 156:333-362

25. Stetsenko AI, Lipner BS (1974) Zh Obshch Khim 44:2289-2293

26. Zorbas-Seifried S, Jakupec MA, Kukushkin NV, Groessl M, Hartinger CG, Semenova O, Zorbas H, Kukushkin VY, Keppler BK (2007) Mol Pharmacol 71:357-365

27. Lippert B (ed) Cisplatin. Chemistry and Biochemistry of a leading anticancer drug (1999) Wiley-VCH, Weinheim, Germany

28. Zenker A, Galanski M, Bereuter TL, Keppler BK, Lindner W (2000) J Biol Inorg Chem 5:498-504

29. Halamikova A, Heringova P, Kasparkova J, Intini FP, Natile G, Nemirovski A, Gibson D, Brabec V (2008) J Inorg Biochem 102:1077-1089

30. Khazanov E, Barenholz Y, Gibson D, Najajreh Y (2002) J Med Chem 45:5196-5204

31. Heringova P, Woods J, Mackay FS, Kasparkova J, Sadler PJ, Brabec V (2006) J Med Chem 49:7792-7798

32. Messori L, Casini A, Gabbiani C, Michelucci E, Cubo L, Rios-Luci C, Padron JM, Navarro-Ranninger C, Quiroga AG ACS Med Chem Letters 1:381-385

33. Perez JM, Montero EI, Gonzalez AM, Solans X, Font-Bardia M, Fuertes MA, Alonso C, Navarro-Ranninger C (2000) J Med Chem 43:2411-2418

34. Kasparkova J, Novakova O, Farrell N, Brabec V (2003) Biochemistry 42:792-800

35. Novakova O, Kasparkova J, Malina J, Natile G, Brabec V (2003) Nucleic Acids Res 31:6450-6460

36. Coluccia M, Nassi A, Boccarelli A, Giordano D, Cardellicchio N, Locker D, Leng M, Sivo M, Intini FP, Natile G (1999) J Inorg Biochem 77:31-35

37. Bursova V, Kasparkova J, Hofr C, Brabec V (2005) Biophysical Journal 88:1207-1214

38. Galanski M, Jakupec MA, Keppler BK (2005) Curr Med Chem 12:2075-2094

SUPPORTING INFORMATION

Cellular accumulation

The comparison of the cellular accumulation of the *cis-* and *trans*-configured platinum(II) oxime complexes after 2 h incubation with 10 µM (Figure S1, A) and 50 µM (Figure S1, B) of the respective compound show outstanding platinum accumulation in the case of the *trans*-complexes, whereas that of their *cis*-congeners is in the same range as cisplatin and transplatin. The *cis*-iodido complex **3c** also shows higher accumulation, exceeding that of cisplatin by 20 times.
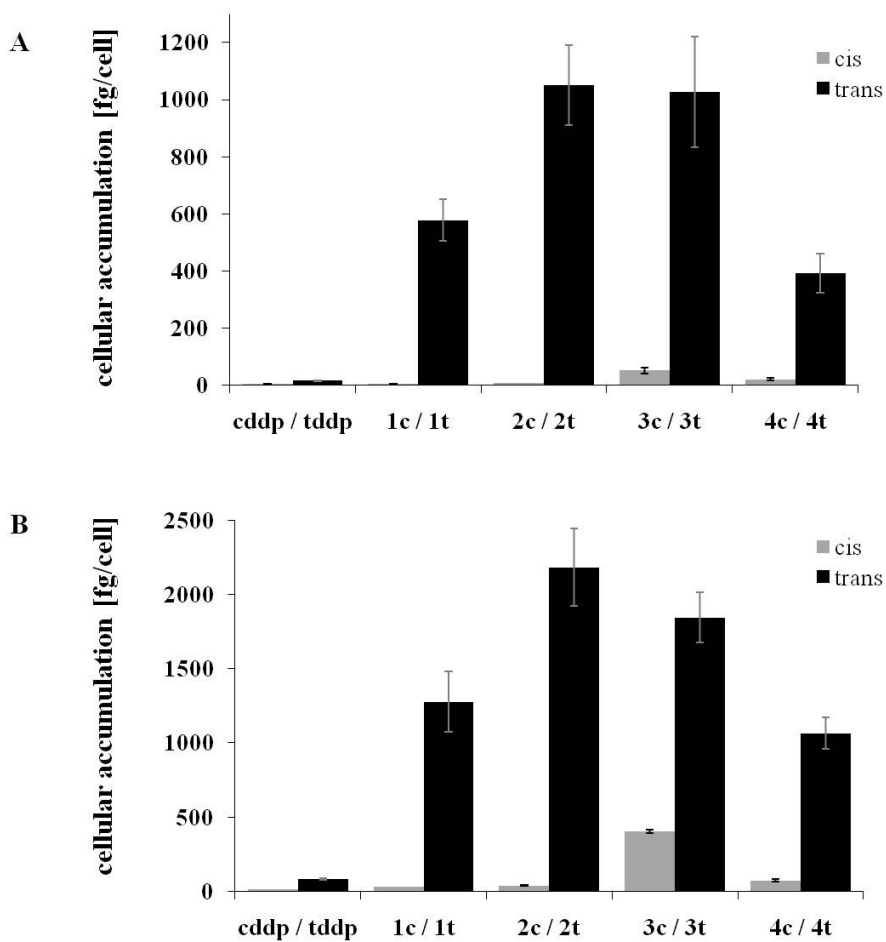
Figure S1. Comparison of cellular platinum accumulation after treatment with cisplatin, transplatin and the complexes under investigation in concentrations of with 10 µM (A) and 50 µM (B)

DNA platination

The r_b values (Pt/P) in DNA isolated from SW480 cells that were treated with the *cis*- and *trans*-configured platinum(II) oxime complexes are listed in Table S1. The *trans*-configured complexes bind to DNA to a considerably higher extent than their *cis*-counterparts. The *cis*-configured iodido complex **3c** induces elevated r_b values compared to the other *cis*-configured complexes, and the DNA binding of the corresponding *trans*-complex is only twice as high. In contrast, the extent of DNA binding of the other *trans*-complexes is 5-25 times higher than that of their corresponding *cis*-isomers.

Table S1. DNA platination induced by cisplatin, transplatin and the complexes under investigation. SW480 cells were incubated for 24 h at 37 °C with 10 µM of the respective compound. The degree of platination is indicated as mean r_b value [Pt/P] ± standard deviation.

cis-configuration		*trans*-configuration	
	r_b [Pt/P] x 10^{-3}		metalation r_b [Pt/P] x 10^{-3}
compound	SW480	compound	SW480
cddp	0.26 ± 0.04	**tddp**	0.40 ± 0.07
1c	0.13 ± 0.01	**1t**	3.71 ± 0.45
2c	0.24 ± 0.05	**2t**	3.86 ± 0.55
3c	1.10 ± 0.06	**3t**	2.06 ± 0.40
4c	0.65 ± 0.10	**4t**	3.78 ± 1.00

Comet Assay

The decrease of MMS-induced DNA damage by cisplatin is based on the cross-linking activity of the compound. We demonstrated a dose-dependent reduction of the MMS-induced tail intensity by cisplatin (Figure S2).
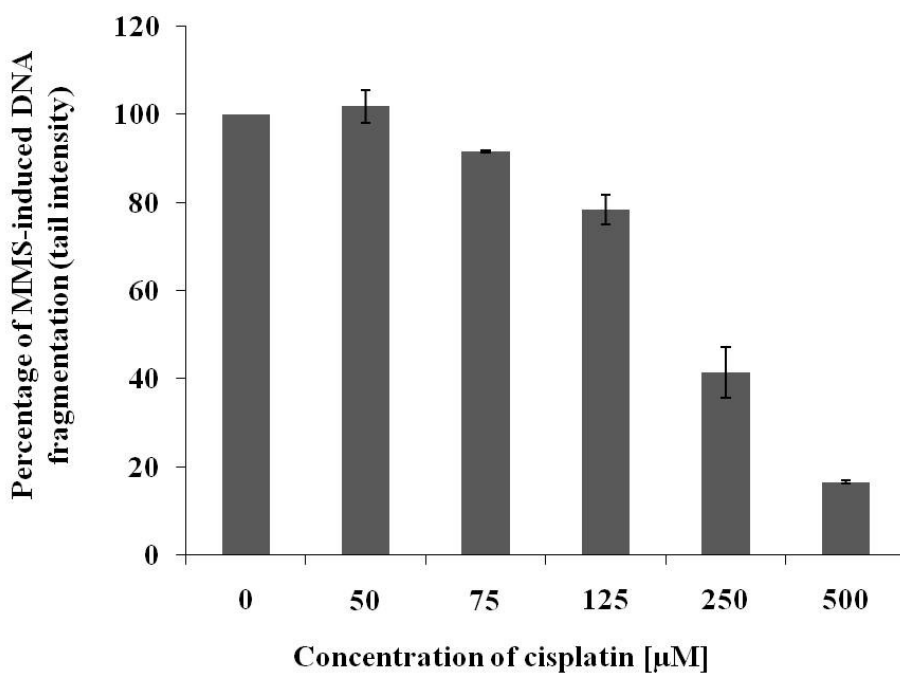
Figure S2. Concentration-dependent decrease of MMS-based DNA fragmentation by cross-linking with cisplatin. SW480 cells were incubated for 2 h at 37 °C with various concentrations of cisplatin.

2.2.   Influence of ascorbic acid on the activity of the investigational anticancer drug KP1019

Bartel C.[a], Egger A.E.[a], Jakupec M.A[a,c]., Heffeter P.[b,c], Galanski M.[a], Berger W[b,c]., Keppler B.K.[a,c]

[a] Institute of Inorganic Chemistry, University of Vienna, Waehringer Strasse 42, 1090 Vienna, Austria

[b] Department of Medicine I, Institute of Cancer Research, Medical University of Vienna, Borschkegasse 8a, 1090 Vienna, Austria

[c] Research Platform ''Translational Cancer Therapy Research'', University of Vienna, Waehringer Strasse 42, & Medical University of Vienna, Borschkegasse 8a, 1090 Vienna, Austria

ORIGINAL PAPER

Influence of ascorbic acid on the activity of the investigational anticancer drug KP1019

**Caroline Bartel · Alexander E. Egger · Michael A. Jakupec ·
Petra Heffeter · Markus Galanski · Walter Berger ·
Bernhard K. Keppler**

Abstract Ascorbic acid has been previously discussed to have antitumor potential through its interaction with transition metal ions such as iron and copper. Furthermore, ascorbic acid may act as a reducing agent for Ru(III) compounds such as indazolium *trans*-[tetrachlorobis(1*H*-indazole)ruthenate(III)] (KP1019), an investigational anticancer drug which is supposed to be activated by reduction, prior to binding to cellular target proteins. Therefore, we investigated the influence of ascorbic acid on the activity of this antitumor metal complex in cell culture studies. We show that co-incubation of equicytotoxic, constant amounts of KP1019 with high concentrations of ascorbic acid (50–700 μM) increases cytotoxicity of the ruthenium anticancer drug in the human colon carcinoma cell line SW480, human cervical carcinoma KB-3-1 cells, and the multidrug-resistant subline KBC-1, whereas addition of low concentrations (2.7–50 μM) has a strong chemoprotective effect in the human colon carcinoma cell line SW480, but not in multidrug-resistant KBC-1 cells. Although cellular uptake of KP1019 is not altered, ascorbic acid induce stronger interaction of the ruthenium compound with DNA both in SW480 cells and under cell-free conditions with plasmid DNA. Even if DNA interactions probably play a subordinate role in vivo given the extensive protein binding of the compound, our data exemplify that ascorbic acid enhances the reactivity of KP1019 with biomolecules. Moreover, we demonstrate that the levels of KP1019-generated reactive oxygen species are markedly decreased by co-incubation with ascorbic acid. Conclusively, our results indicate that application of high doses of ascorbic acid might increase the anticancer effects of KP1019.

Abbreviations

DCFH-DA	$2',7'$-Dichlorodihydrofluorescein diacetate
D-PBS	Dulbecco's phosphate-buffered saline
ICP-MS	Inductively coupled plasma mass spectrometry
KP1019	Indazolium *trans*-[tetrachlorobis-(1*H*-indazole)ruthenate(III)]
MEM	Eagle's minimum essential medium

C. Bartel · A. E. Egger · M. A. Jakupec (✉) · M. Galanski ·
B. K. Keppler
Institute of Inorganic Chemistry,
University of Vienna,
Waehringer Strasse 42,
1090 Vienna, Austria
e-mail: michael.jakupec@univie.ac.at

P. Heffeter · W. Berger
Department of Medicine I,
Institute of Cancer Research,
Medical University of Vienna,
Borschkegasse 8a, 1090 Vienna, Austria

M. A. Jakupec · M. Galanski · B. K. Keppler
Research Platform "Translational Cancer Therapy Research",
University of Vienna,
Waehringer Strasse 42,
1090 Vienna, Austria

P. Heffeter · W. Berger
Research Platform "Translational Cancer Therapy Research",
Medical University of Vienna,
Borschkegasse 8a,
1090 Vienna, Austria

MTT	3-(4,5-Dimethyl-2-thiazolyl)-2,5-diphenyl-2*H*-tetrazolium bromide
NAMI-A	Imidazolium *trans*-[tetrachloro(dimethyl sulfoxide)(1*H*-imidazole)ruthenate(III)]
P-gp	P-glycoprotein
RNS	Reactive nitrogen species
ROS	Reactive oxygen species
TBS	Tris(hydroxymethyl)aminomethane-buffered saline
Tris	Tris(hydroxymethyl)aminomethane

Introduction

Ruthenium is a nonessential transition metal with a versatile coordination chemistry and strong ligand field stabilization, which makes this element attractive for development of pharmacologically active compounds, in particular anticancer drugs [1]. Ruthenium shows various chemical similarities to iron, such as physiologically accessible redox potentials and protein binding behavior. Iron is the most common transition metal in the human body and is essential for many cellular functions, such as oxygen transport, cellular respiration, drug metabolism, and DNA synthesis. Therefore, it is possible that ruthenium interacts with these targets as well, and it seems feasible to use these biological properties for therapeutic strategies. The currently most promising candidates are the two ruthenium(III) complexes imidazolium *trans*-[tetrachloro(dimethyl sulfoxide)(1*H*-imidazole)ruthenate(III)] (NAMI-A) [2, 3] and indazolium *trans*-[tetrachlorobis(1*H*-indazole)ruthenate(III)] (KP1019) [4, 5]. Whereas NAMI-A proved to inhibit the formation of metastases in mouse models [2], KP1019 was recognized as a potent tumor inhibitor in various preclinical models, in particular colorectal carcinomas [4]. Even though the exact mode of action of these compounds is not fully understood, it was suggested that they serve as prodrugs which are activated by reduction. Reduction of ruthenium facilitates ligand exchange and coordination towards biological targets (e.g., proteins) and is therefore assumed to be the first step in the mode of action [6]. Physiological reductants include ascorbic acid, which is the main reducing agent in the blood (12–80 μM) [7], and glutathione, which is the main intracellular reducing agent (0.5–10 mM). The redox potentials of the complex anion of KP1019 and ascorbic acid at pH 7.0 only differ marginally, namely, +0.03 V [8] versus +0.06 V against the hydrogen electrode. Hence, pH and variations in the ratio between oxidized and reduced forms alter the potentials and consequently influence the equilibrium. Lower pH, which is typically found in solid tumor tissue owing to the hypoxic environment, favors reduction and leads to a selective activation in tumor tissue (activation-by-reduction hypothesis) [1].

During recent years various mechanisms contributing to the cytotoxic effect of KP1019 have been explored. Both the induction of apoptosis via the mitochondrial pathway [9] and the formation of oxidative stress [10] have been demonstrated in cell culture settings. It has also been reported that KP1019 interacts with DNA [4, 11] and topoisomerase II [12], but these findings are most likely of subordinate relevance given the extensive protein binding of KP1019 and the high concentrations required, respectively.

The role of ascorbic acid in medicine in general and especially in anticancer therapy has been discussed quite controversially during recent decades. On the one hand, several articles postulate a beneficial role on the basis of the findings that ascorbic acid in combination with transition metal ions produce H_2O_2, leading to reactive oxygen species (ROS) that interact with biomolecules and thereby kill cancer cells [13–15]. This mechanism is assumed to be cancer-cell-specific because cancer cells have lost the efficiency of antioxidative stress defense [16]. On the other hand, some studies claim that ascorbic acid does not have antiproliferative properties [17, 18]. It must be considered that the divergent effects of ascorbic acid are strongly dependent on the route of administration. Oral administration of vitamin C—even in high doses—can only yield blood plasma levels below 100 μM [19]. In contrast, higher plasma levels in a concentration range of 1–5 mM [20], which seem to be beneficial in cancer treatment, can only be achieved by intravenous or intraperitoneal infusion in xenograft animal models [21, 22]. Corresponding to the conflicting data found for ascorbic acid alone, also the coadministration of ascorbic acid and chemotherapeutic drugs is discussed controversially. Whereas Hoffer et al. [17] postulated that this is a promising approach, another study showed that administration of ascorbic acid during chemotherapy decreases the efficiency of anticancer drugs such as cisplatin and doxorubicin and is therefore contraindicated [23]. The mode of action of each drug must be examined carefully because drugs that exert their antiproliferative potential by ROS production such as doxorubicin may lose their activity when coadministered with ascorbic acid, whereas the activity of KP1019—owing to the proposed activation by reduction—may benefit from coadministration. Ascorbic acid was recently shown to be capable of quickly reducing KP1019 in buffered (pH 6.0) and unbuffered (pH approximately 3.5) aqueous solutions, leading to increased reactivity with the nucleotide 5′-GMP [24]. However, the influence on cytotoxicity has never been evaluated and will be presented in this article.

The cell culture setting allows variation of extracellular conditions in a controlled manner, and ascorbic acid was considered the appropriate choice for studies on the influence of biological reductants under these conditions. In this

study the influence of ascorbic acid over a broad concentration range (2.8–700 μM) including the average physiological concentration (50 μM) on cytotoxicity of KP1019 in human cancer cells was analyzed. Furthermore, the influence of ascorbic acid on KP1019-induced intracellular radical formation as well as on cellular uptake of KP1019 and DNA ruthenation in KP1019-treated cells was investigated by the 2′,7′-dichlorodihydrofluorescein diacetate (DCFH-DA) assay and inductively coupled plasma mass spectrometry (ICP-MS), respectively, and the influence of co-incubation with ascorbic acid on the conformational changes induced by KP1019 on plasmid DNA was studied by an electrophoretic mobility shift assay. Finally, we approached the issue of whether reduction of KP1019 takes place mainly extracellularly or intracellularly by means of ^{1}H-NMR spectroscopy.

Materials and methods

Compounds

KP1019 was prepared in high purity at the Institute of Inorganic Chemistry, University of Vienna, according to a procedure published previously [25]. Sodium ascorbate was purchased from Serva (Heidelberg, Germany) and bovine serum albumin (better than 98% purity) was purchased from Sigma (Steinheim, Germany).

Cell lines and culture conditions

SW480 (human colon carcinoma) cells were purchased from the American Type Culture Collection. KB-3-1 (human cervical carcinoma) cells and the colchicine-resistant subline KBC-1 were kindly provided by D.W. Shen (Bethesda, MD, USA). Eagle's minimum essential medium (MEM), Dulbecco's phosphate-buffered saline (D-PBS), sodium pyruvate (100 mM), L-glutamine (200 mM), fetal bovine serum, nonessential amino acids (100×), and trypsin were obtained from Sigma (Schnelldorf, Germany). The six-well plates, 96-well plates, 90-mm tissue culture plates, and 75-cm^2 culture flasks were purchased from Iwaki/Asahi Technoglass (Gyouda, Japan). Cells were grown in 75-cm^2 culture flasks as adherent monolayer cultures in complete culture medium, i.e., MEM supplemented with 10% heat-inactivated fetal bovine serum, 1 mM sodium pyruvate, and 2 mM L-glutamine. For the cell line KBC-1, the culture medium additionally contained 1 μg/mL colchicine to ensure stable expression of the P-glycoprotein (P-gp) transporter. For the 3-(4,5-dimethyl-2-thiazol-yl)-2,5-diphenyl-2H-tetrazolium bromide (MTT) assay, cellular uptake experiments, and DNA ruthenation studies, the following medium composition was used: MEM supplemented with 10% heat-inactivated fetal bovine serum, 1 mM

sodium pyruvate, 4 mM L-glutamine, and 1% nonessential amino acids (100×). Cultures were maintained at 37 °C in a humidified atmosphere containing 5% CO_2.

MTT assay

Cytotoxicity was determined by means of the colorimetric MTT assay (purchased from Fluka, Vienna, Austria). Cells were harvested from culture flasks by trypsinization, counted in a hemocytometer after trypan blue staining of dead cells and seeded in 100-μL aliquots into 96-well microculture plates at densities of 2.5×10^3 viable cells per well to ensure exponential growth of untreated controls throughout the experiment. After a 24-h preincubation, serial dilutions of the test compound in complete culture medium (100 μL) were added and cells were exposed for 96 h. At the end of exposure, drug solutions were replaced by 100 μL RPMI1640 culture medium (supplemented with 10% heat-inactivated fetal bovine serum and 4 mM L-glutamine) per well plus 20 μL MTT solution (5 mg/mL MTT in phosphate-buffered saline) per well. After incubation for 4 h, the medium/MTT mixtures were removed, and the formazan crystals formed in vital cells were dissolved in 150 μL dimethyl sulfoxide per well. Optical densities at 550 nm were measured with a microplate reader (Tecan Spectra Classic), using a reference wavelength of 690 nm to correct for unspecific absorption. The quantity of vital cells was expressed in terms of T/C values relative to untreated control microcultures, and IC_{50} values were calculated from concentration-effect curves by interpolation. To determine the relative number of cells at the beginning of exposure, a separate plate prepared identically to the test plates was stained and measured in the same manner at the beginning of drug exposure. Evaluation was based on means and standard deviations from at least three independent experiments, each comprising six replicates per concentration.

In the experiments using a constant, average physiological concentration (50 μM) of ascorbic acid, the same cell number was seeded in aliquots of only 80 μL, and the appropriate concentration of ascorbic acid was adjusted by addition of 20 μL of a 10× stock solution in the same medium immediately before the addition of serially diluted solutions of KP1019 in another 100 μL culture medium.

The effect of different concentrations of ascorbic acid (2.8–700 μM) on a constant concentration of KP1019 (corresponding to the IC_{50} value in the respective cell line) was investigated in the same manner, and the appropriate amount of ascorbic acid was added prior to addition of KP1019. The T/C values were referenced to the IC_{50} value in the respective cell line, and to rule out any cytotoxic effects of ascorbic acid, ascorbic acid alone (2.8–700 μM) was tested in each cell line.

DCFH-DA assay

Generation of intracellular radicals was studied fluorimetrically by the DCFH-DA assay (Sigma, Schnelldorf, Germany) [26]. One million cells (SW480, KB-3-1, or KBC-1) were suspended in 1 mL Hank's balanced salt solution (Sigma, Schnelldorf, Germany), containing 1% fetal bovine serum (Gibco-Invitrogen, Lofer, Austria), 25 μM DCFH-DA, and appropriate concentrations of ascorbic acid (0, 5.5, 50, or 700 μM). KP1019 was added in effective concentrations of 50, 62.5, and 125 μM, corresponding to the determined equicytotoxic 50% inhibitory concentrations in SW480, KB-3-1, and KBC-1 cells, respectively. To correct for the intrinsic fluorescence of the cells, samples without DCFH-DA and KP1019 were prepared analogously. Furthermore, samples containing only DCFH-DA but no KP1019 were required to consider the fluorescence which is due to DCFH-DA alone. Cells were incubated for 90 min in a total volume of 1 mL in a tissue culture incubator at 37 °C to allow formation of the fluorescent 2′,7′-dichlorofluorescein by ROS and reactive nitrogen species (RNS). Subsequently, intracellular fluorescence was determined by fluorescence-activated cell sorting analysis (FACSCalibur, Becton Dickinson) with 505-nm excitation and 535-nm emission. Experiments were repeated independently three times.

Cellular uptake

Studies on cellular uptake were performed according to the method described previously [27]. Briefly, SW480, KB-3-1, and KBC-1 cells were seeded in six-well plates at densities of 3×10^5 cells per well in aliquots of 2.5 mL complete culture medium. Uptake experiments and corresponding adsorption/desorption controls were located on the same plate. Plates were kept at 37 °C for 24 h prior to addition of appropriate concentrations of ascorbic acid, followed by addition of KP1019 yielding a concentration of 50 μM during exposure (2 h). Afterwards, the medium was removed, cells were washed three times with PBS, lysed with 0.5 mL subboiled HNO_3 per well for 1 h at room temperature, and ruthenium was quantified by ICP-MS in aliquots of 400 μL diluted to a total volume of 8 mL and internally standardized with indium (0.5 ppb). The value for the adsorption/desorption blank was subtracted from that for the corresponding uptake sample, and the uptake of KP1019 in the presence of various concentrations of ascorbic acid (5.5, 50 and 700 μM) was compared with the uptake of KP1019 alone. The results are based on three independent experiments, each consisting of triplicates.

Metal concentrations were determined using an ICP-MS instrument (7500ce, Agilent, Waldbronn, Germany), equipped with a CETAC ASX-520 autosampler and a MicroMist nebulizer, at a sample uptake rate of approximately 0.25 mL/min. Indium and ruthenium standards were obtained from CPI International (Amsterdam, The Netherlands). Standards were prepared in matrices matching the sample matrix with regard to the internal standard and the concentration of the acid. Nitric acid (p.a.) was purchased from Fluka (Buchs, Switzerland) and further purified in a quartz sub-boiling-point distillation unit. All samples and dilutions were prepared with Milli-Q water (18.2 MΩ cm). Concentrations were determined by means of the isotopes ^{115}In and ^{102}Ru.

DNA metallation

SW480 cells were seeded in Petri dishes (Iwaki/Asahi Technoglass, Gyouda, Japan) and grown to about 80% confluence in a total volume of 9 mL complete culture medium at 37 °C. Substances were dissolved in tenfold concentrations in medium and 1 mL was added to each Petri dish. Cells were exposed for 24 h at 37 °C. After incubation, the medium was removed, and cells were washed with tris(hydroxymethyl)aminomethane (Tris)-buffered saline (TBS) and harvested by trypsinization. After centrifugation of the cell suspensions, the pellets were resuspended in TBS, and the number of viable cells was determined after trypan blue staining of dead cells. Six million cells were transferred to a 15-mL tube and centrifuged for 2 min. The cells were washed three times by resuspending the pellets in 1 mL TBS and centrifugation at 900g for 2 min in Eppendorf tubes. The supernatant was discarded, and the cell pellets were resuspended in 500 μL lysis buffer [10 mM Tris–HCl, 1 mM EDTA, 20 μg/mL RNase, 0.2 % Triton X-100, pH 7.4] and incubated for 30 min at 37 °C. The lysate was centrifuged at 10,000g for 8 min. The supernatant was transferred to fresh Eppendorf tubes, 350 μL 2-propanol were added, the tubes were centrifuged at 10,000g for 30 min at 4 °C, and pellets were washed with ethanol and finally centrifuged again. The pellets were dried in air and dissolved in 200 μL Milli-Q water (18.2 MΩ cm) for at least 20 min at 65 °C in a gently shaking thermomixer. To minimize the impact of ^{15}N^{16}O interference with ^{31}P, aliquots (100 μL) of each DNA solution were analyzed in 2% (w/w) hydrochloric acid in a total volume of 5 mL and internally standardized. Beryllium (1 ppb) and indium (0.5 ppb) were used as internal standards for phosphorus and ruthenium, respectively, and concentrations were determined by means of the isotopes ^{9}Be, ^{31}P, ^{115}In, and ^{102}Ru. All standards were obtained from CPI International (Amsterdam, The Netherlands) and prepared in matrices matching the sample matrix with regard to the internal standard and the concentration of the acid. Hydrochloric acid (p.a.) was purchased from Fluka (Buchs, Switzerland) and was further purified in a quartz sub-boiling-point distillation unit. Milli-Q water (18.2 MΩ cm) was used for dilutions. As

phosphate-containing reagents were strictly avoided, phosphorus was measured simultaneously with ruthenium by ICP-MS (as described earlier) and the amount was used for calculation of r_b values (number of ruthenium atoms per nucleotide). The results were based on three independent experiments, each consisting of parallel replicates.

Electrophoretic mobility shift assay

Plasmid pTZ18u (2,860 bp) from Bio-Rad Laboratories (Munich, Germany) was kindly provided by Stefanie Zorbas-Seifried (Max Planck Institute of Biochemistry, Martinsried, Germany). For every time point of the kinetic studies, 1 μg plasmid DNA was incubated with the substances in a total volume of 40 μL in 0.1-fold Tris–EDTA buffer at 37 °C. The incubation time varied from 1 to 15 min. The concentration of KP1019 was 50 μM in all experiments. Ascorbic acid was added in concentrations of 5.5, 50, or 700 μM. After incubation, 4 μL loading dye (6× loading dye, Fermentas) was added to a 20-μL aliquot of the sample, and electrophoresis was performed for 90 min at 80 V in a 1% agarose gel (agarose from Sigma, Schnelldorf, Germany) using Tris–borate–EDTA buffer (5×, Eppendorf, Hamburg, Germany). Gels were stained with 0.2 μg/mL ethidium bromide solution (Serva, Heidelberg, Germany), illuminated by UV light, and photographed using the gel documentation system GelDoc-It (UVP, Upland, CA, USA).

Reduction of KP1019 by ascorbic acid

Stock solutions of KP1019 (5 mM in dimethyl-d_6 sulfoxide), and bovine serum albumin (300 μM in D_2O) were prepared and stored at −20 °C. Sodium ascorbate was freshly dissolved in D_2O in a 20 mM concentration directly prior to ^{1}H-NMR measurements. D-PBS or D_2O was added to adjust the appropriate concentrations for buffered or unbuffered experiments, respectively. Time-dependent reduction of KP1019 by an equimolar concentration of ascorbic acid (effective concentration 0.5 mM) was studied in D_2O or in D-PBS solutions (pH 7.4) of albumin (effective concentrations of albumin 30 or 200 μM). Ascorbic acid was added approximately 5 min after the first ^{1}H-NMR measurement. ^{1}H-NMR spectra were recorded at 26 °C with a Bruker Avance III Fourier transform NMR spectrometer at 500.32 MHz using standard Bruker pulse programs over 1 h.

Results

MTT assay

Concentration–effect curves for KP1019 in SW480, KB-3-1, and KBC-1 cells in the absence and presence of ascorbic
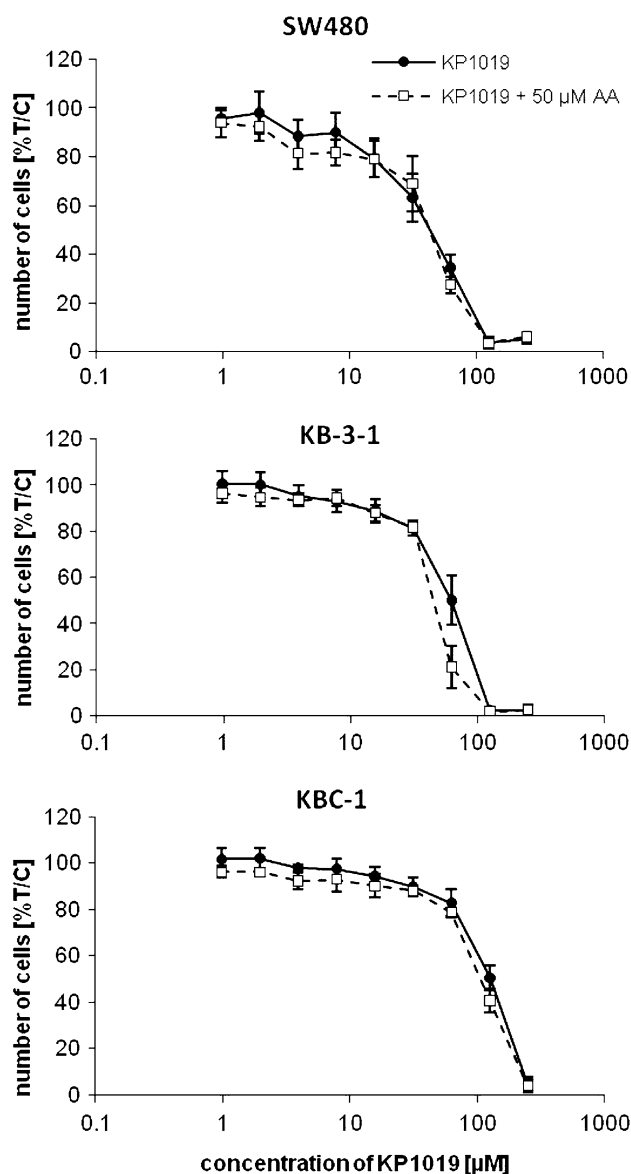

Fig. 1 Cytotoxicity of indazolium *trans*-[tetrachlorobis(1*H*-indazole)ruthenate(III)] (KP1019) in SW480, KB-3-1, and KBC-1 cells without addition of ascorbic acid (*black line*) and in the presence of a constant, physiological amount of 50 μM ascorbic acid (*dashed line*). *AA* ascorbic acid

acid (50 μM) are presented in Fig. 1 and the resulting IC_{50} values are summarized in Table 1. Ascorbic acid did not affect the cytotoxic activity of KP1019 in SW480 cells (43 ± 8 vs. 42 ± 3 μM) and KBC-1 cells (125 ± 10 vs. 106 ± 7 μM), but the IC_{50} value slightly decreased in the presence of 50 μM ascorbic acid in the case of KB-3-1 cells (62 ± 9 vs. 45 ± 2 μM).

However, when KP1019 was adjusted to a constant concentration corresponding roughly to the IC_{50} in the respective cell line (50, 62.5, and 125 μM, for SW480, KB-3-1, and KBC-1 cells, respectively), varying the concentrations of ascorbic acid (2.8–700 μM) dramatically

Table 1 IC$_{50}$ values of indazolium *trans*-[tetrachlorobis(1*H*-indazole)ruthenate(III)] (KP1019)-treated cells (96 h) in the absence of ascorbic acid (AA) and in the presence of an average physiological amount of 50 μM ascorbic acid

	IC$_{50}$	
	Without AA	With 50 μM AA
SW480	43 ± 8	42 ± 3
KB-3-1	62 ± 9	45 ± 2
KBC-1	125 ± 10	106 ± 7

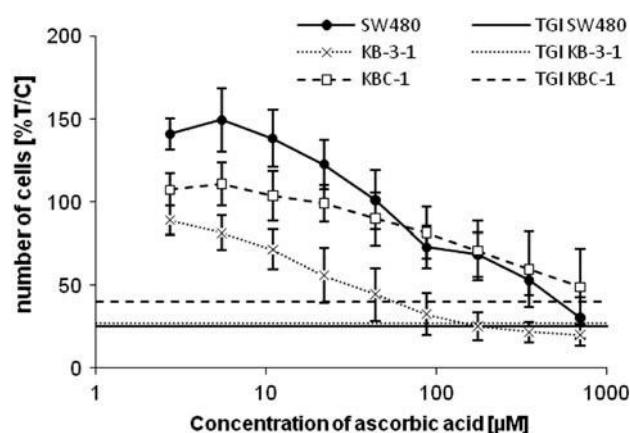Values are given as the mean ± the standard deviation of at least three independent experiments

Fig. 2 Cytotoxicity of KP1019 in SW480 (50 μM), KB-3-1 (62.5 μM), and KBC-1 (125 μM) cells with addition of various concentrations of ascorbic acid. Values are given relative to the values for cells treated only with KP1019 corresponding to the respective IC$_{50}$. Cytotoxicity of KP1019 is enhanced up to the complete inhibition of cell growth (TGI) in all cell lines

affected the cytotoxicity of KP1019 (Fig. 2). In contrast, ascorbic acid alone did not show any influence on cell growth up to a concentration of 700 μM (Fig. S1). Concentrations of ascorbic acid below 50 μM had protective effects in SW480 cells, resulting in an increase of cell number up to 50% compared with controls treated only with KP1019. No such protective effect was observed in KB-3-1 and KBC-1 cells. In contrast, concentrations above 50 μM ascorbic acid increased the cytotoxicity of a constant concentration of KP1019 dramatically in all cell lines, resulting in a complete inhibition of cell growth at a concentration of 700 μM in SW480 and KBC-1 cells. In KB-3-1 cells, an enhancement of the cytotoxicity of KP1019 was observed at concentrations of ascorbic acid as low as 10 μM and total growth inhibition was reached in the presence of 175 μM ascorbic acid. Preincubation of cells for 4 h with various concentrations of ascorbic acid followed by incubation with KP1019 (in a concentration corresponding to the IC$_{50}$ of the cell line tested) for 92 h did not result in altered cytotoxicity compared with KP1019 without preincubation (data not shown).
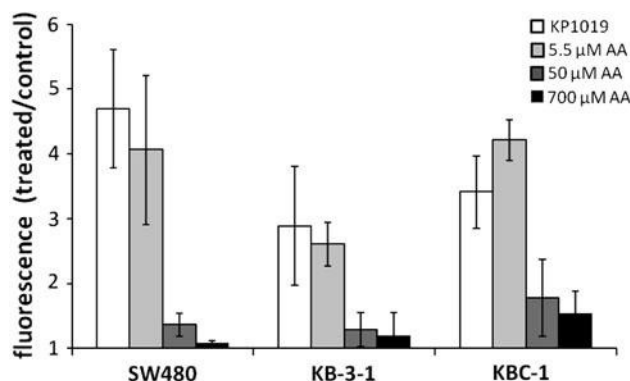

Fig. 3 Intracellular fluorescence in the 2′,7′-dichlorodihydrofluorescein diacetate assay, indicating the formation of reactive oxygen species and reactive nitrogen species in SW480, KB-3-1, and KBC-1 cells treated with KP1019 in the absence and presence of ascorbic acid. *Columns* indicate the factors by which fluorescence is increased beyond that of untreated controls

DCFH-DA assay

The generation of intracellular ROS and RNS induced by treatment with equicytotoxic 50% inhibitory concentrations of KP1019 alone and in the presence of 5.5, 50, and 700 μM ascorbic acid was studied by means of the DCFH-DA assay. The concentrations of ascorbic acid were chosen such that the lowest has partially protective effects whereas the highest enhances the cytotoxicity of KP1019, and the intermediate corresponds to the average concentration in human plasma. Strongest fluorescence was observed in the presence of KP1019 alone, whereas ascorbic acid counteracts KP1019-induced ROS/RNS generation in a concentration-dependent manner. Formation of ROS and RNS increased about 3–4.5 times (depending on the cell line) upon incubation with KP1019 compared with untreated controls and decreased with increasing concentrations of ascorbic acid compared with that induced by KP1019 alone. Intracellular fluorescence decreased to levels slightly above or comparable with that of untreated controls in the presence of 50 or 700 μM ascorbic acid (Fig. 3).

Cellular uptake

The influence of ascorbic acid on the total amount of cellular ruthenium taken up by cells was studied upon exposure of cells to 50 μM KP1019 in the presence of concentrations of ascorbic acid corresponding to the maximum protective effect observed in SW480 cells (5.5 μM), the average plasma level (50 μM), and the maximum activating effect (700 μM). The cellular uptake of KP1019 alone was used as a control.

It is important to mention that adsorption/desorption of KP1019 to/from the plates, which was investigated in detail
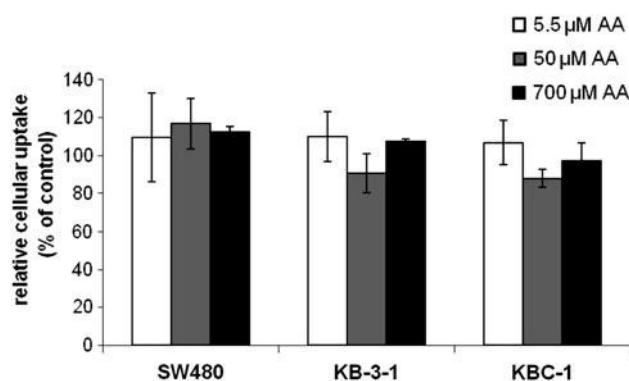
Fig. 4 Cellular uptake of KP1019 under various concentrations of ascorbic acid, normalized to controls treated with KP1019 alone

Fig. 5 Ruthenation of DNA in SW480 cells exposed for 24 h to KP1019 (50 μM) alone and KP1019 in the presence of various concentrations of ascorbic acid (50 or 700 μM). Values are given as the mean ± the standard deviation of three independent experiments. *Asterisk* significantly different from KP1019 alone ($P = 0.032$, paired t test)

previously [27], was found to be influenced by ascorbic acid. Whereas in wells treated only with KP1019 the adsorption was 5.8 ng per well, an increase to 6.0, 8.5, and 9.6 ng per well in the presence of 5.5, 50, and 700 μM ascorbic acid, respectively, was observed. Without correction for adsorption, this increase could be mistaken for enhanced cellular uptake, as the levels of cellular ruthenium and adsorbed ruthenium are in a similar range. However, upon correction for adsorption, no influence of ascorbic acid on the total cellular amount of ruthenium could be observed (Fig. 4).

Ruthenation of cellular DNA

The extent of ruthenium binding to DNA, which was isolated from treated SW480 cells (50 μM KP1019 in the absence or presence of 5.5, 50, or 700 μM ascorbic acid), was measured by ICP-MS. SW480 cells were chosen because ascorbic acid showed the most pronounced impact on cytotoxicity of KP1019 in these cells. The r_b value (determined as Ru per P) in cells treated only with KP1019 was calculated to be 0.00092 ± 0.00029. Addition of 5.5 μM or 50 μM ($r_b = 0.00093 \pm 0.00023$) ascorbic acid did not influence the DNA binding behavior, whereas co-incubation of 50 μM KP1019 with 700 μM ascorbic acid significantly ($P = 0.032$, two-sided paired t test) increased the amount of ruthenium bound to DNA ($r_b = 0.00122 \pm 0.00035$) compared with KP1019 alone (Fig. 5).

Electrophoretic mobility shift assay

Plasmid DNA occurs in two conformations that can be separated by electrophoresis: a slowly migrating open circular form and a faster migrating supercoiled form. Adducts that are able to locally unwind DNA cause a retardation of the faster migrating band of the supercoiled form, whereas substances that are able to bend DNA
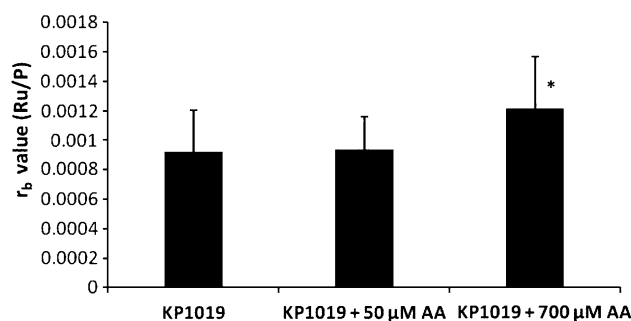
accelerate the migration of the open circular form [28]. The electrophoretic analysis of pTZ18u plasmid treated with 50 μM KP1019 in the absence and presence of ascorbic acid (5.5, 50, and 700 μM) is depicted in Fig. 6. When only ascorbic acid was added to the plasmid (Fig. 6, lanes 6 and 10), migration of plasmid DNA remained unchanged compared with that of untreated plasmid (Fig. 6, lanes 5 and 9), indicating there was no conformational change due to ascorbic acid. Within 15 min of incubation at 37 °C, KP1019-treated DNA showed a slight retardation of the supercoiled form compared with DNA incubated for only 1 min (Fig. 6, lanes 7 and 1, respectively). Co-incubation of a high concentration of ascorbic acid (700 μM) and KP1019 accelerated the alteration of DNA mobility (Fig. 6c, lanes 4 and 8) compared with the effect of KP1019 alone at the same incubation time (Fig. 6c, lanes 3 and 7). The effect of ascorbic acid on KP1019-induced alterations of DNA secondary structure slightly diminished with decreasing concentration, but was still well discernible at a concentration of ascorbic acid as low as 5.5 μM (Fig. 6a, lanes 4 and 8). The addition of ascorbic acid obviously enhanced the DNA-interacting effect of KP1019, resulting in a stronger retardation within the same time of exposure, indicating that the presence of ascorbic acid markedly increased the reactivity of KP1019.

Reduction of KP1019 by ascorbic acid

In the ^{1}H-NMR spectrum of KP1019 two sets of indazole signals can be detected. Indazole resonances of the indazolium counter ion were found in the region between 7.1 and 8.2 ppm. Indazole coordinated to the paramagnetic Ru(III) center, however, gives rise to signals (chemical shifts of less than 3.5 ppm) which are typically shifted upfield. Upon reduction to the diamagnetic Ru(II) complex, resonances of coordinated indazole can be found in the
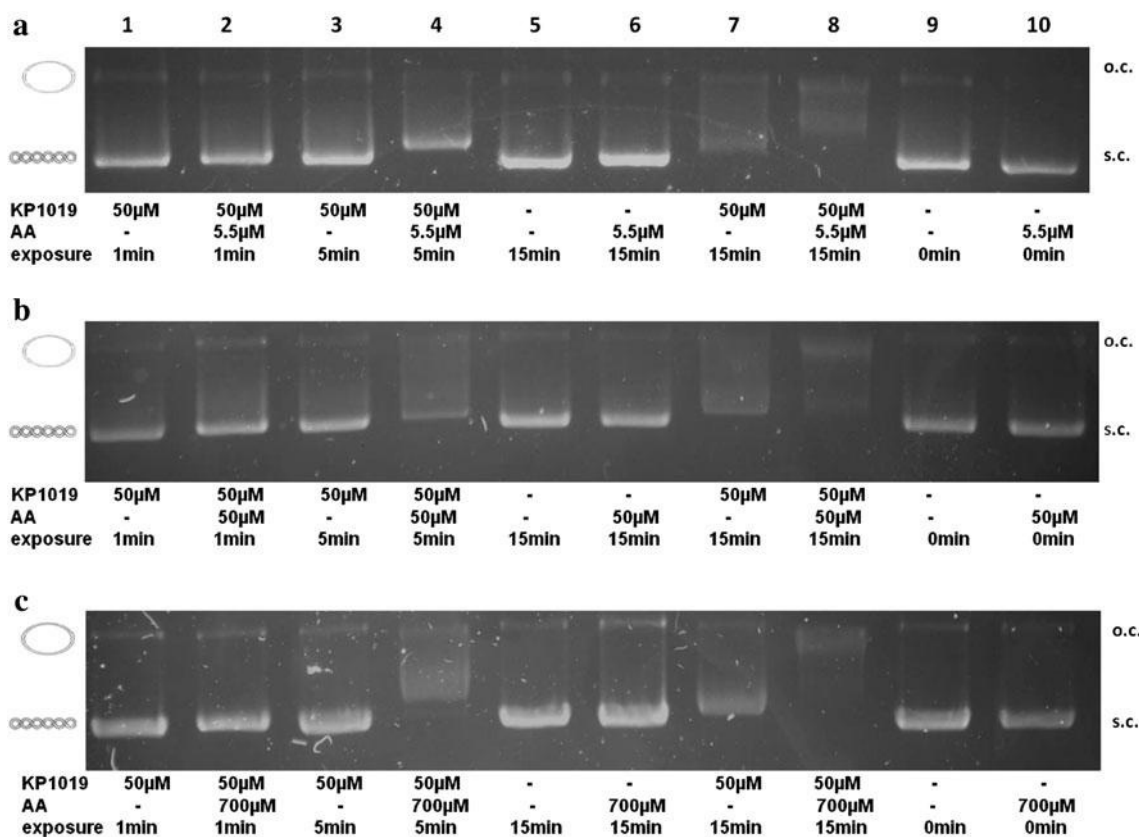
Fig. 6 Electrophoretic mobility of plasmid DNA pTZ18u treated with KP1019 (50 μM) alone and with KP1019 (50 μM) in combination with 5.5 μM (**a**), 50 μM (**b**), and 700 μM (**c**) ascorbic acid. The plasmid was incubated with the substances at 37 °C for different incubation times. *o.c.* open circular., *s.c.* supercoiled

typical aromatic region (7.3–9.0 ppm) slightly downfield from those of the indazolium counter ion. As the stoichiometry between the counter ion and the coordinated indazole is 1:2, the signal intensity ratio allows the relative determination of the reduced form of KP1019. Typical spectra of KP1019 dissolved in D_2O and upon 1 h coincubation with ascorbic acid are presented in Fig. 7. Time-dependent reduction of 0.5 mM KP1019 in D_2O and in phosphate-buffered solution (pH 7.4) in the presence of 30 μM albumin is shown in Fig. S2. Addition of an equimolar amount of ascorbic acid led to a substantial formation of Ru(II) species under all conditions investigated, but the kinetics differed significantly. Whereas in aqueous, unbuffered solution reduction was slowest (signals corresponding to reduced KP1019 increase in intensity for at least 1 h, Fig. S2, top), the presence of albumin in a concentration mimicking cell culture conditions (30 μM) accelerated reduction, leading to stable ratios between free indazole and Ru(II)-coordinated indazole within 15 min. Reduction further accelerated when the albumin-containing solution was buffered to a pH of 7.4 (Fig. S2, bottom): the final ratio was observed in the first spectrum recorded (approximately 5 min after addition of ascorbic acid). A higher concentration of albumin (200 μM) increased the albumin background significantly, but nevertheless signals corresponding to Ru(II)-coordinated indazole were detected in the first spectrum and did not change further within 1 h (data not shown).

Discussion

One of the major features of Ru(III)-based anticancer drugs is the biologically accessible redox potential of Ru(III)/Ru(II). Reduction is supposed to play an important role in the mode of action of Ru(III)-based anticancer compounds; hence, we first studied the impact of ascorbic acid on the cytotoxicity of KP1019 in two ways: the effect of a constant concentration of ascorbic acid on various concentrations of KP1019 and the effect of various concentrations of ascorbic acid on a constant concentration of KP1019 were determined. Consecutively, T/C values for coexposure to an IC_{50} of KP1019 and 50 μM ascorbic acid were determined twice in two different experimental setups, proving validity of the observed results (see Table S1).

Cytotoxicity of a constant concentration of KP1019 was increased in all cell lines investigated in the presence of high concentrations of ascorbic acid (up to 700 μM), but

Fig. 7 ^{1}H-NMR spectra of the time dependence of the reduction of 0.5 mM KP1019 in the presence of an equivalent concentration of ascorbic acid in D$_2$O. Signals originating from reduced species of KP1019 are highlighted
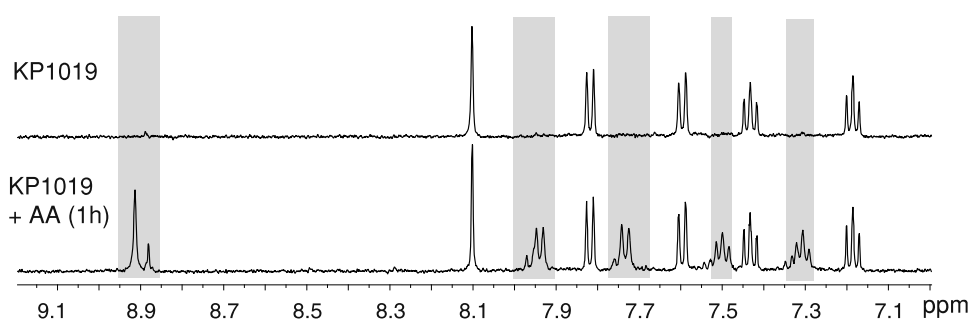
only SW480 cells were protected in the presence of low ascorbic acid concentrations. It is known that millimolar concentrations of ascorbic acid itself cause DNA damage probably owing to a prooxidant action of ascorbic acid, leading to mutations and finally apoptosis of the cell [29–32]. In our experimental setting, ascorbic acid alone showed no cytotoxic effect (Fig. S1). However, as KP1019 also exerts its cytotoxicity partly via generation of ROS/RNS [10], we studied intracellular reactive oxygen/nitrogen production by means of the DCFH-DA assay. The amount of reactive species generated by KP1019 decreased in the presence of low and high concentrations of ascorbic acid, showing its radical scavenging capabilities [33–35], and indicating that increased intracellular radical formation can be ruled out as a possible reason for the increased cytotoxicity in the presence of high concentrations of ascorbic acid.

As ascorbic acid alone neither exhibited cytotoxicity in the MTT assay up to concentrations of 700 μM nor led to increased cell proliferation in lower concentrations nor sensitized the cells to KP1019 when preincubated for 4 h prior to 96 h incubation with KP1019 alone, the mode of action of KP1019 has to be influenced by direct interaction with ascorbic acid. To evaluate if the increase in cytotoxicity originates from higher cellular uptake of KP1019 in the presence of ascorbic acid, ruthenium was quantified in cells which were co-incubated with different concentrations of ascorbic acid for 2 h. No significant influence on the level of cellular ruthenium could be observed. In contrast, the amount of ruthenium adsorbed by the polystyrene of the plates nearly doubled in the presence of 700 μM ascorbic acid compared with adsorption in the absence of ascorbic acid. This may indicate structural changes in the ruthenium compound, most likely due to reduction, associated with a higher reactivity. In accordance with our findings, Sava et al. [36] also demonstrated no enhanced uptake of the Ru(III) complex NAMI-A, which is also supposed to be activated by reduction, by ascorbic acid cotreatment in vitro. Notably, it was discovered that coadministration of ascorbic acid and NAMI-A inhibited metastasis growth to a higher extent than the Ru(III) complex alone. Consequently, it is of interest whether the

anticancer activity of KP1019 might be also enhanced by cotreatment with ascorbic acid in xenograft experiments and the first experiments are currently being planned.

To verify the change in reactivity of KP1019 induced by ascorbic acid we used plasmid DNA as a binding partner in a cell-free experiment as a model for interactions with biomolecules, being aware that DNA is probably not the critical target of KP1019 in vivo. Ascorbic acid increased the interaction of KP1019 with DNA with plasmid DNA in cell-free settings as well as in living SW480 cells. This again suggests that KP1019 shows higher activity when ascorbic acid is coadministered as a result of direct interaction between the two compounds. The KB-3-1/KBC-1 cell panel allowed us to further strengthen this assumption. KBC-1 is the colchicine-resistant subline of KB-3-1, established by long-term exposure to colchicine, which led to P-gp overexpression [40]. As KP1019 is a substrate for P-gp [37], KBC-1 cells were less sensitive than KB-3-1 cells to KP1019 owing to partial cellular efflux of KP1019 by P-gp. The fact, that the sensitizing effect by ascorbic acid cotreatment was weaker in P-gp-overexpressing KBC-1 cells indicates, on the one hand, that the enhanced anticancer activity of KP1019 is based on direct interaction and, on the other hand, that KP1019 in its reduced form still seems to be a P-gp substrate.

Direct interaction between ascorbic acid and KP1019 is supposed to take place outside the cell, namely, in the culture medium. Hence, the question arises of whether ruthenium is reduced outside or inside the cell. Several instrumental settings were previously applied to try to answer this question, but each suffered from drawbacks concerning transferability to conditions in cell culture. A capillary electrophoretic approach by Timerbaev et al. [38] showed no impact of ascorbic acid on albumin–KP1019 adducts in buffered solution; however, ascorbic acid suffered from decomposition and impact of the electric field during separation cannot be ruled out. On the other hand, Piccioli et al. [39] reported changes in UV–vis spectra of KP1019–albumin adducts when ascorbate was added to the reaction mixture, concluding that these are probably due to reduction of ruthenium. Reduction of KP1019 in aqueous solution was recently investigated in our group by

1H-NMR spectroscopy, which allows to unambiguously distinguish between signals originating from free indazole, indazole that is coordinated to paramagnetic Ru(III) in KP1019, and indazole that is coordinated to the diamagnetic Ru(II) center [24]. Hence, we adapted the conditions to those in cell culture. Details of the NMR investigations in protein free solutions were reported by other authors [23]. Although KP1019 quickly and nearly quantitatively binds to albumin [40], an increased concentration of albumin did not decelerate the reduction kinetics, suggesting that reduction of KP1019 cannot be inhibited and, hence, KP1019 is partly reduced in cell culture medium as well. However, as the concentration of KP1019 in NMR studies is approximately 10 times higher and cell culture medium contains further ingredients, it is obvious that reduction in cell culture imperatively neither proceeds equally fast nor leads to comparable amounts of reduced KP1019.

Regarding the possible consequences of these findings in vivo, one should note that cancer cells were found to accumulate more ascorbic acid owing to their alterations in reduction/oxidation processes [41, 42] and, hence, ascorbic acid may possess the ability to selectively activate KP1019 in tumors. The activation through ascorbic acid at the tumor site would be an achievement on the path of target-directed cancer therapy that optimizes the activity in the tumor while leaving other tissues less affected and therefore diminishes the risk of adverse effects. Furthermore, these studies suggest that it may be possible to achieve equal therapeutic benefit with lower amounts of KP1019 when ascorbic acid is present in an optimized concentration by intravenous application of ascorbic acid, which was recently shown to lead to plasma concentrations in the millimolar range for several hours [16].

Even though we do not know the exact mechanism of activation of KP1019 mediated by ascorbic acid, it may be possible that in addition to DNA also a higher reactivity towards protein targets might be induced [43]. Experiments are ongoing to confirm these assumptions.

References

1. Clarke MJ (2003) Coord Chem Rev 236:209–233
2. Alessio E, Mestroni G, Bergamo A, Sava G (2004) Curr Topics Med Chem 4:1525–1535
3. Sava G, Zorzet S, Turrin C, Vita F, Soranzo M, Zabucchi G, Cocchietto M, Bergamo A, DiGiovine S, Pezzoni G, Sartor L, Garbisa S (2003) Clin Cancer Res 9:1898–1905
4. Hartinger CG, Zorbas-Seifried S, Jakupec MA, Kynast B, Zorbas H, Keppler BK (2006) J Inorg Biochem 100:891–904
5. Galanski M, Arion VB, Jakupec MA, Keppler BK (2003) Curr Pharm Des 9:2078–2089
6. Jungwirth U, Kowol CR, Keppler BK, Hartinger CG, Berger W, Heffeter P (2011) Antioxid Redox Signal. doi:10.1089/ars.2010.3663
7. Arrigoni O, De Tullio MC (2002) Biochim Biophys Acta 1569:1–9
8. Reisner E, Arion VB, Guedes da Silva MFC, Lichtenecker R, Eichinger A, Keppler BK, Kukushkin VY, Pombeiro AJL (2004) Inorg Chem 43:7083–7093
9. Kapitza S, Pongratz M, Jakupec MA, Heffeter P, Berger W, Lackinger L, Keppler BK, Marian B (2005) J Cancer Res Clin Oncol 131:101–110
10. Kapitza S, Jakupec MA, Uhl M, Keppler BK, Marian B (2005) Cancer Lett 226:115–121
11. Brabec V, Novakova O (2006) Drug Resist Updat 9:111–122
12. Gopal YNV, Kondapi AK (2001) J Biosci 26:271–276
13. Chen Q, Espey MG, Krishna MC, Mitchell JB, Corpe CP, Buettner GR, Shacter E, Levine M (2005) Proc Natl Acad Sci USA 102:13604–13609
14. Chen Q, Espey MG, Sun AY, Lee J-H, Krishna MC, Shacter E, Choyke PL, Pooput C, Kirk KL, Buettner GR, Levine M (2007) Proc Natl Acad Sci USA 104:8749–8754
15. Chen Q, Espey MG, Sun AY, Pooput C, Kirk KL, Krishna MC, Khosh DB, Drisko J, Leven M (2008) Proc Natl Acad Sci USA 105:11105–11109
16. Oberley TD, Oberley LW (1997) Histol Histopathol 12:525–535
17. Hoffer LJ, Levine M, Assouline S, Melnychuk D, Padayatty SJ, Rosadiuk K, Rousseau C, Robitaille L, Miller WH Jr (2008) Ann Oncol 19:1969–1974
18. Moertel CG, Fleming TR, Creagan ET, Rubin J, O'Connell MJ, Ames MM (1985) N Engl J Med 312:137–141. doi:10.1056/nejm198501173120301
19. Levine M, Conry-Cantilena C, Wang Y, Welch RW, Washiko PW, Dhariwal KR, Park JB, Lazarev A, Graumlich JF et al (1996) Proc Natl Acad Sci USA 93:3704–3709
20. Riordan NH, Riordan HD, Meng X, Li Y, Jackson JA (1995) Med Hypotheses 44:207–213
21. Frei B, Lawson S (2008) Proc Natl Acad Sci USA 105:11037–11038
22. Ohno S, Ohno Y, Suzuki N, Soma G-I, Inoue M (2009) Anticancer Res 29:809–815
23. Heaney ML, Gardner JR, Karasavvas N, Golde DW, Scheinberg DA, Smith EA, O'Connor OA (2008) Cancer Res 68:8031–8038
24. Schluga P, Hartinger CG, Egger A, Reisner E, Galanski M, Jakupec MA, Keppler BK (2006) Dalton Trans 1796–1802
25. Lipponer K-G, Vogel E, Keppler BK (1996) Metal Based Drugs 3:243–260
26. Halliwell B, Whiteman M (2004) Br J Pharmacol 142:231–255
27. Egger AE, Rappel C, Jakupec MA, Hartinger CG, Heffeter P, Keppler BK (2009) J Anal At Spectrom 24:51–61
28. Zorbas-Seifried S, Jakupec MA, Kukushkin NV, Groessl M, Hartinger CG, Semenova O, Zorbas H, Kukushkin VY, Keppler BK (2007) Mol Pharmacol 71:357–365
29. Satoh K, Ida Y, Hosaka M, Arakawa H, Maeda M, Ishihara M, Kunii S, Kanda Y, Toguchi M, Sakagami H (1998) Anticancer Res 18:4371–4375
30. Sakagami H, Satoh K, Fukuchi K, Gomi K, Takeda M (1997) Free Radic Biol Med 23:260–270. doi:S0891584996006211
31. Sakagami H, Satoh K, Hakeda Y, Kumegawa M (2000) Cell Mol Biol (Noisy-le-grand) 46:129–143
32. Amano Y, Sakagami H, Tanaka T, Yamanaka Y, Nishimoto Y, Yamaguchi M, Takeda M (1998) Anticancer Res 18:2503–2506
33. Carr A, Frei B (1999) FASEB J 13:1007–1024

34. Frei B, England L, Ames BN (1989) Proc Natl Acad Sci USA 86:6377–6381
35. Bevan RJ, Mistry N, Patel PR, Halligan EP, Dove R, Lunec J (2010) Br J Nutrit 103:686–695. doi:10.1017/S000711450999 2285
36. Sava G, Bergamo A, Zorzet S, Gava B, Casarsa C, Cocchietto M, Furlani A, Scarcia V, Serli B, Iengo E, Alessio E, Mestroni G (2002) Eur J Cancer 38:427–435
37. Heffeter P, Pongratz M, Steiner E, Chiba P, Jakupec MA, Elbling L, Marian B, Koerner W, Sevelda F, Micksche M, Keppler BK, Berger W (2005) J Pharmacol Exp Ther 312:281–289
38. Timerbaev AR, Foteeva LS, Rudnev AV, Abramski JK, Polec-Pawlak K, Hartinger CG, Jarosz M, Keppler BK (2007) Electrophoresis 28:2235–2240
39. Piccioli F, Sabatini S, Messori L, Orioli P, Hartinger CG, Keppler BK (2004) J Inorg Biochem 98:1135–1142
40. Cetinbas N, Webb MI, Dubland JA, Walsby CJ (2010) J Biol Inorg Chem 15:131–145
41. Langemann H, Torhorst J, Kabiersch A, Krenger W, Honegger CG (1989) Int J Cancer 43:1169–1173
42. Agus DB, Vera JC, Golde DW (1999) Cancer Res 59:4555–4558
43. Heffeter P, Boeck K, Atil B, Hoda MAR, Koerner W, Bartel C, Jungwirth U, Keppler BK, Micksche M, Berger W, Koellensperger G (2010) J Biol Inorg Chem 15:737–748

2.3. Physicochemical studies and anticancer potency of ruthenium(6η-p-cymene) complexes containing antibacterial quinolones

Kljun J.[a], Kandioller W.[b], Bytzek A.K.[b], Bartel C.[b], Jakupec M.A.[b], Hartinger Ch.G.[b], Keppler B.K.[b], Iztok T.[a,c]

[a] Faculty of Chemistry and Chemical Technology, University of Ljubljana, Aškerčeva cesta 5, SI-1000, Ljubljana, Slovenia

[b] Institute of Inorganic Chemistry, University of Vienna, Waehringer Strasse 42, 1090 Vienna, Austria

[c] EN-FIST Centre of Excellence, Dunajska 156, SI-1000 Ljubljana, Slovenia

Physicochemical Studies and Anticancer Potency of Ruthenium η^6-p-Cymene Complexes Containing Antibacterial Quinolones

Jakob Kljun,[†] Anna K. Bytzek,[‡] Wolfgang Kandioller,[‡] Caroline Bartel,[‡] Michael A. Jakupec,[‡] Christian G. Hartinger,[‡] Bernhard K. Keppler,[‡] and Iztok Turel*[,†,§]

[†]Faculty of Chemistry and Chemical Technology, University of Ljubljana, Aškerčeva 5, SI-1000, Ljubljana, Slovenia

[‡]Institute of Inorganic Chemistry, University of Vienna, Währinger Strasse 42, A-1090 Vienna, Austria

[§]EN→FIST Centre of Excellence, Dunajska 156, SI-1000 Ljubljana, Slovenia

Ⓢ *Supporting Information*

ABSTRACT: With the aim of exploring the anticancer properties of organometallic compounds with bioactive ligands, Ru-(arene) compounds of the antibacterial quinolones nalidixic acid (**2**) and cinoxacin (**3**) were synthesized, and their physicochemical properties were compared to those of chlorido(η^6-p-cymene)(ofloxacinato-κ^2O,O)ruthenium(II) (**1**). All compounds undergo a rapid ligand exchange reaction from chlorido to aqua species. **2** and **3** are significantly more stable than **1** and undergo minor conversion to an unreactive $[(\text{cym})\text{Ru}(\mu\text{-OH})_3\text{Ru}(\text{cym})]^+$ species (cym = η^6-p-cymene). In the presence of human serum albumin **1**−**3** form adducts with this transport protein within 20 min of incubation. With guanosine 5′-monophosphate (5′-GMP; as a simple model for reactions with DNA) very rapid reactions yielding adducts via its N7 atom were observed, illustrating that DNA is a possible target for this compound class. A moderate capacity of inhibiting tumor cell proliferation in vitro was observed for **1** in CH1 ovarian cancer cells, whereas **2** and **3** turned out to be inactive.
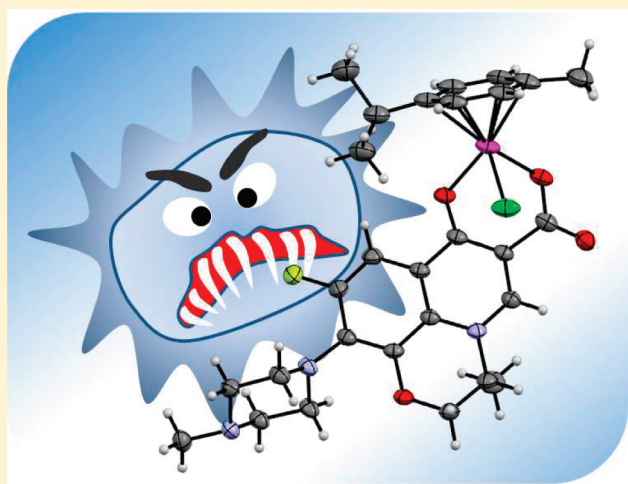
■ INTRODUCTION

In the past two decades ruthenium coordination compounds (Figure 1) have attracted considerable interest as potential anticancer agents because of their low toxicity and their efficacy against platinum-drug-resistant tumors, reflected in promising results in various stages of preclinical to early clinical studies.[1−6] Organometallic ruthenium complexes bearing a π-bonded arene ligand and other simple mono- or bidentate ligands are considered promising candidates for cancer treatment.[7] Compounds containing phosphatriazaadamantane (pta) or its derivatives were developed,[8,9] which show antimetastatic activity but low cytotoxicity in vitro.[9−11] On the other hand, complexes bearing N,N-chelating ligands (Figure 1) have shown cytotoxicity comparable to that of cisplatin in a number of cell lines.[12−14] The first organometallic ruthenium compound with chelating O,O-ligand systems were reported to undergo relatively fast decomposition due to hydrolysis. The biological activity of O,O- and S,O-chelates coordinated to the Ru(II) metal center was investigated recently,[15−22] and some of the compounds were shown to be potent protein kinase inhibitors.[20]

Quinolones are synthetic antibacterial agents, which are widely used in clinical practice. They are also suitable as ligands,

RAPTA-C   **[Ru(η⁶-biphenyl)Cl(en)]⁺**
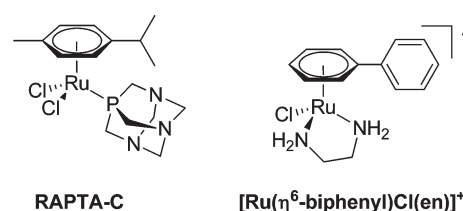
Figure 1. Structures of anticancer ruthenium complexes: RAPTA-C and $[\text{Ru}(\eta^6\text{-biphenyl})\text{Cl}(\text{en})]\text{PF}_6$ (en = ethylene-1,2-diamine).

featuring an O,O-chelate motif (Figure 2). Since the introduction of nalidixic acid into clinical use in 1962 more than 10 000 related compounds were synthesized and tested as potential antibacterial agents, and more than 30 were or still are in clinical or veterinary use.[23−25] In addition to their antibacterial activity, they were also shown to exhibit tumor-inhibiting properties.[26,27]

The mechanism of action of quinolones is not yet fully understood. It is supposed that the quinolones bind to DNA,
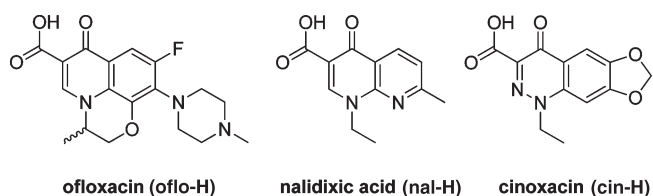
Figure 2. Chemical structures of the clinically applied quinolone antibacterials ofloxacin (oflo-H), nalidixic acid (nal-H), and cinoxacin (cin-H) used in this study.

inhibiting bacterial topoisomerase and thus preventing the bacteria from replicating.[23−25] The DNA interactions of quinolones[28,29] and their metal complexes[30−32] as well as their affinity to serum proteins[33] have been studied by applying different techniques. However, their mode of binding to DNA is uncertain. The quinolone molecule either forms hydrogen bonds to the nucleobases through the ketocarboxylate moiety or may bind to the phosphate backbone with the aid of magnesium ions that act as a bridge between the ketocarboxylate moiety and the DNA phosphates.[34] Recently, the crystal structure of a topoisomerase−DNA−quinolone complex was reported which shows that the magnesium ion is bidentately coordinated by the quinolone and four additional aqua ligands, which in turn form hydrogen bonds with DNA nucleobases.[35]

Since the approach to attach a bioactive ligand to a Ru(arene) moiety has been previously successfully used,[36−38] and keeping in mind the various biological properties of quinolones, we have recently prepared the first organometallic ruthenium complex with ofloxacin (oflo-H; Figure 2) and studied its interactions with DNA.[39] Herein, we describe an extended study comprising the synthesis and characterization of Ru(arene) complexes of the first-generation quinolone agents nalidixic acid (nal-H) and cinoxacin (cin-H) and comparisons of these complexes to the analogous ofloxacin derivative with regard to stability in aqueous solution and reactivity toward the DNA model 5′-guanosine monophosphate (5′-GMP) and the serum transport protein human serum albumin (HSA) as well as anticancer activity in human tumor cell lines.

■ EXPERIMENTAL SECTION

Materials and Methods. The starting materials were purchased from Sigma-Aldrich and were used as received. All the solvents were of reagent grade and were purchased from Fluka. The synthesis of [(cym)RuCl(oflo)] (**1**) was performed as reported recently.[39] ^{1}H NMR spectra were recorded with Bruker Avance DPX 300 (at 29 °C and 300.13 MHz) or Avance III 500 spectrometers (at 25 °C and 500.10 MHz). ^{31}P{^{1}H} NMR spectra were recorded at 25 °C on the latter instrument at 161.98 MHz. Elemental analyses (C, H, N) were performed with a Perkin-Elmer 2400 Series II CHNS/O analyzer. Infrared spectra were recorded with a Perkin-Elmer Spectrum 100 FTIR spectrometer, equipped with a Specac Golden Gate Diamond ATR as a solid sample support. X-ray diffraction data (Supporting Information) for **2** and **3** were collected on a Nonius Kappa CCD difractometer at 293(2) K equipped with a Mo anode (K$_\alpha$ radiation, λ = 0.710 73 Å) and a graphite monochromator. The structures were solved by direct methods implemented in SIR92[40] and refined by a full-matrix least-squares procedure based on F^2 using SHELXL-97.[41] All non-hydrogen atoms were refined anisotropically. The hydrogen atoms were either placed at calculated positions and treated using appropriate riding models or determined from the difference Fourier map. The programs Mercury[42] and ORTEP[43] were used for data analysis and figure preparation.

Synthesis. *Chlorido(η^6-p-cymene)(nalidixicato-κ^2O,O)ruthenium (II)* (**2**). [(Cym)RuCl(μ-Cl)]$_2$ (40.0 mg, 0.065 mmol) and nalidixic acid sodium salt hydrate (33.2 mg, 0.130 mmol) were dissolved in chloroform/methanol (1/1; 15 mL), and the reaction mixture was refluxed for 6 h. The obtained NaCl was removed by filtration through Celite, toluene (10 mL) was slowly added, and the solution was left in an open flask. Orange-brown crystals were obtained after 3 days at room temperature. The crystals were collected and washed with hexane. Yield: 50 mg, 65%.

^{1}H NMR (CDCl$_3$, 300.13 MHz): δ 9.02 (s, 1H, H2 nal), 8.67 (d, ^3J(H,H) = 8 Hz, 1H, H6 nal), 7.34−7.13 (m, 1H, H-2 nal), 5.64−5.57 (m, 2H, Ar-H cym), 5.35−5.32 (m, 2H, Ar-H cym), 4.50 (q, ^3J(H,H) = 7 Hz, 2H, NCH_2CH$_3$), 3.12−3.03 (m, 1H, Ar-CH(CH$_3$)$_2$ cym), 2.69 (s, 3H, Ar-CH_3 cym), 2.35 (s, 3H, Ar-CH_3 nal), 1.42 (t, ^3J(H,H) = 7 Hz, 3H, NCH$_2$CH_3 nal), 1.39 (d, ^3J(H,H) = 7 Hz, 6H, Ar-CH(CH_3)$_2$ cym). IR (cm^{-1}, ATR): 3045, 2963, 1624, 1607, 1560, 1517, 1490, 1444, 1362, 1342, 1315, 1286, 1250, 1231, 1160, 1124, 1091, 1031, 895, 858, 805, 771, 736, 700, 670, 636. Anal. Calcd for C$_{22}$H$_{27}$ClN$_2$O$_3$Ru·C$_7$H$_8$: C, 58.43; H, 5.92; N, 4.70. Found: C, 58.63; H, 5.60; N, 4.72.

Chlorido(η^6-p-cymene)(cinoxacinato-κ^2O,O)ruthenium(II) (**3**). [(Cym)RuCl(μ-Cl)]$_2$ (40.0 mg, 0.065 mmol) and cinoxacin (34.2 mg, 0.130 mmol) were dissolved in chloroform/methanol (1/1; 15 mL). NaOMe (5.2 mg, 0.130 mmol) was added, and the reaction mixture was refluxed for 6 h. The obtained NaCl was removed by filtration through Celite, toluene (10 mL) was slowly added, and the solution was left in an open flask. Orange-brown crystals were obtained after 3 days at room temperature. The crystals were collected and washed with hexane. Yield: 42 mg, 55%.

^{1}H NMR (CDCl$_3$, 300.13 MHz): δ 7.69 (s, 1H, H5 cin), 6.94 (s, 1H, H8 cin), 6.20 (s, 2H, O−CH_2O cin), 5.65−5.58 (m, 2H, Ar-H cym), 5.36−5.33 (m, 2H, Ar-H cym), 4.58 (q, ^3J(H,H) = 7 Hz, 2H, NCH_2CH$_3$), 3.11−3.06 (m, 1H, Ar-CH(CH$_3$)$_2$ cym), 2.35 (s, 3H, Ar-CH_3 cym), 1.48 (t, ^3J(H,H) = 7 Hz, 3H, NCH$_2$CH_3 cin), 1.40 (d, 6H, ^3J(H,H) = 7 Hz, Ar-CH(CH_3)$_2$ cym). IR (cm^{-1}, ATR): 3538, 3436, 2970, 1620, 1517, 1494, 1471, 1461, 1277, 1241, 1159, 1124, 1086, 1034, 938, 899, 882, 868, 850, 812, 787, 747, 700, 666, 648, 610. Anal. Calcd for C$_{22}$H$_{23}$ClN$_2$O$_5$Ru·H$_2$O·0.5C$_7$H$_8$: C, 51.39; H, 4.90; N, 4.70. Found: C, 51.40; H, 4.75; N, 4.74.

Aquation Experiments by Means of NMR Spectroscopy. For aquation studies, **1**−**3** (1−2 mg/mL) were dissolved in D$_2$O and the samples were analyzed by ^{1}H NMR spectroscopy immediately after dissolution and after 18 h.

pK_a Determination. pK_a values were determined by dissolving **1**−**3** in MeOD-d_4/D$_2$O (5/95). The pH values were measured directly in the NMR tubes with an Eco Scan pH6 pH meter equipped with a glass micro combination pH electrode (Orion 9826BN) and calibrated with standard buffer solutions of pH 4.00, 7.00, and 10.00. The pH titration was performed with NaOD (0.4−0.0004% in D$_2$O) and DNO$_3$ (0.4−0.0004% in D$_2$O).

5′-GMP Interaction Study. 5′-GMP binding experiments were carried out by titrating solutions of **1**−**3** (1−2 mg/mL) in D$_2$O with a 5′-GMP solution (10 mg/mL D$_2$O) in 50 μL increments. The reaction was monitored by ^{1}H and ^{31}P{^{1}H} NMR spectroscopy until unreacted 5′-GMP was detected.

Aqueous Stability and Interactions with Human Serum Albumin. *Instrumentation.* Capillary zone electrophoresis (CZE) separations were carried out on an HP[3D] CE system (Agilent, Waldbronn, Germany) equipped with an on-column diode array detector. Detection was carried out either by UV (200 nm) or with an Agilent 7500ce inductively coupled plasma mass spectrometer (ICP-MS) interfaced to the CE system utilizing a CETAC CEI-100 microconcentric nebulizer. For all experiments with UV detection, capillaries of 48.5 cm total length (40 cm effective length; 50 μm i.d.) were used (Polymicro Technologies, Phoenix, AZ); in the case of ICP-MS detection

(Supporting Information), the capillary length was extended to 60 cm. For the hydrolysis studies in water the capillary and sample tray were thermostated at 25 °C, whereas the HSA binding experiments were done at 37 °C. Injections were performed by applying a pressure of 25 mbar for 4 s and a constant voltage of 25 kV. Prior to the first use, the capillary was flushed at 1 bar with 0.1 M HCl, water, 0.1 M NaOH, and again with water (10 min each). Before each injection, the capillary was purged for 2 min with both water and the background electrolyte (BGE). The nebulizer was employed in self-aspiration mode with the sheath liquid closing the electrical circuit and spraying a fine aerosol. The working conditions were daily optimized using a 1 μg L^{-1} tuning solution containing ^{7}Li, ^{89}Y, and ^{205}Tl in 2% HNO$_3$. Doubly charged ions and oxide levels were minimized by using ^{140}Ce and were typically <2.5%. To improve precision and to ensure interday reproducibility, the peak area responses of the two monitored Ru isotopes as well as of the ^{34}S trace were normalized with the total ion current of the internal standard (^{72}Ge). Analyses were only started if a sufficiently stable signal (RSD ^{72}Ge <5%) was attained. The kinetics of the hydrolysis and the binding of the three compounds toward HSA were determined by monitoring the time-dependent changes in the peak area.

Reagents. Sodium hydroxide, sodium chloride, sodium dihydrogen-phosphate, and sodium bicarbonate were obtained from Fluka (Buchs, Switzerland). Disodium hydrogenphosphate was purchased from Riedel-de Haen (Seelze, Germany), and 1,2-dibromoethane and human serum albumin (ca. 99%) were obtained from Sigma-Aldrich (Vienna, Austria). The ICP-MS tuning solution was from Agilent Technologies (Vienna, Austria) and the ^{72}Ge standard from CPI international (Santa Rosa, CA). High-purity water used throughout this study was obtained from a Millipore Synergy 185 UV Ultrapure water system (Molsheim, France).

Sample Preparation. The hydrolysis studies were done in water at 25 °C, and solutions of the Ru complexes 1−3 were analyzed immediately and after 1 h and 1 and 2 days. In order to work at concentrations similar to those used in NMR investigations, 1 mM solutions of the complexes were prepared in water and diluted 1/10 with water before analysis by CZE-ICP-MS. Due to the poor aqueous solubility of the complexes, the dissolution was supported by ultrasonification for 15, 20, and 5 min for 1−3, respectively. For the in vitro protein binding studies, solutions containing 0.1 mM of the ruthenium compound and 0.05 mM of HSA in physiological buffer (25 mM NaHCO$_3$, 4 mM NaHPO$_4$, 100 mM NaCl) were prepared and incubated at 37 °C in order to simulate physiological conditions. The samples were analyzed by CZE-ICP-MS immediately after mixing and after 0.5, 1, and 1.5 h.

In Vitro Anticancer Activity. *Cell Lines and Cell Culture Conditions.* The human nonsmall cell lung carcinoma cell line A549 and colon adenocarcinoma cell line SW480 were kindly provided by Brigitte Marian (Institute of Cancer Research, Department of Medicine I, Medical University of Vienna, Vienna, Austria). CH1 cells (ovarian cancer, human) were a gift from Lloyd R. Kelland (CRC Centre for Cancer Therapeutics, Institute of Cancer Research, Sutton, U.K.). Cells were grown in 75 cm^2 culture flasks (Iwaki/Asahi Technoglass, Gyouda, Japan) in complete medium [Minimum Essential Medium supplemented with 10% heat-inactivated fetal bovine serum, 1 mM sodium pyruvate, 4 mM L-glutamine, and 1% nonessential amino acids (100×)] as adherent monolayer cultures. All media and supplements were purchased from Sigma-Aldrich, Vienna, Austria. Cultures were maintained at 37 °C under a humidified atmosphere containing 5% CO$_2$ and 95% air.

MTT Assay. Cytotoxicity was determined by a colorimetric micro-culture assay (MTT assay, MTT = 3-(4,5-dimethyl-2-thiazolyl)-2,5-diphenyl-2H-tetrazolium bromide, Fluka). For this purpose, cells were harvested from culture flasks by use of trypsin and seeded in 100 μL per well into 96-well plates (Iwaki/Asahi Technoglass, Gyouda,

Japan) in cell densities of 4 × 10^3 (A549), 1.5 × 10^3 (CH1), and 2.5 × 10^3 (SW480) cells per well, respectively. These cell numbers ensure exponential growth of untreated controls throughout drug exposure of treated microcultures. Cells were allowed to adhere and resume proliferation in drug-free complete culture medium for 24 h. Drugs were dissolved in complete medium and appropriately diluted, and instantly 100 μL of the drug dilutions were added per well. After exposure for 96 h at 37 °C and 5% CO$_2$, drug solutions were replaced by 100 μL/well RPMI 1640 culture medium (supplemented with 10% heat-inactivated fetal bovine serum and 4 mM L-glutamine) plus 20 μL/well MTT solution in phosphate-buffered saline (5 mg/mL) and incubated for 4 h. Subsequently, the medium/MTT mixture was removed and the formazan crystals that were formed in vital cells were dissolved in 150 μL of DMSO (dimethyl sulfoxide) per well. Optical densities were measured with a microplate reader (Tecan Spectra Classic) at 550 nm (and a reference wavelength of 690 nm) to yield relative quantities of viable cells as percentages of untreated controls, and 50% inhibitory concentrations (IC$_{50}$) were calculated from concentration−effect curves by interpolation. Calculations are based on at least three independent experiments, each consisting of three replicates per concentration level.

■ RESULTS AND DISCUSSION

The combination of biologically active precursors with metals is a promising strategy to develop new anticancer agents.[7,44−46] In a recent study, the antibacterial quinolone ofloxacin was used as a bidentate chelating ligand to form a Ru(cym) complex.[39] In an attempt to extend the series of compounds the quinolones nalidixic acid and cinoxacin were included into this study. The synthesis of 2 and 3 differs slightly from that of 1, which is obtained by reaction of the precursor [(cym)RuCl(μ-Cl)]$_2$ with ofloxacin and NaOH in MeOH. In contrast, 2 was prepared in chloroform/methanol (1/1) by reaction of the sodium salt of nalidixic acid (nal-Na), due to the commercial availability of the latter (Scheme 1). Compound 3 was synthesized in dry methanol/chloroform (1:1) by addition of sodium methoxide, in order to avoid aquation in the reaction mixture. In all cases, the solvent system was evaporated from the reaction mixture, the crude product was dissolved in dichloromethane, and insoluble NaCl was removed by filtration over Celite. Finally, toluene was added to aid crystallization, which yielded crystals suitable for X-ray diffraction analysis.

The molecular structures of the Ru(cym) complexes 2 and 3 adopt a pseudo-octahedral "piano-stool" geometry, which is typical for this compound class, with ruthenium(II) π-bonded to the p-cymene ring and σ-bonded to a chloride as well as the pyridone and carboxylato oxygen atoms of the chelating quinolone ligands (Figure 3, Table 1, and the Supporting Information). In case of 1 and 3, the Ru atom is located out of the plane of the six-membered chelate ring with Ru−centroid$_{O,O}$−C$_3$ angles of 151.72 and 151.39°, respectively, whereas this kinking is only marginal in the structure of 2 (175.72°). The unit cell of 2

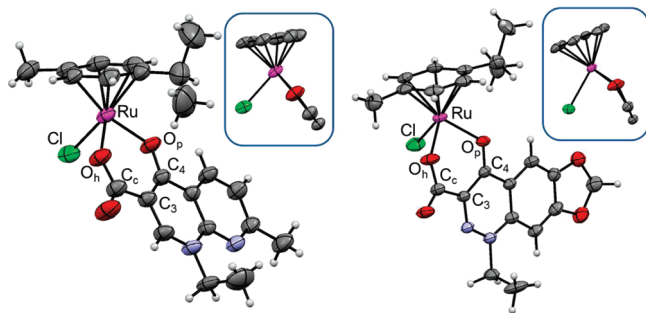**Scheme 1. Synthetic Pathways Applied to Prepare 1−3**
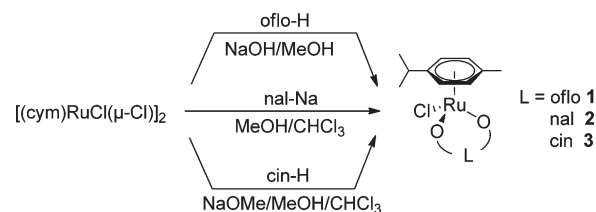
Figure 3. X-ray structures of **2** (left) and **3** (right). The insets show the Ru atom and its coordinated ligands along the plane of the chelating ring system. The thermal ellipsoids are shown at the 50% probability level, and the solvent molecules are omitted for clarity.

Table 1. X-ray Structure Numbering Scheme and Selected Bond Lengths (Å) and Angles (deg) for 1–3

bond length/angle	$1 \cdot 2.8H_2O^{39}$	$2 \cdot C_7H_8$	$3 \cdot H_2O$
Ru–O_p	2.0713(18)	2.0866(19)	2.099(2)
Ru–O_h	2.069(2)	2.070(2)	2.071(2)
Ru–Cl	2.4183(7)	2.4155(10)	2.4153(8)
Ru–$cym_{centroid}$	1.6345(14)	1.6421(15)	1.644(3)
O_p–C_4	1.275(3)	1.273(3)	1.272(3)
C_c–O_h	1.293(3)	1.276(4)	1.280(3)
C_c–O_c	1.232(4)	1.226(4)	1.226(4)
O_h–Ru–O_p	85.30(7)	87.30(8)	84.94(8)
O_p–Ru–Cl	86.92(6)	84.73(7)	84.95(6)
O_h–Ru–Cl	83.73(6)	85.63(8)	86.89(7)

contains a toluene solvate, while **3** cocrystallized with a water molecule, which forms a hydrogen bond with the carbonyl oxygen ($d(O_c–O_{water})$ = 2.917 Å). The Ru–O (Ru–O_p, Ru–O_h) distances in both **2** and **3** as in the structure of **1** range from 2.070 to 2.099 Å, while the Ru–Cl bond is longer (2.415–2.418 Å).[39] In contrast to the case for **1**, the molecules in the structures of **2** and **3** show distinct π-interactions between the quinolone ligands with a more stacked arrangement in the case of **2** as compared to **3** (Supporting Information). The difference Fourier map of **3** showed high residual density peaks which could not be refined due to high disorder and partial occupancy. In the final model, the scattering contributions were removed from all of these diffuse moieties using the SQUEEZE routine in PLATON.[47] A potential solvent-accessible volume of 192.5 Å³ was found, which corresponds to the volume of a small organic molecule such as toluene. ¹H NMR spectroscopy of a crystal sample revealed peaks corresponding to toluene protons, which confirms the used model. The O–Ru–Cl and O–Ru–O angles are between 83.73 and 87.30°. This is in the same range as

Table 2. Stability (%) of Compounds 1–3 as Determined by ¹H NMR and CZE-ICP-MS[a]

compd	¹H NMR[b]	CZE-ICP-MS[b]
1	45	56
2	94	93
3	90	87

[a] The values represent the amount of aqua complex in the solution. [b] Determined after 18 or 24 h incubation.
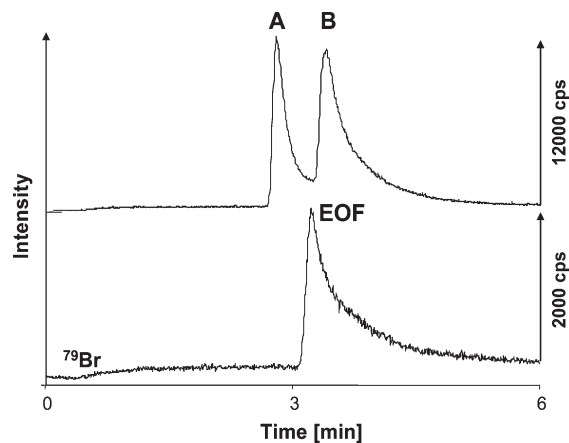

Figure 4. CZE-ICP-MS electropherogram of **1** in water at 25 °C after 1 h. Shown are the traces of ^{102}Ru and ^{79}Br (1,2-dibromoethane as EOF marker). Peak identifications: (**A**) hydrolysis product $[Ru_2(cym)_2(OH)_3]^+$; (**B**) $[Ru(cym)(CO_3)(oflo)]^-$.

for other organometallic ruthenium compounds bearing maltolato ligands, although six-membered chelate ring systems are present in **2** and **3**, whereas five-membered rings are formed with maltol.[20]

Behavior and Stability in Aqueous Solution. Aquation of Ru(arene) complexes is supposed to be an essential step for activation of these compounds.[48] Replacing the chlorido ligand by a water molecule leads to the more reactive aqua species, which can react with biological target molecules. The stability of these aqua species constitutes an essential requirement for pharmaceutical formulation and subsequently also intravenous administration of the substance. The aqueous stability of **1–3** was studied by means of ¹H NMR spectroscopy (Supporting Information) and CZE with spectrophotometric and ICP-MS detection (Table 2). All of the complexes undergo a quick first hydrolytic step by releasing the chlorido ligand and filling the coordination sphere with a water molecule. The stability of the aqua species differs significantly among the three compounds. The aqua species of **1** decomposes slowly over 24 h, resulting in more than 40% of free ligand and the previously reported hydrolytic product $[(cym)Ru(\mu\text{-}OH)_3Ru(cym)]^+$,[16,17,39,49] whereas complexes **2** and **3** were found to possess a higher stability, with only a small fraction of the ligand dissociating. The hydrolyzed fraction was determined by ¹H NMR spectroscopy, comparing the peak area of the aromatic hydrogen atoms of cymene (δ 5.6 and 6.0 ppm) and of the hydroxido-bridged dimer (δ 5.2 and 5.5 ppm), and by a complementary CZE-ICP-MS study. The migration behavior of the two Ru species in the CZE mode is an indication of the charge of the analyte. The electroosmotic flow (EOF), and therewith neutral species in the sample,
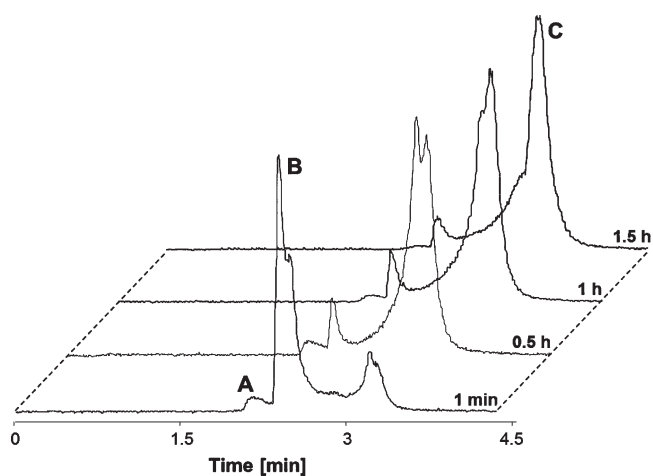
Figure 5. Electropherograms illustrating the kinetics of the interaction of **3** with HSA by monitoring the ^{102}Ru signal at different incubation times, normalized for the migration of **3** and HSA: (**A**) hydrolysis product; (**B**) **3**; (**C**) HSA adduct.

was marked by adding 1,2-dibromoethane (Figure 4). The peak migrating with higher velocity is a positively charged species, most probably the highly stable dinuclear complex $[Ru_2(cym)_2(OH)_3]^+$. The second peak is a negatively charged complex, possibly a carbonate adduct formed by replacement of the chlorido/aqua ligand due to the use of carbonate buffer as BGE. The behavior in aqueous solution was monitored for 2 days, but no additional peaks were detected.

The pK_a values of the aquated Ru(arene) complexes can be determined by stepwise titration of the primary hydrolysis products and analysis by ^{1}H NMR spectroscopy. In this case, fast decomposition of the compounds was observed under alkaline conditions (pD >9). The major products were identified as the released ligand and dimeric $[Ru_2(cym)_2(OD)_3]^+$. Similar observations were made by CZE with spectrophotometric detection. Accordingly, the pK_a values of **1**–**3** can only be estimated from the amount of hydroxido species formed at pD <9, which indicates pK_a values greater than 8.5. This fact confirms that the complexes are present as reactive aqua species under physiological conditions.

Interactions with Human Serum Albumin (HSA) and the DNA Model 5′-GMP. As the most abundant protein in the circulatory system, HSA plays an important role in the binding and delivery of many pharmaceuticals to sites of disease.[50] Ruthenium complexes such as KP1019 and NAMI-A have a high affinity for HSA and other serum proteins,[51,52] which may also contribute to the selective accumulation of ruthenium complexes within tumor cells.[5]

The binding kinetics for the reactions of the three ruthenium compounds with HSA were characterized by CZE-ICP-MS. Electropherograms illustrating the interaction with HSA were recorded immediately after mixing HSA and the complex and after 0.5, 1, and 1.5 h of incubation. Quantification of non-metal-containing proteins by ICP-MS is only feasible via determination of the sulfur content (the amino acids methionine and cysteine are present in many proteins).[53] The results demonstrate that the protein binding occurs rapidly, as indicated by a fast disappearance of the peaks of the unbound complex (Figure 5). The binding kinetics for the ruthenium complexes are rather similar, and 90% of the total ruthenium content is bound to HSA within

Table 3. Cytotoxicity of 1–3 and the Respective Ligands in Human A549, CH1, and SW480 Cancer Cell Lines[a]

	IC$_{50}$ [μM]		
compd	A549	CH1	SW480
oflo-H	>320	>320	>320
1	>320	18 ± 7	225 ± 39
nal-H	>320	>320	>320
2	>320	>320	>320
cin-H	>320	>320	>320
3	>320	>320	>320

[a] Presented are the 50% inhibitory concentrations obtained by the MTT assay. Values are the means ± standard deviations obtained from at least three independent experiments using exposure times of 96 h.
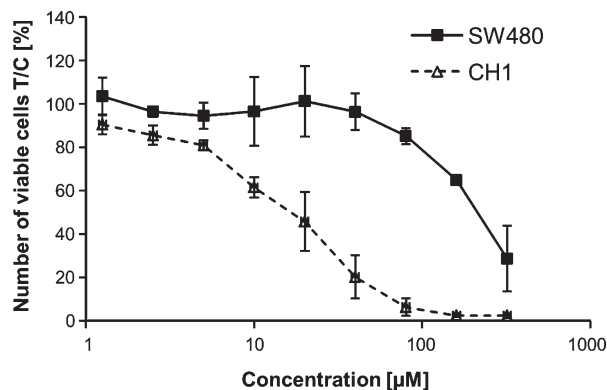

Figure 6. Concentration–effect curves of **1** in human CH1 and SW480 cancer cells. Values were obtained by the MTT assay and are means ± standard deviations from at least three independent experiments using exposure times of 96 h.

20 min (Supporting Information). Only two minor additional peaks which do not correspond to HSA-bound ruthenium but might be attributable to hydrolysis products were observed in the ^{102}Ru trace of the electropherogram (Figure 5).

DNA is one of the potential biological targets for metal-based anticancer drugs. Sadler et al. proposed that Ru complexes, such as $[Ru(\eta^6\text{-biphenyl})Cl(en)]^+$ (see Figure 1), initially bind to the phosphate backbone of DNA, followed by rearrangement to adducts with softer nucleobase donor atoms.[14] Similarly, the interactions between **1** and DNA appear to be of an electrostatic kind initially, but the exact binding mode was not determined.[39] Furthermore, competitive DNA binding experiments revealed that **1** prevents the binding of cisplatin and vice versa, indicating either competition for the same binding sites or major conformational changes of the macromolecule.

In order to determine a possible binding site on DNA, **1**–**3** were reacted with 5′-GMP (used as a model for DNA binding), and these interactions were characterized by means of ^{1}H and ^{31}P{^{1}H} NMR spectroscopy. Aqua species of **1**–**3** are formed immediately after dissolution (see above), and they react quickly and selectively with N7 of 5′-GMP, as indicated by a shift of the H8 proton signal.[54] However, it cannot be excluded that the first interaction occurs via the phosphate backbone, followed by the formation of a covalent bond to N7. Furthermore, the reaction of metal ions with isolated nucleotides is not necessarily comparable to that with the macromolecule DNA.[55]

In Vitro Anticancer Activity. Preliminary cytotoxicity experiments with rat skeletal myoblasts in vitro were previously reported for **1**, but no significant activity was observed.[39] In this study, the biological activities of **1** and of the related quinolone complexes **2** and **3** were studied more in detail. The in vitro anticancer activities of compounds **1**−**3** were determined in human A549 (nonsmall cell lung carcinoma), CH1 (ovarian carcinoma), and SW480 (colon carcinoma) cells by means of the colorimetric MTT assay and compared to the tumor-inhibiting properties of the respective ligands (Table 3, Figure 6). CH1 cells were found to be about 10 times more sensitive to **1** (IC_{50} 18 μM) than the intrinsically resistant SW480 cells (IC_{50} 225 μM), whereas the complex does not show marked activity in A549 cells, which is reflected in an IC_{50} value higher than 320 μM. Moreover, **2** and **3** and all the ligands are inactive in the three cell lines, resulting in IC_{50} values higher than 320 μM. Even though the compounds were shown to be mostly noncytotoxic to the various cell lines, this is not necessarily a negative property for an anticancer drug candidate. The mechanisms of anticancer activity of ruthenium compounds are still not fully understood, and the example of NAMI-A, which is noncytotoxic in vitro but exhibits a high activity against metastases in vivo, has shown that mere IC_{50} values are not a sufficient reason to discard a compound as a potential drug candidate.[2,56,57]

It is known that fluoroquinolone antibiotics are not completely devoid of cytotoxicity in mammalian cells, but due to their rather low potency the side effects of anti-infective treatment are usually tolerable. Although the cytotoxicity of ofloxacin in vitro has been reported to be somewhat lower than that of the more commonly used ciprofloxacin, IC_{50} values in the 10^{-4} molar range in bladder and lung cancer cell lines can be inferred from literature data.[58−60] Still, the cytotoxicity of the organometallic ruthenium complex **1** with ofloxacin in CH1 ovarian cancer cells (IC_{50} = 18 μM) is remarkable and is not paralleled by the two analogues with other quinolone ligands. Which of the structural features account for the observed differences in cytotoxicity remains unclear and requires more extensive structure−activity relationship studies. In analogy to their mechanism of action in bacteria, inhibition of topoisomerase II with the consequence of DNA cleavage is considered the primary cellular effect of ofloxacin and other fluoroquinolones, with prokaryotic topoisomerase being more sensitive by orders of magnitude,[61] and ofloxacin was shown to synergize with the topoisomerase II inhibitor doxorubicin in bladder cancer cells in vitro.[59] However, very little topoisomerase II inhibition was observed in an electrophoretic assay with plasmid DNA, no matter whether ofloxacin or complex **1** was applied, whereas **1** yielded DNA interactions in addition to those observed with ofloxacin alone, most likely as a result of ruthenium binding to DNA.[39]

CONCLUSIONS

In this paper the synthesis of organometallic Ru(cym) complexes with quinolone ligands is reported. In addition to ofloxacin, the antibacterials nalidixic acid and cinoxacin were selected as ligands to prepare **1**−**3**. The structures were established by X-ray diffraction analysis and spectroscopic methods. Furthermore, they were characterized with regard to drug-like properties, such as stability in aqueous solution and reaction with biological target molecules, as well as their tumor-inhibiting potential in a cancer cell line panel. NMR and CZE-ICP-MS studies revealed that the compounds undergo a quick activation step by releasing the chlorido ligand and replacing it with a labile water molecule that allows the compounds to readily interact with target molecules, such as blood proteins and DNA. Compounds **2** and **3** are more stable in aqueous solution than **1**; however, all react with similar kinetics with HSA. The binding to 5′-GMP occurs via its nucleophilic N7, but a preassociation via the negatively charged phosphate backbone of DNA cannot be excluded. In an anticancer assay in vitro, only the ofloxacin derivative **1** was active in relevant concentrations in two cell lines.

Further work will be directed toward the development of new complexes with ligands of the quinolone family in order to elucidate the influence of the structure and substitution pattern of the ligands on the anticancer activity of the compound class. Additional studies will aim to enlighten the potential of such compounds, comprising the influence on cancer cell adhesion, migration, and invasion and the use in alternative anticancer treatment approaches, such as electrochemotherapy.[62−65]

■ ASSOCIATED CONTENT

Ⓢ Supporting Information. Figures, tables, and CIF files giving X-ray diffraction data for compounds **2** and **3**, ^{1}H NMR spectra, the CZE-ICP-MS operational parameters, and HSA binding data. This material is available free of charge via the Internet at http://pubs.acs.org.

■ ACKNOWLEDGMENT

■ REFERENCES

(1) Heffeter, P.; Jungwirth, U.; Jakupec, M.; Hartinger, C.; Galanski, M.; Elbling, L.; Micksche, M.; Keppler, B.; Berger, W. *Drug Res. Upd.* **2008**, *11*, 1–16.

(2) Rademaker-Lakhai, J. M.; Van Den Bongard, D.; Pluim, D.; Beijnen, J. H.; Schellens, J. H. M. *Clin. Cancer Res.* **2004**, *10*, 3717–3727.

(3) Depenbrock, H.; Schmelcher, S.; Peter, R.; Keppler, B. K.; Weirich, G.; Block, T.; Rastetter, J.; Hanauske, A. R. *Eur. J. Cancer* **1997**, *33*, 2404–2410.

(4) Kapitza, S.; Pongratz, M.; Jakupec, M. A.; Heffeter, P.; Berger, W.; Lackinger, L.; Keppler, B. K.; Marian, B. *J. Cancer Res. Clin. Oncol.* **2005**, *131*, 101–110.

(5) Hartinger, C. G.; Zorbas-Seifried, S.; Jakupec, M. A.; Kynast, B.; Zorbas, H.; Keppler, B. K. *J. Inorg. Biochem.* **2006**, *100*, 891–904.

(6) Hartinger, C. G.; Jakupec, M. A.; Zorbas-Seifried, S.; Groessl, M.; Egger, A.; Berger, W.; Zorbas, H.; Dyson, P. J.; Keppler, B. K. *Chem. Biodiversity* **2008**, *5*, 2140–2155.

(7) Hartinger, C. G.; Dyson, P. J. *Chem. Soc. Rev.* **2009**, *38*, 391–401.

(8) Allardyce, C. S.; Dyson, P. J.; Ellis, D. J.; Heath, S. L. *Chem. Commun.* **2001**, 1396–1397.

(9) Scolaro, C.; Bergamo, A.; Brescacin, L.; Delfino, R.; Cocchietto, M.; Laurenczy, G.; Geldbach, T. J.; Sava, G.; Dyson, P. J. *J. Med. Chem.* **2005**, *48*, 4161–4171.

(10) Dyson, P. J. *Chimia* **2007**, *61*, 698–703.

(11) Chatterjee, S.; Kundu, S.; Bhattacharyya, A.; Hartinger, C. G.; Dyson, P. J. *J. Biol. Inorg. Chem.* **2008**, *13*, 1149–1155.

(12) Morris, R. E.; Aird, R. E.; Murdoch Pdel, S.; Chen, H.; Cummings, J.; Hughes, N. D.; Parsons, S.; Parkin, A.; Boyd, G.; Jodrell, D. I.; Sadler, P. J. *J. Med. Chem.* **2001**, *44*, 3616–21.

(13) Chen, H.; Parkinson, J. A.; Parsons, S.; Coxall, R. A.; Gould, R. O.; Sadler, P. J. *J. Am. Chem. Soc.* **2002**, *124*, 3064–3082.

(14) Chen, H.; Parkinson, J. A.; Morris, R. E.; Sadler, P. J. *J. Am. Chem. Soc.* **2003**, *125*, 173–186.

(15) Mendoza-Ferri, M. G.; Hartinger, C. G.; Eichinger, R. E.; Stolyarova, N.; Jakupec, M. A.; Nazarov, A. A.; Severin, K.; Keppler, B. K. *Organometallics* **2008**, *27*, 2405–2407.

(16) Kandioller, W.; Hartinger, C. G.; Nazarov, A. A.; Bartel, C.; Skocic, M.; Jakupec, M. A.; Arion, V. B.; Keppler, B. K. *Chem. Eur. J.* **2009**, *15*, 12283–12291.

(17) Kandioller, W.; Hartinger, C. G.; Nazarov, A. A.; Kuznetsov, M. L.; John, R. O.; Bartel, C.; Jakupec, M. A.; Arion, V. B.; Keppler, B. K. *Organometallics* **2009**, *28*, 4249–4251.

(18) Mendoza-Ferri, M. G.; Hartinger, C. G.; Nazarov, A. A.; Eichinger, R. E.; Jakupec, M. A.; Severin, K.; Keppler, B. K. *Organometallics* **2009**, *28*, 6260–6265.

(19) Nováková, O.; Nazarov, A. A.; Hartinger, C. G.; Keppler, B. K.; Brabec, V. *Biochem. Pharmacol.* **2009**, *77*, 364–374.

(20) Hanif, M.; Henke, H.; Meier, S. M.; Martic, S.; Labib, M.; Kandioller, W.; Jakupec, M. A.; Arion, V. B.; Kraatz, H. B.; Keppler, B. K.; Hartinger, C. G. *Inorg. Chem.* **2010**, *49*, 7953–7963.

(21) Hanif, M.; Schaaf, P.; Kandioller, W.; Hejl, M.; Jakupec, M. A.; Roller, A.; Keppler, B. K.; Hartinger, C. G. *Aust. J. Chem.* **2010**, *63*, 1521–1528.

(22) Kasser, J. H.; Kandioller, W.; Hartinger, C. G.; Nazarov, A. A.; Arion, V. B.; Dyson, P. J.; Keppler, B. K. *J. Organomet. Chem.* **2010**, *695*, 875–881.

(23) Andriole, V. T., Ed. *The Quinolones.*, 3rd ed.; Academic Press: San Diego, CA, 2000; p 517.

(24) Hooper, D., Rubinstein, E., Eds. *Quinolone Antimicrobial Agents.*, 3rd ed.; ASM Press: Washington, DC, 2003; p 485.

(25) Ronald, A. R., Low, D. E., Eds. *Fluoroquinolone Antibiotics*; Birkhäuser: Basel, Switzerland, 2003; p 250.

(26) Kwok, Y.; Sun, D.; Clement, J. J.; Hurley, L. H. *Anti-Cancer Drug Des.* **1999**, *14*, 443–50.

(27) Yu, H.; Kwok, Y.; Hurley, L. H.; Kerwin, S. M. *Biochemistry* **2000**, *39*, 10236–46.

(28) Vilfan, I. D.; Drevensek, P.; Turel, I.; Poklar Ulrih, N. *Biochim. Biophys. Acta, Gene Struct. Expression* **2003**, *1628*, 111–122.

(29) Drevensek, P.; Turel, I.; Poklar Ulrih, N. *J. Inorg. Biochem.* **2003**, *96*, 407–415.

(30) Turel, I. *Coord. Chem. Rev.* **2002**, *232*, 27–47.

(31) Drevensek, P.; Kosmrlj, J.; Giester, G.; Skauge, T.; Sletten, E.; Sepcic, K.; Turel, I. *J. Inorg. Biochem.* **2006**, *100*, 1755–1763.

(32) Drevensek, P.; Ulrih, N. P.; Majerle, A.; Turel, I. *J. Inorg. Biochem.* **2006**, *100*, 1705–1713.

(33) Skyrianou, K. C.; Perdih, F.; Turel, I.; Kessissoglou, D. P.; Psomas, G. *J. Inorg. Biochem.* **2010**, *104*, 161–170.

(34) Mitscher, L. A. *Chem. Rev.* **2005**, *105*, 559–592.

(35) Wohlkonig, A.; Chan, P. F.; Fosberry, A. P.; Homes, P.; Huang, J.; Kranz, M.; Leydon, V. R.; Miles, T. J.; Pearson, N. D.; Perera, R. L.; Shillings, A. J.; Gwynn, M. N.; Bax, B. D. *Nat. Struct. Mol. Biol.* **2010**, *17*, 1152–1153.

(36) Vock, C. A.; Ang, W. H.; Scolaro, C.; Phillips, A. D.; Lagopoulos, L.; Juillerat-Jeanneret, L.; Sava, G.; Scopelliti, R.; Dyson, P. J. *J. Med. Chem.* **2007**, *50*, 2166–2175.

(37) Ang, W. H.; De Luca, A.; Chapuis-Bernasconi, C.; Juillerat-Jeanneret, L.; Lo Bello, M.; Dyson, P. J. *ChemMedChem* **2007**, *2*, 1799–1806.

(38) Mulcahy, S.; Meggers, E., Organometallics as Structural Scaffolds for Enzyme Inhibitor Design. In *Medicinal Organometallic Chemistry*; Jaouen, G., Metzler-Nolte, N., Eds.; Springer: Berlin/Heidelberg, 2010; Vol. 32, pp 141−153.

(39) Turel, I.; Kljun, J.; Perdih, F.; Morozova, E.; Bakulev, V.; Kasyanenko, N.; Byl, J. A. W.; Osheroff, N. *Inorg. Chem.* **2010**, *49*, 10750–10752.

(40) Altomare, A.; Burla, M. C.; Camalli, M.; Cascarano, G. L.; Giacovazzo, C.; Guagliardi, A.; Moliterni, A. G. G.; Polidori, G.; Spagna, R. *J. Appl. Crystallogr.* **1999**, *32*, 115–119.

(41) Sheldrick, G. M. *Acta Crystallogr., Sect. A: Found. Crystallogr.* **2008**, *A64*, 112–122.

(42) Macrae, C. F.; Edgington, P. R.; McCabe, P.; Pidcock, E.; Shields, G. P.; Taylor, R.; Towler, M.; van de Streek, J. *J. Appl. Crystallogr.* **2006**, *39*, 453–457.

(43) Farrugia, L. J. *J. Appl. Crystallogr.* **1997**, *30*, 565.

(44) Debreczeni, J. É.; Bullock, A. N.; Atilla, G. E.; Williams, D. S.; Bregman, H.; Knapp, S.; Meggers, E. *Angew. Chem., Int. Ed. Engl.* **2006**, *45*, 1580–1585.

(45) Nguyen, A.; Vessieres, A.; Hillard, E. A.; Top, S.; Pigeon, P.; Jaouen, G. *Chimia* **2007**, *61*, 716–724.

(46) Ott, I.; Kircher, B.; Bagowski, C. P.; Vlecken, D. H. W.; Ott, E. B.; Will, J.; Bensdorf, K.; Sheldrick, W. S.; Gust, R. *Angew. Chem., Int. Ed. Engl.* **2009**, *48*, 1160–1163.

(47) Van der Sluis, P.; Spek, A. L. *Acta Crystallogr., Sect. A: Found. Crystallogr.* **1990**, *A46*, 194–201.

(48) Peacock, A. F. A.; Sadler, P. J. *Chem. Asian J.* **2008**, *3*, 1890–1899.

(49) Peacock, A. F. A.; Melchart, M.; Deeth, R. J.; Habtemariam, A.; Parsons, S.; Sadler, P. J. *Chem. Eur. J.* **2007**, *13*, 2601–2613.

(50) Timerbaev, A. R.; Hartinger, C. G.; Aleksenko, S. S.; Keppler, B. K. *Chem. Rev.* **2006**, *106*, 2224–2248.

(51) Groessl, M.; Reisner, E.; Hartinger, C. G.; Eichinger, R.; Semenova, O.; Timerbaev, A. R.; Jakupec, M. A.; Arion, V. B.; Keppler, B. K. *J. Med. Chem.* **2007**, *50*, 2185–2193.

(52) Groessl, M.; Hartinger, C. G.; Polec-Pawlak, K.; Jarosz, M.; Keppler, B. K. *Electrophoresis* **2008**, *29*, 2224–2232.

(53) Groessl, M.; Bytzek, A.; Hartinger, C. G. *Electrophoresis* **2009**, *30*, 2720–2727.

(54) Dorcier, A.; Hartinger, C. G.; Scopelliti, R.; Fish, R. H.; Keppler, B. K.; Dyson, P. J. *J. Inorg. Biochem.* **2008**, *102*, 1066–1076.

(55) Zorbas-Seifried, S.; Hartinger, C. G.; Meelich, K.; Galanski, M.; Keppler, B. K.; Zorbas, H. *Biochemistry* **2006**, *45*, 14817–14825.

(56) Sava, G.; Capozzi, I.; Clerici, K.; Gagliardi, G.; Alessio, E.; Mestroni, G. *Clin. Exp. Metastasis* **1998**, *16*, 371–379.

(57) Sava, G.; Gagliardi, R.; Cocchietto, M.; Clerici, K.; Capozzi, I.; Marrella, M.; Alessio, E.; Mestroni, G.; Milanino, R. *Pathol. Oncol. Res.* **1998**, *4*, 30–36.

(58) Seay, T. M.; Peretsman, S. J.; Dixon, P. S. *J. Urol.* **1996**, *155*, 757–762.

(59) Kamat, A. M.; DeHaven, J. I.; Lamm, D. L. *Urology* **1999**, *54*, 56–61.

(60) Chen, C.-Y.; Chen, Q.-Z.; Wang, X.-F.; Liu, M.-S.; Chen, Y.-F. *Transition Met. Chem.* **2009**, *34*, 757–763.

(61) Yamashita, Y.; Ashizawa, T.; Morimoto, M.; Hosomi, J.; Nakano, H. *Cancer Res.* **1992**, *52*, 2818–22.

(62) Bicek, A.; Turel, I.; Kanduser, M.; Miklavcic, D. *Bioelectrochemistry* **2007**, *71*, 113–117.

(63) Sersa, G.; Miklavcic, D.; Cemazar, M.; Rudolf, Z.; Pucihar, G.; Snoj, M. *Eur. J. Surg. Oncol.* **2008**, *34*, 232–40.

(64) Hudej, R.; Turel, I.; Kanduser, M.; Scancar, J.; Kranjc, S.; Sersa, G.; Miklavcic, D.; Jakupec, M. A.; Keppler, B. K.; Cemazar, M. *Anticancer Res.* **2010**, *30*, 2055–2063.

(65) Kljun, J.; Petricek, S.; Zigon, D.; Hudej, R.; Miklavcic, D.; Turel, I. *Bioinorg. Chem. Appl.* **2010**, Article ID 183097.

2.4. **Intracellular protein binding patterns of the anticancer ruthenium drugs KP1019 and KP1339**

Heffeter P.[a], Boeck K.[b], Atil B.[a], Hoda M.A.R.[a], Koerner W.[c], Bartel C.[d], Jungwirth U.[a], Keppler B.K.[d], Micksche M.[a], Berger W.[a]

[a] Department of Medicine I, Institute of Cancer Research, Medical University of Vienna,
Borschkegasse 8a, 1090 Vienna, Austria

[b] Division of Analytical Chemistry, Department of Chemistry, University of Natural Resources and Applied Life Sciences, BOKU, Vienna, Austria

[c] Institute for Geological Sciences, University of Vienna, Vienna, Austria

[d] Institute of Inorganic Chemistry, University of Vienna, Waehringer Strasse 42, 1090 Vienna, Austria

ORIGINAL PAPER

Intracellular protein binding patterns of the anticancer ruthenium drugs KP1019 and KP1339

**Petra Heffeter · Katharina Böck · Bihter Atil · Mir Ali Reza Hoda ·
Wilfried Körner · Caroline Bartel · Ute Jungwirth · Bernhard K. Keppler ·
Michael Micksche · Walter Berger · Gunda Koellensperger**

Abstract The ruthenium compound KP1019 has demonstrated promising anticancer activity in a pilot clinical trial. This study aims to evaluate the intracellular uptake/binding patterns of KP1019 and its sodium salt KP1339, which is currently in a phase I–IIa study. Although KP1339 tended to be moderately less cytotoxic than KP1019, IC_{50} values in several cancer cell models revealed significant correlation of the cytotoxicity profiles, suggesting similar targets for the two drugs. Accordingly, both drugs activated apoptosis, indicated by caspase activation via comparable pathways. Drug uptake determined by inductively coupled plasma mass spectrometry (ICP-MS) was completed after 1 h, corresponding to full cytotoxicity as early as after 3 h of drug exposure. Surprisingly, the total cellular drug uptake did not correlate with cytotoxicity. However, distinct differences in intracellular distribution patterns suggested that the major targets for the two ruthenium drugs are cytosolic rather than nuclear. Consequently, drug–protein binding in cytosolic fractions of drug-treated cells was analyzed by native size-exclusion chromatography (SEC) coupled online with ICP-MS. Ruthenium–protein binding of KP1019- and KP1339-treated cells distinctly differed from the platinum binding pattern observed after cisplatin treatment. An adapted SEC-SEC-ICP-MS system identified large protein complexes/aggregates above 700 kDa as initial major binding partners in the cytosol, followed by ruthenium redistribution to the soluble protein weight fraction below 40 kDa. Taken together, our data indicate that KP1019 and KP1339 rapidly enter tumor cells, followed by binding to larger protein complexes/organelles. The different protein binding patterns as compared with those for cisplatin suggest specific protein targets and consequently a unique mode of action for the ruthenium drugs investigated.

Keywords Ruthenium · Size exclusion chromatography–inductively coupled plasma mass spectrometry · Drug uptake · Intracellular distribution · Anticancer

P. Heffeter · B. Atil · M. A. Reza Hoda · U. Jungwirth ·
M. Micksche · W. Berger (✉)
Department of Medicine I,
Institute of Cancer Research,
Medical University Vienna,
Borschkegasse 8a,
1090 Vienna, Austria
e-mail: walter.berger@meduniwien.ac.at

K. Böck · G. Koellensperger
Division of Analytical Chemistry,
Department of Chemistry,
University of Natural Resources and Applied Life Sciences,
BOKU, Vienna, Austria

W. Körner
Institute for Geological Sciences,
University of Vienna,
Vienna, Austria

C. Bartel · B. K. Keppler
Institute of Inorganic Chemistry,
University of Vienna,
Vienna, Austria

Abbreviations

GSH	Glutathione
HMW/LMW	Ruthenium-content ratio between the high molecular weight fraction and the low molecular weight fraction
ICP-MS	Inductively coupled plasma mass spectrometry
JC-1	5,5′,6,6′-Tetrachloro-1,1′,3,3′-tetraethylbenzimidazolylcarbocyanine iodide

🖉 Springer

KP1019	Indazolium *trans*-[tetrachlorobis (1*H*-indazole)ruthenate(III)]
KP1339	Sodium *trans*-[tetrachlorobis(1*H*-indazole) ruthenate(III)]
PARP	Poly(ADP-ribosyl)polymerase
PBS	Phosphate-buffered saline
SEC	Size-exclusion chromatography
Tris	Tris(hydroxymethyl)aminomethane

Introduction

Besides surgery and radiation therapy, chemotherapy is still one of the major therapy options for treatment of human malignancies. Platinum-containing drugs such as cisplatin and oxaliplatin are frequently used in diverse therapeutic regimens [1, 2]. However, owing to often observed complications, including severe side effects or ineffectiveness through drug resistance, the need for better chemotherapeutics still exists [3]. Ruthenium compounds belong to the most promising candidates of non-platinum-containing metal complexes for cancer therapy. Recently, indazolium *trans*-[tetrachlorobis(1*H*-indazole)ruthenate (III)] (KP1019) demonstrated exciting anticancer activity in a pilot clinical phase I study with disease stabilization for 8–10 weeks in five of six treated patients [2, 4]. Notably, only mild treatment-related toxicities were observed in this study, encouraging further clinical development of KP1019 [4]. On the basis of its higher water solubility, the sodium salt of KP1019, sodium *trans*-[tetrachlorobis(1*H*-indazole)ruthenate(III)] (KP1339), has been selected as a lead candidate for further clinical development. With regard to the mode of action, KP1019 has been suggested to induce oxidative stress and DNA damage comparable to that for other metal drugs such as cisplatin [5]. Moreover, treatment with KP1019 led to apoptosis via the mitochondrial pathway [6]. Profound depolarization of the mitochondrial membrane potential was observed after 24-h incubation with KP1019 in this study, indicating that there might be additional targets involved. KP1019 is known to strongly bind to serum proteins, including albumin and transferrin [4, 7, 8]. Consequently, it has been postulated that this serum protein binding is important for the drug accumulation into the tumor, probably involving the transferrin pathway [4, 7]. As cancer cells generally express elevated levels of transferrin receptor to serve their higher need for iron [9], KP1019 was expected to accumulate preferentially in tumor tissues to exert its anticancer activity. This hypothesis of "transferrin-mediated tumor targeting" is supported by the low toxicity of KP1019 observed in the clinical

phase I trial [4]. Moreover, the binding of KP1019 to serum proteins hampered P-glycoprotein-mediated KP1019 efflux, making this ruthenium drug interesting for treatment of multidrug-resistant tumor types [10].

Numerous studies have focused on the interaction of KP1019 with serum proteins, and the intracellular fate of KP1019 and KP1339 after uptake into tumor cells is widely unknown. Thus, the aim of this study was to gain more insight into the pharmacokinetics and intracellular distributions of KP1019 and KP1339, which should help to identify additional targets of these promising ruthenium compounds.

Materials and methods

Drugs

KP1019 and KP1339 were synthesized at the Institute of Inorganic Chemistry, University of Vienna, Austria, and by ChemCon (Freiburg, Germany), respectively, as previously reported [11, 12]. For in vitro studies, the compounds were dissolved in dimethyl sulfoxide and diluted into culture media at the concentrations indicated (dimethyl sulfoxide concentrations were always below 1%). Eluents were prepared from sodium hydroxide (pure pellets, Acros Organics, Geel, Belgium), hydrochloric acid (p.a. Merck, Darmstadt, Germany), tris(hydroxymethyl)aminomethane (Tris; p.a. Merck), and water purified in a water purification system (more than 18 MΩ cm resistance; HQ, USF, Vienna, Austria). HNO_3 was prepared by double subboiling distillation (Milestone-MLS, Leutkirch, Germany) of analytical reagent grade acid (Merck). H_2O_2 (ultrapure grade) was purchased from Merck. All other substances were from Sigma-Aldrich (St. Louis, MO, USA).

Cell culture

The cervical carcinoma-derived human cell line KB-3-1 was generously donated by D.W. Shen (Bethesda, MD, USA) [13]. The primary hepatocellular carcinoma cell lines HCC1.1 and HCC1.2 had been previously established at the Institute of Cancer Research, Vienna [14]. The mesothelioma cell model P31 and its respective cisplatin-resistant subline P31/cis were generously donated by K. Grankvist (Umeå University, Sweden) [15]. The colon carcinoma cell line HCT116 was generously donated by B. Vogelstein (Johns Hopkins University, Baltimore, MD, USA) [16]. The primary mesothelioma cell line VMC was established from patient material at the Institute of Cancer Research, Vienna. Additionally, the hepatocellular carcinoma cell line Hep3B and the colon carcinoma cell line SW480 (both from American Type Culture Collection,

Manassas, VA, USA) were used. SW480 cells were grown in minimal essential medium, HCT116 cells in McCoy's culture medium, and P31 cells in Eagle's minimal essential medium. All other cell lines were grown in RMPI 1640 supplemented with 10% fetal bovine serum. Cultures were regularly checked for *Mycoplasma* contamination.

Cytotoxicity assays

Cells were plated (2×10^3 cells in 100 µl per well) in 96-well plates and allowed to recover for 24 h. Drugs were added in another 100 µl of growth medium and cells were exposed for the time periods indicated. For pulsing experiments, test medium was replaced with fresh (drug-free) culture medium after the exposure times indicated. After 72-h drug treatment, the proportion of viable cells was determined by 3-(4,5-dimethylthiazol-2-yl)-2,5-diphenyltetrazolium bromide assay following the manufacturer's recommendations (EZ4U kit, Biomedica, Vienna, Austria).

Total ruthenium uptake levels

Cell lines derived from diverse cell models (1×10^5 per well) were exposed to 50 µM KP1019 or KP1339 for 60 min at 37 °C. After three washes with ice-cold phosphate-buffered saline (PBS), cells were lysed by incubation at room temperature in 400 µl tetramethylammonium hydroxide. Lysates were diluted in 0.6 N HNO_3 and ruthenium concentrations were determined by inductively coupled plasma mass spectrometry (ICP-MS) using an ELAN 6100 (PerkinElmer Sciex) at the Institute for Geological Sciences, University of Vienna. The values represent means of at least three independent experiments. As unspecific binding to cell culture plastic has been shown for KP1019 [17], the results were corrected for ruthenium levels of a blank well containing no cells.

Preparation of cytosolic versus nucleic fractions

KB-3-1 cells (2×10^6) were seeded in a T25 culture flask and allowed to attach for 24 h. Drugs were added in 5 ml of fresh growth medium. Cells were collected by trypsinization, washed twice with ice-cold PBS, and counted. For lysis, cell pellets were resuspended in lysis buffer containing 50 mM Tris–HCl, 300 mM NaCl, 0.5% Triton X-100. Additionally, 1 mM phenylmethylsulfonyl fluoride and 25 µl/ml "complete" protease inhibitor mix (Roche, Mannheim, Germany) were added to the buffer immediately before use. Proper cell lysis was checked microscopically by trypan blue staining. After 5-min centrifugation (14,000 rpm) at 4 °C, supernatant (cytosolic fraction) was separated from the pellet (nucleic fraction)

and fractions were stored at −80 °C. Protein concentrations of the cytosolic fractions were determined using a micro bicinchoninic acid protein assay reagent kit (Pierce Biotechnology, Rockford, IL, USA).

Ruthenium levels in cytosolic and nucleic fractions

A 100-µl volume of cytosolic fraction and the full nucleic fraction of each experiment were digested with 2 ml 20% HNO_3, 1 ml H_2O, and 200 µl H_2O_2 in a high-performance microwave (MLS 1200 microwave, MLS, Leutkirch, Germany). Ruthenium levels were determined by ICP-MS. The quadrupole-based system used for these measurements was equipped with a dynamic reaction cell (ELAN DRC-II, PerkinElmer Sciex, Woodbridge, ON, Canada). Oxygen (purity 4.5, Linde Gas, Vienna, Austria) was used as the reaction gas. The values represent means of at least two independent experiments and were adjusted to the previously determined cell numbers. The values (arbitrary units) were expressed relative to the total ruthenium levels (cytosolic + nucleic) at 1-h exposure (50 µM) set arbitrarily as 1.

Size-exclusion chromatography–inductively coupled plasma mass spectrometry

Size-exclusion chromatography (SEC) was combined with ICP-MS detection using the ELAN DRC-II (PerkinElmer Sciex, Woodbridge, ON, Canada). The metal-free chromatographic system consisted of an AS 50 autosampler (including a custom-made temperature-control device), a GP 40 gradient pump, and the Chromeleon Chromatography Management System (version 6.40), all from Dionex (Sunnyvale, CA, USA). The injection volume was 25 µl. Injected samples were filtered in-line using a 0.45-µm PEEK filter located in front of the column. A BioSuite™ 125 column (300 mm × 4.6 mm UHR SEC, 4-µm particle diameter) from Waters (Milford, MA, USA) was used as the stationary phase for SEC. The eluent containing 150 mM NaCl and 20 mM Tris–HCl, pH 7.4 was delivered at a flow rate of 350 µl/min. The SEC eluent was transferred directly to the ICP-MS introduction system consisting of a perfluoroalkoxy nebulizer and a cyclonic spray chamber. The values were assessed from four independently prepared samples.

The SEC column utilized for these experiments provided a size-exclusion limit of 150 kDa; hence, proteins larger than 150 kDa could not be separated and eluted in the void volume of the column at 6 min. A retention time of 8 min corresponded to the size range 80–60 kDa. Low molecular weight compounds as, e.g., peptides or metallothioneins, had a retention time of more than 10 min. A retention time of 13–14 min corresponded to small molecules (e.g. inorganic salts) [18]. The low molecular weight

fraction was defined as the integral of the ruthenium response from 11 to 14 min in the SEC chromatogram.

Tandem size-exclusion chromatography–inductively coupled plasma mass spectrometry

SEC-SEC-ICP-MS was performed by coupling two separation columns in-line in combination with ICP-MS detection using the ELAN DRC-II (PerkinElmer Sciex, Woodbridge, ON, Canada). The first column (BioSep-SEC-S 4000, 300 mm × 7.8 mm, 5 μm particle diameter) had an exclusion limit of 2,000 kDa and the second had a separation range from 66 to 670 kDa (BioSep-SEC-S 3000, 300 mm × 7.8 mm, 5-μm particle diameter), both from Phenomenex (Phenomenex, Aschaffenburg, Germany). The flow rate applied was 1 ml/min (injection volume 25 μl).

Cell fractionation

KB-3-1 cells (10^7) were seeded in a T150 culture flask and allowed to attach for 24 h. KP1019 or KP1339 was added in 20 ml of fresh growth medium. After 3-h drug incubation, cells were collected by trypsinization, washed twice with ice-cold PBS, and counted. After another centrifugation step, cell pellets were resuspended in Douce buffer containing 10 mM Tris–HCl pH 7.6 and 0.5 mM $MgCl_2$. Additionally, 1 mM phenylmethylsulfonyl fluoride and 25 μl/ml "complete" protease inhibitor mix (Roche, Mannheim, Germany) were added to the buffer immediately before use. After 15-min incubation on ice, cells were lysed by Douce homogenization. Total cell lysis was checked microscopically by trypan blue staining. After addition of NaCl (final concentration 150 mM), homogenates were centrifuged for 5 min at 3,500g. Pellets were separated from supernatants, washed once, and stored at −80 °C (fraction I). The supernatants were supplemented with EDTA (final concentration 5 mM) and centrifuged at 100,000g for 1 h at 4 °C. The resulting supernatant was stored at −80 °C (fraction II). The pellets (fraction III) were resuspended in lysis buffer containing 50 mM Tris–HCl, 300 mM NaCl, 0.5% Triton X-100, 1 mM phenylmethylsulfonyl fluoride, and 25 μl/ml "complete" protease inhibitor mix (Roche, Mannheim, Germany). Also this fraction was stored at −80 °C. Protein concentrations of the cytosolic fractions were determined using a micro bicinchoninic acid protein assay reagent kit (Pierce Biotechnology, Rockford, IL, USA).

4′,6-Diamidino-2-phenylindole staining

KB-3-1 cells (1×10^5 per well) were plated in six well plates and after 24 h of recovery were treated with various concentrations of KP1019 and KP1339. After 24 h, cells were harvested, cytospins were prepared, and apoptosis was evaluated by staining with 4′,6-diamidino-2-phenylindole (DAPI) containing antifade solution (Vector Laboratories, Burlingame, CA, USA). The nuclear morphology of cells was examined with a Leica DMRXA fluorescence microscope (Leica Mikroskopie and System, Wetzlar, Germany) equipped with appropriate epifluorescence filters and a Cohu charge-coupled-device camera. For each concentration at least two slides were evaluated, whereby at least 250 nuclei per experimental group were analyzed.

Western blot analyses

After 24 h of drug exposure, proteins were isolated, resolved by sodium dodecyl sulfate polyacrylamide gel electrophoresis, and transferred onto a poly(vinylidene difluoride) membrane for western blotting as described in [19, 20]. The anti-poly(ADP-ribosyl)polymerase (PARP), cleaved PARP, caspase 3, caspase 9, caspase 7, and cleaved caspase 7 antibodies (all polyclonal rabbit) from an apoptosis sampler kit (Cell Signalling Technology, Beverly, MA, USA) and the anti-β-actin monoclonal mouse AC-15 (Sigma) were used in a 1:1,000 dilution. Additionally, horseradish peroxidase labeled antibodies from Santa Cruz Biotechnology were used at working dilutions of 1:10,000.

Mitochondrial membrane potential detection

KB-3-1 cells (1×10^6 per well) were seeded in T25 flasks. After 24-h recovery, cells were treated with various concentrations of KP1019 and KP1339 for another 24 h. Cell staining was performed as published [21]. Cell suspensions were incubated with 10 μl/ml of the fluorescent dye 5,5′,6,6′-tetrachloro-1,1′,3,3′-tetraethylbenzimidazolylcarbocyanine iodide (JC-1; mitochondrial membrane potential detection kit; Stratagene, La Jolla, CA, USA) in full culture medium for 10 min at 37 °C. At the end of the incubation period, cells were washed twice with cold PBS, resuspended in PBS, and analyzed by flow cytometry using a Calibur fluorescence-activated cell sorting instrument (Becton-Dickinson, Palo Alto, CA, USA).

Statistical analysis

Linear regression analyses were performed using GraphPad Prism 4.0 (GraphPad Software, La Jolla, CA, USA).

Results

Exposure-time dependency of cytotoxicity

The anticancer activity of KP1339 was compared with that of KP1019 after 72 h in several cancer cell lines (Table 1).

Table 1 IC$_{50}$ values after 72 h

	KP1019 (μM)		KP1339 (μM)	
	IC$_{50}$	SD	IC$_{50}$	SD
KB-3-1	99.3	29.3	135.3	25.8
HCC1.1	108.1	56.0	148.9	42.1
HCC1.2	82.9	0.2	88.3	26.4
Hep3B	98.4	25.3	143.1	15.3
SW480	58.2	21.4	110.2	31.7
HCT116	36.6	17.0	34.7	3.6
P31	151.2	12.9	148.0	9.2
P31/cis	147.0	8.0	150.0	0.8
VMC	56.4	9.6	77.5	6.3

SD standard deviation

For both drugs, the colon cancer cell line HCT116 was found to be most responsive, whereas the mesothelioma cell model P31 and P31/cis displayed the highest resistance. In general, KP1339 tended to be less cytotoxic than KP1019, with a mean IC$_{50}$ values of 93.1 μM for KP1019 and 115.1 μM for KP1339 over all cell lines tested. However, linear regression analysis of the respective IC$_{50}$ values revealed significant correlation of the anticancer activity of KP1019 and KP1339 ($p = 0.0035$). With regard to exposure time dependency, the ruthenium drugs were tested by pulsing experiments using KB-3-1 cells. To this end, KP1019- and KP1339-containing test mediums were replaced with fresh culture medium after 1-, 2-, and 3-h exposure for a total experimental time of 72 h (Fig. 1). Again KP1019 displayed moderately enhanced cytotoxicity at all time points tested. With regard to the exposure-time dependency, as little as 1 h of drug contact induced significant anticancer activity, with IC$_{50}$ values of 136 μM for KP1019 and 182 μM for KP1339. Moreover, 3 h of drug contact was found to be sufficient for about 95% anticancer activity (3-h IC$_{50}$ values of KP1019 and KP1339 were 85.0 and 117.6 μM, respectively, versus 82.6 and 108.9 μM after 72 h).

Comparison of KP1019 and KP1339 drug uptake

To evaluate whether the higher cytotoxicity of KP1019 (compared with KP1339) might be based on enhanced drug uptake, total intracellular ruthenium levels were determined by ICP-MS after 1-h incubation. In general, drug uptake was detectable at levels of nanograms of ruthenium per 10^5 cells for both drugs. In most cell lines tested, KP1019 accumulation was up to twofold higher than KP1339 uptake (mean of all cell lines, 4.4 ng ruthenium per 10^5 cells for KP1019 vs. 2.3 ng ruthenium per 10^5 cells for KP1339; Table 2). Comparable to the vitality assays, linear regression analysis revealed significant correlation of
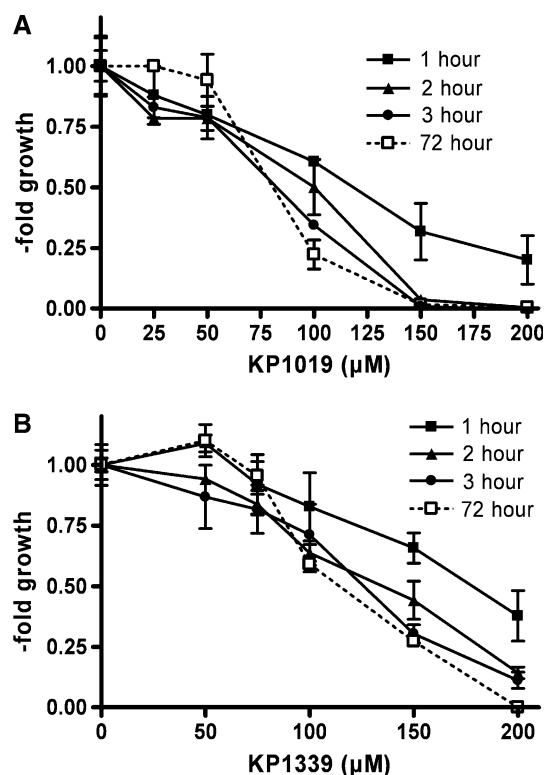

Fig. 1 Exposure-time dependency of KP1019 and KP1339 cytotoxicity. Pulsing experiments were performed in KB-3-1 cells by replacing **a** KP1019- and **b** KP1339-containing test mediums after 1, 2, and 3 h with fresh culture medium. Following a total experimental time of 72 h, cell vitality was determined by 3-(4,5-dimethylthiazol-2-yl)-2,5-diphenyltetrazolium bromide assays. The values given are means and standard deviations (SD) of three independent experiments in triplicate

Table 2 Total uptake after 1-h exposure using 50 μM of the respective drug

	KP1019		KP1339	
	Ru/10^5 cells (ng)	±SD	Ru/10^5 cells (ng)	±SD
KB-3-1	5.3	0.56	3.0	0.06
HCC1.1	7.7	2.55	5.1	0.96
HCC1.2	4.4	0.35	3.1	0.46
Hep3B	7.5	0.43	3.2	0.14
SW480	2.6	0.15	2.4	0.40
HCT116	3.0	0.3	1.4	1.5
P31	2.4	0.66	0.24	0.36
P31/cis	1.9	0.35	ND	–
VMC	5.59	0.51	1.97	0.15

ND below detection limit

KP1019 and KP1339 uptake ($p = 0.049$). However, no correlation between total cellular drug uptake and cytotoxicity was found in the case of both drugs (KP1019 $p = 0.76$ and KP1339 $p = 0.81$), indicating that mere drug

Fig. 2 Comparison of the apoptosis-inducing potential of KP1019 with KP1339. **a** Induction of apoptosis in KB-3-1 cells was determined after treatment for 24 h. 4′,6-Diamidino-2-phenylindole (DAPI) staining of nuclei is shown in untreated controls and cells treated with the drug concentrations indicated. **b** Morphological features of 300–500 nuclei of at least two slides for each concentration were analyzed by DAPI staining. The percentages of normal, mitotic, and apoptotic/necrotic nuclei at the concentrations indicated are shown. **c** Apoptosis-induced cleavage of poly(ADP-ribosyl)polymerase (PARP), caspase 7, and caspase 3 in KB-3-1 and Hep3B cells after 24-h treatment was determined via western blot. The antibodies used are described in "Materials and methods"
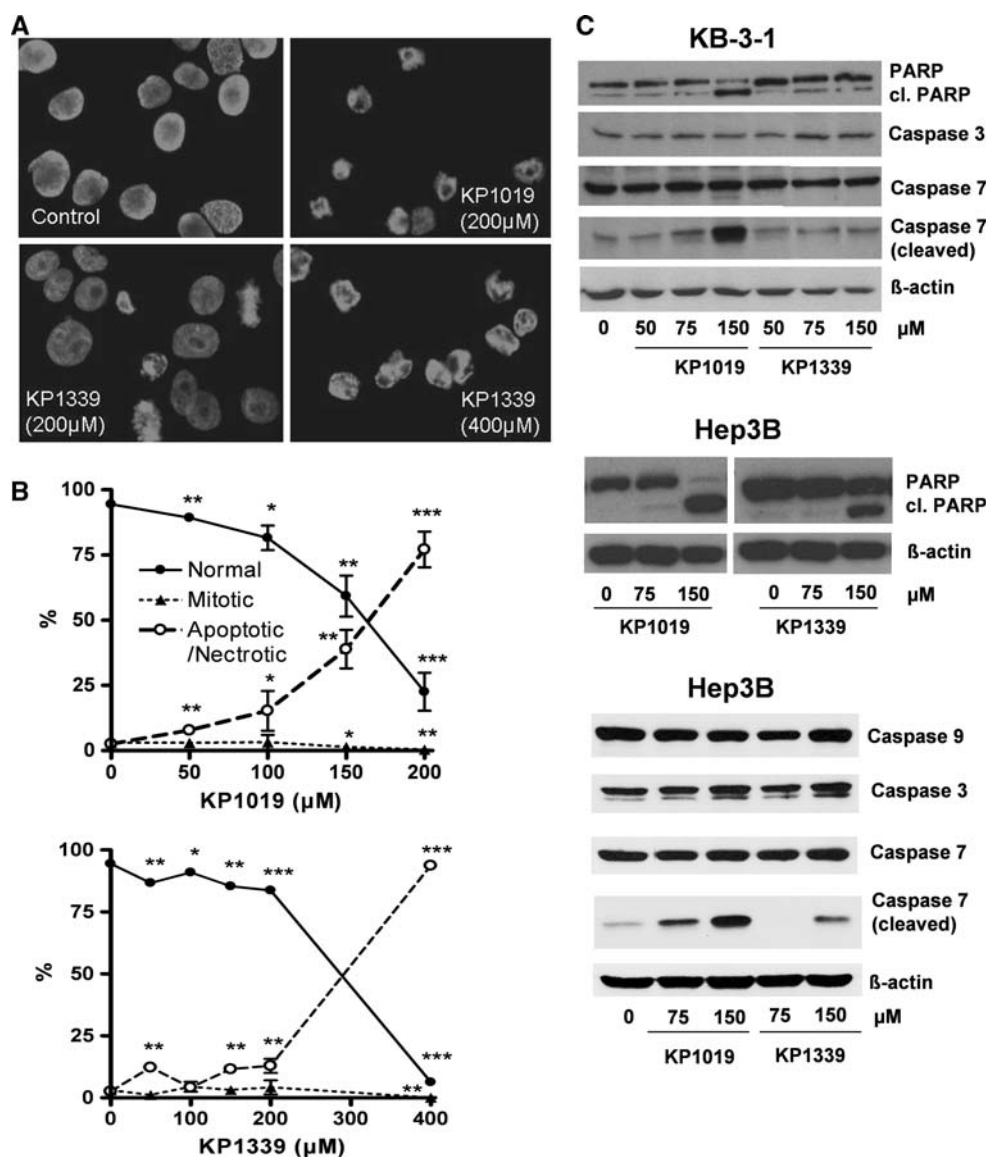
accumulation is not decisive for the exerted level of cytotoxicity.

Comparison of KP1019- and KP1339-induced apoptosis

Next, it was tested whether the difference in activity of KP1019 and KP1339 is accompanied by differences in the induction of apoptosis. To this end KB-3-1 cells were treated with increasing concentrations of KP1019 and KP1339 for 24 h (Fig. 2a, b). Pronounced apoptosis induction was observed after treatment with 150 μM (38.9%) and 200 μM (77.1%) KP1019. In accordance with the cytotoxicity and uptake data, apoptosis levels induced by KP1339 were distinctly lower at these concentrations (11.5 and 12.9%, respectively). Treatment with 400 μM KP1339 strongly increased the proportion of apoptotic cells to 93.7%. Additionally, apoptotic body formation after KP1019 and KP1339 treatment was accompanied with an increase in cleavage of caspase 7 as well as of the caspase substrate PARP, another indicator for apoptotic cell death (Fig. 2c). In contrast to reports on SW480 cells [6], no caspase 3 cleavage was observed.

As a next step, the mitochondrial integrity was determined by JC-1 staining after 24-h treatment with KP1019 and KP1339 (Fig. 3a). A detectable increase (from 4.57 to 8.33%) of cells with depolarized mitochondria was observed using only 100 μM KP1019. Treatment with 200 μM KP1019 resulted in profound mitochondrial depolarization (78.72%). KP1339 was about half as active as KP1019, with 7.03% of cells with depolarized mitochondria at 200 μM and 65.67% of cells at 400 μM.
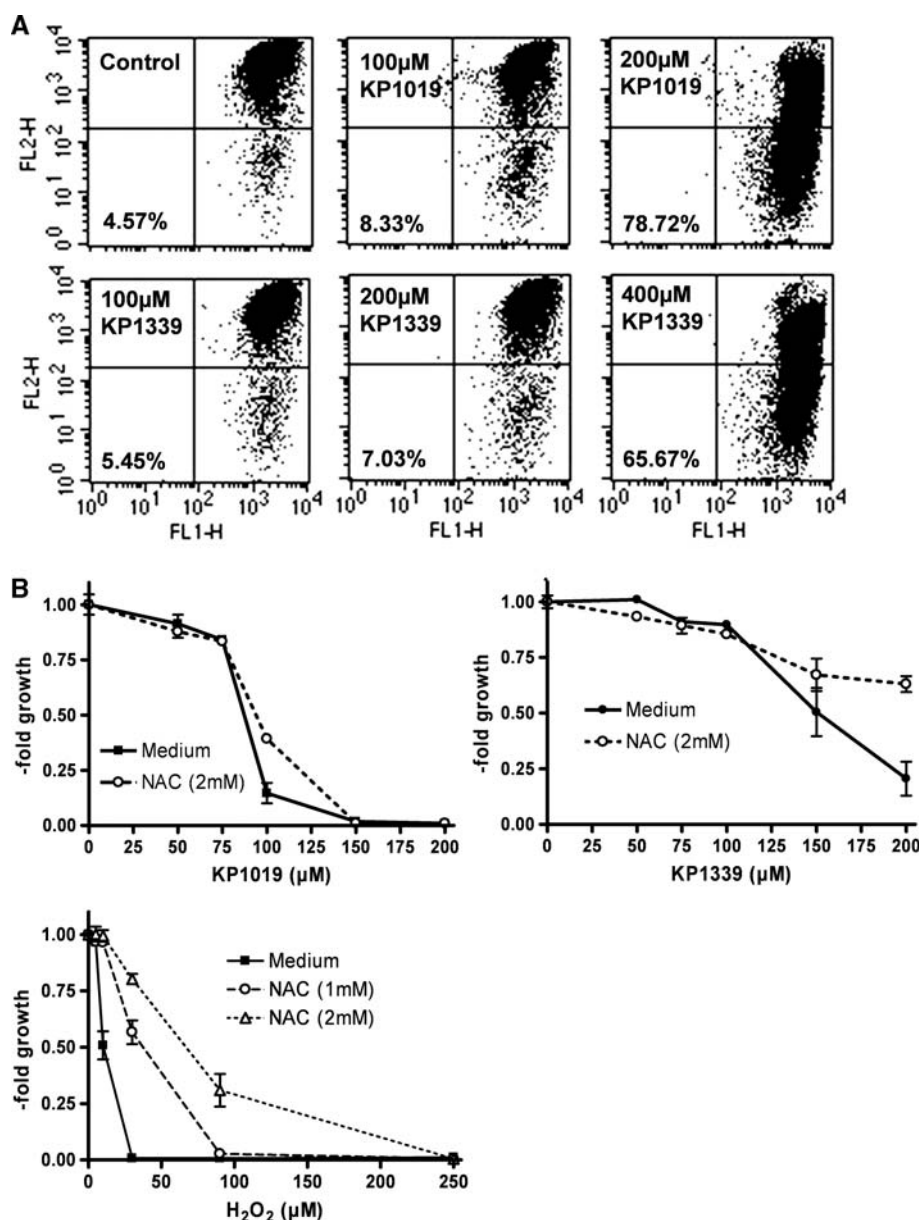
Fig. 3 Characterization of KP1019 and KP1339 apoptosis. **a** Loss of mitochondrial membrane potential after 24-h treatment was determined by 5,5′,6,6′-tetrachloro-1,1′,3,3′-tetraethylbenzimidazolylcarbocyanine iodide (JC-1) staining. Increase of the green fluorescent apoptotic populations of KB-3-1 cells at the drug concentrations indicated (cells in the lower right field) are indicated (30,000 events were analyzed in total per group). **b** Effects of 30-min pretreatment with the radical scavenger N-acetylcysteine (NAC) on the anticancer activity of KP1019, KP1339, and H_2O_2 (positive control) were analyzed after 72-h drug exposure by an EZ4U kit

Earlier studies indicated that oxidative stress might be involved in apoptosis induction by KP1019 [5, 6]. Thus, the impact of the radical scavenger N-acetylcysteine (NAC) on the cytotoxic activity of KP1019 and KP1339 was compared. Protective NAC effects were observed for both drugs at concentrations in their IC50 range (Fig. 3b). However, this effect was significantly less pronounced as compared with that for H_2O_2, the positive control for oxidative stress production.

Intracellular distribution of KP1019 and KP1339

The intracellular fate of the ruthenium compounds tested is still widely unknown. Figure 4 shows the ruthenium distribution between cytoplasm and nucleic cell fractions after 1-, 3-, and 6-h treatment with 50, 75, and 150 μM KP1019 and KP1339, respectively. In accordance with already published observations [10], KP1019 and KP1339 were significantly and completely accumulated in tumor cells
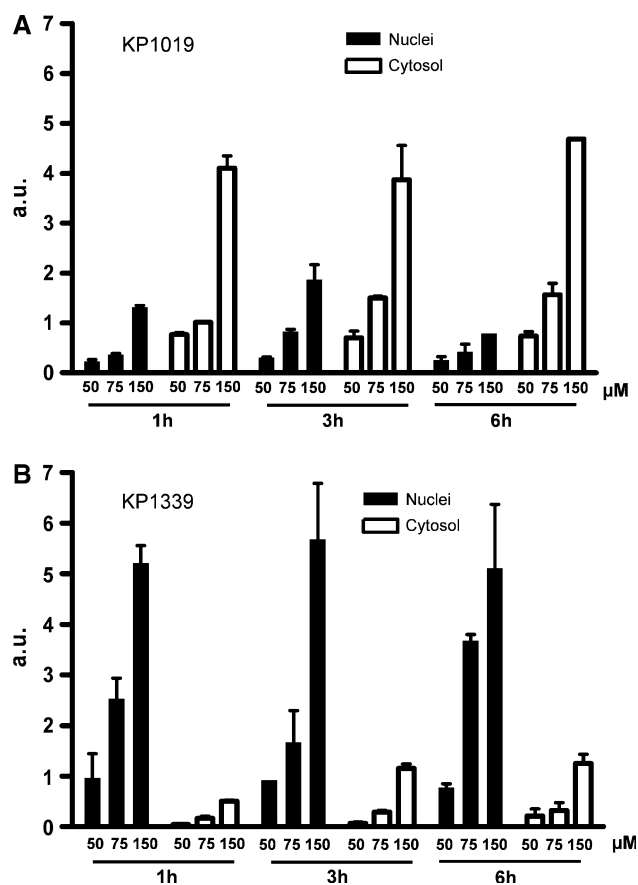
Fig. 4 Drug accumulation and intracellular drug distribution. Cytosolic and nucleic ruthenium levels of **a** KP1019- and **b** KP1339-treated KB-3-1 cells were determined after 1-, 3-, and 6-h drug exposure by inductively coupled plasma mass spectrometry (ICP-MS). The values given are relative means and the SD from at least two independent experiments

Fig. 5 Drug–protein binding patterns of KP1019. **a** Size-exclusion chromatography (SEC)–ICP-MS determination of cell culture medium supplemented with fetal calf serum after 3 h of incubation with KP1019. **b** Cytosolic fractions of KP1019-treated KB-3-1 cells were isolated after 3-h treatment and protein-bound ruthenium was determined by SEC-ICP-MS. **c** Cytosolic fractions of cisplatin-treated KB-3-1 cells were isolated after 3-h treatment with 50 μM cisplatin and protein-bound platinum was determined by SEC-ICP-MS. One representative experiment out of three is shown

within the first hour of drug incubation. Further increase of the incubation time up to 6 h did not result in a change of total drug uptake or the patterns of distribution between the nucleus and the cytoplasm. This was also in good agreement with the findings of the pulsing experiment data (see Fig. 1), which had already indicated that only short drug contact is sufficient for full KP1019 and KP1339 anticancer activity. Drug uptake of KP1019 as well as KP1339 followed a linear and dose-dependent pattern. With regard to intracellular distribution at all concentrations and time points tested, about 75% of KP1019 was detected in the cytosolic fraction. In contrast, KP1339 accumulated preferentially in the nuclei (approximately 90%).

Protein binding patterns of KP1019 and KP1339

As a next step, the protein binding of the drugs tested was investigated in culture medium as well as in cytoplasm samples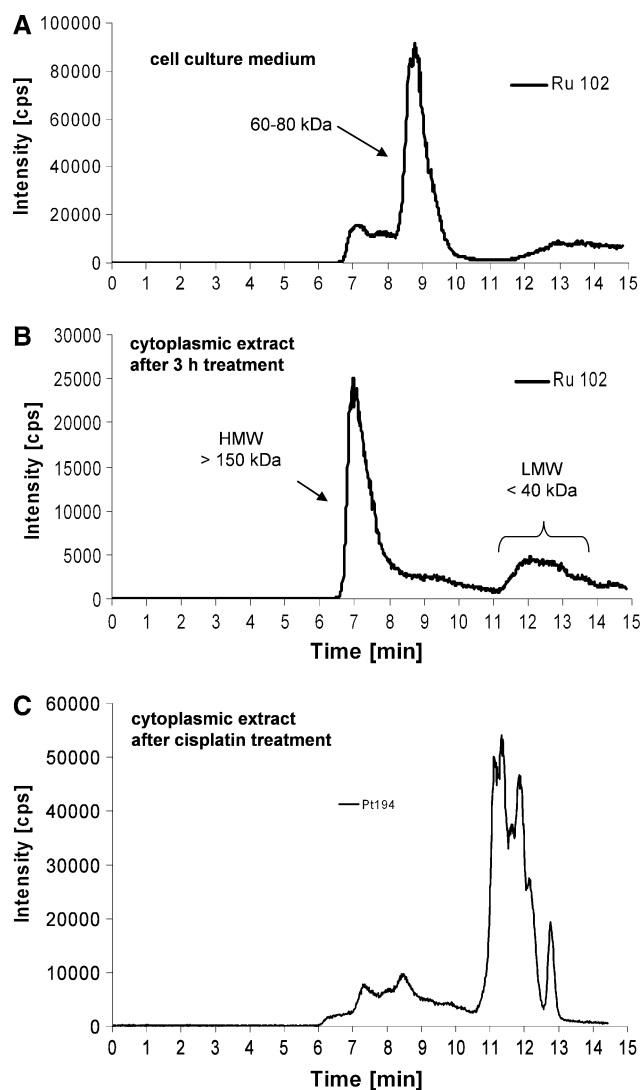 from drug-exposed cells. For this purpose SEC was combined with element-selective detection by ICP-MS [22, 23]. Figure 5a shows the protein binding pattern of the cell culture medium of cells after 3-h incubation with 50 μM KP1019. The major fraction of ruthenium was detected on proteins in the size range 60–80 kDa, i.e., the fraction of albumin and transferrin, present in the medium owing to fetal calf serum supplementation. Only small amounts of KP1019 (including free KP1019) could be detected in the low molecular weight fraction. The column recovery was 70% in these experiments. This is in

accordance with findings of earlier studies on drug–protein binding in human serum of patients [8].

In the cytoplasmic fraction isolated from drug-treated cells (Fig. 5b), KP1019 delivered basically two ruthenium-containing peaks: a prominent high molecular weight peak close to the exclusion limit of the column and a broad peak after 11–14 min corresponding to the low molecular weight fraction. The ruthenium-content ratio between the high molecular weight fraction and the low molecular weight fraction (HMW/LMW) was 3.5 ± 0.8 ($n = 5$ independently prepared samples) upon 3 h of drug exposure. Comparable intracellular protein binding patterns were also observed in Hep3B, HCC1.2, and HL60 cells (data not shown). Comparative experiments with KP1339 revealed concordant protein binding in the culture medium and in the cytoplasm (data not shown). KP1339 exposure for 3 h resulted in an HMW/LMW of 4 ± 0.8 ($n = 2$ independently prepared samples). Although KP1339 exhibits less accumulation in the cytoplasm, the cytoplasmic protein binding pattern was comparable to that of KP1019. Thus, for further analysis only KP1019-treated cells were used. Notably, the ruthenium binding patterns of KP1019 and KP1339 were in contrast to the platinum binding pattern of cisplatin-treated cells (Fig. 5c), which were characterized by distinct protein binding in the low molecular weight fraction.

As a next step, KP1019 incubation was extended from 3 to 24 h (Fig. 6a). A significantly changed HMW/LMW of 1.0 ± 0.4 ($n = 2$ independently performed experiments) was observed in the cytoplasmic samples; hence, the drug binding shifted toward low molecular weight proteins. To test the hypothesis that these observations resulted from changes in the distribution of the early accumulated
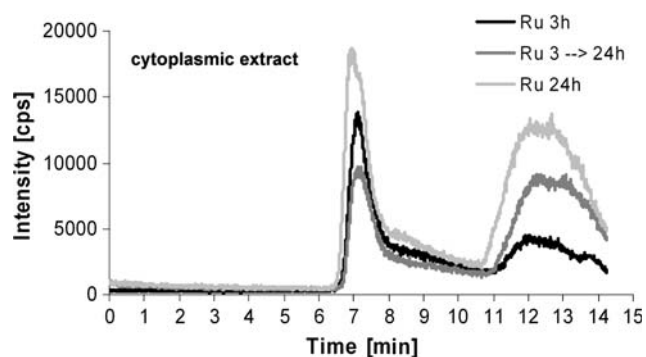

Fig. 6 Drug–protein binding patterns of KP1019 in pulsing experiments. KB-3-1 cells were treated with 50 μM KP1019, and after 3-h drug exposure drug-containing medium was replaced with fresh, drug-free cell culture medium. SEC-ICP-MS of cytosolic fractions was performed 24 h after the beginning of the experiment. Cytosolic fractions of cells treated for 3 and 24 h were prepared and analyzed in parallel. The respective cell numbers for the experiment were 1.58×10^7, 3.2×10^7, and 2.95×10^7 for the 3-, 3–24-, and 24-h samples

KP1019, pulsing experiments were performed. To this end, KP1019-containing medium was replaced after 3 h with drug-free cell culture medium. SEC-ICP-MS was performed 24 h after the beginning of the experiment. In analogy to the 24-h continuous incubation experiments, the low molecular weight fraction increased, giving an HMW/LMW of 0.5 in this experiment (Fig. 6b).

Characterization of the high molecular weight fraction

The column utilized for the SEC-ICP-MS measurements provided a size-exclusion limit of 150 kDa; hence proteins larger than 150 kDa could not be separated and eluted in the void volume of the column at 6 min. To further characterize the high molecular weight fraction, which was observed in all cytoplasmic samples, an alternative size-exclusion system was implemented. This new high-end technology allowed the separation of large proteins by increasing the protein size-exclusion limit from 150 to 2,000 kDa. The separation efficiency for the low molecular weight fraction was retained by setting up a novel SEC-SEC-ICP-MS method with two size-exclusion columns online. The first column was designed for separation of large proteins (exclusion limit 2,000 kDa, separation range 66–670 kDa), and the second column provided separation for mid-to-large proteins (exclusion limit 700 kDa, 5–700 kDa separation range). Notably, the SEC-SEC-ICP-MS investigation of KB-3-1 cells incubated with 50 μM KP1019 for 3 h (Fig. 7a) again revealed only two peaks: one at high molecular weight (again at the exclusion limit of the column, corresponding to proteins larger than 2,000 kDa), and the other at low molecular weight. Similar to our previous experiments, an HMW/LMW of 3.6 was observed. Hence, it could be concluded that monomeric proteins in the size range 60–700 kDa were not major targets of the ruthenium compounds in the cytoplasm. Since the native fractionation protocol applied did not separate cytoplasm from membrane-bound proteins and cell organelles, the metallodrug adducts detected in the void volume of the SEC-SEC-ICP-MS system can be explained by drug bound to membrane protein agglomerates, large protein complexes (e.g., ribosomes, vaults), and/or other cell organelles. This hypothesis was further confirmed by applying a different cell lysis protocol ($n = 2$). This allowed the separation of different cell compartments: the nucleic fraction (fraction I), a fraction containing all soluble (cytoplasmic) proteins (fraction II), as well as a particular fraction containing all membrane proteins and organelles (fraction III). The overall ruthenium levels in fractions I, II, and III were 2.9 ± 0.6, 1.8 ± 0.1, and 2.8 ± 1.8 fg per cell, respectively. Figure 7b shows the intracellular/cytoplasmic distribution obtained of 50 μM KP1019 in the soluble
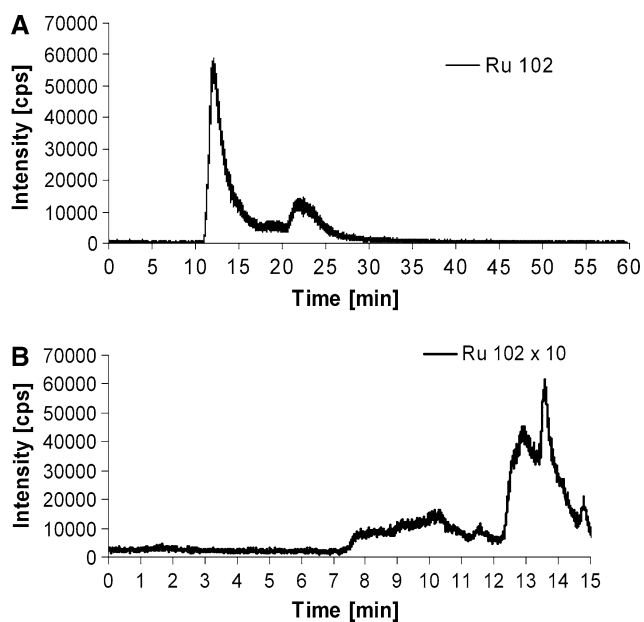
fraction (fraction II) of KB-3-1 cells after 3 h of incubation. In accordance with the above-mentioned hypothesis, only the low molecular weight fraction was detectable, and the prominent high molecular weight peak was missing from the SEC-ICP-MS spectrum. This indicates that KP1019 does not bind to soluble, monomeric proteins larger than 100 kDa. The low molecular weight ruthenium peaks correspond to small protein- and/or peptide-bound drug. Detection of free drug is unlikely as comparable amounts of KP1019 from protein-free solutions could not be recovered from the column (data not shown).

Discussion

Metal compounds belong to the most important chemotherapeutics for the treatment of human malignancies at the disseminated stage. In addition to platinum-containing drugs, ruthenium compounds such as KP1019 and KP1339 are also promising candidates in the development of new cancer therapeutics [4]. Recently, KP1019—containing an indazolium counterion—demonstrated considerable anticancer activity in a pilot clinical phase I study with low

side effects [2, 4]. However, KP1019's poor pharmaceutical properties, especially its poor aqueous solubility, did not allow the dose escalation in the trial to be done beyond a certain point. The maximum tolerated dose and optimal dose could not be reached. Hence, the sodium salt (KP1339) was selected for further clinical development. KP1339 has superior pharmaceutical properties, including more than 30 times better aqueous solubility. In this study, we compared the modes of action and activity patterns of these two ruthenium compounds in vitro. KP1019 was generally more active than KP1339. Nevertheless, linear regression analyses showed that both cytotoxic activity and the drug accumulation profile correlated between both drugs, indicating that they share similar modes of action. Moreover, both drugs were found to induce caspase-mediated apoptosis via the mitochondrial pathway, which is in agreement with previous data showing mitochondrial membrane depolarization and apoptosis induction by KP1019 in SW480 cells [5, 6]. Experiments using the glutathione (GSH) precursor and radical scavenger NAC indicated that the mechanisms underlying the anticancer activity of KP1019 and KP1339 share common effectors and/or metabolic pathways.

The present study reveals that KP1019 and KP1339 distinctly differ in their intracellular distribution: KP1339 preferentially accumulated into the nucleus (approximately 90%), whereas KP1019 was mainly localized in the cytoplasm (approximately 75%). This is of special interest as it challenges the widespread view that DNA is the major target of ruthenium drugs [24]. Pronounced nucleic localization has been reported for several DNA-damaging agents such as cisplatin [25] and doxorubicin [26]. Unlike the cytotoxicity of cisplatin or other DNA-damaging agents, our studies show that the KP1019 and KP1339 cytotoxicity is independent of p53 status ([10], data not shown). Similarly, the caspase activation and cytosolic drug–protein binding profiles indicate that both ruthenium drugs exert apoptosis via similar pathways, despite their different intracellular distribution pattern. Therefore, it seems unlikely that nucleic localization and DNA targeting is the primary mechanism underlying the anticancer activity of KP1019 and KP1339. In support of this, ruthenium compounds have been shown to involve targets other than DNA [27]. For example, the designed ruthenium-containing glycogen synthase kinase-3β inhibitor DW1/2 was recently reported to reduce the intracellular levels of MDM2 and MDM4. Consequently, p53 is stabilized, leading to apoptosis via the mitochondrial pathway in melanoma cells [28]. Moreover, DW1/2 was found to potently inhibit phosphatidylinositol 3-kinase [29] as well as the serine/threonine kinase PIM1 [30]. Also, for NAMI-A, a specific antimetastatic activity was described independent from DNA targeting [31, 32]. Altogether, these

reports and our data suggest that cytosolic protein targets are involved in the anticancer activity of some ruthenium compounds including KP1019 and KP1339.

KP1019 has been repeatedly shown to bind to serum proteins in vitro as well as in patient blood samples [4, 7, 8]. However, the intracellular protein binding patterns of anticancer drugs, in general, and of ruthenium compounds such as KP1019 and KP1339, in particular, are widely unexplored. This is the first study to elucidate the intracellular distribution and protein binding patterns of KP1019 and KP1339. A highly advanced SEC-ICP-MS analytical method has been adapted to address ruthenium contents of native (cytosolic) protein preparations from drug-exposed human cancer cells [22, 23]. This method is an ideal tool for studying interactions between metallo-drugs and proteins in live cells on a quantitative basis. It combines native protein separation with ICP-MS detection, allowing the determination of covalent as well as noncovalent drug–protein binding. Such noncovalent interactions (e.g., with serum proteins) are believed to play a crucial role in the anticancer activity of KP1019 and KP1339 [4]. Our time-course activity and cellular accumulation experiments show that uptake and damage leading to cytotoxicity of KP1019 and KP1339 is rapid and completed within the first hours of drug incubation. Moreover, the cytosol to nucleus distribution remained unchanged for more than 6 h, arguing for rapid drug compartmentalization. With regard to the binding of KP1019 or KP1339 to cyctosolic proteins, ruthenium binding was predominantly found in the high molecular weight fraction (more than 700 kDa). This fraction probably contains mainly polymeric proteins (e.g., cyto-skeleton components) or large protein complexes (e.g., ribosomes, proteins from the respiratory chain, multi-meric channels). Accordingly, preliminary proteome profiling using shotgun analyses identified multiple ribosomal and cytoskeletal proteins in this fraction (data not shown). To further dissect the observed ruthenium–protein binding patterns, a second cell fractionation approach using detergent-free buffer for separation of nuclei and large (protein) particles from smaller, soluble proteins was employed. Corroborating the data above, the larger ruthenium binding fraction was completely lost following 100,000g centrifugation in these settings. Only ruthenium bound to cytosolic proteins smaller than 100 kDa was still detectable, with distinct separation into several subpeaks. The characterization of these KP1019 and KP1339 targets is currently being addressed by developing immunoaffinity-assisted SEC-ICP-MS methods with higher selectivity for potential protein targets. Notably, the intracellular drug binding patterns of KP1019- and KP1339-treated cells strongly differed from those exposed to cisplatin, where cytosolic platinum

binding was mainly detected in the low molecular weight protein fraction. This again illustrates that KP1019 and KP1339 have a mechanism of action different from that of cisplatin.

To further investigate the intracellular processing of ruthenium binding, protein extracts of KP1019-treated cells were prepared after a longer drug-free recovery period (21 h). Notably, the initiative ruthenium–protein binding pattern shifted to the low molecular weight fraction (below 40 kDa) in these experiments. Again the underlying mechanisms are widely speculative and need further evaluation. However, one explanation for the increase in small ruthenium-bound proteins could be the appearance of KP1019 and KP1339 detoxification products. In SEC-ICP-MS measurements, peptides or metal-lothioneins have a retention time of more than 10 min [18]. Thus, GSH conjugation or metallothionein binding would explain the increased ruthenium content in this fraction. This is supported by the interaction and coordination of KP1019 to GSH [33] and metallothioneins (unpublished results) in cell-free systems. Also, the protective activity of NAC against KP1339- and KP1019-mediated cytotoxicity would support this hypothesis (see Fig. 3b and [5]). However, our previous studies revealed that KP1019 is not a substrate for the GSH conjugate efflux pump MRP1 and long-term KP1019 treatment did not induce expression of any GSH-dependent ABC transporters [2, 10]. This suggests that GSH conjugation is not a major factor protecting cells from KP1019. Another explanation for the increased low molecular weight ruthenium-containing protein peaks might be the proteosomal degradation of damaged proteins due to ruthenium-adduct formation [34, 35]. KP1019 has previously been shown to induce the formation of reactive (oxygen) species [5]. Moreover, preliminary results revealed induction of several chaperons including heat shock proteins after KP1339 treatment (unpublished results), which also points toward induction of protein stress. Accordingly, in a recent study activation of endoplasmic reticulum stress was described as a major contributor to the cytotoxic activity of the poorly DNA interacting ruthenium compound RDC11 [36].

Taken together, the findings of our study revealed that KP1019 and KP1339 rapidly enter tumor cells, where they bind to multiple small soluble proteins as well as large (multimeric) complexes/organelles. The higher cytosolic retention of the more cytotoxic compound KP1019 suggests that protein targets in the cytoplasm are key components of the cytotoxicity exerted. Moreover, the cytosolic protein binding pattern strongly differs from that observed for cisplatin, supporting the hypothesis that KP1019 and KP1339 exert a specific mode of action different from that of platinum drugs.

References

1. Bruijnincx PC, Sadler PJ (2008) Curr Opin Chem Biol 12:197–206
2. Heffeter P, Jungwirth U, Jakupec M, Hartinger C, Galanski M, Elbling L, Micksche M, Keppler B, Berger W (2008) Drug Resist Updat 11:1–16
3. Cossa G, Gatti L, Zunino F, Perego P (2009) Curr Med Chem 16:2355–2365
4. Hartinger CG, Zorbas-Seifried S, Jakupec MA, Kynast B, Zorbas H, Keppler BK (2006) J Inorg Biochem 100:891–904
5. Kapitza S, Jakupec MA, Uhl M, Keppler BK, Marian B (2005) Cancer Lett 226:115–121
6. Kapitza S, Pongratz M, Jakupec MA, Heffeter P, Berger W, Lackinger L, Keppler BK, Marian B (2004) J Cancer Res Clin Oncol 226:115–121
7. Cetinbas N, Webb MI, Dubland JA, Walsby CJ (2010) J Biol Inorg Chem 15:131–145
8. Sulyok M, Hann S, Hartinger CG, Keppler BK, Stingeder G, Koellensperger G (2005) J Anal At Spectrom 20:856–863
9. MacKenzie EL, Iwasaki K, Tsuji Y (2008) Antioxid Redox Signal 10:997–1030
10. Heffeter P, Pongratz M, Steiner E, Chiba P, Jakupec MA, Elbling L, Marian B, Korner W, Sevelda F, Micksche M, Keppler BK, Berger W (2005) J Pharmacol Exp Ther 312:281–289
11. Lipponer KG, Vogel E, Keppler BK (1996) Met Based Drugs 3:243–260
12. Peti W, Pieper T, Sommer, Keppler BK, Giester G (1999) Eur J Inorg Chem 1551–1555
13. Heffeter P, Jakupec MA, Korner W, Wild S, von Keyserlingk NG, Elbling L, Zorbas H, Korynevska A, Knasmuller S, Sutterluty H, Micksche M, Keppler BK, Berger W (2006) Biochem Pharmacol 71:426–440
14. Sagmeister S, Eisenbauer M, Pirker C, Mohr T, Holzmann K, Zwickl H, Bichler C, Kandioler D, Wrba F, Mikulits W, Gerner C, Shehata M, Majdic O, Streubel B, Berger W, Micksche M, Zatloukal K, Schulte-Hermann R, Grasl-Kraupp B (2008) Br J Cancer 99:151–159
15. Janson V, Andersson B, Behnam-Motlagh P, Engstrom KG, Henriksson R, Grankvist K (2008) Cell Physiol Biochem 22:45–56
16. Bunz F, Fauth C, Speicher MR, Dutriaux A, Sedivy JM, Kinzler KW, Vogelstein B, Lengauer C (2002) Cancer Res 62:1129–1133
17. Egger A, Rappel C, Jakupec MA, Hartinger CG, Heffeter P, Keppler BK (2009) J Anal At Spectrom 24:51–61
18. Koellensperger G, Daubert S, Erdmann R, Hann S, Rottensteiner HP (2007) Chem Biol 388:1209–1214
19. Heffeter P, Jakupec MA, Korner W, Chiba P, Pirker C, Dornetshuber R, Elbling L, Sutterluty H, Micksche M, Keppler BK, Berger W (2007) Biochem Pharmacol 73:1873–1886
20. Berger W, Elbling L, Micksche M (2000) Int J Cancer 88:293–300
21. Korynevska A, Heffeter P, Matselyukh B, Elbling L, Micksche M, Stoika R, Berger W (2007) Biochem Pharmacol 74:1713–1726
22. Hall AG (1999) Adv Exp Med Biol 457:199–203
23. Hann S, Obinger C, Stingeder G, Paumann M, Furtmüller PG, Koellensperger G (2006) J Anal At Spectrom 21:1224–1231
24. Pizarro AM, Sadler PJ (2009) Biochimie 91:1198–1211
25. Sakurai H, Okamoto M, Hasegawa M, Satoh T, Oikawa M, Kamiya T, Arakawa K, Nakano T (2008) Cancer Sci 99:901–904
26. Pawarode A, Shukla S, Minderman H, Fricke SM, Pinder EM, O'Loughlin KL, Ambudkar SV, Baer MR (2007) Cancer Chemother Pharmacol 60:179–188
27. Brabec V, Novakova O (2006) Drug Resist Updat 9:111–122
28. Smalley KS, Contractor R, Haass NK, Kulp AN, Atilla-Gokcumen GE, Williams DS, Bregman H, Flaherty KT, Soengas MS, Meggers E, Herlyn M (2007) Cancer Res 67:209–217
29. Xie P, Williams DS, Atilla-Gokcumen GE, Milk L, Xiao M, Smalley KS, Herlyn M, Meggers E, Marmorstein R (2008) ACS Chem Biol 3:305–316
30. Bullock AN, Russo S, Amos A, Pagano N, Bregman H, Debreczeni JE, Lee WH, von Delft F, Meggers E, Knapp S (2009) PLoS One 4:e7112
31. Bergamo A, Sava G (2007) Dalton Trans 1267–1272
32. Alessio E, Mestroni G, Bergamo A, Sava G (2004) Curr Top Med Chem 4:1525–1535
33. Schluga P, Hartinger CG, Egger A, Reisner E, Galanski M, Jakupec MA, Keppler BK (2006) Dalton Trans 1796–1802
34. Bursch W, Karwan A, Mayer M, Dornetshuber J, Frohwein U, Schulte-Hermann R, Fazi B, Di Sano F, Piredda L, Piacentini M, Petrovski G, Fesus L, Gerner C (2008) Toxicology 254:147–157
35. Jung T, Grune T (2008) IUBMB Life 60:743–752
36. Meng X, Leyva ML, Jenny M, Gross I, Benosman S, Fricker B, Harlepp S, Hebraud P, Boos A, Wlosik P, Bischoff P, Sirlin C, Pfeffer M, Loeffler JP, Gaiddon C (2009) Cancer Res 69:5458–5466

2.5. Maltol-derived ruthenium-cymene complexes with tumor inhibiting properties: the impact of ligand-metal bond stability on anticancer activity *in vitro*

Kandioller W.[a], Hartinger C.G.[a], Nazarov A.A.[a,b], Bartel C.[a], Skocic M.[a], Jakupec M.A.[a], Arion V.B.[a], Keppler B.K.[a]

[a] Institute of Inorganic Chemistry, University of Vienna, Waehringer Strasse 42, 1090 Vienna, Austria

[b] Institut des Sciences et Ingenierie Chimiques, Ecole Polytechnique Federale de Lausanne (EPFL), CH-1015, Lausanne, Switzerland

Maltol-Derived Ruthenium–Cymene Complexes with Tumor Inhibiting Properties: The Impact of Ligand–Metal Bond Stability on Anticancer Activity In Vitro

Wolfgang Kandioller,[a] Christian G. Hartinger,*[a] Alexey A. Nazarov,*[a, b] Caroline Bartel,[a] Matthias Skocic,[a] Michael A. Jakupec,[a] Vladimir B. Arion,[a] and Bernhard K. Keppler[a]

Abstract: Organometallic ruthenium–arene compounds bearing a maltol ligand have been shown to be nearly inactive in in vitro anticancer assays, presumably due to the formation of dimeric Ru^{II} species in aqueous solutions. In an attempt to stabilize such complexes, $[Ru(\eta^6\text{-}p\text{-cymene})(XY)Cl]$ (XY = pyrones or thiopyrones) complexes with different substitution pattern of the (thio)pyrone ligands have been synthesized, their structures characterized spectroscopically, and their aquation behavior investigated as well as their tumor-inhibiting potency. The aquation behavior of pyrone systems with electron-donating substituents and of thiopyrone complexes was found to be significantly different from that of the maltol-type complex reported previously. However, the formation of the dimer can be excluded as the primary reason for the inactivity of the complex because some of the stable compounds are not active in cancer cell lines either. In contrast, studies of their reactivity towards amino acids demonstrate different reactivities of the pyrone and thiopyrone complexes, and the higher stability of the latter probably renders them active against human tumor cells.

Keywords: amino acids · antitumor agents · heterocycles · O ligands · ruthenium

Introduction

Metal complexes play an important role in the treatment of cancer. One of the most widely used compounds is cisplatin, which was developed by Rosenberg in the 1960s.[1] Due to severe side-effects, activity in a limited range of tumors, and the occurrence of resistance,[2] the development of new antitumor agents with other metal ions as the central atom is an area of intense research.[1,3–7] Ruthenium complexes have shown the most promising results in preclinical and clinical studies.[8–11] NAMI-A and KP1019 are at the most advanced stage of development and are currently undergoing clinical trials (Figure 1).[8–10] The low general toxicity of these complexes reflects a more selective activity in tumor tissue compared with platinum-based compounds, mediated by transport into the cell in the form of protein adducts and reduction in the tumor.[12–16]

More recently, the potential of organometallic Ru^{II}–arene compounds as anticancer agents has been recognized.[4,7,11,17] This compound type bears an arene ligand that facilitates diffusion through the cell membrane (and thereby enhances cellular uptake). The coordination sphere is filled with mono- or bidentate ligands, which control the reactivity with biomolecules, and these moieties also appear to be determinants for the mode of action.[7,14,18–22]

RAPTA (containing the 1,3,5-triaza-7-phoshatricyclo-[3.3.1.1]decane (pta) ligand) and $[Ru^{II}\text{–}(arene)(en)]$ complexes (en = 1,2-diaminoethane) are the best studied ruthenium organometallics.[4,11,23] The pta complexes have been shown to be, similarly to NAMI-A, active against metastasis, but inactive in in vitro cell assays,[24,25] whereas the en complexes have potential as anticancer agents against primary

[a] Dr. W. Kandioller, Dr. C. G. Hartinger, Dr. A. A. Nazarov, C. Bartel, M. Skocic, Dr. M. A. Jakupec, Prof. V. B. Arion, Prof. B. K. Keppler
Institute of Inorganic Chemistry, University of Vienna
Waehringer Str. 42, Vienna (Austria)
Fax: (+43) 1-4277-9526
E-mail: christian.hartinger@univie.ac.at
        alex.nazarov@univie.ac.at

[b] Dr. A. A. Nazarov
Institut des Sciences et Ingénierie Chimiques
Ecole Polytechnique Fédérale de Lausanne (EPFL), 1015 Lausanne (Switzerland)

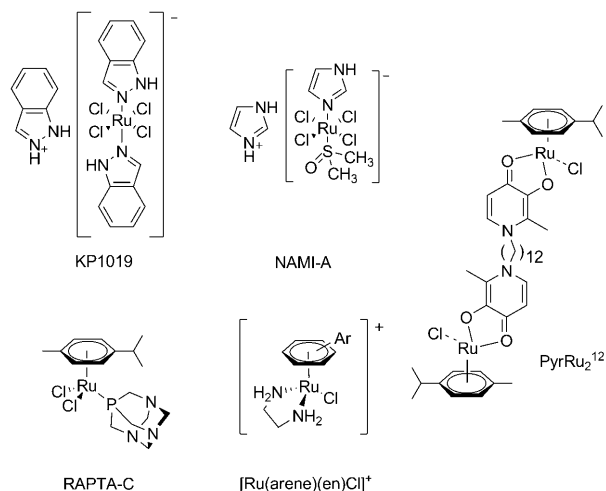Supporting information for this article is available on the WWW under http://dx.doi.org/10.1002/chem.200901939.

Figure 1. Structures of the anticancer compounds KP1019, NAMI-A, [Ru(η^6-p-cymene)(pta)Cl$_2$] (RAPTA-C), [Ru(arene)(acac)Cl]$^+$, [Ru-(arene)(en)Cl]$^+$, and the dinuclear compound PyrRu$_2$^{12}.

tumors.[26] Besides pta and en, several other ligand systems have been studied in ruthenium-based organometallics, including moieties containing O,O, N,O, N,N, and S,O donor sets.[19,22,27–35] The nature of the donor atoms was shown to influence the in vitro anticancer activity significantly, and the low potency of some of the synthesized compounds appears to be related to the instability of the ruthenium–ligand interaction, which results in the formation of dimeric Ru^{II} species with the arene moiety remaining attached to the metal center. Recently we demonstrated that the replacement of the O,O donor set of maltol by S,O leads to a significantly increased stability and the compounds are anticancer-active in the low μM range.[34] This ligand type has also found application, for example, in the removal or supplementation of iron, or in imaging contrast agents.[36] However, a switch from pyrone to pyridone systems in the case of this particular ligand also afforded stable compounds in aqueous solution that exhibit promising anticancer activity.[21,29,30,33]

Herein, the synthesis and characterization of a series of (thio)pyrone-derived Ru^{II}–cymene complexes are described, and the data are compared with other recent results.[34] The molecular structures of the complexes with kojic acid, pyromeconic acid, and maltol were determined by single-crystal X-ray diffraction analysis. The aquation behavior and the interactions with small biomolecules were investigated, and the cytotoxic activity in different human cancer cell lines was studied. The influence of the substitution pattern of the (thio)pyrone moiety on the stability of the complexes and their anticancer activity in human tumor cell lines is discussed.

Results and Discussion

Synthesis: The ligand **1b** (allomaltol) was synthesized in two steps starting from kojic acid (**1a**) by reaction with thionyl chloride followed by a reductive step using Zn/HCl (60% yield; Scheme 1).[37] Ligand **1e** was obtained by conversion
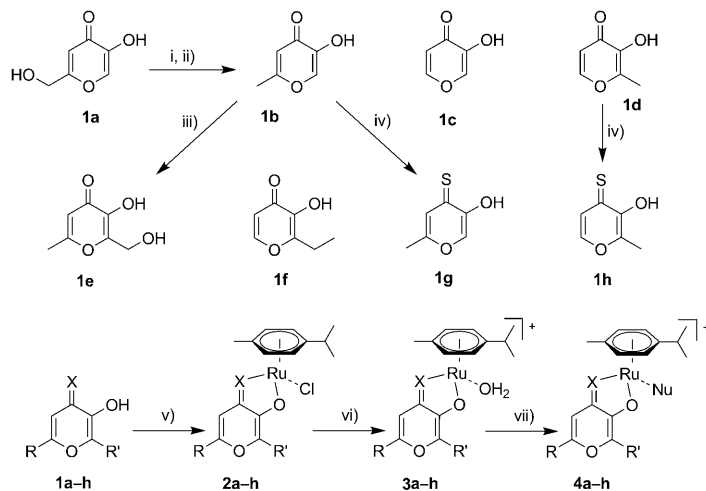
Scheme 1. Synthesis of ligands and complexes. Reagents and conditions: i) SOCl$_2$; ii) Zn/HCl; iii) formaldehyde, NaOH; iv) P$_4$S$_{10}$, dioxane; v) [Ru(η^6-p-cymene)Cl$_2$]$_2$, NaOMe; vi) H$_2$O; vii) nucleophiles (Nu) such as 5′-GMP or amino acids.

of **1b** with formaldehyde under alkaline conditions (70%).[37] The thiopyrones **1g** and **1h** were prepared by reaction of P$_4$S$_{10}$ with the corresponding pyrones **1b** and **1d** (40–60%).[38] Ligands **1a–h** were converted with bis[dichlorido(η^6-p-cymene)ruthenium(II)] under alkaline conditions into the corresponding Ru^{II} complexes **2a–h** in good yields (61–85%) (Scheme 1).[39] The reaction was performed with a slight excess of ligand to facilitate the purification step.

All complexes were characterized by 1D and 2D NMR spectroscopy, mass spectrometry, and elemental analysis. The influence of the solvent on the inversion of the ruthenium center is significant: In protic solvents, fast inversion of the ruthenium center was observed, as evidenced by the formation of two doublets for the p-cymene ligand, whereas in CDCl$_3$, the aromatic protons are detected as four doublets. Similar behavior was also observed in the ^{13}C NMR spectra, in accord with related Ru^{II}–arene complexes.[39] In the ^{1}H NMR spectrum of **2e** in CDCl$_3$, two doublets with a coupling constant of 17 Hz were observed, which were assigned to the protons of the CH$_2$ group (see the Supporting Information). This geminal splitting can be explained by the formation of an intramolecular hydrogen bond between the hydroxymethyl moiety and the coordinated O3 atom. ESI mass spectra were recorded after dissolving the samples in methanol and the predominant peak for the complexes **2a–h** was assigned to [M−Cl]$^+$ (good agreement between the measured and theoretical isotopic patterns was observed).

Molecular structure determination: Single crystals of the Ru[II] complexes **2a**, **2c**, and **2d** suitable for X-ray diffraction analysis were obtained by recrystallization from ethyl acetate. The results of the X-ray diffraction studies are shown
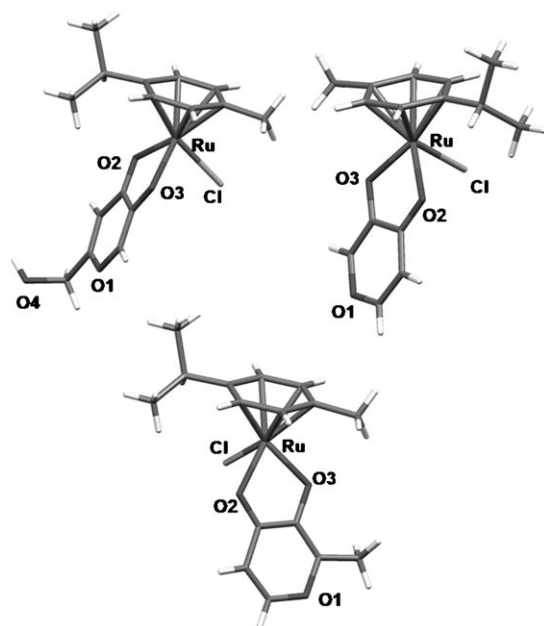

Figure 2. Molecular structures of the Ru[II] complexes **2a** (top left), **2c** (top right), and **2d** (bottom).

in Figure 2. These compounds crystallized in the monoclinic $P2_1/n$ (**2a**), triclinic $P\bar{1}$ (**2c**), and monoclinic $P2_1/c$ (**2d**) space groups, respectively. All the complexes have a piano-stool configuration. The pyrones act as bidentate ligands and form a five-membered chelate cycle with an envelope-like conformation on binding to ruthenium. The Ru–Cl bond lengths are in the same range as those of recently published compounds [2.4200(11)–2.4273(8) Å].[29,32] The largest torsion angle Ru-O2-C-C (12°) was found for **2c**.

In contrast to the crystal structure reported previously for **2d**,[19] the two Ru–O bonds in **2a**, **2c**, and **2d** were found to be slightly different, with the Ru–O2 distance marginally shorter than the Ru–O3 bond. The largest difference was found for **2d**, with bond lengths of 2.078(2) (Ru–O2) and 2.117(2) Å (Ru–O3). For complexes **2c** and **2d**, short contacts between two independent molecules were found. The H2 atom of the arene and one proton of the isopropyl group have short contacts to the O3 of the neighboring molecule. Intermolecular hydrogen bonds between the hydroxymethyl group and the O3 of the neighboring molecule were observed for **2a**. The *R* and *S* stereoisomers of **2a** are connected in an alternating manner through hydrogen bonds to form a syndiotactic chain (Figures S3 and S4 in the Supporting Information). The distance between the O3 atom of the *R* enantiomer and the OH group of the *S* isomer is 1.969 Å, whereas the length of the hydrogen bond between the O3 atom of the *S* enantiomer and the OH of the *R* isomer is 1.931 Å. Connections between adjacent chains through short

contacts of the isopropyl protons to O2 (2.527 Å) and *p*-cymene (2.983 Å) are responsible for the observed layer-type structure (see the Supporting Information).

Aquation: Aquation and the stability of the complexes in water were investigated by ^{1}H NMR spectroscopy. Owing to the higher lipophilicity of the thiopyrone complexes, all experiments with **2g** and **2h** were performed in 10% [D6]DMSO/D2O solutions. No coordination of [D6]DMSO was observed in preliminary experiments, although small amounts of degradation products were detected after 18 h in this solvent mixture.

The complexes **2a–h** were hydrolyzed in aqueous solution within seconds to give the charged complexes **3a–h** by exchange of the chlorido ligand with a neutral water molecule, and identical NMR spectra were obtained after the induced release of the chlorido ligands with equimolar amounts of AgNO3. NMR experiments with **2b** in physiological NaCl solution (100 mM), which should shift the aquation equilibrium from **3b** to **2b**,[40] showed no influence on the aquation process. For complexes **3a–d**, the formation of the identical dimeric hydrolysis side-product $[Ru_2(cym)_2(OH)_3]^+$ was observed (detected by positive ion mode ESI mass spectrometry and ^{1}H NMR spectroscopy), which is thought to be responsible for the inactivity of the compound type against cancer cells.[19] The amount of side-product formed depends on the concentration, the incubation time, and the pH value of the solution. In contrast to **3a–d**, compounds **3e–h** are stable for more than 24 h in aqueous solution, conceivably due to a stronger binding of the ligands **3e** and **3f** to ruthenium relative to pyrones.[34]

To stabilize the complexes against hydrolysis and the concomitant dimer formation, **2a–d** were treated with imidazole in aqueous solution to form the corresponding positively charged complex. The reactions proceeded very quickly (within seconds) and the resulting imidazole complexes did not reveal the formation of a dimeric species within 18 h (Figure 3).

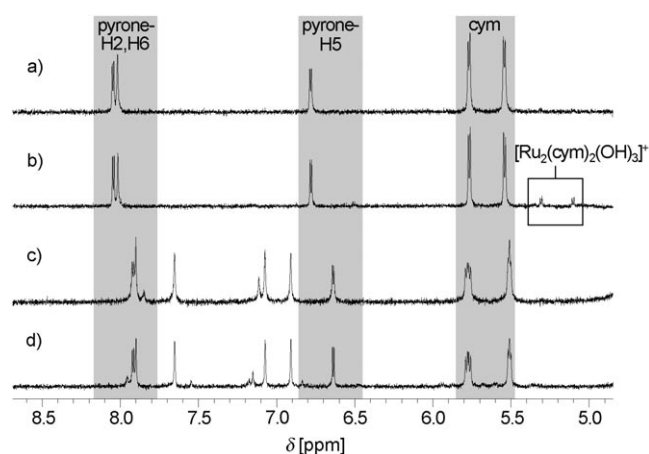Figure 3. ^{1}H NMR spectra of the reaction of **3c** with imidazole in D2O: a) **3c** in D2O after 5 min, b) **3c** after 18 h, c) imidazole/**3c** reaction mixture after 5 min (molar ratio 1:1), and d) imidazole/**3c** reaction mixture after 18 h.

The pK_a values of **3a–f** were determined by stepwise deprotonation of the aqua species with NaOD. The chemical shifts of the *p*-cymene protons were monitored by ^{1}H NMR spectroscopy and plotted against the pH value of the solution to give the pK_a values (corrected as reported recently;[32] see Table 1 and the Supporting Information). The pK_a

Table 1. pK_a values of **3a–h** and IC$_{50}$ values of **2a–h** (96 h exposure).

Complex	pK_a	IC$_{50}$ [μM]		
		CH1	SW480	A549
a	8.93 ± 0.02	234 ± 21	429 ± 10	n.d.
b[a]	9.01 ± 0.03	239 ± 22	359 ± 119	518 ± 65
c	8.91 ± 0.02	112 ± 50	206 ± 94	490 ± 43
d[a]	9.23[19]	81 ± 14	159 ± 41	482 ± 20
e	8.92 ± 0.02	242 ± 39	457 ± 33	510 ± 29
f	9.12 ± 0.04	81 ± 8	165 ± 31	389 ± 37
g[a]	>10 $(12.8$[b]$)$	35 ± 8	20 ± 7	n.d.
h[a]	>10 $(12.5$[b]$)$	13 ± 4	5.1 ± 0.5	n.d.

[a] See ref. [34]. [b] Obtained by DFT calculation.

values of the thiopyrone complexes **3g** and **3h** could not be determined due to precipitation of the complexes at pH 10.0. However, the theoretical DFT calculations[34] indicate that the pK_a values of the thiopyrone species are higher than those of the corresponding pyrone complexes by a factor of 1.5–1.7. The pK_a values for **3a–f** are comparable to those published recently for other pyrone- and pyridone-based Ru^{II}–arene complexes (8.99–9.64).[19,32,33] The pK_a values indicate that **3a–h** are present as reactive aqua species under physiological conditions.

Cytotoxicity: The cytotoxic activity was assayed in the human tumor cell lines SW480 (colon carcinoma), CH1 (ovarian carcinoma), and A549 (non-small cell lung carcinoma) by means of the colorimetric MTT assay (Table 1). Note that the chlorido complexes **2a–h** were rapidly converted in the medium into the corresponding aqua complexes **3a–h** prior to contact with the cells. The recently reported maltol complex **2d** does not exhibit activity in human tumor cells to a meaningful extent. This behavior is thought to be related to the formation of the inactive [Ru$_2$(*p*-cymene)$_2$(OH)$_3$]$^+$ in aqueous solution.[19,29] Similarly, the structurally related compounds **2a–c** show no noteworthy cytotoxic activity in the tested cell lines.

In contrast to **2a–d**, **2e–h** do not form such dimeric species. However, the in vitro activities of **2e** and **2f** were of a dimension similar to those of **2a–d**. Switching from pyrone to the analogous thiopyrone compounds **2g** and **2h** resulted in IC$_{50}$ values in the low μM range. Notably, these compounds were more active in the SW480 cell line than in the otherwise more chemosensitive CH1 cells. These results suggest that dimer formation is not responsible for the inactivity of **2a–f** (Table 1).

Reaction with small biomolecules: The interactions of the aqua species **3a–h** with small biomolecules, such as the

DNA model compound 5′-GMP and amino acids, were investigated by ^{1}H NMR spectroscopy.

The reaction of 5′-GMP can easily be monitored in ^{1}H NMR spectroscopy due to the shift of the N7 atom of 5′-GMP from $\delta = 8.1$ to approximately 7.9 ppm.[41] The reaction was completed within seconds and the adducts formed were stable in solution for more than 18 h. Accordingly, DNA is a possible target for these Ru^{II}–cymene complexes, as suggested for related organometallic ruthenium(II) compounds.[19]

However, many drugs are administered intravenously, and amino acids and proteins are the first potential binding partners for the complexes in the bloodstream. Therefore, the reactions with the amino acids glycine, L-histidine, L-methionine, and L-cysteine were investigated to gain an insight into the possible interactions with proteins and the pharmacokinetic pathways. Complexes **3a–h** were treated with an equimolar amount of the respective amino acid, and the reaction progress was monitored for 18 h. The addition of L-cysteine led to fast decomposition of all the complexes within minutes, most probably due to the strong *trans* effect exhibited by the thiol functionality. The reactions of the pyrone-derived complexes **3a–f** with L-methionine, L-histidine, and glycine to give **4a–f** differ significantly from those of the thiopyrone complexes **3g** and **3h**. All the compounds reacted immediately with 1 equiv of L-methionine by replacement of the aqua ligand with the amino acid (bound through the thioether moiety, see below). In the case of **3a–f**, the pyrone ligands **1a–f** were cleaved quantitatively by the amino acid within 18 h. In contrast, **4g** and **4h** were stable in solution over the period of analysis and no free ligands were detected. Similar results were obtained for the reactions with L-histidine. In all cases the Ru^{II} centers were coordinated to the amino acid in a ratio of 1:1 through the N1 or N3 atoms of the imidazole moiety. As in the case of L-Met, the pyrone ligands **1a–f** were released upon coordination of the amino acid, whereas for **3g** and **3h** stable species were obtained. The reactions of glycine with **3a–h** were significantly slower than those with the other investigated amino acids: After an incubation time of 18 h, the ^{1}H NMR spectra of the reaction mixtures showed the formation of two doublets at approximately $\delta = 3.1$ ppm with a geminal coupling of 17 Hz (Figure 4). These signals were assigned to the CH$_2$ group of glycine, which acts as a chelating ligand and is coordinated through the amino and carboxylic groups to the Ru^{II} center forming a five-membered ring structure. No adducts of **3g** and **3h** with glycine were observed, probably due to the inability of the amino acid to coordinate in a bidentate manner. This also demonstrates the greater stability of the thiopyrone complexes.

Notably, no ruthenium dimer signals (at approximately $\delta = 5.0$ and 5.5 ppm) were observed in the NMR experiments within 18 h when amino acids were present. The high reactivity towards amino acids and the prevention of the formation of dimeric species by coordination to amino acids make it unlikely that dimerization is the reason for the anticancer inactivity of the maltol complex and the related
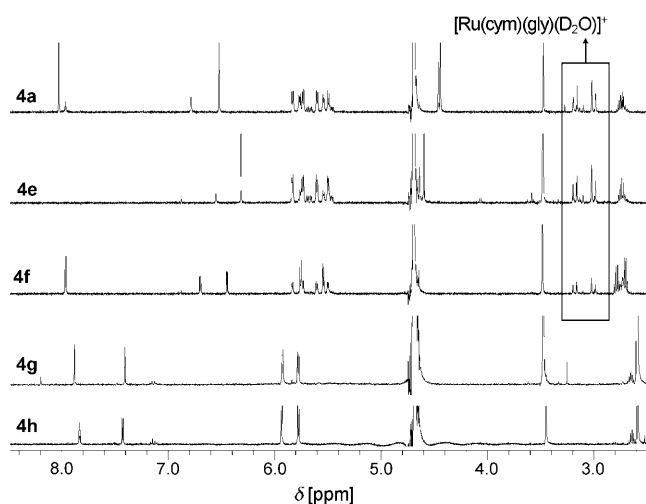
Figure 4. The reactions of **3a** and **3e–h** with glycine to yield **4a** and **4e–h**, monitored by ^{1}H NMR spectroscopy for 18 h.

pyrone-based compounds. In contrast, the slower degradation in the presence of amino acids might allow the thiopyrone complexes to enter the cells to a higher degree in their unmodified form.

To characterize the coordination compound obtained upon reaction of **3c** with L-methionine by NMR spectroscopy, **3c** was treated with an equimolar amount of the L-Met-analogous *Se*-methyl-L-selenocysteine. ^{1}H, ^{13}C, and ^{77}Se NMR spectra were recorded over a period of 18 h. The selenium signal of *Se*-methyl-L-selenocysteine at −419 ppm vanished within 10 min after the addition of **3c**, and two new signals at −283 and −265 ppm appeared (Figure 5 and the Supporting Information). The signal at −283 ppm disappears over time, probably due to completion of *N*,*Se*-chelation to the Ru^{II} center (Figure 5). The ^{13}C NMR spectrum obtained after 18 h shows signals at 176.3 ppm, which could
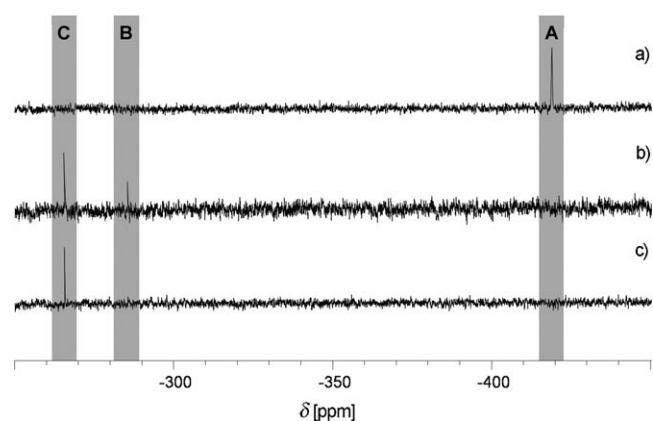

Figure 5. Time course for the reaction of *Se*-methyl-L-selenocysteine (**A**) with **3c**, followed by ^{77}Se NMR spectroscopy. a) *Se*-Methyl-L-selenocysteine and the *Se*-methyl-L-selenocysteine/**3c** reaction mixture after b) 5 min and c) 18 h showing the formation of the intermediate [Ru-(cym)(*Se*-methyl-L-selenocysteine-κ*Se*)(**1c**)] (**B**) and eventually [Ru-(cym)(*Se*-methyl-L-selenocysteine-κ^2*N*,*Se*)(D$_2$O)] (**C**).

be assigned to the carbonyl functionality of the free pyrone, and at 180.5 ppm, which corresponds to the uncoordinated carboxylate of the amino acid. Therefore it is proposed that the amino acid binds in a bidentate fashion through the selenium and nitrogen atoms to the Ru^{II} center with the release of the pyrone ligand.

In an attempt to overcome the rapid decomposition of **3g** and **3h** in the presence of L-cysteine, the chlorido ligands in the Ru^{II} complexes were exchanged for L-histidine in situ. The new compounds were, similarly to the reactions with imidazole, significantly more stable under the applied conditions, and no degradation products were observed in the ^{1}H NMR spectra after the addition of an equimolar amount of L-cysteine (monitored for 18 h).

Conclusion

Bio-organometallic chemistry is an emerging field of research and, in particular, the use of ruthenium–arene compounds as anticancer agents appears to be promising. The ruthenium–arene complex with the O,O-bound maltol ligand was shown to be inactive in in vitro anticancer assays. The inactivity of the compound was assumed to be related to the formation of dimeric Ru^{II} species in aqueous solutions.[19] In contrast, the analogous thiomaltol complexes exhibit anticancer activity in the low μM range and are not prone to dimer formation.[34] The formation of the dimeric species can also be inhibited by modification of the substitution pattern of the pyrone scaffold. The introduction of electron-donating groups on the pyrone leads to compounds with higher stability. However, these compounds were also found to be inactive in vitro, which demonstrates that dimer formation is not the main reason for the inactivity of the compounds. Aquation of the ruthenium center appears to be a prerequisite for the release of pyrone ligands, and replacement of the chlorido ligand by imidazole was shown to be an effective alternative to obtain [Ru^{II}(arene)(pyrone)] complexes that are stable in aqueous solutions.

To gain a deeper insight into the chemical behavior of these compounds, their reactions with the amino acids Gly, L-His, L-Met, and L-Cys were followed by NMR spectroscopy. These studies revealed that the thiopyrone complexes are significantly more stable. This greater stability gives them more time to be taken up by tumor cells, whereas the pyrone complexes decompose as coordination of the amino acid leads to cleavage of the pyrone. It is assumed that N,O and S,O chelates are thermodynamically preferred over the O,O coordination of pyrone ligands, leading to the release of the pyrone ligand if appropriate molecules are present, as is the case in a biological environment.

Experimental Section

ylmaltol (**1f**; Aldrich), formaldehyde solution (Aldrich), P_4S_{10} (Aldrich), and sodium methoxide (Aldrich) were purchased and used without further purification. Bis[dichlorido(η^6-*p*-cymene)ruthenium(II)], 2-chloromethyl-5-hydroxypyran-4(1*H*)-one (chlorokojic acid), 5-hydroxy-2-methylpyran-4(1*H*)-one (**1b**), 3-hydroxypyran-4(1*H*)-one (**1c**), 2-hydroxymethyl-3-hydroxy-6-methylpyran-4(1*H*)-one (**1e**), 5-hydroxy-2-methylpyran-4(1*H*)-thione (**1g**), and 3-hydroxy-2-methylpyran-4(1*H*)-thione (**1h**) were synthesized as described elsewhere.[37,38] Melting points were determined with a Büchi B-540 apparatus and are uncorrected. Elemental analyses were carried out with a Perkin–Elmer 2400 CHN Elemental Analyzer at the Microanalytical Laboratory of the University of Vienna. NMR spectra were recorded at 25 °C by using a Bruker FT Avance III™ 500 spectrometer at 500.10 (^{1}H), 125.75 (^{13}C{^{1}H}), 202.44 (^{31}P{^{1}H}), and 95.38 MHz (^{77}Se{^{1}H}, referenced to diphenyl diselenide) in [D$_6$]DMSO, D$_2$O, or CDCl$_3$. The 2D NMR spectra were recorded in gradient-enhanced mode. An esquire$_{3000}$ ion-trap mass spectrometer (Bruker Daltonics, Bremen, Germany) equipped with an orthogonal ESI ion source was used for MS measurements. The solutions were introduced by flow injection using a Cole-Parmer 74900 single-syringe infusion pump (Vernon Hills, IL).

X-ray diffraction measurements were performed with single crystals of **2a**, **2c** and **2d** on a Bruker X8 APEXII CCD diffractometer at 100 K. The single crystals were positioned 40 mm from the detector. 2710 frames for 5 s exposure time over 2° scan width were measured for **2a**, 1007 frames for 10 s over 1° for **2c**, and 2173 frames for 4 s over 1° for **2d**. The data were processed by using the SAINT software package.[43] Crystal data, data collection parameters, and structure refinement details are given in Tables S1–S4 of the Supporting Information. The structures were solved by direct methods and refined by full-matrix least-squares techniques. Non-hydrogen atoms were refined with anisotropic displacement parameters. Hydrogen atoms were inserted at calculated positions and refined with a riding model. The following software, computer, and tables were used: Structure solution, SHELXS-97;[44] refinement, SHELXL-97;[45] molecular diagrams, ORTEP-3;[46] computer, Pentium IV; scattering factors.[47]

CCDC-739426 (**2a**), 739427 (**2c**), and 739425 (**2d**) contain the supplementary crystallographic data for this paper. These data can be obtained free of charge from The Cambridge Crystallographic Data Centre via www.ccdc.cam.ac.uk/data_request/cif.

General procedure for the synthesis of the ruthenium(II)(η^6-*p*-cymene) complexes: The ligand (1 equiv) and sodium methoxide were dissolved in methanol and stirred for 5 min under an inert atmosphere (clear solution). A solution of [Ru(η^6-*p*-cymene)Cl$_2$]$_2$ in MeOH/CH$_2$Cl$_2$ (1:1) was added and the reaction mixture was stirred for 5–18 h. The reaction mixture was concentrated under reduced pressure and the residue was extracted with CH$_2$Cl$_2$. The combined organic layers were filtered and the solvent was removed. The crude product was purified by recrystallization.

Chlorido[2-hydroxymethyl-5-(oxo-κ*O*)-4-(1*H*)-pyronato-κ*O*^{4}](η^6-*p*-cymene)ruthenium(II) (2a): The reaction was performed according to the general complexation protocol by using **1a** (113 mg, 0.73 mmol, 1 equiv), NaOMe (43 mg, 0.8 mmol, 1.1 equiv), and [Ru(η^6-*p*-cymene)Cl$_2$]$_2$ (200 mg, 0.33 mmol, 0.45 equiv). The crude product was recrystallized from acetone/*n*-hexane to afford an orange powder (200 mg, 67%). Single crystals suitable for X-ray diffraction analysis were grown from ethyl acetate. M.p. > 180 °C (decomp.); ^{1}H NMR (500.10 MHz, CDCl$_3$): δ = 1.31 (d, ^{3}*J*(H,H) = 7 Hz, 6 H; CH$_{3,Cym}$), 2.29 (s, 3 H; CH$_{3,Cym}$), 2.90 (m, 1 H; CH$_{Cym}$), 3.83 (br s, 1 H; OH), 4.40 (d, ^{2}*J*(H,H) = 17 Hz, 1 H; CH$_2$), 4.46 (d, ^{2}*J*(H,H) = 17 Hz, 1 H; CH$_2$), 5.30 (dd, ^{3}*J*(H,H) = 5 Hz, ^{3}*J*(H,H) = 5 Hz, 2 H; 3-H/5-H$_{Cym}$), 5.53 (dd, ^{3}*J*(H,H) = 5 Hz, ^{3}*J*(H,H) = 5 Hz, 2 H; 2-H/6-H$_{Cym}$), 6.63 (s, 1 H; 3-H), 7.65 ppm (s, 1 H; 6-H); ^{13}C NMR (125.75 MHz, CDCl$_3$) δ = 18.6 (CH$_{3,Cym}$), 22.3 (CH$_{3,Cym}$), 31.1 (CH$_{Cym}$), 60.7 (CH$_2$), 78.0 (C-3/C-5$_{Cym}$), 79.6 (C-2/C-6$_{Cym}$), 95.6 (C-4$_{Cym}$), 100.1 (C-1$_{Cym}$), 107.5 (C-3), 141.1 (C-6), 159.3 (C-2), 167.9 (C-5), 185.7 ppm (C-4); elemental analysis calcd (%) for C$_{16}$H$_{19}$ClO$_4$Ru: C 46.66 H 4.65; found: C 46.43 H 4.56.

Chlorido[2-methyl-5-(oxo-κ*O*)-4-(1*H*)-pyronato-κ*O*^{4}](η^6-*p*-cymene)ruthenium(II) (2b): The reaction was performed according to the general com-

plexation procedure by using **1b** (92 mg, 0.73 mmol, 1 equiv), NaOMe (43 mg, 0.8 mmol, 1.1 equiv), and [Ru(η^6-*p*-cymene)Cl$_2$]$_2$ (200 mg, 0.33 mmol, 0.45 equiv). The crude product was recrystallized from MeOH/*n*-hexane to afford a deep-red crystalline solid (207 mg, 73%). M.p. > 200 °C (decomp.); ^{1}H NMR (500.10 MHz, CDCl$_3$): δ = 1.33 (d, ^{3}*J*(H,H) = 7 Hz, 6 H; CH$_{3,Cym}$), 2.26 (s, 3 H; CH$_3$), 2.32 (s, 3 H; CH$_{3,Cym}$), 2.93 (m, 1 H; CH$_{Cym}$), 5.32 (dd, ^{3}*J*(H,H) = 5 Hz, ^{3}*J*(H,H) = 5 Hz, 2 H; 3-H/5-H$_{Cym}$), 5.53 (dd, ^{3}*J*(H,H) = 5 Hz, ^{3}*J*(H,H) = 5 Hz, 2 H; 2-H/6-H$_{Cym}$), 6.34 (s, 1 H; 3-H), 7.66 ppm (s, 1 H; 6-H); ^{13}C NMR (125.75 MHz, CDCl$_3$): δ = 18.6 (CH$_{3,Cym}$), 19.8 (CH$_3$), 22.3 (CH$_{3,Cym}$), 31.1 (CH$_{Cym}$), 78.8 (C-3/C-5$_{Cym}$), 79.8 (C-2/C-6$_{Cym}$), 95.6 (C-4$_{Cym}$), 100.1 (C-1$_{Cym}$), 109.6 (C-3), 141.1 (C-6), 159.3 (C-2), 165.2 (C-5), 185.7 ppm (C-4); elemental analysis calcd (%) for C$_{16}$H$_{19}$ClO$_3$Ru·0.25H$_2$O: C 48.00, H 4.91 found: C 47.94, H 4.76.

Chlorido[3-(oxo-κ*O*)-4-(1*H*)-pyronato-κ*O*^{4}](η^6-*p*-cymene)ruthenium(II) (2c): The reaction was performed according to the general complexation procedure by using pyromeconic acid (81 mg, 0.72 mmol, 1 equiv), NaOMe (43 mg, 0.8 mmol, 1.1 equiv), and [Ru(η^6-*p*-cymene)Cl$_2$]$_2$ (200 mg, 0.326 mmol, 0.45 equiv). The crude product was recrystallized from ethyl acetate/*n*-hexane to afford a deep-red crystalline solid (202 mg, 73%). Single crystals suitable for X-ray diffraction analysis were grown from ethyl acetate. M.p. > 200 °C (decomp.); ^{1}H NMR (500.10 MHz, CDCl$_3$): δ = 1.34 (d, ^{3}*J*(H,H) = 7 Hz, 6 H; CH$_{3,Cym}$), 2.32 (s, 3 H; CH$_{3,Cym}$), 2.90–2.96 (m, 1 H; CH$_{Cym}$), 5.32 (dd, ^{3}*J*(H,H) = 5 Hz, 2 H; 3-H/5-H$_{Cym}$); 5.55 (dd, ^{3}*J*(H,H) = 5 Hz, ^{3}*J*(H,H) = 5 Hz, 2 H; 2-H/6-H$_{Cym}$), 6.57 (d, ^{3}*J*(H,H) = 7 Hz, 1 H; 5-H), 7.66 (d, ^{3}*J*(H,H) = 7 Hz, 1 H; 6-H), 7.77 ppm (s, 1 H; 2-H); ^{13}C NMR (125.75 MHz, CDCl$_3$): δ = 18.6 (CH$_{3,Cym}$), 22.3 (CH$_{3,Cym}$), 31.1 (CH$_{Cym}$), 76.9 (C-3/C-5$_{Cym}$), 79.6 (C-2/C-6$_{Cym}$), 95.6 (C-4$_{Cym}$), 100.1 (C-1$_{Cym}$), 111.4 (C-5), 142.6 (C-2), 153.8 (C-6), 161.0 (C-3), 185.3 ppm (C-4); elemental analysis calcd (%) for C$_{15}$H$_{17}$ClO$_3$Ru·0.5H$_2$O: C 46.10, H 4.64; found: C 45.92, H 4.37.

Chlorido[2-methyl-3-(oxo-κ*O*)-4-(1*H*)-pyronato-κ*O*^{4}](η^6-*p*-cymene)ruthenium(II) (2d): The reaction was performed according to the general complexation procedure by using **1d** (92 mg, 0.73 mmol, 1 equiv), NaOMe (43 mg, 0.8 mmol, 1.1 equiv), and [Ru(η^6-*p*-cymene)Cl$_2$]$_2$ (200 mg, 0.33 mmol, 0.45 equiv). The crude product was recrystallized from ethyl acetate/*n*-hexane to afford a deep-red crystalline solid (164 mg, 64%). Single crystals suitable for X-ray diffraction analysis were grown from ethyl acetate. M.p. > 200 °C (decomp.); ^{1}H NMR (500.10 MHz, CDCl$_3$): δ = 1.32 (d, ^{3}*J*(H,H) = 7 Hz, 6 H; CH$_{3,Cym}$), 2.32 (s, 3 H; CH$_3$), 2.41 (s, 3 H; CH$_3$), 2.91 (m, 1 H; CH$_{Cym}$), 5.30 (dd, ^{3}*J*(H,H) = 6 Hz, ^{3}*J*(H,H) = 6 Hz, 2 H; 3-H/5-H$_{Cym}$), 5.52 (dd, ^{3}*J*(H,H) = 6 Hz, ^{3}*J*(H,H) = 6 Hz, 2 H; 2-H/6-H$_{Cym}$), 6.51 (d, ^{3}*J*(H,H) = 5 Hz, 1 H; 5-H), 7.56 ppm (d, ^{3}*J*(H,H) = 5 Hz, 1 H; 6-H); ^{13}C NMR (125.75 MHz, CDCl$_3$): δ = 14.6 (CH$_3$), 18.6 (CH$_{3,Cym}$), 22.3 (CH$_{3,Cym}$), 31.1 (CH$_{Cym}$), 77.8 (C-3/C-5$_{Cym}$), 79.6 (C-2/C-6$_{Cym}$), 95.8 (C-4$_{Cym}$), 99.7 (C-1$_{Cym}$), 111.1 (C-5), 151.7 (C-6), 153.9 (C-2), 157.8 (C-3), 182.7 ppm (C-4); elemental analysis calcd (%) for C$_{16}$H$_{19}$ClO$_3$Ru: C 48.55, H 4.84; found: C 48.45, H 4.63.

Chlorido[2-hydroxymethyl-6-methyl-3-(oxo-κ*O*)-4-(1*H*)-pyronato-κ*O*^{4}]-(η^6-*p*-cymene)ruthenium(II) (2e): The reaction was performed according to the general complexation protocol by using 2-hydroxymethyl-3-hydroxy-6-methyl-pyran-4(1*H*)-one (**1e**; 113 mg, 0.73 mmol, 1 equiv), NaOMe (43 mg, 0.8 mmol, 1.1 equiv), and [Ru(η^6-*p*-cymene)Cl$_2$]$_2$ (200 mg, 0.33 mmol, 0.45 equiv). The crude product was recrystallized from ethyl acetate/*n*-hexane to afford a red crystalline solid (250 mg, 81%). M.p. 193–196 °C (decomp.); ^{1}H NMR (500.10 MHz, CDCl$_3$): δ = 1.33 (d, ^{3}*J*(H,H) = 7 Hz, 6 H; CH$_{3,Cym}$), 2.27 (s, 3 H; CH$_{3,Cym}$), 2.31 (s, 3 H; CH$_{3,Cym}$), 2.88 (m, 1 H; CH$_{Cym}$), 4.05 (br s, 1 H; OH), 4.63 (d, ^{2}*J*(H,H) = 14 Hz, 1 H; CH$_2$), 4.80 (d, ^{2}*J*(H,H) = 14 Hz, 1 H; CH$_2$), 5.30 (dd, ^{3}*J*(H,H) = 4 Hz, ^{3}*J*(H,H) = 4 Hz, 2 H; 3-H/5-H$_{Cym}$), 5.53 (dd, ^{3}*J*(H,H) = 6 Hz, ^{3}*J*(H,H) = 6 Hz, 2 H; 2-H/6-H$_{Cym}$), 6.31 ppm (s, 1 H; 5-H); ^{13}C NMR (125.75 MHz, CDCl$_3$): δ = 19.1 (CH$_{3,Cym}$), 20.3 (CH$_3$), 22.8 (CH$_{3,Cym}$), 31.5 (CH$_{Cym}$), 59.4 (CH$_2$), 78.1 (C-3/C-5$_{Cym}$), 80.3 (C-2/C-6$_{Cym}$), 96.2 (C-4$_{Cym}$), 100.0 (C-1$_{Cym}$), 109.9 (C-5), 152.1 (C-6), 156.5 (C-2), 164.5 (C-3), 185.3 ppm (C-4); elemental analysis calcd (%) for C$_{17}$H$_{21}$ClO$_4$Ru: C 47.94, H 4.97; found: C 48.00, H 5.02.

Chlorido[2-ethyl-3-(oxo-κ*O*)-4-(1*H*)-pyronato-κ*O*^{4}](η^6-*p*-cymene)ruthenium(II) (2f): The reaction was performed according to the general complexation procedure by using ethylmaltol (**1g**; 102 mg, 0.72 mmol,

1 equiv), NaOMe (43 mg, 0.8 mmol, 1.1 equiv), and [Ru(η⁶-*p*-cyme-ne)Cl₂]₂ (200 mg, 0.33 mmol, 0.45 equiv). The crude product was dissolved in a minimum amount of CH_2Cl_2 and precipitated with diethyl ether to afford a deep-red solid (181 mg, 61%). M.p. >140°C (decomp.); ¹H NMR (500.10 MHz, CDCl₃): $\delta = 1.22$ (t, ³*J*(H,H) = 7 Hz, 3H; CH₃,Cym), 1.32 (d, ³*J*(H,H) = 7 Hz, 6H; CH₃,Cym), 2.34 (s, 3H; CH₃), 2.80 (m, 1H; CH_Cym), 2.91 (q, ³*J*(H,H) = 7 Hz, 2H; CH₂), 5.30 (dd, ³*J*(H,H) = 6 Hz, ³*J*-(H,H) = 6 Hz, 2H; 3-H/5-H_Cym), 5.52 (dd, ³*J*(H,H) = 6 Hz, ³*J*(H,H) = 6 Hz, 2H; 2-H/6-H_Cym), 6.52 (d, ³*J*(H,H) = 5 Hz, 1H; 5-H), 7.59 ppm (d, ³*J*-(H,H) = 5 Hz, 1H; 6-H); ¹³C NMR (125.75 MHz, CDCl₃): $\delta = 10.8$ (CH₃), 18.6 (CH₃,Cym), 21.6 (CH₂), 22.3 (CH₃,Cym), 31.1 (CH_Cym), 77.8 (C-3/C-5_Cym), 79.6 (C-2/C-6_Cym), 95.9 (C-4_Cym), 99.6 (C-1_Cym), 111.0 (C-5), 151.6 (C-6), 157.3 (C-2), 158.3 (C-3), 182.9 ppm (C-4); elemental analysis calcd (%) for C₁₇H₂₁ClO₃Ru: C 49.81, H 5.16; found: C 49.49, H 5.10.

Chlorido[2-methyl-5-(oxo-κ*O*)-pyran-4(1*H*)-thionato-κ*S*](η⁶-*p*-cymene)-ruthenium(II) (2g): The reaction was performed according to the general complexation protocol by using thioallomaltol (**1g**; 103 mg, 0.72 mmol, 1 equiv), NaOMe (43 mg, 0.8 mmol, 1.1 equiv), and [Ru(η⁶-*p*-cy-mene)Cl₂]₂ (200 mg, 0.33 mmol, 0.45 equiv). The crude product was re-crystallized from ethyl acetate/*n*-hexane to afford a red crystalline solid (230 mg, 85%). M.p. >190°C (decomp.); ¹H NMR (500.10 MHz, CDCl₃): $\delta = 1.26$ (d, ³*J*(H,H) = 7 Hz, 6H; CH₃), 2.23 (s, 3H; CH₃,Cym), 2.27 (s, 3H; CH₃), 2.76 (m, 1H; CH_Cym), 5.51 (d, ³*J*(H,H) = 5 Hz, 2H; 3'-H/5'-H), 5.71 (d, ³*J*(H,H) = 6 Hz, 2H; 2'-H/6 '-H), 7.09 (s, 1H; 5-H), 7.87 ppm (s, 1H; 2-H); ¹³C NMR (125.75 MHz, CDCl₃): $\delta = 18.6$ (CH₃,Cym), 19.0 (CH₃), 22.1 (CH₃,Cym), 30.9 (CH_Cym), 80.5 (C-3/C-5_Cym), 81.3 (C-2/C-6_Cym), 99.5 (C-4_Cym), 100.9 (C-1_Cym), 119.4 (C-3), 139.6 (C-6), 157.1 (C-2), 166.0 (C-5), 187.0 ppm (C-4); elemental analysis calcd (%) for C₁₆H₁₉ClO₂RuS: C 46.65, H 4.65, S 7.78; found: C 46.24, H 4.61, S 8.04.

Chlorido[2-methyl-3-(oxo-κ*O*)-pyran-4(1*H*)-thionato-κ*S*](η⁶-*p*-cymene)-ruthenium(II) (2h): The reaction was performed according to the general complexation protocol by using thiomaltol (**1h**; 103 mg, 0.72 mmol, 1 equiv), NaOMe (43 mg, 0.8 mmol, 1.1 equiv), and [Ru(η⁶-*p*-cy-mene)Cl₂]₂ (200 mg, 0.33 mmol, 0.45 equiv). The crude product was re-crystallized from ethyl acetate/*n*-hexane to afford a red crystalline solid (200 mg, 74%). M.p. >190°C (decomp.); ¹H NMR (500.10 MHz, CDCl₃): $\delta = 1.28$ (d, ³*J*(H,H) = 7 Hz, 6H; CH₃,Cym), 2.21 (s, 3H; CH₃,Cym), 2.50 (s, 3H; CH₃), 2.76 (m, 1H; CH_Cym), 5.49 (br s, 2H; 3-H/5-H_Cym), 5.71 (br s, 2H; 2-H/6-H_Cym), 7.18 (d, ³*J*(H,H) = 5 Hz, 1H; 5-H), 7.43 ppm (d, ³*J*-(H,H) = 5 Hz, 1H; 6-H); ¹³C NMR (125.75 MHz, CDCl₃): $\delta = 15.4$ (CH₃), 18.4 (CH₃,Cym), 22.1 (CH₃,Cym), 31.0 (CH_Cym), 80.5 (C-3/C-5_Cym), 81.3 (C-2/C-6_Cym), 98.2 (C-4_Cym), 100.0 (C-1_Cym), 120.2 (C-5), 143.9 (C-6), 153.3 (C-2), 165.4 (C-3), 180.5 ppm (C-4); elemental analysis calcd (%) for C₁₆H₁₉ClO₂SRu: C 46.65, H 4.65, S 7.75; found: C 47.03, H 4.57, S 7.67.

p*K*ₐ determination: To determine the p*K*ₐ values, **2a–f** were dissolved in D₂O and the pH of the solution in the NMR tube was determined with an Eco Scan pH6 pH meter equipped with a glass-micro combination pH electrode (Orion 9826BN) and calibrated with standard buffer solutions of pH 4.00, 7.00, and 10.00. The pH titration was performed by the addition of NaOD (0.4–0.0004% in D₂O) to a DNO₃ acidified solution (0.4–0.0004% in D₂O). The shifts of the 2-H/6-H cymene protons observed in the ¹H NMR spectra were plotted against the pH value and the curves obtained were fitted by using the Henderson–Hasselbalch equation with Excel software (Microsoft® Office Excel 2003, SP3, Microsoft Corporation). The experimentally obtained p*K*ₐ* values were corrected with Equation (1)[48] in order to convert the p*K*ₐ* values determined in D₂O to the corresponding p*K*ₐ values in aqueous solutions.

$$pK_a = 0.929\, pK_{a*} + 0.42 \tag{1}$$

Computational details: Full geometry optimization of all the structures was carried out at the DFT level of theory by using Becke's three-parameter hybrid exchange functional[49] in combination with the gradient-corrected correlation functional of Lee, Yang, and Parr[50] (B3LYP) and with the Gaussian 03[51] program package. Symmetry operations were not applied to all structures. The geometry optimizations were carried out by using a quasi-relativistic Stuttgart pseudo-potential described 28 core electrons and the appropriate contracted basis set (8s7p6d)/[6s5p3d][52]

for the ruthenium atom and the 6-31G(d) basis set for the other atoms. Then, single-point calculations were performed on the basis of the equilibrium geometries determined by using the 6-31+G(d,p) basis set for non-metal atoms. The experimental X-ray structure of **2h**[34] was chosen as the starting geometry for the optimizations. The Hessian matrix was calculated analytically for all optimized structures to prove the location of the correct minima (no "imaginary" frequencies) and to estimate thermodynamic parameters, the latter were calculated at 25°C.

Solvent effects were taken into account in the single-point calculations based on the gas-phase equilibrium geometries at the CPCM-B3LYP/6-31+G(d,p)//gas-B3LYP/6-31G(d) level of theory using the polarizable continuum model (CPCM version)[53,54] with H₂O as solvent and UAKS atomic radii. The Gibbs free-energies in solution (G_s) were estimated by addition of the solvation energy δG_{solv} to the gas-phase Gibbs free-energies (G_g).

p*K*ₐ values were calculated for the reaction HA⁺ + H₂O → A + H₃O⁺ (HA⁺: cationic complexes **3'b**, **3'd**, **3g**, and **3h**; A: corresponding neutral hydroxo complexes **5'b**, **5'd**, **5g**, and **5h**; 1 atm standard state) by using Equation (2)

$$pK_a = \frac{\Delta G}{2.303 RT} - 1.74 \tag{2}$$

The vertical heterolytic bond energies in solution were calculated at the CPCM-B3LYP/6-31+G(d,p)//gas-B3LYP/6-31G(d) level of theory.

Interaction with small biomolecules: Complexes **2a–h** (1–2 mg mL⁻¹) were dissolved in D₂O (containing 5% [D₆]DMSO for **2g** and **2h**) to yield the aqua species **3a–h**, which were titrated against 5'-GMP solution (10 mg mL⁻¹) in 50 μL steps, and the reaction was monitored by ¹H and ³¹P NMR spectroscopy until unreacted 5'-GMP was detected.

To investigate their reactivity towards amino acids and imidazole, the aqua complexes **3a–h** (1 mg mL⁻¹) were treated with equimolar amounts of amino acids and the ¹H NMR spectra were recorded after 5 min and 18 h.

Cytotoxicity in cancer cell lines

Cell lines and culture conditions: CH1 cells originate from an ascites sample of a patient with a papillary cystadenocarcinoma of the ovary and were a generous gift from Lloyd R. Kelland (CRC Centre for Cancer Therapeutics, Institute of Cancer Research, Sutton, UK). SW480 (adeno-carcinoma of the colon, human) and A549 (non-small cell lung cancer, human) cells were kindly provided by Brigitte Marian (Institute of Cancer Research, Department of Medicine I, Medical University of Vienna, Austria). All cell culture reagents were obtained from Sigma–Aldrich, Austria. Cells were grown in 75 cm² culture flasks (Iwaki) as adherent monolayer cultures in Minimal Essential Medium (MEM) supplemented with 10% heat-inactivated fetal calf serum, 1 mM sodium pyruvate, 4 mM L-glutamine, and 1% nonessential amino acids (100×). Cultures were maintained at 37°C in a humidified atmosphere containing 95% air and 5% CO₂.

MTT assay conditions: The cytotoxicity was determined by the colorimetric MTT (3-(4,5-dimethyl-2-thiazolyl)-2,5-diphenyl-2*H*-tetrazolium bromide, purchased from Fluka) microculture assay. For this purpose, cells were harvested from culture flasks by trypsinization and seeded in 100 μL aliquots into 96-well microculture plates (Iwaki). Cell densities of 1.5×10³ (CH1), 2.5×10³ (SW480), and 4×10³ cells per well (A549) were chosen to ensure exponential growth of untreated controls throughout the experiment. Cells were allowed to settle and resume exponential growth in a drug-free complete culture medium for 24 h. Stocks of the test compounds in DMSO were appropriately diluted in complete culture medium such that the maximum DMSO content did not exceed 1% (this procedure yielded opaque but colloidal solutions from which no precipitates could be separated by centrifugation). These dilutions were added in 100 μL aliquots to the microcultures (if necessary due to limited solubility, the maximum concentration tested was added in 200 μL aliquots after removal of the preincubation medium) and cells were exposed to the test compounds for 96 h. At the end of exposure, all media were replaced by 100 μL per well RPMI1640 culture medium (supplemented with 10% heat-inactivated fetal bovine serum) plus 20 μL per well MTT

solution in phosphate-buffered saline (5 mg mL^{-1}). After incubation for 4 h, the supernatants were removed and the formazan crystals formed by vital cells were dissolved in 150 μL DMSO per well. Optical densities at 550 nm were measured with a microplate reader (Tecan Spectra Classic) using a reference wavelength of 690 nm to correct for unspecific absorption. The quantity of vital cells was expressed in terms of T/C (treated/control) values by comparison with untreated control microcultures and 50% inhibitory concentrations (IC$_{50}$) were calculated from concentration-effect curves by interpolation. The evaluations were based on the means from at least three independent experiments, each comprising at least three replicates per concentration level.

Acknowledgements

[1] M. A. Jakupec, M. Galanski, V. B. Arion, C. G. Hartinger, B. K. Keppler, *Dalton Trans.* **2008**, 183–194.

[2] P. Heffeter, U. Jungwirth, M. Jakupec, C. Hartinger, M. Galanski, L. Elbling, M. Micksche, B. Keppler, W. Berger, *Drug Resist. Updates* **2008**, *11*, 1–16.

[3] M. J. Clarke, F. Zhu, D. R. Frasca, *Chem. Rev.* **1999**, *99*, 2511–2533.

[4] W. H. Ang, P. J. Dyson, *Eur. J. Inorg. Chem.* **2006**, 4003–4018.

[5] P. J. Dyson, G. Sava, *Dalton Trans.* **2006**, 1929–1933.

[6] K. Strohfeldt, M. Tacke, *Chem. Soc. Rev.* **2008**, *37*, 1174–1187.

[7] C. G. Hartinger, P. J. Dyson, *Chem. Soc. Rev.* **2009**, *38*, 391–401.

[8] J. M. Rademaker-Lakhai, D. Van Den Bongard, D. Pluim, J. H. Beijnen, J. H. M. Schellens, *Clin. Cancer Res.* **2004**, *10*, 3717–3727.

[9] C. G. Hartinger, M. A. Jakupec, S. Zorbas-Seifried, M. Groessl, A. Egger, W. Berger, H. Zorbas, P. J. Dyson, B. K. Keppler, *Chem. Biodiversity* **2008**, *5*, 2140–2155.

[10] C. G. Hartinger, S. Zorbas-Seifried, M. A. Jakupec, B. Kynast, H. Zorbas, B. K. Keppler, *J. Inorg. Biochem.* **2006**, *100*, 891–904.

[11] A. F. A. Peacock, P. J. Sadler, *Chem. Asian J.* **2008**, *3*, 1890–1899.

[12] M. Pongratz, P. Schluga, M. A. Jakupec, V. B. Arion, C. G. Hartinger, G. Allmaier, B. K. Keppler, *J. Anal. At. Spectrom.* **2004**, *19*, 46–51.

[13] M. Sulyok, S. Hann, C. G. Hartinger, B. K. Keppler, G. Stingeder, G. Koellensperger, *J. Anal. At. Spectrom.* **2005**, *20*, 856–863.

[14] P. Schluga, C. G. Hartinger, A. Egger, E. Reisner, M. Galanski, M. A. Jakupec, B. K. Keppler, *Dalton Trans.* **2006**, 1796–1802.

[15] M. A. Jakupec, E. Reisner, A. Eichinger, M. Pongratz, V. B. Arion, M. Galanski, C. G. Hartinger, B. K. Keppler, *J. Med. Chem.* **2005**, *48*, 2831–2837.

[16] M. Groessl, C. G. Hartinger, K. Polec-Pawlak, M. Jarosz, B. K. Keppler, *Electrophoresis* **2008**, *29*, 2224–2232.

[17] G. Jaouen, *Bioorganometallics*, Wiley-VCH, Weinheim, **2006**, p. 444.

[18] C. S. Allardyce, P. J. Dyson, D. J. Ellis, S. L. Heath, *Chem. Commun.* **2001**, 1396–1397.

[19] A. F. A. Peacock, M. Melchart, R. J. Deeth, A. Habtemariam, S. Parsons, P. J. Sadler, *Chem. Eur. J.* **2007**, *13*, 2601–2613.

[20] H. Chen, J. A. Parkinson, S. Parsons, R. A. Coxall, R. O. Gould, P. J. Sadler, *J. Am. Chem. Soc.* **2002**, *124*, 3064–3082.

[21] O. Nováková, A. A. Nazarov, C. G. Hartinger, B. K. Keppler, V. Brabec, *Biochem. Pharmacol.* **2009**, *77*, 364–374.

[22] R. Fernandez, M. Melchart, A. Habtemariam, S. Parsons, P. J. Sadler, *Chem. Eur. J.* **2004**, *10*, 5173–5179.

[23] P. J. Dyson, *Chimia* **2007**, *61*, 698–703.

[24] C. Scolaro, A. Bergamo, L. Brescacin, R. Delfino, M. Cocchietto, G. Laurenczy, T. J. Geldbach, G. Sava, P. J. Dyson, *J. Med. Chem.* **2005**, *48*, 4161–4171.

[25] S. Chatterjee, S. Kundu, A. Bhattacharyya, C. G. Hartinger, P. J. Dyson, *J. Biol. Inorg. Chem.* **2008**, *13*, 1149–1155.

[26] R. E. Aird, J. Cummings, A. A. Ritchie, M. Muir, R. E. Morris, H. Chen, P. J. Sadler, D. I. Jodrell, *Br. J. Cancer* **2002**, *86*, 1652–1657.

[27] A. Habtemariam, M. Melchart, R. Fernandez, S. Parsons, I. D. H. Oswald, A. Parkin, F. P. A. Fabbiani, J. E. Davidson, A. Dawson, R. E. Aird, D. I. Jodrell, P. J. Sadler, *J. Med. Chem.* **2006**, *49*, 6858–6868.

[28] W. H. Ang, E. Daldini, C. Scolaro, R. Scopelliti, L. Juillerat-Jeannerat, P. J. Dyson, *Inorg. Chem.* **2006**, *45*, 9006–9013.

[29] M. G. Mendoza-Ferri, C. G. Hartinger, R. E. Eichinger, N. Stolyarova, M. A. Jakupec, A. A. Nazarov, K. Severin, B. K. Keppler, *Organometallics* **2008**, *27*, 2405–2407.

[30] M. G. Mendoza-Ferri, C. G. Hartinger, A. A. Nazarov, W. Kandioller, K. Severin, B. K. Keppler, *Appl. Organomet. Chem.* **2008**, *22*, 326–332.

[31] R. Schuecker, R. O. John, M. A. Jakupec, V. B. Arion, B. K. Keppler, *Organometallics* **2008**, *27*, 6587–6595.

[32] W. Kandioller, C. G. Hartinger, A. A. Nazarov, J. Kasser, R. John, M. A. Jakupec, V. B. Arion, P. J. Dyson, B. K. Keppler, *J. Organomet. Chem.* **2009**, *694*, 922–929.

[33] M. G. Mendoza-Ferri, C. G. Hartinger, M. A. Mendoza, M. Groessl, A. E. Egger, R. E. Eichinger, J. B. Mangrum, N. P. Farrell, M. Maruszak, P. J. Bednarski, F. Klein, M. A. Jakupec, A. A. Nazarov, K. Severin, B. K. Keppler, *J. Med. Chem.* **2009**, *52*, 916–925.

[34] W. Kandioller, C. G. Hartinger, A. A. Nazarov, M. L. Kuznetsov, R. John, C. Bartel, M. A. Jakupec, V. B. Arion, B. K. Keppler, *Organometallics* **2009**, *28*, 4249–4251.

[35] W. H. Ang, Z. Grote, R. Scopelliti, L. Juillerat-Jeanneret, K. Severin, P. J. Dyson, *J. Organomet. Chem.* **2009**, *694*, 968–972.

[36] K. H. Thompson, C. A. Barta, C. Orvig, *Chem. Soc. Rev.* **2006**, *35*, 545–556.

[37] Z. D. Liu, H. H. Khodr, D. Y. Liu, S. L. Lu, R. C. Hider, *J. Med. Chem.* **1999**, *42*, 4814–4823.

[38] J. A. Lewis, D. T. Puerta, S. M. Cohen, *Inorg. Chem.* **2003**, *42*, 7455–7459.

[39] R. Lang, K. Polborn, T. Severin, K. Severin, *Inorg. Chim. Acta* **1999**, *294*, 62–67.

[40] I. Berger, M. Hanif, A. A. Nazarov, C. G. Hartinger, R. O. John, M. L. Kuznetsov, M. Groessl, F. Schmitt, O. Zava, F. Biba, V. B. Arion, M. Galanski, M. A. Jakupec, L. Juillerat-Jeanneret, P. J. Dyson, B. K. Keppler, *Chem. Eur. J.* **2008**, *14*, 9046–9057.

[41] A. Dorcier, C. G. Hartinger, R. Scopelliti, R. H. Fish, B. K. Keppler, P. J. Dyson, *J. Inorg. Biochem.* **2008**, *102*, 1066–1076.

[42] W. L. F. Armarego, C. Chai, *Purification of Laboratory Chemicals*, 5th ed., Butterworth Heinemann, Oxford, **2003**.

[43] SAINT + Integration Engine, Program for Crystal Structure Integration, M. R. Pressprich, J. Chambers, Bruker Analytical X-ray systems, Madison, **2004**.

[44] SHELXS-97, Program for Crystal Structure Solution, G. M. Sheldrick, Göttingen (Germany), **1997**.

[45] SHELXL-97, Program for Crystal Structure Refinement, G. M. Sheldrick, Göttingen (Germany), **1997**.

[46] L. J. Farrugia, *J. Appl. Crystallogr.* **1997**, *30*, 565.

[47] *International Tables for X-ray Crystallography, Vol. C*, Kluwer Academic, Dordrecht, **1992**.

[48] A. Krezel, W. Bal, *J. Inorg. Biochem.* **2004**, *98*, 161–166.

[49] A. D. Becke, *J. Chem. Phys.* **1993**, *98*, 5648–5652.

[50] C. Lee, W. Yang, R. G. Parr, *Phys. Rev. B* **1988**, *37*, 785–789.

[51] Gaussian 03, Revision D.01, M. J. Frisch, G. W. Trucks, H. B. Schlegel, G. E. Scuseria, M. A. Robb, J. R. Cheeseman, J. Montgomery, Jr., J. A., T. Vreven, K. N. Kudin, J. C. Burant, J. M. Millam, S. S. Iyengar, J. Tomasi, V. Barone, B. Mennucci, M. Cossi, G. Scalmani, N. Rega, G. A. Petersson, H. Nakatsuji, M. Hada, M. Ehara, K. Toyota, R. Fukuda, J. Hasegawa, M. Ishida, T. Nakajima, Y. Honda, O. Kitao, H. Nakai, M. Klene, X. Li, J. E. Knox, H. P.

Hratchian, J. B. Cross, V. Bakken, C. Adamo, J. Jaramillo, R. Gomperts, R. E. Stratmann, O. Yazyev, A. J. Austin, R. Cammi, C. Pomelli, J. W. Ochterski, P. Y. Ayala, K. Morokuma, G. A. Voth, P. Salvador, J. J. Dannenberg, V. G. Zakrzewski, S. Dapprich, A. D. Daniels, M. C. Strain, O. Farkas, D. K. Malick, A. D. Rabuck, K. Raghavachari, J. B. Foresman, J. V. Ortiz, Q. Cui, A. G. Baboul, S. Clifford, J. Cioslowski, B. B. Stefanov, G. Liu, A. Liashenko, P. Piskorz, I. Komaromi, R. L. Martin, D. J. Fox, T. Keith, M. A. Al-Laham, C. Y. Peng, A. Nanayakkara, M. Challacombe, P. M. W. Gill, B. Johnson, W. Chen, M. W. Wong, C. Gonzalez, J. A. Pople, Gaussian, Inc., Wallingford CT, **2004**.

[52] D. Andrae, U. Haeussermann, M. Dolg, H. Stoll, H. Preuss, *Theor. Chim. Acta* **1990**, *77*, 123–141.

[53] J. Tomasi, M. Persico, *Chem. Rev.* **1994**, *94*, 2027–2094.

[54] V. Barone, M. Cossi, *J. Phys. Chem. A* **1998**, *102*, 1995–2001.

2.6.   From pyrone to thiopyrone ligands-rendering maltol-derived ruthenium(II)-arene complexes that are anticancer active *in vitro*

Kandioller W.[a], Hartinger C.G.[a,b], Nazarov A.A.[a,b,c], Kuznetsov M.L.[c], John R.O.[a], Bartel C.[a], Jakupec M.A.[a], Arion V.B.[a], Keppler B.K.[a]

[a] Institute of Inorganic Chemistry, University of Vienna, Waehringer Strasse 42, 1090 Vienna, Austria

[b] Institut des Sciences et Ingenierie Chimiques, Ecole Polytechnique Federale de Lausanne (EPFL), CH-1015, Lausanne, Switzerland

[c] Centro de Quimica Estrutural, Complexo I, Instituto Superior Tecnico, Technical University of Lisbon, Av. Rovisco Pais, 1049-001 Lisbon, Portugal

From Pyrone to Thiopyrone Ligands—Rendering Maltol-Derived Ruthenium(II)—Arene Complexes That Are Anticancer Active in Vitro

Wolfgang Kandioller,[†] Christian G. Hartinger,*,[†] Alexey A. Nazarov,*,[†,‡]
Maxim L. Kuznetsov,[§] Roland O. John,[†] Caroline Bartel,[†] Michael A. Jakupec,[†]
Vladimir B. Arion,[†] and Bernhard K. Keppler[†]

[†]*University of Vienna, Institute of Inorganic Chemistry, Waehringer Str. 42, A-1090 Vienna, Austria,*
[‡]*Institut des Sciences et Ingénierie Chimiques, Ecole Polytechnique Fédérale de Lausanne (EPFL), CH-1015*
Lausanne, Switzerland, and [§]Centro de Química Estrutural, Complexo I, Instituto Superior Técnico,
*Technical University of Lisbon, Av. Rovisco Pais, 1049-001 Lisbon, Portugal*

Summary: Ru(II)—arene complexes with pyrone-derived ligands are rendered active against cancer cells by replacement of the coordinated O,O donor with an S,O donor. The different stabilities of these systems may explain the observed influence of the donor atoms on the anticancer activity in vitro.

Metal complexes are playing an important role in the treatment of cancer, and many promising compounds have been developed in recent years.[1–4] Ruthenium complexes have been shown to be among the most promising candidates for new metal-based anticancer drugs. Two of them, KP1019 and NAMI-A, are currently undergoing clinical trials.[2,5] Their low general toxicity might be explained by their modes of action, including protein binding and activation by reduction.[5–7]

More recently, bioorganometallic chemistry has emerged as a new source of anticancer metallodrugs, with titanocene dichloride being the prototype agent of this compound class.[4,8,9] Furthermore, organometallic Ru(II) compounds that are stabilized in their +2 oxidation state by coordination of an arene ligand have been investigated for their anticancer properties. These piano-stool complexes have been pioneered by the Dyson and Sadler groups,[10,11] who developed compounds with pta (1,3,5-triaza-7-phosphatricyclo[3.3.1.1]-decane) and en (ethylenediamine) ligands, respectively.[10] For the [(η^6-arene)Ru[II](X)(Y)] complexes, DNA base selectivity strongly depends on the character of the chelating ligand Y—exchange of the neutral ethylenediamine by anionic acetyla-

Scheme 1. Synthesis of the Complexes 2a–d

a	R1 = H, R2 = CH$_3$, X = O
b	R1 = H, R2 = CH$_3$, X = S
c	R1 = CH$_3$, R2 = H, X = O
d	R1 = CH$_3$, R2 = H, X = S
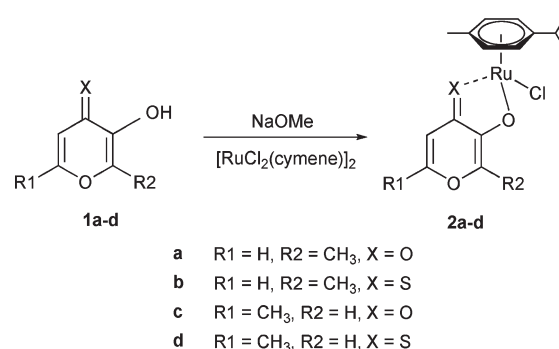
cetonate shifts the affinity from guanine to adenine.[12] In addition to en and pta complexes, maltol-derived mono- and polynuclear ruthenium and osmium complexes have been developed.[13–15] The linking of two pyridone moieties opened up new possibilities for tuning the in vitro anticancer activity and lipophilicity, and compounds with interduplex cross-linking capacity were obtained.[14,16–18] In the case of the mononuclear Ru(II) complexes, an increase in cytotoxic activity was achieved by derivatization of the pyrone ring with lipophilic aromatic substituents.[13]

In order to study the Ru—ligand interaction and its effect on the in vitro anticancer activity, Ru(II)—cymene complexes (Scheme 1) with pyrones and their corresponding, more lipophilic thiopyrones as chelating agents were prepared.[15,19] Such (thio)pyrone systems have already found application in

---

*To whom correspondence should be addressed. E-mail: christian.hartinger@univie.ac.at (C.G.H.); alex.nazarov@univie.ac.at (A.A.N.).

(1) Guo, Z.; Sadler, P. J. *Adv. Inorg. Chem.* **2000**, *49*, 183–306.
(2) Alessio, E.; Mestroni, G.; Bergamo, A.; Sava, G. *Curr. Top. Med. Chem.* **2004**, *4*, 1525–35.
(3) Jakupec, M. A.; Galanski, M.; Arion, V. B.; Hartinger, C. G.; Keppler, B. K. *Dalton Trans.* **2008**, 183–194.
(4) Strohfeldt, K.; Tacke, M. *Chem. Soc. Rev.* **2008**, *37*, 1174–1187.
(5) Hartinger, C. G.; Zorbas-Seifried, S.; Jakupec, M. A.; Kynast, B.; Zorbas, H.; Keppler, B. K. *J. Inorg. Biochem.* **2006**, *100*, 891–904.
(6) Groessl, M.; Reisner, E.; Hartinger, C. G.; Eichinger, R.; Semenova, O.; Timerbaev, A. R.; Jakupec, M. A.; Arion, V. B.; Keppler, B. K. *J. Med. Chem.* **2007**, *50*, 2185–2193.
(7) Dyson, P. J.; Sava, G. *Dalton Trans.* **2006**, 1929–1933.
(8) Hartinger, C. G.; Dyson, P. J. *Chem. Soc. Rev.* **2009**, *38*, 391–401.
(9) Jaouen, G., *Bioorganometallics*; Wiley-VCH: Weinheim, Germany, 2006; p 444.
(10) Ang, W. H.; Dyson, P. J. *Eur. J. Inorg. Chem.* **2006**, 4003–4018.
(11) Yan, Y. K.; Melchart, M.; Habtemariam, A.; Sadler, P. J. *Chem. Commun.* **2005**, 4764–4776.
(12) Fernandez, R.; Melchart, M.; Habtemariam, A.; Parsons, S.; Sadler, P. J. *Chem. Eur. J.* **2004**, *10*, 5173–5179.

(13) Peacock, A. F. A.; Melchart, M.; Deeth, R. J.; Habtemariam, A.; Parsons, S.; Sadler, P. J. *Chem. Eur. J.* **2007**, *13*, 2601–2613.
(14) Mendoza-Ferri, M. G.; Hartinger, C. G.; Eichinger, R. E.; Stolyarova, N.; Jakupec, M. A.; Nazarov, A. A.; Severin, K.; Keppler, B. K. *Organometallics* **2008**, *27*, 2405–2407.
(15) Kandioller, W.; Hartinger, C. G.; Nazarov, A. A.; Kasser, J.; John, R.; Jakupec, M. A.; Arion, V. B.; Dyson, P. J.; Keppler, B. K. *J. Organomet. Chem.* **2009**, *694*, 922–929.
(16) Mendoza-Ferri, M. G.; Hartinger, C. G.; Nazarov, A. A.; Kandioller, W.; Severin, K.; Keppler, B. K. *Appl. Organomet. Chem.* **2008**, *22*, 326–332.
(17) Mendoza-Ferri, M. G.; Hartinger, C. G.; Mendoza, M. A.; Groessl, M.; Egger, A.; Eichinger, R. E.; Mangrum, J. B.; Farrell, N. P.; Maruszak, M.; Bednarski, P. J.; Klein, F.; Jakupec, M. A.; Nazarov, A. A.; Severin, K.; Keppler, B. K. *J. Med. Chem.* **2009**, *52*, 916–925.
(18) Nováková, O.; Nazarov, A. A.; Hartinger, C. G.; Keppler, B. K.; Brabec, V. *Biochem. Pharmacol.* **2009**, *77*, 364–374.
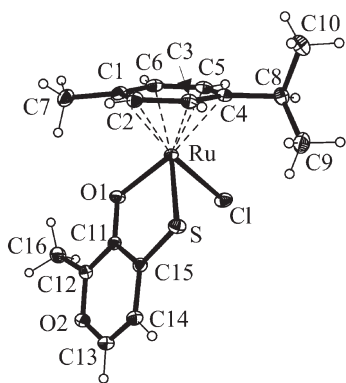(19) Lewis, J. A.; Puerta, D. T.; Cohen, S. M. *Inorg. Chem.* **2003**, *42*, 7455–7459.

Figure 1. ORTEP plot of the molecular structure of **2b**.

medicinal chemistry.[20,21] The Ru(II)−cymene complexes were obtained in good yields (64−85%) by deprotonation of the ligand with sodium methoxide and reaction with bis[dichlorido-(η^6-*p*-cymene)ruthenium(II)]. The reaction was performed with a slight excess of ligand to facilitate the purification. All complexes have been fully characterized by 1D and 2D NMR spectroscopy, mass spectrometry, and elemental analysis.

Single crystals of **2b** were obtained from ethyl acetate, and the molecular structure was determined by X-ray diffraction analysis. The ruthenium center was found to adopt a piano-stool configuration (Figure 1 and the Supporting Information). Due to the larger sulfur atom in **2b**, as compared to the oxygen in maltol-derived ligands, the Ru−S bond (2.3730(3) Å) is significantly longer than the Ru−O bond (2.0808(10) Å). This leads to a strong distortion of the five-membered chelate ring of the complex. The length of the Ru−Cl bond in **2b** (2.4331(4) Å) is comparable to the corresponding bond lengths of pyrone and pyridone Ru(II)−arene complexes.[14,15]

The antiproliferative activities of **2a−d** were investigated in the human tumor cell lines SW480 (colon carcinoma) and CH1 (ovarian carcinoma) by using the colorimetric MTT assay (Figure 2). The IC$_{50}$ values are presented in Table 1. As reported earlier,[14] the maltol complex **2a** shows limited cytotoxic activity, and the allomaltol derivative **2c** has IC$_{50}$ values > 200 μM. In contrast, the thiopyrone complexes **2b,d** are at least by an order of magnitude (in IC$_{50}$) more active than their pyrone analogues. For complexes **2b,d**, an inverted sensitivity of SW480 cells and CH1 cells was observed, which is in contrast with the case for a broad spectrum of other compounds but parallels that observed with Ru(II)−arene complexes containing an 8-quinolinolato ligand.[22] The substitution pattern influences the activity, as inferred from the 2.7−3.9 times higher activity of **2b** as compared to **2d**. These compounds are less cytotoxic than other ruthenium complexes[23] but are still in a reasonable range of activity in vitro in comparison to other Ru−arene species.[22] However, the in vitro effects are only a first indication for potential activity, which needs to be verified in vivo.

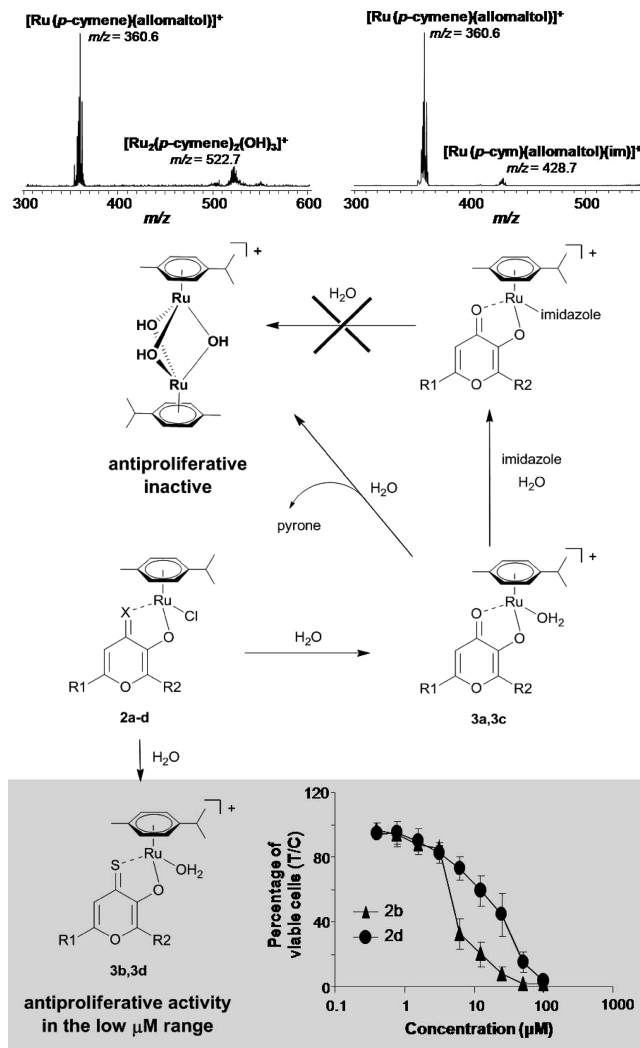The in vitro inactivity of the maltolato complexes has been attributed to the formation of dimers in aqueous solution.[13]

Figure 2. Hydrolysis of Ru−(thio)pyronato complexes (X=O, S), yielding in the case of the pyrone ligands the dimeric [Ru$_2$-(cym)$_2$(OH)$_3$]$^+$ species (as demonstrated by ESI-MS; top left). When the aqua complexes **3a,c** were reacted with imidazole, no dimerization was observed (top right), as was the case for the thiopyrone compounds **3b,d**, which show significant cytotoxic activity in human cancer cell lines (bottom).

Accordingly, hydrolysis and stability in water were investigated by NMR spectroscopy in D$_2$O or 10% DMSO-d_6/90% D$_2$O solutions for the maltol and thiomaltol compounds, respectively. The complexes **2a−d** hydrolyze within seconds to charged complexes by exchange of the chlorido ligand with a water molecule (Figure 2). No coordination of DMSO-d_6 was observed, and identical NMR spectra were obtained by activation of **2a,c** with an equimolar amount of AgNO$_3$, which confirms the obtained results. Similarly to the case of **2a**,[13] the formation of a dimeric species was observed for **2c** (Figure 2, top left), as demonstrated by ESI-MS with a sample of 25 μM; this concentration was chosen in order to obtain a mass spectrum containing both the intact complex and the dimeric species. The amount of side product formed depends on the concentration, time, and pH value of the solution, and its formation can be prevented by addition of an equimolar amount of imidazole, as also demonstrated by means of ESI-MS (Figure 2, top right).

(20) Lewis, J. A.; Mongan, J.; McCammon, J. A.; Cohen, S. M. *ChemMedChem* **2006**, *1*, 694−697.

(21) Thompson, K. H.; Barta, C. A.; Orvig, C. *Chem. Soc. Rev.* **2006**, *35*, 545−556.

(22) Schuecker, R.; John, R. O.; Jakupec, M. A.; Arion, V. B.; Keppler, B. K. *Organometallics* **2008**, *27*, 6587−6595.

(23) Jakupec, M. A.; Reisner, E.; Eichinger, A.; Pongratz, M.; Arion, V. B.; Galanski, M.; Hartinger, C. G.; Keppler, B. K. *J. Med. Chem.* **2005**, *48*, 2831−2837.

Table 1. Antiproliferative Activity, ΔG of Hydrolysis, and Bond Energies (kcal/mol) of 2a−d (2′a−d)

	IC$_{50}$ (μM)			
	2a	**2b**	**2c**	**2d**
CH1	> 100	13 ± 4	239 ± 22	35 ± 8
SW480	> 100	5.1 ± 0.5	359 ± 119	20 ± 7
	2′a	**2′b**	**2′c**	**2′d**
ΔG_{hydr}	4.2	3.3	4.9	3.6
E(Ru−Cl)	10.6	7.1	11.1	7.9
E(Ru−O/S)$_{O/S=C}$	26.8	34.6	26.4	34.4
E(Ru−O)$_{O−C}$	36.9	35.7	36.6	36.2

Hydrolysis of **2b**,**d** in 10% DMSO-d_6/D$_2$O results in the rapid formation of aqua species, which are stable for more than 24 h; in contrast to the case for the maltolato complexes, no dimers have been observed. To explain these observations, theoretical DFT calculations (B3LYP, Gaussian 03 program package;[24] see the Supporting Information for computational details) of the metal−ligand bond energies have been performed. They reveal that the Ru−S$_{S=C}$ bond energies in the model complexes **2′b**,**d** (bearing benzene instead of cymene in **2b**,**d**) are higher by 7.8−8.0 kcal/mol than the Ru−O$_{O=C}$ bond energies in **2′a**,**c**, respectively. In contrast, the Ru−O$_{O−C}$ bond energies in thiopyrone complexes are lower than those in pyrone species, but only by 0.4−1.2 kcal/mol. The stronger binding of thiopyrones to Ru as compared to pyrones explains why thiopyrone complexes are stable in aqueous solution while pyrone complexes undergo decomposition with release of the ligands **1a**,**c**.

Theoretical calculations of **2′a−d** and **3′a−d** show that ΔG values for the substitution of chloride with H$_2$O are only slightly positive (3.3−4.9 kcal/mol). Taking into account the large excess of water, complexes **3a−d** are the predominant species in aqueous solutions. Lower Ru−Cl bond energies in **2′b**,**d** as compared to **2′a**,**c**, respectively, correlate with ΔG values of hydrolysis (Table 1).

In summary, the modification of the first ligand sphere and therewith of the stability of the complexes influences significantly the in vitro anticancer activity. Pyrone and thiopyrone compounds behave quite differently in water (dimer formation). These features have important implications for the mode of action of the compounds and result in considerably active thiopyrone vs minimally active pyrone complexes. Furthermore, complexes **2b**,**d** are slightly more active in SW480 cells, though CH1 cells are in our experience more chemosensitive to the vast majority of metal-based and other tumor-inhibiting compounds tested so far.

Supporting Information Available: Text, tables, figures, and a CIF file giving the general procedure for the synthesis of the complexes, characterization, elemental analysis data, X-ray diffraction data, and computational details. This material is available free of charge via the Internet at http://pubs.acs.org. Crystallographic data for this paper are also available from the Cambridge Crystallographic Database (CCDC 720741).

(24) *Gaussian 03, Revision D.01*; Gaussian, Inc., Wallingford, CT, 2004.

2.7. Synthesis, x-ray diffraction structure, spectroscopic properties and antiproliferative activity of a novel ruthenium complex with constitutional similarity to cisplatin

Grguric-Sipka S.[a], Stepanenko I.N.[b], Lazic J.M.[a], Bartel C.[b], Jakupec M.A.[b], Arion V.B.[b], Keppler B.K.[b]

[a] University of Belgrade, Faculty of Chemistry, Studentski trg 12-16, 11000, Belgrade, Serbia

[b] Institute of Inorganic Chemistry, University of Vienna, Waehringer Strasse 42, 1090 Vienna, Austria

Synthesis, X-ray diffraction structure, spectroscopic properties and antiproliferative activity of a novel ruthenium complex with constitutional similarity to cisplatin†

Sanja Grguric-Sipka,[a] Iryna N. Stepanenko,[b] Jelena M. Lazic,[a] Caroline Bartel,[b] Michael A. Jakupec,[b] Vladimir B. Arion*[b] and Bernhard K. Keppler*[b]

The light-protected reaction of $[(\eta^6\text{-}p\text{-cymene})\text{Ru}^{II}\text{Cl}_2]_2$ with 1-(2-hydroxyethyl)piperazine in dry methanol, followed by addition of excess NH_4PF_6, afforded the complex $[(\eta^6\text{-}p\text{-cymene})\text{Ru}^{II}(\text{NH}_3)_2\text{Cl}]$-$(\text{PF}_6)$ (**1**) in 47% yield. Attempts to use the same protocol for the synthesis of $[(\eta^6\text{-}p\text{cymene})\text{Os}^{II}(\text{NH}_3)_2\text{Cl}](\text{PF}_6)$ led to the isolation of the binuclear triply methoxido-bridged arene-osmium compound $[\{(\eta^6\text{-}p\text{-cymene})\text{Os}\}_2(\mu\text{-OCH}_3)_3](\text{PF}_6)$ (**3**). Both compounds were characterised by X-ray crystallography and ^1H NMR spectroscopy, and the ruthenium complex also by spectroscopic techniques (IR and UV-vis spectroscopies). The antiproliferative activity of complex **1** *in vitro* was studied in A549 (non-small cell lung carcinoma), CH1 (ovarian carcinoma), and SW480 (colon carcinoma) cells and compared to that of $[(\eta^6\text{-}p\text{-cymene})\text{Ru}^{II}(\text{en})\text{Cl}](\text{PF}_6)$ (**2**). In contrast to the latter compound, **1** is only modestly cytotoxic in all three cell lines (IC$_{50}$: 293–542 µM), probably due to the instability of the diammine ruthenium complex in aqueous solution.

Introduction

The first ruthenium complex which showed antiproliferative activity *in vitro* was $[\text{Ru}^{III}\text{Cl}_3(\text{NH}_3)_3]$.[1] The synthesis of this compound was prompted by the clinical success of *cis*-$[\text{Pt}^{II}\text{Cl}_2(\text{NH}_3)_2]$,[2] which is currently one of the most widely and routinely used metal-based anticancer drugs. Further development of $[\text{Ru}^{III}\text{Cl}_3(\text{NH}_3)_3]$ was, however, precluded by its low aqueous solubility, which made its administration difficult. These findings led to the synthesis of novel water-soluble platinum and ruthenium complexes with a different number of ammine, aliphatic and aromatic amine or polyamine ligands and investigation of their antiproliferative activity.[3–8]

The well-established mechanism of cytotoxic action of cisplatin is the alteration of DNA secondary structure *via* coordination to the N^7 atom of a guanine or adenine base, which implies its prior aquation in the cell to the activated complexes $[\text{Pt}(\text{NH}_3)_2(\text{H}_2\text{O})\text{Cl}]^+$ and $[\text{Pt}(\text{NH}_3)_2(\text{H}_2\text{O})_2]^{2+}$.[9,10]

The cytotoxicity of ruthenium compounds correlates with their ability for DNA binding as well. As for cisplatin, aquation

is a requisite for the formation of active species. In addition, the activity of Ru(III) complexes, which are relatively inert towards ligand substitution, was found to depend on the ease of reduction to more labile Ru(II) complexes.[11] As a consequence, organometallic ruthenium(II) compounds attracted the attention of researchers in their search for novel antiproliferative agents. The use of arene ligands, which stabilise ruthenium in the +2 oxidation state, initiated a new phase in the development of potential ruthenium anticancer drugs.

The structure of the "piano-stool" $[(\eta^6\text{-arene})\text{Ru}^{II}(\text{X})(\text{Y})(\text{Z})]$ complexes allows for a variation of the three monodentate ligands X, Y and Z. Linking Y and Z to a bidentate chelating ligand (diamine, deprotonated amino acid or β-diketonate) is also well documented.[5,12,13] The complexes $[(\eta^6\text{-}p\text{-cymene})\text{Ru}^{II}(\text{X})(\text{Y})(\text{Z})]$ (X, Y or Z = halide, acetonitrile or isonicotinamide), with three monodentate ligands, are inactive in A2780 human ovarian cancer cells.[14] At the same time ruthenium complexes $[(\eta^6\text{-arene})\text{M}^{II}(\text{en})\text{Cl}](\text{PF}_6)$ (en = ethylendiamine) show cytotoxicity comparable to cisplatin.[15–17] Intriguingly, the complexes $[(\eta^6\text{-arene})\text{Ru}^{II}(\text{NH}_3)_2\text{Cl}](\text{PF}_6)$, which at least constitutionally possess more similarity to cisplatin (three of four ligands are the same as in cisplatin), have not been studied for their antiproliferative activity. The first investigations of the ruthenium/osmium complexes $[(\eta^6\text{-benzene})\text{M}(\text{NH}_3)_2\text{Cl}](\text{PF}_6)$ were reported thirty years ago, but were focused mainly on photochemical properties.[18–20] Low analytical purity and difficulties with the reproducibility encountered upon synthesis of these compounds were probably the main reasons which prevented their earlier evaluation for cytotoxicity.

Herein we report on (i) the synthesis of $[(\eta^6\text{-}p\text{-cymene})\text{Ru}^{II}(\text{NH}_3)_2\text{Cl}](\text{PF}_6)$ (**1**) and attempts to prepare its osmium congener, which led to the isolation of $[\{(\eta^6\text{-}p\text{-cymene})\text{Os}^{II}\}_2(\mu\text{-OCH}_3)_3](\text{PF}_6)$ (**3**), (ii) the study of their structures, the

^{a}University of Belgrade, Faculty of Chemistry, Studentski trg 12-16, 11000, Belgrade, Serbia
^{b}University of Vienna, Institute of Inorganic Chemistry, Währinger Str. 42, A-1090, Vienna, Austria. E-mail: vladimir.arion@univie.ac.at (V.B.A.), bernhard.keppler@univie.ac.at (B.K.K.); Fax: +43 1 427752680.

spectroscopic characterization of **1** and its behaviour in aqueous and alcohol solutions, and (iii) the evaluation of antiproliferative activity of **1** *in vitro* in three human cancer cell lines in comparison with that of $[(\eta^6\text{-}p\text{-cymene})Ru^{II}(en)Cl]$-(PF$_6$) (**2**).

Result and discussion

Synthesis

We discovered that the reaction of $[(\eta^6\text{-}p\text{-cymene})RuCl_2]_2$ with 1-(2-hydroxyethyl)piperazine (HEPA) in 1:2.5 molar ratio in dry methanol followed by addition of excess NH$_4$PF$_6$, concentration of the final solution and prolonged standing at 4 °C gave rise to X-ray diffraction quality orange crystals of $[(\eta^6\text{-}p\text{-cymene})\text{-}Ru(NH_3)_2Cl](PF_6)$ (**1**, Chart 1) in 47.2% yield. The same reaction starting from $[(\eta^6\text{-}p\text{-cymene})OsCl_2]_2$ produced yellow crystals of $[\{(\eta^6\text{-}p\text{-cymene})Os\}_2(\mu\text{-OCH}_3)_3](PF_6)$ (**3**, Chart 1). Variation of the reaction stoichiometry, temperature or use of a stronger base, *e.g.* triethylamine instead of HEPA, did not lead to the osmium analogue of **1**. Moreover, the formation of an unidentified black precipitate was observed upon crystallization of **3** at room temperature. Interestingly, the use of triethylamine instead of HEPA in the case of ruthenium also enabled the synthesis of **1**. The role of the base used appears to consist in deprotonation of the ammonium cation, which serves as an ammonia source. Examples of ruthenium complexes with piperazine or their derivatives described in the literature are scarce.[21–23]
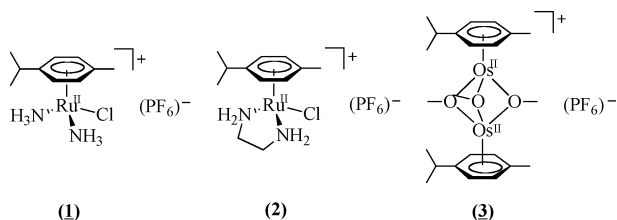

Chart 1 Complexes reported in this work; underlined compounds have been characterised by X-ray crystallography.

Although the preparation of $[(\eta^6\text{-benzene})Ru(NH_3)_2Cl](PF_6)$ was reported many years ago, this turned out to be unreliable, and later attempts were undertaken to improve the available literature protocols. The reaction was carried out in concentrated aqueous ammonia in methanol, and saturated aqueous NH$_4$PF$_6$ solution was used for the precipitation of the complex as hexafluorophosphate $[(\eta^6\text{-benzene})Ru(NH_3)_2Cl](PF_6)$.[18,19] The same experimental conditions were applied to the synthesis of $[(\eta^6\text{-benzene})Os(NH_3)_2Cl](PF_6)$. The synthesis, however, was accompanied by concurrent reactions which led to low yield and unsatisfactory purity of the desired product.[20]

Attempts to produce $[(\eta^6\text{-}p\text{-cymene})Os(NH_3)_2Cl](PF_6)$ by using the protocol optimised for ruthenium complex **1** resulted in the methoxido-bridged arene complex $[\{(\eta^6\text{-}p\text{-cymene})Os\}_2(\mu\text{-OCH}_3)_3](PF_6)$ (**3**). Although the synthesis of the complex with a $[\{(\eta^6\text{-benzene})Os\}_2(\mu\text{-OCH}_3)_3]^+$ cation is well documented in the literature,[24] X-ray diffraction data on binuclear hydroxido- or

alkoxido-bridged osmium-arene compounds were not found in the Cambridge Structural Database.[25]

Crystal structures of 1 and 3

Complex **1** crystallised in the triclinic centrosymmetric space group $P\bar{1}$. The structure of the cation is shown in Fig. 1. Selected bond distances (Å) and angles (deg) are quoted in the legend to Fig. 1. The cation $[(\eta^6\text{-}p\text{-cymene})Ru(NH_3)_2Cl]^+$ has the characteristic "three-leg piano stool" geometry with an η^6 π-bound *p*-cymene ring forming the seat and three other monodentate ligands, namely chlorido and two ammonia, as the legs of the stool. The X-ray structure of $[(\eta^6\text{-benzene})Ru(NH_3)_2Cl](PF_6)\cdot$ 0.33NH$_4$PF$_6$ determined at room temperature and published in 1978[26,27] is of poor quality [Ru–C$_{av}$ 2.185(4), Ru–N 2.129 and Ru–Cl 3.384 Å, N1–Ru–N1^i 83.98, N1–Ru–Cl 83.69°] to make a close comparison with geometrical parameters of the cation in **1** (see legend to Fig. 1). The Ru–C(1–6)$_{av}$ in **1** is very similar to that in $[(\eta^6\text{-}p\text{-cymene})Ru(en)Cl]^+$ at 2.187(9) Å, while the Ru–Cl bond is markedly shorter than that in $[(\eta^6\text{-}p\text{-cymene})Ru(en)Cl]^+$ at 2.442 Å.[14,28] The N1–Ru–N2 angle in the ethylendiamine complex at 78.97° is only *ca.* 3.7° smaller than the corresponding angle in **1**.

Fig. 1 ORTEP view of the cation $[(\eta^6\text{-}p\text{-cymene})Ru(NH_3)_2Cl]^+$ in **1** with atom labeling scheme. Selected bond lengths (Å) and angles (deg): Ru–C(1–6)$_{av}$ 2.183(7), Ru–Cl 2.4146(4), Ru–N1 2.1504(15), Ru–N2 2.1425(15); N1–Ru–N2 82.70(6), N1–Ru–Cl 84.60(4), N2–Ru–Cl 84.68(4).

The result of the X-ray diffraction study of complex **3**, which crystallised in the orthorhombic space group $P2_12_12_1$, is shown in Fig. 2. The geometry of both crystallographically independent cations can be described as confacial-bipseudooctahedral with Os1···Os2 and Os3···Os4 separations of 3.0748(2) and 3.0820(2) Å, respectively, which are larger than those found for the triply hydroxido-bridged arene-ruthenium cations $[Ru_2(\eta^6\text{-}C_6H_6)_2(\mu\text{-OH})_3]^+$[29] 2.9812(7), $[Ru_2(\eta^6\text{-}1,3,5\text{-}C_6H_3Me_3)_2(\mu\text{-OH})_3]^+$[30] 2.989(3) and $[Ru_2(\eta^6\text{-}p\text{-cymene})_2(\mu\text{-OH})_3]^+$[31] 2.990(3) or the triply methoxido-bridged arene-ruthenium cation $[Ru_2(\eta^6\text{-}C_6H_6)_2(\mu\text{-OMe})_3]^+$[32] and very similar to those found in a tetrameric osmium complex $[Os_4(\eta^6\text{-}C_6H_6)_4(\mu_2\text{-OH})_4(\mu_4\text{-O})](BPh_4)_2\cdot 2Me_2CO$[30] of 3.0768(25) and 3.0777(23) for Os1···Os2 and Os3···Os4 distances, correspondingly.

The bond angles for the bridging methoxido ligands Os1–O1–Os2, Os1–O2–Os2, Os1–O3–Os2, Os3–O4–Os4, Os3–O5–Os4 and Os3–O6–Os4 at 94.36(12), 95.90(12), 95.88(11), 94.70(12), 96.40(12) and 95.68(11)° are comparable with those found in
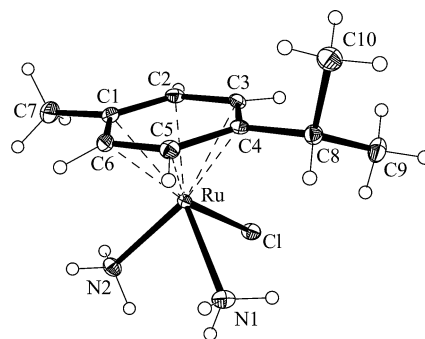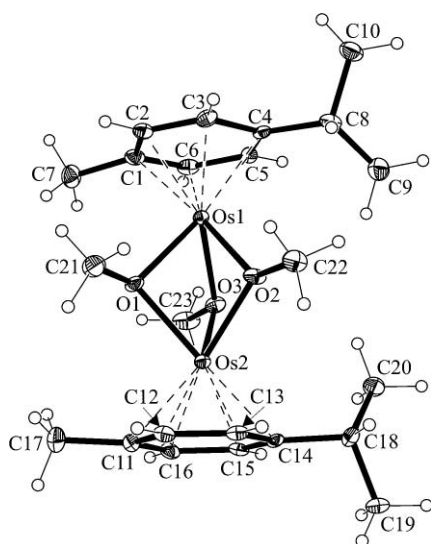
Fig. 2 ORTEP view of the cation $[\{(\eta^6\text{-}p\text{-cymene})Os\}_2(\mu\text{-OCH}_3)_3]^+$ in **3** with atom labeling scheme. Selected bond lengths (Å) and angles (deg): Os1–O1 2.093(3), Os1–O2 2.069(3), Os1–O3 2.068(3), Os2–O1 2.099(3), Os2–O2 2.072(3), Os2–O3 2.073(3) Å; Os1–O1–Os2 94.36(12), Os1–O2–Os2 95.90(12), Os1–O3–Os2 95.88(11).

$[Ru_2(\eta^6\text{-}C_6H_6)_2(\mu\text{-OMe})_3]^+$ [32] with Ru1–O1–Ru2, Ru1–O2–Ru2 and Ru1–O3–Ru2 of 93.9(3), 94.6(3) and 92.6(3)°, respectively.

Stability of 1 in different solvents

We investigated the stability of **1** in dry methanol, water, and 0.1 M NaCl (a similar concentration to that in blood plasma) by UV-vis spectroscopy (Figs. 3, S1–S3†). Fast changes in UV-vis spectra of **1** in H_2O and in aqueous 0.1 M NaCl solution indicate that the complex undergoes substitution reactions at the ruthenium centre upon dissolution. The complex does not remain intact even in methanol, and its UV-vis spectra change rapidly with time. Such behaviour of **1** can be explained by solvolysis of Ru–N and Ru–Cl bonds. Evidence of formation of a dimer of the type **3** in methanol is furnished by ESI mass spectrometry, which showed the presence of the peak with m/z 564 assignable to $[\{(\eta^6\text{-}p\text{-}cymene)Ru\}_2(\mu\text{-OCH}_3)_3]^+$. The experimental isotopic pattern, which agrees well with that calculated, is shown in Fig. S4.† Instability of the species generated by reaction of **1** with $AgPF_6$ "$[(\eta^6\text{-}p\text{-cymene})Ru(NH_3)_2(H_2O)]^{2+}$" in H_2O (Fig. S5†) indicates
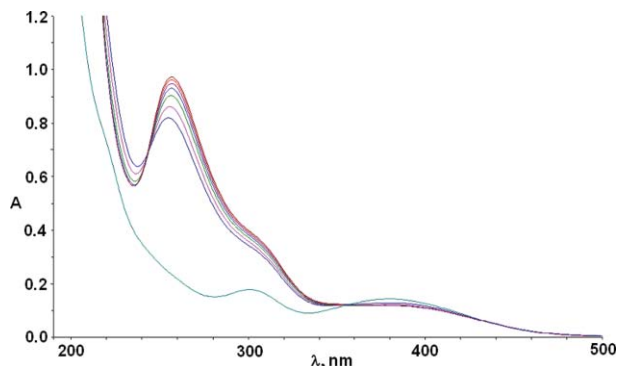

Fig. 3 UV-vis spectra of **1** in H_2O: 24 × 1 h (cycles 1, 2, 4, 8, 12, 16, 20 and 24).

its further hydrolysis with involvement of Ru–N bonds in further substitution reactions.

The solution behaviour of **1** was also investigated by ^{1}H NMR spectroscopy. ^{1}H NMR spectra were recorded in DMSO-d_6 and D_2O. For the freshly prepared DMSO-d_6 solution of **1** a typical spectrum for a metal-coordinated cymene ligand is observed (see Experimental). The spectrum in D_2O changes dramatically and five sets of cymene signals can be observed very quickly (Figs. 4, S6–S8†). One cymene set disappears after 1 h, whereas the other four sets are still present with changing intensities after 13 days. Also of note is that signals which can be attributed to metal-free cymene were not observed during the present experiment.
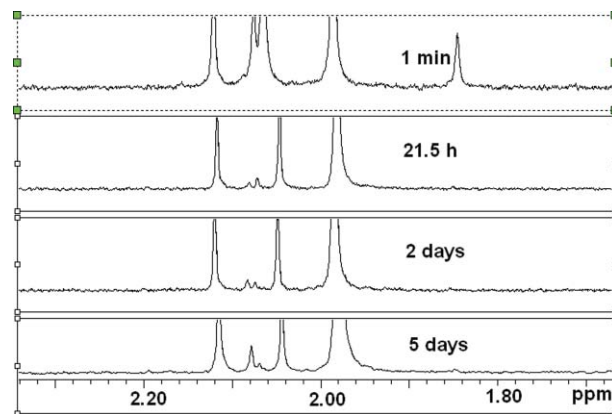
Fig. 4 ^{1}H NMR spectra of **1** in D_2O (CH_3 region).

The ^{1}H NMR spectrum of the elusive "$[(\eta^6\text{-}p\text{-cymene})Ru(NH_3)_2(H_2O)]^{2+}$" species in D_2O showed four sets of metal-bound cymene signals (see the CH(CH_3)$_2$ region of the spectrum in Fig. S9†). The equilibrium was achieved after 2 days with two sets of signals. These two species were also found in D_2O solution of **1** (see Fig. S9†).

Cytotoxicity of 1

In vitro anticancer activity of compounds **1** and **2** was determined in human A549 (non-small cell lung carcinoma), CH1 (ovarian carcinoma) and SW480 (colon carcinoma) cells by means of the colorimetric MTT assay. IC_{50} values were calculated and are quoted in Table 2, and complete concentration–effect curves are displayed in Fig. 5. CH1 cells were found to be more sensitive to **1**, followed by SW480 and A549 cells. In contrast, complex **2** shows the strongest effect in SW480 cells, followed by that in CH1 and A549 cells. Compound **2** has a higher level of antiproliferative activity in all three cell lines, with IC_{50} values lower than 10 μM. In contrast, compound **1** has very low cytotoxic potential with IC_{50} values between 293 μM in the cisplatin-sensitive cell line CH1 and 542 μM in the cisplatin-resistant cell line A549. Complex **2** is almost a hundredfold more cytotoxic than its structural analogue, **1**. We also performed an MTT test with a shorter exposure time in SW480 cells. It clearly points out that compound **1** requires more than 6 h contact with cells to exert its full cytotoxic effect, indicating at the same time that the species present in the medium after 6 h contribute considerably to total cytotoxic activity. The IC_{50} value could not be reached within this time and the chosen range of concentration.

Table 1 Crystal data and details of data collection for **1** and **3**

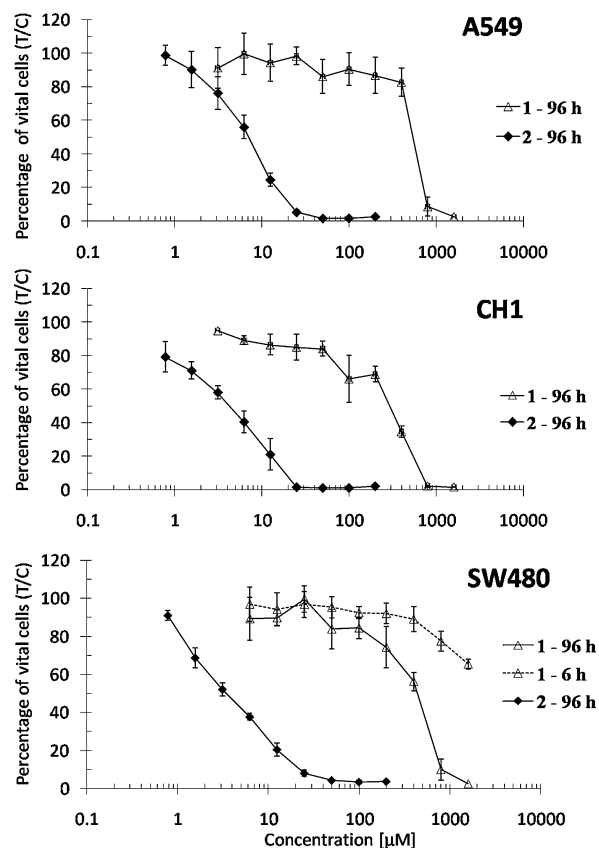| Complex	**1**	**3**
CCDC no.	707426	707427
empirical formula	$C_{10}H_{20}ClF_6N_2PRu$	$C_{23}H_{37}F_6O_6Os_2P$
fw	449.77	886.89
space group	$P\bar{1}$ (No 2)	$P2_12_12_1$ (No 19)
a, Å	8.0544(2)	11.2483(3)
b, Å	8.8166(2)	13.6694(4)
c, Å	11.2876(3)	34.2630(9)
α, deg	87.861(2)	
β, deg	88.256(2)	
γ, deg	78.272(2)	
V, Å^3	784.07(3)	5268.2(3)
Z	2	8
λ, Å	0.71073	0.71073
ρ_{calcd}, g cm^{-3}	1.905	2.236
crystal size, mm^3	$0.40 \times 0.38 \times 0.38$	$0.38 \times 0.28 \times 0.22$
T, K	100	100
μ, cm^{-1}	13.27	97.65
reflns collected/unique [R_{int}]	16677/4586 [0.0323]	140298/15486 [0.0601]
$R1^a$	0.0237	0.0228
$wR2^b$	0.0612	0.0489
Flack parameter		0.006(5)
GOF^c	1.075	0.993

^{a} $R1 = \sum ||F_o| - |F_c||/\sum |F_o|$, ^{b} $wR2 = \{\sum[w(F_o^2 - F_c^2)^2]/\sum[w(F_o^2)^2]\}^{1/2}$. ^{c} $GOF = \{\sum[w(F_o^2 - F_c^2)^2]/(n-p)\}^{1/2}$, where n is the number of reflections and p is the total number of parameters refined.

Table 2 Cytotoxicity of ruthenium complexes **1** and **2** in three human cancer cell lines. Presented are the 50% inhibitory concentrations in A549, CH1 and SW480 cells in the MTT assay. Values are the means ± standard deviations obtained from at least three independent experiments using exposure times of 96 h

	IC$_{50}$, μM		
Compound	A549	CH1	SW480
1	542 ± 12	293 ± 24	437 ± 23
2	7.1 ± 1.1	4.4 ± 0.9	3.5 ± 0.5

Low levels of cytotoxicity in A2780 human ovarian cancer cells with IC$_{50}$ > 150 μM have been documented for related organometallic compounds with three monodentate ligands, e.g. $[(\eta^6\text{-}p\text{-cymene})Ru^{II}(CH_3CN)_2Cl](PF_6)$, $[(\eta^6\text{-}p\text{-cymene})Ru^{II}\text{-}(CH_3CN)_2Br](PF_6)$, and $[(\eta^6\text{-}p\text{-cymene})Ru^{II}(\text{isonicotinamide})\text{-}Cl_2]$.[14] It was suggested that the observed level of their cytotoxicity, which further decreased with time, is presumably due to their deactivation by components of the cell culture medium and/or the cells before they reach their target sites.[5] The formation of the dimer $[\{(\eta^6\text{-biphenyl})Os\}_2(\mu\text{-OH})_3]^+$ in aqueous solution accounted for the inactivity of $[(\eta^6\text{-biphenyl})Os(CH_3CN)Cl_2]$ in the human lung A549 cancer cell line.[33] In line with these results, we believe that compound **1** has the same fate because of the observed instability in organic and aqueous medium. In contrast to classic platinum(II) complexes, where the presence of ethylenediamine instead of two ammonia ligands is usually disadvantageous for biological activity, the stabilising effect of the bidentate ligand seems to be essential in the case of Ru(II)–arene complexes.

Fig. 5 Concentration–effect curves of ruthenium complexes **1** and **2** in the human cancer cell lines A549, CH1 and SW480. Values were obtained by the MTT assay and are means ± standard deviations from at least three independent experiments using exposure times of 96 h, with the exception of the dotted curve of complex **1** in SW480 cells (exposure time 6 h).

Experimental

Starting materials

RuCl$_3$·3H$_2$O and OsO$_4$ were purchased from Johnson Matthey. $[(\eta^6\text{-}p\text{-cymene})RuCl_2]_2$ and $[(\eta^6\text{-}p\text{-cymene})OsCl_2]_2$ were prepared according to literature protocols.[34,35] 1-(2-hydroxyethyl)piperazine (HEPA) and triethylamine were purchased from Aldrich. All chemicals were used without further purification. $[(\eta^6\text{-}p\text{-cymene})Ru^{II}(en)Cl](PF_6)$ (**2**) was prepared as reported by Sadler et al.[36]

Synthesis of complexes

$[(\eta^6\text{-}p\text{-cymene})Ru^{II}(NH_3)_2Cl](PF_6)$ (**1**). To a suspension of $[(\eta^6\text{-}p\text{-cymene})Ru^{II}Cl_2]_2$ (0.12 g, 0.2 mmol) in dry methanol (15 mL) a solution of 1-(2-hydroxyethyl)piperazine (0.065 g, 0.5 mmol) in dry methanol (5 mL) was added. The light-protected reaction mixture was stirred at room temperature for 2 h. Then NH$_4$PF$_6$ (0.25 g, 1.6 mmol) was added as a solid, the orange solution was concentrated by rotary evaporation under reduced pressure to 10 mL and allowed to stand at 4 °C for 24 h. The orange crystals formed were filtered off and re-crystallised in ethanol (0.085 g, 47.2%). Found: C, 26.86; H, 4.43; N, 6.12. Calc. for $C_{10}H_{20}ClF_6N_2PRu$: C, 26.69; H, 4.45; N, 6.23%. δ_H (200 MHz; d_6-DMSO) 5.60–5.33 (4H, dd, $-C_6H_4-$), 2.80 (1H, m, $CHMe_2$),

2.10 (3H, s, $C_6H_4CH_3$) and 1.20 (6H, d, $(CH_3)_2CH$); ν_{max},cm^{-1} 3381 (m), 3335 (m), 3249 (m), 3193 (m), 1626 (m), 1280 (m), 1255 (m), 1062 (w), 1035 (w), 823 (s) and 553 (s).

Generation of "$[(\eta^6\text{-}p\text{-cymene})Ru(NH_3)_2(H_2O)]^{2+}$" species. $AgPF_6$ (8 mg, 0.03 mmol) was added to a solution of **1** (11.1 mg, 0.025 mmol) in H_2O (5 mL). The light-protected mixture was stirred at room temperature for 17 h and then filtered to remove AgCl. The resulting aqueous solution was diluted to 100 mL and used for UV-vis spectroscopy investigation. 10 mL of this solution were lyophilised and studied by NMR spectroscopy.

$[\{(\eta^6\text{-}p\text{-cymene})Os^{II}\}_2(\mu\text{-OCH}_3)_3](PF_6)$ (3). To a suspension of $[(\eta^6\text{-}p\text{-cymene})OsCl_2]_2$ (60.6 mg, 0.077 mmol) in methanol (15 mL) a solution of 1-(2-hydroxyethyl)piperazine (30.5 mg, 0.23 mmol) in methanol (2 mL) was added. The light-protected reaction mixture was stirred at room temperature for 3.5 h. Then NH_4PF_6 (92.4 mg, 0.57 mmol) was added, and the yellow solution was concentrated by rotary evaporation under reduced pressure to *ca.* 5 mL and allowed to stand at –20 °C. The yellow crystals of **3** were studied by X-ray diffraction and NMR spectroscopy. δ_H (500.10 MHz; DMSO-d_6): 6.18–5.97 (8H, dd, $-C_6H_4-$), 4.48 (9H, s, μ-OCH$_3$), 2.70 (2H, m, CHMe$_2$), 2.23 (6H, s, $C_6H_4CH_3$) and 1.23 (12H, d, $(CH_3)_2CH$).

Physical measurements

Elemental analyses were carried out with an Elemental Vario EL III microanalyser at the Faculty of Chemistry, University of Belgrade, Serbia. UV-vis spectra were recorded on a Perkin-Elmer Lambda 20 UV-vis spectrophotometer using samples dissolved in dry methanol, water, and 0.1 M NaCl at 298 K. The ^{1}H NMR spectra were recorded with a Bruker FT-NMR spectrometer Avance II™ 500 MHz using standard pulse programs at 500.10 MHz (in D_2O, DMSO-d_6) and on a Varian Gemini 200 instrument at 200 MHz (in DMSO-d_6). Chemical shifts for ^{1}H spectra were referenced to residual ^{1}H present in DMSO-d_6 (D_2O). Infrared spectra were recorded on a Nicolet 6700 FT-IR spectrometer using the ATR technique. Electrospray ionisation mass spectra of samples dissolved in methanol/acetonitrile were measured with a Finnigan Mat 900S instrument. Expected and experimental isotope distributions were compared.

Crystallographic structure determination

X-ray diffraction measurements were performed on a Bruker X8 APEXII CCD diffractometer at 100 K. Single crystals were positioned at 40 and 60 mm from the detector, and 1033 and 2133 frames were measured, each for 3 and 15 s over 1° scan width for **1** and **3**, correspondingly. The data were processed using SAINT software.[37] Crystal data, data collection parameters, and structure refinement details for **1** and **3** are given in Table 1. Both structures were solved by direct methods and refined by full-matrix least-squares techniques. Non-hydrogen atoms were refined with anisotropic displacement parameters. H atoms were placed at calculated positions and refined as riding atoms in the subsequent least squares model refinements. The isotropic thermal parameters were estimated to be 1.2 times the values of the equivalent isotropic thermal parameters of the non-hydrogen atoms to which hydrogen atoms are bonded. The following computer programs, equipment and table were used: structure solution, *SHELXS*-

97;[38] refinement, *SHELXL-973*;[39] molecular diagrams, *ORTEP*;[40] computer, Pentium IV; scattering factors were taken from the literature.[41]

Cell lines and culture conditions

Human A549 (non-small cell lung carcinoma) and SW480 (adenocarcinoma of the colon) cells were kindly provided by Brigitte Marian (Institute of Cancer Research, Department of Medicine I, Medical University of Vienna, Austria). CH1 cells originate from an ascites sample of a patient with a papillary cystadenocarcinoma of the ovary and were a generous gift from Lloyd R. Kelland (CRC Centre for Cancer Therapeutics, Institute of Cancer Research, Sutton, UK). Cells were grown in 75 cm^2 culture flasks (Iwaki/Asahi Technoglass, Gyouda, Japan) as adherent monolayer cultures in complete medium (Minimum Essential Medium supplemented with 10% heat-inactivated fetal bovine serum, 1 mM sodium pyruvate, 4 mM L-glutamine and 1% non-essential amino acids (100×)). All media and supplements were purchased from Sigma-Aldrich, Vienna, Austria. Cultures were maintained at 37 °C in a humidified atmosphere containing 5% CO_2.

Cytotoxicity test in cancer cell lines

Cytotoxicity was determined by means of a colorimetric microculture assay (MTT assay, MTT = 3-(4,5-dimethyl-2-thiazolyl)-2,5-diphenyl-2H-tetrazolium bromide, Fluka). Cells were harvested from culture flasks by trypsinization and seeded in 100 µL aliquots into 96-well plates (Iwaki/Asahi Technoglass, Gyouda, Japan) in densities of 4×10^3 (A549), 1.5×10^3 (CH1) and 2.5×10^3 (SW480) cells per well, respectively, to ensure exponential growth of untreated controls throughout the experiment. Cells were allowed to settle in drug-free complete culture medium for 24 h. Drugs were dissolved and appropriately diluted in complete medium shortly before application. Subsequently 100 µL of the drug dilutions were added per well, and cells were incubated for 96 h. An MTT assay in SW480 cells was also performed with a shorter exposure time. For this purpose, the drug solution was removed after 6 h and cells were incubated with drug-free medium for the remaining 90 h. After exposure, drug solutions or medium, respectively, were replaced by 100 µL/well RPMI 1640 culture medium (supplemented with 10% heat-inactivated fetal bovine serum and 4 mM L-glutamine) plus 20 µL/well MTT solution in phosphate-buffered saline (5 mg/mL). At the end of incubation for 4 h, the medium/MTT mixture was removed and the formazan crystals that were formed in vital cells were dissolved in 150 µL DMSO (dimethyl sulfoxide) per well. Optical densities were measured at 550 nm with a microplate reader (Tecan Spectra Classic), using a reference wavelength of 690 nm. The quantity of vital cells was expressed in terms of T/C values by comparison with untreated control microcultures, and 50% inhibitory concentrations (IC$_{50}$) were calculated from concentration–effect curves by interpolation. Evaluation is based on means from at least three independent experiments, each comprising three replicates per concentration level.

Conclusion

A novel ruthenium compound, namely $[(\eta^6\text{-}p\text{-cymene})Ru^{II}\text{-}(NH_3)_2Cl](PF_6)$ (**1**), which had remained elusive for preparative organometallic chemists engaged in the development of antitumour drugs for quite a long time, was prepared in good yield

and comprehensively characterised. However, the presence of two ammonia ligands instead of ethylenediamine results in a tremendous loss of cytotoxicity, probably due to increased susceptibility to inactivating reactions leading to formation (among others) of $[\{(\eta^6\text{-}p\text{-cymene})Ru\}_2(\mu\text{-OH})_3]^+$ species.

Attempts to apply an analogous approach for the synthesis of the osmium counterpart $[(\eta^6\text{-}p\text{-cymene})Os^{II}(NH_3)_2Cl](PF_6)$ failed. Instead a novel binuclear triply methoxido-bridged arene–osmium(II) compound, $[\{(\eta^6\text{-}p\text{-cymene})Os\}_2(\mu\text{-OCH}_3)_3](PF_6)$ **(3)**, was isolated and studied by X-ray crystallography and ^{1}H NMR spectroscopy. This is a further example that the synthesis of osmium analogues cannot be performed by simply following the protocols for ruthenium species, and very often non-trivial approaches, particular skills, experience and knowledge of the systems are required.

References

1 M. J. Clarke, *Metal Ions Biol. Syst.*, 1980, **11**, 231–283.
2 B. Rosenberg, L. VanCamp, J. E. Trosko and V. H. Mansour, *Nature*, 1969, **222**, 385–386.
3 W. H. Ang and P. J. Dyson, *Eur. J. Inorg. Chem.*, 2006, **20**, 4003–4018.
4 M. A. Jakupec, M. Galanski, V. B. Arion, C. G. Hartinger and B. K. Keppler, *Dalton Trans.*, 2008, **2**, 183–194.
5 L. Ronconi and P. J. Sadler, *Coord. Chem. Rev.*, 2007, **251**, 1633–1648.
6 M. Galanski, V. B. Arion, M. A. Jakupec and B. K. Keppler, *Curr. Pharm. Des.*, 2003, **9**, 2078–2089.
7 C. A. Vock, W. H. Ang, C. Scolaro, A. D. Phillips, L. Lagopoulos, L. Juillerat-Jeanneret, G. Sava, R. Scopelliti and P. J. Dyson, *J. Med. Chem.*, 2007, **50**, 2166–2175.
8 C. A. Vock, C. Scolaro, A. D. Phillips, R. Scopelliti, G. Sava and P. J. Dyson, *J. Med. Chem.*, 2006, **49**, 5552–5561.
9 Y. Jung and S. J. Lippard, *Chem. Rev.*, 2007, **107**, 1387–1407.
10 S. van Zutphen and J. Reedijk, *Coord. Chem. Rev.*, 2005, **249**, 2845–2853.
11 M. J. Clarke, *Coord. Chem. Rev.*, 2003, **236**, 209–233.
12 Y. K. Yan, M. Melchart, A. Habtemariam and P. J. Sadler, *Chem. Comm.*, 2005, **38**, 4764–4776.
13 A. Habtemariam, M. Melchart, R. Fernandez, S. Parsons, I. D. H. Oswald, A. Parkin, F. P. A. Fabbiani, J. E. Davidson, A. Dawson, R. E. Aird, D. I. Jodrell and P. J. Sadler, *J. Med. Chem.*, 2006, **49**, 6858–6868.
14 R. E. Morris, R. E. Aird, P. S. Murdoch, H. Chen, J. Cummings, N. D. Hughes, S. Parsons, A. Parkin, G. Boyd, D. I. Jodrell and P. J. Sadler, *J. Med. Chem.*, 2001, **44**, 3616–3621.
15 F. Wang, H. Chen, S. Parsons, I. D. H. Oswald, J. E. Davidson and P. J. Sadler, *Chem. Eur. J.*, 2003, **9**, 5810–5820.
16 H. Chen, J. A. Parkinson, S. Parsons, R. A. Coxall, R. O. Gould and P. J. Sadler, *J. Am. Chem. Soc.*, 2002, **124**, 3064–3082.
17 H. Chen, J. A. Parkinson, R. E. Morris and P. J. Sadler, *J. Am. Chem. Soc.*, 2003, **125**, 173–186.
18 D. R. Robertson, T. A. Stephenson and T. Arthur, *J. Organomet. Chem.*, 1978, **162**, 121–136.
19 W. Weber and P. C. Ford, *Inorg. Chem.*, 1986, **25**, 1088–1092.
20 Y. Hung, W.-J. Kung and H. Taube, *Inorg. Chem.*, 1981, **20**, 457–463.
21 G. Sanchez, C. Bifano and H. Krentzien, *Acta Cientifica Venezolana*, 1984, **35**, 44–47.
22 K. S. Siddiqi, P. Khan, N. Singhal and S. A. A. Zaidi, *Indian J. Chem.*, 1980, **19A**, 265–267.
23 S. Grguric-Sipka, M. Al. A. M. Alshtewi, D. Jeremic, G. N. Kaluderovic, S. Gomez-Ruiz, Z. Zizak, Z. Juranic and T. J. Sabo, *J. Serb. Chem. Soc.*, 2008, **73**, 619–630.
24 T. Arthur, D. R. Robertson, D. A. Tocher and T. A. Stephenson, *J. Organomet. Chem.*, 1981, **208**, 389–400.
25 CSD version 5.29, November 2007.
26 R. O. Gould, C. L. Jones, D. R. Robertson and T. A. Stephenson, *Cryst. Structure Comm.*, 1978, **7**, 27–32.
27 CSD version 5.29, November 2007 (ABZRUP code).
28 CSD version 5.29, November 2007 (CAFPOP code).
29 T. D. Kim, T. J. McNeese and A. L. Rheingold, *Inorg. Chem.*, 1988, **27**, 2554–2555.
30 R. O. Gould, C. L. Jones, T. A. Stephenson and D. A. Tocher, *J. Organomet. Chem.*, 1984, **264**, 365–378.
31 V. Artero, A. Proust, P. Herson and P. Gouzerh, *Chem. Eur. J.*, 2001, **7**, 3901–3910.
32 R. O. Gould, T. A. Stephenson and D. A. Tocher, *J. Organomet. Chem.*, 1984, **263**, 375–384.
33 A. F. A. Peacock, A. Habtemariam, S. A. Moggach, A. Prescimone, S. Parsons and P. J. Sadler, *Inorg. Chem.*, 2007, **46**, 4049–4059.
34 M. A. Bennett and A. K. Smith, *J. Chem. Soc., Dalton Trans.*, 1974, **2**, 233–241.
35 W. A. Kiel, R. G. Ball and W. A. G. Graham, *J. Organomet. Chem.*, 1990, **383**, 481–496.
36 *PCT Int. Appl.*, WO 2001030790, 2001.
37 *SAINT-Plus (Version 7.06a) and APEX2*. Bruker-Nonius AXS Inc. 2004, Madison, Wisconsin, USA.
38 G. M. Sheldrick, *SHELXS-97, Program for Crystal Structure Solution* University of Göttingen, Göttingen, Germany, 1997.
39 G. M. Sheldrick, *SHELXS-97, Program for Crystal Structure Refinement*, University of Göttingen, Göttingen, Germany, 1997.
40 G. K. Jonson, *Report ORNL-5138*, Oak Ridge National Laboratory, Oak Ridge, TN, 1976.
41 *International Tables for X-ray Crystallography*, ed. A. J. C. Wilson, Kluwer Academic Press, Dodrecht, The Netherlands, 1992; Vol. C, Tables 4.2.6.8 and 6.1.1.4.

3. Conclusion and Perspectives

Severe side effects, a limited panel of treatable tumors and resistance are the limiting factors in platinum-based anticancer treatment in the clinic nowadays. To overcome resistance and to limit the risk of adverse effects, the development of new drugs with a different mode of action and a more selective activity especially against tumor cells became of particular interest. Within this PhD thesis, cellular accumulation and the interaction with DNA were studied for the investigational anticancer ruthenium(III) complex KP1019 and for a group of active *trans*-platinum(II) oxime complexes with regard to biological differences compared to cisplatin.

The mode of action of KP1019 is not completely elucidated by now, but interactions with various biomolecules have been demonstrated. The binding to transferrin and the transport into the cell *via* the transferrin receptor are supposed to play an important role in selective transport to cancer cells that normally show enhanced expression of transferrin receptors. Another hypothesis that is discussed as an important step in the mode of action is the activation by reduction. It is supposed that Ru(III) is reduced at the tumor site to the active Ru(II) species. The activation is based on the reductive environment in solid tumors and contributes to selective effects at the tumor site, leaving normal tissue unharmed. The impact of the natural antioxidant ascorbic acid on the cytotoxic activity of KP1019 was investigated within this work. Ascorbic acid enhanced the cytotoxicity of KP1019 in the cancer cell lines SW480 (colon carcinoma), KB-3-1 (cervix carcinoma) and its multidrug resistant P-gp overexpressing subclone KBC-1. Furthermore it was demonstrated that the reactivity of KP1019 towards DNA could be enhanced by co-incubation with ascorbic acid. Elevated cellular accumulation and increased generation of ROS could be excluded as explanations for the stronger activity, and based on the finding that preincubation with ascorbic acid prior to incubation with KP1019 did not result in an increase in cytotoxicity, the effect must be based on direct interaction of the two compounds. ^{1}H-NMR measurements revealed accelerated reduction of KP1019 in the presence of ascorbic acid even in a system roughly adapted to cell culture conditions, and therefore the accelerated reduction seems to contribute to the enhanced cytotoxic effects.

Beside the development of antitumor complexes based on various metals such as ruthenium, gallium and osmium, the investigation of non-classical platinum-based drugs is of great interest. Therefore, the cellular accumulation and DNA interaction of *cis*- and *trans*-configured platinum(II) oxime complexes was studied and compared with the parental drug cisplatin and its inactive counterpart transplatin. Interestingly, the *trans*-configured complexes showed higher cytotoxicity than their *cis*-configured analogues, with the exception of the iodido complex, and are comparable with regard to their cytotoxic potency to cisplatin. The cellular accumulation and the binding towards DNA of the *trans*-complexes were much higher than for cisplatin. Additionally, it was demonstrated that the *trans*-configured complexes cause strand breaks in the comet assay, whereas cisplatin leads to crosslinks, which was

proven by reduction of chemically induced DNA fragmentation. The corresponding *cis*-isomers did not alter the DNA in the tested concentrations but those platinum amounts might be too low to reveal possible cross-linking effects. The only exception was the *cis*-iodido complex, which was more cytotoxic than its *trans*-congener, led to enhanced cellular platinum accumulation and DNA platination and caused strand breaks comparable to the *trans*-complexes and thus might exert a distinct mode of action. The adduct formation with dGMP was demonstrated by means of capillary zone electrophoresis (CZE) and showed faster adduct formation of the *trans*-configured complexes compared to their *cis*-congeners, corresponding to higher r_b values (Pt/P) in the cellular DNA platination experiments. Based on findings from the literature and the obtained results it may be suggested that the *trans*-platinum(II) oxime complexes form monoadducts which reduce DNA stability and thus contribute to the cytotoxic activity. Furthermore, differences in the uptake mechanisms between the *cis*- and *trans*-configured congeners must be considered, and more experiments are planned the elucidate these hypotheses. The differences in the biological behavior of the *trans*-platinum(II) complexes and cisplatin seem to be based on the distinct DNA binding behavior and the adduct formation with nucleobases and might contribute to activity in cisplatin-resistant tumors.

In vitro assays are an important instrument in preclinical development, but nevertheless they only draw a very simplified picture of the effects caused by a drug. To examine the anticancer activity in an organism in which the substance is metabolized and therefore may act differently, studies in animal models should be carried out and are currently planned. Those studies will demonstrate whether the antitumor potential of KP1019 can also be enhanced by ascorbic acid *in vivo,* which would be an important factor in ruthenium-based chemotherapy. The co-administration of KP1019 and ascorbic acid could allow giving lower doses with the same therapeutic effect but lessen the risk of side effects. Beside the reduction of adverse effects, overcoming of cisplatin resistance is a great challenge in metal-based antitumor drug development. Therefore, the *in vivo* activity of selected *trans*-configured platinum(II) oxime complexes will be examined in mouse models and compared to cisplatin treatment with an emphasis on cisplatin-resistant tumors.

4. References

1. Weinberg, R.A., *The biology of cancer*. 2006, New York: Garland Science.
2. Pecorino, L., *Molecular biology of cancer*. 2005, New York: Oxford University Press.
3. Zielonke, N., M. Hackl, and E. Baldaszti, *Krebsinzidenz und Krebsmortalität in Österreich*. 2010: Statistik Austria.
4. Yokota, J., *Tumor progression and metastasis.* Carcinogenesis, 2000.**21**(3):p.497-503.
5. Shaw, P.H., *The role of p53 in cell cycle regulation.* Pathol., Res. Pract., 1996. **192**(7): p. 669-675.
6. Peto, J., *Cancer epidemiology in the last century and the next decade.* Nature (London, U. K.), 2001. **411**(6835): p. 390-395.
7. Hanahan, D. and R.A. Weinberg, *The hallmarks of cancer.* Cell, 2000. **100**(1):p.57-70.
8. Paolo Fedi, A.K., Stuart A Aaronson, *Growth Factor Signal Transduction in Cancer*, in *Cancer Medicine, 5th edition*, D.W.K. Robert C Bast Jr, Raphael E Pollock, Ralph R Weichselbaum, James F Holland, Emil Frei III, Editor. 2000, Hamilton (ON): BC Decker.
9. Yarden, Y. and A. Ullrich, *Growth factor receptor tyrosine kinases.* Annu. Rev. Biochem., 1988. **57**: p. 443-78.
10. Medema, R.H. and J.L. Bos, *The role of p21ras in receptor tyrosine kinase signaling.* Crit Rev Oncog, 1993. **4**(6): p. 615-61.
11. Hanahan, D. and R.A. Weinberg, *Hallmarks of cancer: the next generation.* Cell (Cambridge, MA, U. S.). **144**(5): p. 646-674.
12. Harris, C.C., *p53 Tumor suppressor gene: from the basic research laboratory to the clinic - an abridged historical perspective.* Carcinogenesis, 1996. **17**(6): p. 1187-1198.
13. Christofori, G. and H. Semb, *The role of the cell-adhesion molecule E-cadherin as a tumor-suppressor gene.* Trends Biochem. Sci., 1999. **24**(2): p. 73-76.
14. Kimball, J.W. *Kimball's Biology Pages.* March 2011 [cited 2011 May 2011]; Available from: http://users.rcn.com/jkimball.ma.ultranet/BiologyPages/.
15. Krauss, G., *Biochemistry of Signal Tranduction and Regulation*. 4th ed. 2008: Wiley-VCH.
16. Alberts Bruce, J.A., Lewis Julian, Raff Martin, Roberts Keith, Walter Peter, *Molecular Biology of the cell*. 5th ed. 2008, New York: Garland Science Taylor & Francis Group.
17. Murray, A., *Cell cycle checkpoints.* Current Opinion in Cell Biology, 1994. **6**(6): p. 872-876.
18. Elledge, S.J., *Cell Cycle Checkpoints: Preventing an Identity Crisis.* Science, 1996. **274**(5293): p. 1664-1672.
19. Kastan, M.B. and J. Bartek, *Cell-cycle checkpoints and cancer.* Nature, 2004. **432**(7015): p. 316-323.
20. Levesque, A.A. and A. Eastman, *p53-based cancer therapies: is defective p53 the Achilles heel of the tumor?* Carcinogenesis, 2006. **28**(1): p. 13-20.
21. Sancar, A., *DNA excision repair.* Annu Rev Biochem, 1996. **65**: p. 43-81.
22. Reardon, J.T., et al., *Efficient nucleotide excision repair of cisplatin, oxaliplatin, and Bis-aceto-ammine-dichloro-cyclohexylamine-platinum(IV) (JM216) platinum intrastrand DNA diadducts.* Cancer Res, 1999. **59**(16): p. 3968-71.
23. Chválová, K., V. Brabec, and J. Kaspárková, *Mechanism of the formation of DNA-protein cross-links by antitumor cisplatin.* Nucleic Acids Res., 2007. **35**(6): p. 1812-1821.

24. Saunders, W.M., *Radiation oncology: the use of beams of photons or particles for the treatment of tumors.* Radiat. Phys. Chem., 1984. **24**(3-4): p. 357-64.

25. Lassmann, M., C. Reiners, and M. Luster, *Dosimetry and thyroid cancer: the individual dosage of radioiodine.* Endocr.-Relat. Cancer. **17**(3): p. R161-R172.

26. Zhang, L., et al., *Delivery of therapeutic radioisotopes using nanoparticle platforms: potential benefit in systemic radiation therapy.* Nanotechnol., Sci. Appl. **3**: p. 159-170.

27. Mierzwa, M.L., et al., *Recent advances in combined modality therapy.* Oncologist. **15**(4): p. 372-381.

28. Papac, R.J., *Origins of cancer therapy.* Yale J Biol Med, 2001. **74**(6): p. 391-8.

29. Chabner, B.A. and T.G. Roberts, *Chemotherapy and the war on cancer.* Nat. Rev. Cancer, 2005. **5**(1): p. 65-72.

30. DeVita, V.T., Jr. and E. Chu, *A History of Cancer Chemotherapy.* Cancer Res., 2008. **68**(21): p. 8643-8653.

31. Galanski, M., et al., *Recent developments in the field of tumor-inhibiting metal complexes.* Curr Pharm Des, 2003. **9**(25): p. 2078-89.

32. Kelland, L., *The resurgence of platinum-based cancer chemotherapy.* Nat. Rev. Cancer, 2007. **7**(8): p. 573-584.

33. Skladanowski, A., P. Bozko, and M. Sabisz, *DNA Structure and Integrity Checkpoints during the Cell Cycle and Their Role in Drug Targeting and Sensitivity of Tumor Cells to Anticancer Treatment.* Chem.Rev.(Washington,DC, U.S.),2009.**109**(7):p.2951-2973

34. Takeshita, M., et al., *Interaction of bleomycin with DNA.* Proceedings of the National Academy of Sciences, 1978. **75**(12): p. 5983-5987.

35. Jamieson, E.R. and S.J. Lippard, *Structure, recognition, and processing of cisplatin-DNA adducts.* Chem. Rev. (Washington, D. C.), 1999. **99**(9): p. 2467-2498.

36. Pil P., L.S.J. Encyclopedia of Cancer, ed. B.J. R. 1997, San Diego: Academia Press.

37. Loenn, U. and S. Loenn, *Interaction between 5-fluorouracil and DNA of human colon adenocarcinoma.* Cancer Res., 1984. **44**(8): p. 3414-18.

38. Qian, Z.M., et al., *Targeted drug delivery via the transferrin receptor-mediated endocytosis pathway.* Pharmacol. Rev., 2002. **54**(4): p. 561-587.

39. Sun, H., H. Li, and P.J. Sadler, *Transferrin as a Metal Ion Mediator.* Chemical Reviews, 1999. **99**(9): p. 2817-2842.

40. Daniels, T.R., et al., *The transferrin receptor part I: Biology and targeting with cytotoxic antibodies for the treatment of cancer.* Clin Immunol, 2006.**121**(2):p.144-58.

41. Gatter, K.C., et al., *Transferrin receptors in human tissues: their distribution and possible clinical relevance.* J Clin Pathol, 1983. **36**(5): p. 539-45.

42. Pongratz, M., et al., *Transferrin binding and transferrin-mediated cellular uptake of the ruthenium coordination compound KP1019, studied by means of AAS, ESI-MS and CD spectroscopy.* J. Anal. At. Spectrom., 2004. **19**(1): p. 46-51.

43. Guo, M., et al., *Ti(IV) uptake and release by human serum transferrin and recognition of Ti(IV)-transferrin by cancer cells: understanding the mechanism of action of the anticancer drug titanocene dichloride.* Biochemistry, 2000. **39**(33): p. 10023-33.

44. Li, H., H. Sun, and Z.M. Qian, *The role of the transferrin-transferrin-receptor system in drug delivery and targeting.* Trends in Pharmacological Sciences, 2002. **23**(5): p. 206-209.

45. Valko, M., et al., *Free radicals, metals and antioxidants in oxidative stress-induced cancer.* Chem Biol Interact, 2006. **160**(1): p. 1-40.

46. Hancock, J.T., *The Role of Redox Mechanisms in Cell Signalling.* Mol. Biotechnol., 2009. **43**(2): p. 162-166.

47. Cooke, M.S., et al., *Oxidative DNA damage: mechanisms, mutation, and disease.* The FASEB Journal, 2003. **17**(10): p. 1195-1214.

48. Benhar, M., D. Engelberg, and A. Levitzki, *ROS, stress-activated kinases and stress signaling in cancer.* EMBO Rep, 2002. **3**(5): p. 420-5.

49. Trachootham, D., J. Alexandre, and P. Huang, *Targeting cancer cells by ROS-mediated mechanisms: a radical therapeutic approach?* Nat Rev Drug Discov, 2009. **8**(7): p. 579-591.

50. Jungwirth, U., et al., *Anticancer Activity of Metal Complexes: Involvement of Redox Processes.* Antioxidants & Redox Signaling, 2011. **in press**.

51. Kapitza, S., et al., *The heterocyclic ruthenium(III) complex KP1019 (FFC14A) causes DNA damage and oxidative stress in colorectal tumor cells.* Cancer Lett. (Amsterdam, Neth.), 2005. **226**(2): p. 115-121.

52. Szeto, H.H., *Mitochondria-targeted peptide antioxidants: novel neuroprotective agents.* AAPS J., 2006. **8**(3): p. E521-31.

53. Costantini, P., et al., *Mitochondrion as a Novel Target of Anticancer Chemotherapy.* Journal of the National Cancer Institute, 2000. **92**(13): p. 1042-1053.

54. Kapitza, S., et al., *Heterocyclic complexes of ruthenium(III) induce apoptosis in colorectal carcinoma cells.* J. Cancer Res. Clin. Oncol., 2005. **131**(2): p. 101-110.

55. Szekeres, T., et al., *The Enzyme Ribonucleotide Reductase: Target for Antitumor and Anti-HIV Therapy.* Critical Reviews in Clinical Laboratory Sciences, 1997. **34**(6): p. 503-528.

56. Cerqueira, N.M.F.S.A., et al., *Overview of Ribonucleotide Reductase Inhibitors: An Appealing Target in Anti-Tumour Therapy.* Curr. Med. Chem., 2005. **12**: p. 1283-1294.

57. Giles, F.J., et al., *Phase I and pharmacodynamic study of Triapine, a novel ribonucleotide reductase inhibitor, in patients with advanced leukemia.* Leuk. Res., 2003. **27**(12): p. 1077-1083.

58. Greeno, E., et al., *A phase II study of triapine in combination with gemcitabine (G) in patients (pts) with unresectable or metastatic pancreatic cancer (PC).* 2006, Amer soc clinical oncology.

59. Rosenberg, B., L. Van Camp, and T. Krigas, *Inhibition of cell division in Escherichia coli by electrolysis products from a platinum electrode.* Nature (London, U. K.), 1965. **205**(4972): p. 698-9.

60. Rosenberg, B., et al., *Platinum compounds: a new class of potent antitumor agents.* Nature, 1969. **222**(5191): p. 385-6.

61. Einhorn, L.H., *Curing metastatic testicular cancer.* Proc. Natl. Acad. Sci. U. S. A., 2002. **99**(7): p. 4592-4595.

62. Zamble, D.B. and S.J. Lippard, *Cisplatin and DNA repair in cancer chemotherapy.* Trends Biochem Sci, 1995. **20**(10): p. 435-9.

63. Harmers, F.P., W.H. Gispen, and J.P. Neijt, *Neurotoxic side-effects of cisplatin.* Eur J Cancer, 1991. **27**(3): p. 372-6.

64. Andrews, P.A. and S.B. Howell, *Cellular pharmacology of cisplatin: perspectives on mechanisms of acquired resistance.* Cancer Cells, 1990. **2**(2): p. 35-43.

65. Perez, R.P., T.C. Hamilton, and R.F. Ozols, *Resistance to alkylating agents and cisplatin: insights from ovarian carcinoma model systems.* Pharmacol. Ther., 1990. **48**(1): p. 19-27.

66. Perez, R.P., *Cellular and molecular determinants of cisplatin resistance.* Eur. J. Cancer, 1998. **34**(10): p. 1535-1542.

67. Eastman, A., *Cross-linking of glutathione to DNA by cancer-chemotherapeutic platinum coordination complexes.* Chem.-Biol. Interact., 1987. **61**(3): p. 241-8.

68. Kelley, S.L., et al., *Overexpression of metallothionein confers resistance to anticancer drugs.* Science (Washington, D. C., 1883-), 1988. **241**(4874): p. 1813-15.

69. Andrews, P.A., M.P. Murphy, and S.B. Howell, *Metallothionein-mediated cisplatin resistance in human ovarian carcinoma cells.* Cancer Chemother. Pharmacol., 1987. **19**(2): p. 149-54.

70. Masuda, H., et al., *Increased DNA repair as a mechanism of acquired resistance to cis-diamminedichloroplatinum(II) in human ovarian cancer cell lines.* Cancer Res., 1988. **48**(20): p. 5713-16.

71. Wang, D. and S.J. Lippard, *Cellular processing of platinum anticancer drugs.* Nat. Rev. Drug Discovery, 2005. **4**(4): p. 307-320.

72. Fichtinger-Schepman, A.M.J., et al., *Adducts of the antitumor drug cis-diamminedichloroplatinum(II) with DNA: formation, identification, and quantitation.* Biochemistry, 1985. **24**(3): p. 707-13.

73. Knox, R.J., et al., *Mechanism of cytotoxicity of anticancer platinum drugs: evidence that cis-diamminedichloroplatinum(II) and cis-diammine(1,1-cyclobutanedicarboxylato)platinum(II) differ only in the kinetics of their interaction with DNA.* Cancer Res., 1986. **46**(4, Pt. 2): p. 1972-9.

74. Woynarowski, J.M., et al., *Sequence- and region-specificity of oxaliplatin adducts in naked and cellular DNA.* Mol. Pharmacol., 1998. **54**(5): p. 770-777.

75. Noordhuis, P., et al., *Oxaliplatin activity in selected and unselected human ovarian and colorectal cancer cell lines.* Biochem. Pharmacol., 2008. **76**(1): p. 53-61.

76. Malina, J., et al., *Conformation of DNA GG Intrastrand Cross-Link of Antitumor Oxaliplatin and Its Enantiomeric Analog.* Biophysical journal, 2007. **93**(11): p. 3950-3962.

77. Masters, J.R.W. and B. Koberle, *Curing metastatic cancer: lessons from testicular germ-cell tumours.* Nat Rev Cancer, 2003. **3**(7): p. 517-525.

78. Cleare, M.J. and J.D. Hoeschele, *Antitumor platinum compounds. Relation between structure and activity.* Platinum Metals Rev., 1973. **17**(1): p. 2-13.

79. Hambley, T.W., *The influence of structure on the activity and toxicity of Pt anticancer drugs.* Coord. Chem. Rev., 1997. **166**: p. 181-223.

80. Farrell, N., *DNA binding and chemistry of dinuclear platinum complexes.* Comments Inorg. Chem., 1995. **16**(6): p. 373-389.

81. Mangrum, J.B. and N.P. Farrell, *Excursions in polynuclear platinum DNA binding.* Chem. Commun. (Cambridge, U. K.). **46**(36): p. 6640-6650.

82. Di Blasi, P., et al., *Cytotoxicity, cellular uptake and DNA binding of the novel trinuclear platinum complex BBR 3464 in sensitive and cisplatin resistant murine leukemia cells.* Anticancer Res., 1998. **18**(4C): p. 3113-3117.

83. Wong, E. and C.M. Giandomenico, *Current Status of Platinum-Based Antitumor Drugs.* Chem. Rev. (Washington, D. C.), 1999. **99**(9): p. 2451-2466.

84. Giandomenico, C.M. and E. Wong, *Discovery and development of third-generation platinum antitumor agents with oral activity.* ACS Symp. Ser., 2005. **903**(Medicinal Inorganic Chemistry): p. 30-43.

85. Lebwohl, D. and R. Canetta, *Clinical development of platinum complexes in cancer therapy: an historical perspective and an update.* Eur. J. Cancer, 1998. **34**(10): p. 1522-1534.

86. Farrell, N., et al., *Cytostatic trans-platinum(II) complexes.* J. Med. Chem., 1989. **32**(10): p. 2240-1.

87. Farrell, N., et al., *Activation of the trans geometry in platinum antitumor complexes: a survey of the cytotoxicity of trans complexes containing planar ligands in murine L1210 and human tumor panels and studies on their mechanism of action.* Cancer Res., 1992. **52**(18): p. 5065-72.

88.   Martinez, A., et al., *Synthesis, characterization and biological activity of trans-platinum(II) and trans-platinum(IV) complexes with 4-hydroxymethylpyridine.* ChemBioChem, 2005. **6**(11): p. 2068-2077.

89.   Coluccia, M., et al., *Platinum(II) complexes containing iminoethers: a trans platinum antitumor agent.* Chem.-Biol. Interact., 1995. **98**(3): p. 251-66.

90.   Zaludova, R., et al., *DNA modifications by antitumor trans-[PtCl2(E-iminoether)2].* Mol. Pharmacol., 1997. **52**(3): p. 354-361.

91.   Coluccia, M., et al., *In vitro and in vivo antitumor activity and cellular pharmacological properties of new platinum-iminoether complexes with different configuration at the iminoether ligands.* J. Inorg. Biochem., 1999. **77**(1-2): p. 31-35.

92.   Novakova, O., et al., *DNA-protein cross-linking by trans-[PtCl2(E-iminoether)2]. A concept for activation of the trans geometry in platinum antitumor complexes.* Nucleic Acids Res., 2003. **31**(22): p. 6450-6460.

93.   Montero, E.I., et al., *Preparation and Characterization of Novel trans-[PtCl2(amine)(isopropylamine)] Compounds: Cytotoxic Activity and Apoptosis Induction in ras-Transformed Cells.* J. Med. Chem., 1999. **42**(20): p. 4264-4268.

94.   Prokop, R., et al., *DNA interactions of new antitumor platinum complexes with trans geometry activated by a 2-methylbutylamine or sec-butylamine ligand.* Biochem. Pharmacol., 2004. **67**(6): p. 1097-1109.

95.   Najajreh, Y., et al., *Structure and unique interactions with DNA of a cationic trans-platinum complex with the nonplanar bicyclic piperidinopiperidine ligand.* Angew. Chem., Int. Ed., 2005. **44**(19): p. 2885-2887.

96.   Kasparkova, J., et al., *Activation of Trans Geometry in Bifunctional Mononuclear Platinum Complexes by a Piperidine Ligand: Mechanistic Studies on Antitumor Action.* J. Biol. Chem., 2003. **278**(48): p. 47516-47525.

97.   Zorbas-Seifried, S., et al., *Reversion of structure-activity relationships of antitumor platinum complexes by acetoxime but not hydroxylamine ligands.* Molecular Pharmacology, 2007. **71**(1): p. 357-65.

98.   Quiroga, A.G., et al., *Trans platinum complexes design: One novel water soluble oxime derivative that contains aliphatic amines in trans configuration.* J. Inorg. Biochem., 2007. **101**(1): p. 104-110.

99.   Perez, J.M., et al., *Current status of the development of trans-platinum antitumor drugs.* Crit Rev Oncol Hematol, 2000. **35**(2): p. 109-20.

100.   Farrell, N., *Current status of structure-activity relationships of platinum anticancer drugs: activation of the trans geometry.* Met. Ions Biol. Syst., 1996. **32**(Interactions of Metal Ions with Nucleotides, Nucleic Acids, and Their Constituents): p. 603-639.

101.   Frausin, F., et al., *Free exchange across cells, and echistatin-sensitive membrane target for the metastasis inhibitor NAMI-A (imidazolium trans-imidazole dimethyl sulfoxide tetrachlororuthenate) on KB tumor cells.* J. Pharmacol. Exp. Ther., 2005. **313**(1): p. 227-233.

102.   Hartinger, C.G., et al., *From bench to bedside--preclinical and early clinical development of the anticancer agent indazolium trans-[tetrachlorobis(1H-indazole)ruthenate(III)] (KP1019 or FFC14A).* Journal of Inorganic Biochemistry, 2006. **100**(5-6): p. 891-904.

103.   Reisner, E., et al., *Tuning of Redox Potentials for the Design of Ruthenium Anticancer Drugs - an Electrochemical Study of [trans-RuCl4L(DMSO)]- and [trans-RuCl4L2]-Complexes, where L = Imidazole, 1,2,4-Triazole, Indazole.* Inorg. Chem., 2004. **43**(22): p. 7083-7093.

104.   Heffeter, P., et al., *Intracellular protein binding patterns of the anticancer ruthenium drugs KP1019 and KP1339.* JBIC, J. Biol. Inorg. Chem. **15**(5): p. 737-748.

105. Rademaker-Lakhai, J.M., et al., *A Phase I and Pharmacological Study with Imidazolium-trans-DMSO-imidazole-tetrachlororuthenate, a Novel Ruthenium Anticancer Agent.* Clin. Cancer Res., 2004. **10**(11): p. 3717-3727.

106. Dyson, P.J. and G. Sava, *Metal-based antitumor drugs in the post genomic era.* Dalton Trans., 2006(16): p. 1929-1933.

107. Jakupec, M.A. and B.K. Keppler, *Gallium and other main group metal compounds as antitumor agents.* Metal Ions in Biolgical Systems, Vol 42: Metal Complexes in Tumor Diagnosis and as Anticancer Agents, 2004. **42**: p. 425-62.

108. Seligman, P.A. and E.D. Crawford, *Treatment of Advanced Transitional Cell Carcinoma of the Bladder With Continuous-Infusion Gallium Nitrate.* Journal of the National Cancer Institute, 1991. **83**(21): p. 1582-1584.

109. Foster, B.J., et al., *Gallium nitrate: the second metal with clinical activity.* Cancer Treat Rep, 1986. **70**(11): p. 1311-9.

110. Valiahdi, S.M., et al., *The gallium complex KP46 exerts strong activity against primary explanted melanoma cells and induces apoptosis in melanoma cell lines.* Melanoma Research, 2009. **19**(5): p. 283-93.

111. Doadrio, A., D. Craciunescu, and C. Ghirvu, *Structure-antitumor activity relationship for the platinum(2+), palladium(2+), palladium(4+), and osmium(4+) complexes and complex salts with sulfonamide derivatives.* An. R. Acad. Farm., 1980. **46**(2): p. 153-66.

112. Moucheron, C., A. Kirsch-De Mesmaeker, and J.M. Kelly, *Photoreactions of ruthenium(II) and osmium(II) complexes with deoxyribonucleic acid (DNA).* J. Photochem. Photobiol., B, 1997. **40**(2): p. 91-106.

113. Cebrian-Losantos, B., et al., *Osmium NAMI-A analogues: synthesis, structural and spectroscopic characterization, and antiproliferative properties.* Inorganic Chemistry, 2007. **46**(12): p. 5023-33.

114. Luemmen, G., et al., *Phase II trial of titanocene dichloride in advanced renal-cell carcinoma.* Cancer Chemother. Pharmacol., 1998. **42**(5): p. 415-417.

115. Oberschmidt, O., et al., *Antiproliferative activity of Titanocene Y against tumor colony-forming units.* Anti-Cancer Drugs, 2007. **18**(3): p. 317-321.

116. Koepf-Maier, P. and H. Koepf, *Non-platinum group metal antitumor agents. History, current status, and perspectives.* Chem. Rev., 1987. **87**(5): p. 1137-52.

117. Hartinger Christian, G. and J. Dyson Paul, *Bioorganometallic chemistry--from teaching paradigms to medicinal applications.* Chem Soc Rev, 2009. **38**(2): p. 391-401.

118. van Rijt, S.H. and P.J. Sadler, *Current applications and future potential for bioinorganic chemistry in the development of anticancer drugs.* Drug Discovery Today, 2009. **14**(23/24): p. 1089-1097.

119. Allard, E., et al., *Dose effect activity of ferrocifen-loaded lipid nanocapsules on a 9L-glioma model.* Int. J. Pharm., 2009. **379**(2): p. 317-323.

120. Nguyen, A., et al., *Ferrocifens and ferrocifenols as new potential weapons against breast cancer.* Chimia, 2007. **61**(11): p. 716-724.

DI (FH) Caroline Bartel

PERSONAL DATA

Date of Birth	April 17th, 1981
Place of Birth	Vienna
Nationality	Austrian
Civil status	unmarried
Place of Living	Vienna
Mail	caroline.bartel@univie.ac.at

WORK EXPERIENCE

since 11.2007   **University of Vienna,** *Institute of Inorganic Chemistry, Research Associate, Cell biology laboratory*
PhD thesis "Cellular Accumulation and DNA Interaction Studies of anti-tumor metal complexes", Supervision of undergraduate students in lab courses on Biological Inorganic Chemistry

02.2006 – 06.2006   **Medical University of Vienna, AKH,** *Institute of Medical and Chemical Laboratory Diagnostics, Diploma thesis*
"Assay for the Characterization and Quantification of Microparticles in Plasma", Establishment of a method to analyze human plasma microparticles by means of FACS

07.2005 – 08.2005   **Öko Orange,** *Vienna, Traineeship*
Support in issuing a waste management concept and in market analysis

10.2004 – 03.2005   **Boehringer Ingelheim Austria GmbH,** *Vienna, Traineeship*
Process Science, Biopharmaceutical Production,
Microorganism fermentation, Establishment of a method for
size analysis of protein inclusion bodies

06.2004 – 07.2004   **Novartis Forschungsinstitut GmbH,** *Vienna, Traineeship*

06.2003 – 07.2003   **Frenkel Chemie GmbH,** *Perchtoldsdorf, Traineeship*

09.2001 – 12.2002   **SHG – Schreiber HandelsgmbH,** *Vienna, Marginally Employment*
General office work, Translation of data sheets and documentation
components (English - German), Assistance in trade fairs

LANGUAGE AND EDV SKILLS

German	native language
English	fluently
French	high school level
Russian	basic knowledge

Profound knowledge of Microsoft Office (Excel, Word, Power Point, Outlook)

EDUCATION

2008 - 2011	PhD Study of Chemistry, University of Vienna Specialization: Bioinorganic Chemistry
2006 – 2008	Study of Technical Chemistry, Technical University Vienna Specialization: Biotechnology und Bioanalytics
2002 – 2006	Study of Chemistry, HBLVA for chem. Industry and FH Fresenius, Vienna (A)/Idstein (D), Specialization: Bioanalytics and Management
1999 – 2002	Study of Nutritional Science and Biology, University of Vienna
1987 – 1999	Elementary and Grammar school, Vienna

RESEARCH SKILLS

Cell Culture, Molecular Biology, Analytical Chemistry, Drug Development and Biological Studies of active Compounds, Medicinal Chemistry, Cancer Research, Biochemistry, Biotechnology, Fermentation of Microorganisms

PUBLICATIONS IN SCIENTIFIC JOURNALS

Influence of ascorbic acid on the activity of the investigational anticancer drug KP1019

Bartel C., Egger A.E., Jakupec M.A., Heffeter P., Berger W., Keppler B.K.

Journal of Biological Inorganic Chemistry, **2011**, online June 25th, 2011

Physicochemmical studies and anticancer potency of ruthenium($^6\eta$-*p*-cymene) complexes containing antibacterial quinolones

Kljun J., Kandioller W., Bytzek A.K., Bartel C., Jakupec M.A., Hartinger Ch.G., Keppler B.K., Iztok T.

Organometallics, **2011**, 30(9): 2506-2512

Intracellular protein binding patterns of the anticancer ruthenium drugs KP1019 and KP1339

Heffeter P., Boeck K., Atil B., Hoda M.A.R., Koerner W., Bartel C., Jungwirth U., Keppler B.K., Micksche M., Berger W.

Journal of Biological Inorganic Chemistry, **2010**, 15, 737-748.

Maltol-derived ruthenium-cymene complexes with tumor inhibiting properties: the impact of ligand-metal bond stability on anticancer activity *in vitro*

Kandioller W., Hartinger C.G., Nazarov A.A., Bartel C., Skocic M., Jakupec M.A., Arion V.B., Keppler B.K.

Chemistry – A European Journal, **2009**, 15, 12283-12291

From pyrone to thiopyrone ligands-rendering maltol-derived ruthenium(II)-arene complexes that are anticancer active *in vitro*

Kandioller W., Hartinger C.G., Nazarov A.A., Kuznetsov M.L., John R.O., Bartel C., Jakupec M.A., Arion V.B., Keppler B.K.

Organometallics, **2009**, 28, 4249-4251.

Synthesis, x-ray diffraction structure, spectroscopic properties and antiproliferative activity of a novel ruthenium complex with constitutional similarity to cisplatin

Grguric-Sipka S., Stepanenko I.N., Lazic J.M., Bartel C., Jakupec M.A., Arion V.B., Keppler B.K.

Dalton Transaction, **2009**, 17, 3334-3339.

PUBLICATIONS IN SUBMISSION

Cellular accumulation and DNA interaction studies of active *trans*-platinum(II) anticancer compounds

Bartel C., Bytzek A.K., Scaffidi-Domianello Y.Yu., Grabmann G., Jakupec M.A., Hartinger Ch., Galanski M., Keppler B.K.

Submitted: Journal of Biological Inorganic Chemistry

Synthesis, crystal structures and properties of the complexes of N-hydroxyethyl-N-benzimidazolyl-methylethylendiaminediacetic acid with group 12 metals and with vanadyl

Habala L., Bartel C., Giester G., Ionita G. ,Jakupec M.A., Keppler B.K., Rompel A.

Submitted: Journal of Inorganic Biochemistry

Targeting the DNA-topoisomerase complex in a double-strike approach with a topoisomerase inhibiting moiety and covalent DNA binder

Kurzwernhart A, Kandioller W., Bartel C., Bächler S., Trondl R., Mühlgassner G., Jakupec M.A., Arion V.B., Marko D., Keppler B.K., Hartinger C.

Submitted:

Biological activity of ruthenium- and osmium-arene complexes with bidentate paullone-based ligands in human cancer cells

Mühlgassner G., Bartel C., Schmid W.F., Jakupec M.A., Arion V.B., Keppler B.K.

Submitted: Journal of Inorganic Biochemistry

ORAL PRESENTATIONS

Influence of ascorbic acid on the mode of action of the ruthenium complex KP1019: cytotoxicity, cellular uptake and interaction with DNA

Bartel C., Egger A.E., Jakupec M.A., Berger W., Heffeter P., Keppler B.K.

9th European Biological Inorganic Chemistry Conference
Wroclaw, Poland, September 2nd – September 6th, 2008.

From small molecule anticancer compounds to organometallics with targeting potential

Hartinger C.G., Kurzwernhart A., Trondl R., Kandioller W., Bartel C., Mühlgassner G., Jakupec M.A., Keppler B.K.

10th European Biological Inorganic Chemistry Conference
Thessaloniki, Greece, June 22nd – June 26th, 2010.

Organometallic anticancer compounds targeted by linking the flavopiridol backbone to ruthenium-cymene moieties

Kurzwernhart A., Kandioller W., Mühlgassner G., Bartel C., Jakupec M.A., Arion V.B., Hartinger C.G., Keppler B.K.

6. Workshop Anorganische Chemie in Österreich (6. WACÖ)
Linz, Austria, March 29th – March 30th, 2010

POSTER PRESENTATIONS

Cellular uptake and DNA interaction studies of active *trans*-platinum anticancer compounds

Bartel C., Meelich K., Scaffidi-Domianello Y.Y., Kukushkin N.V., Jakupec M.A., Kukushkin V.Y., Galanski M., Keppler B.K.

10th European Biological Inorganic Chemistry Conference
Thessaloniki, Greece, June 22nd – 26th, 2010.

Pyrone vs. pyridinone as ligands for Ru-arene anticancer agents

Kandioller W., Henke H., Hanif M., Schaaf P., Bartel C., Jakupec M.A., Nazarov A.A., HartingerC.G., Keppler B.K.

10th European Biological Inorganic Chemistry Conference
Thessaloniki, Greece, June 22nd – 26th, 2010.

The cytotoxic potential of 4-pyrone and 4-thiopyrone derived Ru(II)-cymene complexes and their behaviour in aqueous solution

Kandioller W., Hartinger C., Nazarov A., John R., Bartel C., Jakupec M.A., Arion V.B. Keppler B.K.

10th International Symposium on Applied Bioinorganic Chemistry,
Debrecen, Hungary, September 25th – 28th, 2009.